AD NUMBER
ADA800876
CLASSIFICATION CHANGES
TO: **unclassified**
FROM: **confidential**
LIMITATION CHANGES
TO: **Approved for public release; distribution is unlimited.**
FROM: **Distribution authorized to DoD only; Administrative/Operational Use; JUN 1947. Other requests shall be referred to National Aeronautics and Space Administration, Washington, DC. Pre-dates formal DoD distribution statements. Treat as DoD only.**
AUTHORITY
NASA TR Server website; NASA TR Server website

COPY NO. 72

CONFIDENTIAL

6505
NACA - 1947/8

NATIONAL ADVISORY COMMITTEE FOR AERONAUTICS

NACA CONFERENCE ON AIRCRAFT ICE PREVENTION

A COMPILATION OF THE PAPERS PRESENTED BY NACA STAFF MEMBERS

Flight Propulsion Research Laboratory
Cleveland, Ohio

June 26–27, 1947

NACA

CLASSIFIED DOCUMENT

This document contains classified information affecting the National Defense of the United States within the meaning of the Espionage Act, USC 50:31 and 32. Its transmission or the revelation of its contents in any manner to an unauthorized person is prohibited by law. Information so classified may be imparted only to persons in the military and naval Services of the United States, appropriate civilian officers and employees of the Federal Government who have a legitimate interest therein, and to United States citizens of known loyalty and discretion who of necessity must be informed thereof.

CONFIDENTIAL

NACA CONFERENCE ON AIRCRAFT ICE PREVENTION

A COMPILATION OF THE PAPERS PRESENTED

BY NACA STAFF MEMBERS

Flight Propulsion Research Laboratory
Cleveland, Ohio

June 26-27, 1947

CONTENTS

The authors are members of the staffs of the NACA laboratories at Moffett Field, California and Cleveland, Ohio.

INTRODUCTION

The conference on Aircraft Ice Prevention was organized by the NACA to convey the Committee's latest research results to those individuals and organizations responsible for the design, development, and flight application of aircraft ice-prevention equipment.

The technical discussions are reproduced herewith in the same form in which they were presented so that distribution might be prompt. The original presentations in this record are considered as complementary to, rather than as substitutes for, the Committee's system of complete and formal reports.

A list of the conferees is included.

NATIONAL ADVISORY COMMITTEE
FOR AERONAUTICS

LIST OF CONFEREES

The following conferees were registered at the NACA conference on Aircraft Ice Prevention, Flight Propulsion Research Laboratory, Cleveland, Ohio, June 26-27, 1947:

Alford, W. M.	Hamilton Standard Propellers, Div. United Aircraft
Anderson, Herbert	Airplane Div., Curtiss-Wright
Atkin, E. H.	A. V. Roe, Canada Limited
Bartlett, Parker M.	U. S. Navy, Bureau of Aeronautics
Bell, R. A.	Surface Combustion
Bement, Herman	Grumman Aircraft
Bergrun, Norman R.	NACA
Bjerke, A. E.	Goodyear Aircraft
Boeke, F.	North American Aviation
Bowers, J. S.	Engine Div., Packard Aircraft
*Brown, A. A.	Pratt & Whitney
Butcher, J. A.	Northwest Airlines
Callaghan, E. E.	NACA
Chandler, H. C., Jr.	NACA
Chasman, B.	AAF, Air Materiel Command
Clark, Victor F.	Harvard University, Blue Hill Meteorological Observatory
Cook, L. V.	AAF, Air Materiel Command
Dodd, W.	AAF, Air Materiel Command
Doherty, T. E.	Hamilton Standard Propellers, Div. United Aircraft
Drell, Harry	Lockheed Aircraft
Dyment, J. T.	Trans-Canada Air Lines
Empey, Lt. R. E.	Naval Air Test Center
Erdman, Mr.	McDonnell Aircraft
Fairbank, Lt. C. E.	AAF Liaison Office, Cleveland
Fleming, William A.	NACA
Flower, Scott	Pan American Airways
Frantz, J. G.	Pittsburgh Plate Glass

*Member of NACA Subcommittee on De-Icing Problems.

Gleason, T. C.	Chrysler
Gough, W. V., Jr.	NACA
Gray, Vernon H.	NACA
Grimac, Theodore E.	United Aircraft
Grosselfinger, R. A.	DeLaval Steam Turbine
Haines, J. F.	Aeroproducts Div., General Motors
Hammen, T. F., Jr.	Ranger Aircraft Engines Div., Fairchild Engine & Airplane
Harris, Lt. F. L.	Naval Air Test Center
Harris, T. J.	American Overseas Airlines
Harrison, Lt. Comdr. B. K.	Office of Naval Research
Hartman, E. P.	NACA
Hawn, R. J.	U. S. Army, Aeronautical Ice Research Laboratory
*Haynes, B. C.	U. S. Weather Bureau
Hemans, Major John	U. S. Air Weather Service
Hermanson, Comdr. W. L.	Naval Air Transport Service
Hill, J. F.	Douglas Aircraft
Holdaway, George H.	NACA
Howell, Wallace E.	Harvard University, Blue Hill Meteorological Observatory
*Hunter, Willson H.	NACA
Jacob, Dr. Max	Allis-Chalmers Manufacturing
Jewett, Charles	Wright Aeronautical
Johnson, Robert E.	Wright Aeronautical
Johnson, W. C.	Goodyear Aircraft
Johnston, J. Ford	NACA
*Jones, Alun R.	NACA
*Jones, B. F.	B. F. Goodrich
Jones, Clyde B.	Hughes Aircraft
Jukkola, Dr. E. E.	AAF, Air Materiel Command
Kalberer, Karl	Aero Insurance Underwriters
Kemper, Carlton	NACA
Kepple, William L.	NACA
Kinnucan, J. W.	Continental Motors
Kline, Dwight B.	U. S. Weather Bureau
Koneczny, W. E.	Civil Aeronautics Board

*Member of NACA Subcommittee on De-Icing Problems.

Laing, R. W.	Smith, Hinchman, & Grylls
Lawrence, W. C.	American Overseas Airlines
Leach, Mr.	Naval Air Experimental Station
Lewis, J. P.	NACA
Lewis, William	NACA
Linforth, Robert L.	Boeing Aircraft
Littell, R. E.	NACA
Loughborough, Dr. D. L.	B. F. Goodrich
McCartan, Lt. Col. Arthur	U. S. Air Weather Service
Meckley, W. O.	General Electric
Merkle, R. R.	Aeroproducts Div., General Motors
Mershon, C. L.	Westinghouse Electric
Murray, Major James	AAF Liaison Office, Moffett Field
Neel, Carr B., Jr.	NACA
North, D. A.	American Airlines
Nunn, W. S.	Stewart-Warner
Olsen, A. F.	Northwest Airlines
Orr, A. W., Jr.	Holley Carburetor
Orr, J. L.	National Research Council
*Patterson, D. M.	AAF, Air Materiel Command
Pelster, A. F.	Westinghouse Electric
Pettit, K. G.	National Research Council
Pesman, Gerard J.	NACA
Potter, D. A.	Stewart-Warner
Potter, Ray M.	U. S. Army, Aeronautical Ice Research Laboratory
Powell, Lt. Comdr. L. R.	Naval Air Transport Service
Preston, G. Merritt	NACA
Rausch, Paul	B. F. Goodrich
Ray, George	Bell Aircraft
Rethman, Major V. C.	AAF Liaison Office, Cleveland
Ring, W. A.	Consolidated Vultee Aircraft
*Rodert, Lewis A.	NACA
Rothrock, Addison M.	NACA
Sanborn, Lt. Comdr. V. C.	Naval Air Transport Service
Sand, E. J.	Propeller Div., Curtiss-Wright

*Member of NACA Subcommittee on De-Icing Problems.

Sayre, Daniel	Princeton University
Schreiber, J. F.	U. S. Rubber
Scott, R. L.	Naval Air Experimental Station
Scott, Lt. S. V.	Naval Air Transport Service
Selvia, Paul H.	AAF, Air Materiel Command
Sharp, Edward R.	NACA
Shaw, W. C.	United Air Lines
Sheets, J. H.	Propeller Div., Curtiss-Wright
Shippen, William B.	Glenn L. Martin
Silverstein, Abe	NACA
Smith-Johannsen, Robert	General Electric
Smull, T. L. K.	NACA
*Sontag, H. C.	U. S. Navy, Bureau of Aeronautics
Spaulding, M. B., Jr.	Air Transport Association of America
Staley, A. C.	Chrysler
Stark, Robert	Eastern Airlines
Stephen, Gene	Fredric Flader
Stevens, Robert	Airplane Div., Curtiss-Wright
Tanchel, Melvin	AAF, Air Materiel Command
Taylor, W. H.	Goodyear Tire & Rubber
Thompson, James G.	NACA
Tifford, Arthur N.	Westinghouse Electric
Trussell, J.	Glenn L. Martin
*Valentine, C. I.	AAF, Air Materiel Command
von Glahn, Uwe H.	NACA
Walker, R. A.	Transcontinental & Western Airlines
Watson, W. O.	Allison Div., General Motors
Weitzen, W.	AAF, Air Materiel Command
Weldy, Robert	Ex-Cell-O
Weller, D. W.	Fairchild Aircraft Div., Fairchild Engine & Airplane
Wheatley, John	Allison Div., General Motors
Whitney E. G.	Ranger Aircraft Engines Div., Fairchild Engine & Airplane
Whittemore, R. G.	Pittsburgh Plate Glass
Willis, C. E.	Fairchild Aircraft Div., Fairchild Engine & Airplane
Wittner, H.	Republic Aviation
York, Mr.	Continental Motors

*Member of NACA Subcommittee on De-Icing Problems.

REVIEW OF NACA RESEARCH ON THE THERMAL ICE-PREVENTION SYSTEM

By Lewis A. Rodert

Flight Propulsion Research Laboratory

INTRODUCTION

When an unprotected airplane encounters icing conditions, its usefulness is reduced because of the detrimental effects of ice on performance, dependability, and safety. The research of the NACA on ice prevention has been directed to a very large extent toward the use of heat.

A solution to a problem such as that presented by the formation of ice can usually be found, but the solution always involves penalties. In order to judge the relative importance of penalties and benefits connected with thermal ice prevention, it is necessary to understand the severity of the problem when no protection is provided. One phase of the research has therefore been concerned with evaluating the changes in lift and drag of lifting surfaces, loss of thrust, unbalance of propellers, loss of vision through windshields, increased structural loads in external fittings such as radio antennas, and structural damage due to ice being thrown from propellers or shed from one part and striking another, which occurs when an airplane is flown in icing conditions.

The research on the thermal system was concerned first with discovering heating arrangements for the various vulnerable parts of the airplane. Through these arrangements heat could be delivered to the wings, the windshield, and the propeller. Upon discovery of what appeared to be workable constructional arrangements for heating these parts, the next concern was the quantity and distribution of the heat required.

Inasmuch as the heat required is determined not by the configuration of the vulnerable part alone, but also by the nature of the icing cloud, the research also included a study of meteorological conditions.

The scope of the research has been to determine the detrimental effects of ice, to investigate means for applying heat to the vulnerable parts, to establish design procedures for calculating the heat required, and to determine the cloud characteristics which cause the ice.

In the conduct of the research, useful data has been obtained that is applicable to the range of airplane speeds, sizes, and variations in form that exist or are apt to be found in the near future.

Acknowledgment is made to the United Air Lines, Northwest Airlines, and the Air Materiel Command and the pilots of these organizations for their contributions in making possible the extensive flight operations in natural icing conditions.

PROCEDURES AND RESULTS

During the 1920's, flights with unprotected airplanes into icing conditions demonstrated that a major problem existed and as a result research on ice prevention by the NACA was started. The nature of the problem was further evaluated by wind-tunnel and flight research in which the effects on lift and drag on airfoils were measured. Typical of these studies was one conducted in 1939 on the Lockheed 12A airplane (fig. 1), in which protuberances intended to simulate ice were attached to a wing and the aerodynamic characteristics were measured. The simulated formation shown on the wing caused a reduction in $C_{L_{max}}$ of 40 percent and and increase in C_D of the wing at cruising speed of 450 percent. More recently, the effects on airplane performance have been measured by the use of aircraft with which flight may be safely made into icing conditions, which is presented by Gough. Ice has been observed to cause radio-antenna wires to break and a study of this particular problem was made, the results of which are given by Kepple. Ice thrown from propellers has penetrated $\frac{1}{4}$-inch plastic windows and the sides of the airplane fuselages with sufficient velocity to cause some damage on the interior of the craft (fig. 2). Ice shed from the forward portions of the airplane has seriously damaged the tail structure (fig. 2). The simple conclusion from this evidence is that protection is required if operations into icing conditions are to be attempted.

The use of heat as a means of preventing ice was initiated prior to 1930 and reported by Theodorsen and Clay (reference 1). Ice-tunnel and flight investigations using model wings and simulated icing conditions were conducted (fig. 3). At this date, a material such as 18-8 stainless steel was not available and therefore the exhaust-air heat exchanger or other high-operating-temperature equipment was not given serious consideration. The early models were heated with steam because it was thought that a practical

system might be found with such a heating medium and because steam provided a practical method, through the measurement of the rate of precipitation, of determining the heat required. It was concluded from this work that there was adequate heat in the engine exhaust to protect the airplane wing against ice and that protection could be obtained by heating about 10 percent of the leading edge of the wing.

In 1937, when the air line operators had become more in need of an answer to the ice problem and when better materials were available, other heating means were examined. Again, in the icing tunnel and in flight, models were studied.

The trend toward all-metal construction and the possible use of heated air or engine-exhaust gas in the wing structure required investigation of various leading-edge heating arrangements (fig. 4). The passage of exhaust through a tube within the wing leading edge and the passage of heated air within the wing were examined in the flight model (fig. 5). Ice was permitted to form on this model (fig. 6); the quantity of heat required to remove the ice was found to be less than that required to prevent the formation of ice. It was also concluded from this investigation that less than 20 percent of the engine-exhaust heat would be required to prevent ice on large aircraft having the power-area ratios of 1937 period. It was further concluded that by heating the leading-edge 10-percent region to a temperature 100° F above the ambient-air temperature, when flying in dry air, would supply sufficient heat to prevent ice at the same airspeed. This has been the basis of the dry-air method of analysis of heat requirements.

On the basis of these results, a full-scale application was made on the Lockheed 12A airplane (fig. 7). The design of this equipment was started in 1939 and the first flights in natural icing conditions were made in the early part of 1941 from the NACA laboratory at Moffett Field, California. The first Lockheed 12A design employed an exhaust-gas tube within the wing leading edge. The flights in natural icing conditions confirmed in full scale the results of earlier model research and provided the tool with which the problem could be generally treated; that is, an airplane was provided that could be deliberately and safely flown into icing conditions. The ice, so to speak, had been broken. An exhaust tube in the wing did not have wide application and therefore investigations were started on air heating methods. The arrangement shown in figure 4(E) was found to be satisfactory in these investigations. This led to the work on heat exchangers.

A number of heat-exchanger development projects was started by the NACA in industrial concerns in 1941 whereby it was hoped that a satisfactory heated-air source would be found. Many firms responded and several serviceable exchangers were produced. The tube-bundle type exchanger resulted from this activity (fig. 8). The heat exchanger made possible several applications of the thermal system to wartime airplanes, the experimental versions of which were designed and constructed by the NACA. The B-24 was the first of these projects (fig. 9). This craft used four tube-bundle type exchangers to supply heated air to the wings, empennage, and windshield. Modifications were also made for the B-17 and C-46 airplanes and the Lockheed 12A airplane was converted to the heated-air system. The full-scale applications made during the war demonstrated, through actual service, the practicability of the thermal system.

The weight, structural complications, and maintenance difficulties of the thermal system were indicated from the full-scale applications. The thermal protection was found to add about 1 percent of the gross weight. By careful design, cabin heating might also be obtained without further weight.

The wing leading edge (fig. 10) was found to add some structural complications. Metallurgical and structural investigations indicated no serious penalty although flight tests with the C-46 showed that some skin structure might have to be made thicker by about 10 percent. The circulation of air through the heating system caused a small loss in performance. The exhaust-heat exchangers did not have a significant effect on engine power.

The heating of windshields was first examined in tunnel and flight models in 1938. Using a section of a Stinson airplane windshield (fig. 11) and simulated icing conditions, data were taken on the quantity of heat required to prevent ice formations. The windshields were heated by passing heated air between two closely spaced panes and by the use of electric power. From these studies it was concluded that about 1000 Btu per hour per square foot would protect the windshield at airspeeds up to 150 miles per hour. The results of this research were later confirmed on the Lockheed 12A and recently extended on the B-24 and C-46 airplanes, a discussion of which is presented by Holdaway.

The initial research on the heating of propellers was concerned with evaluating the effects of aerodynamic heating. The National Research Council of Canada made the first full-scale applications of the thermal system to propellers and demonstrated

that power for the heating could be provided by hub-type generators. The topic of propeller heating is covered in several papers presented by Gray, Lewis, and Pesman.

While the dry-air method of determining the quantity of heat required for ice protection has been useful as demonstrated by the success of air research airplanes, it has not been considered adequate. It was early recognized that the design should be based on specified meteorological conditions and the quantity of heat as calculated from the impingement rate and pattern when operating in these conditions. A study was made by Kantrowitz (reference 2) of the impingement pattern in 1939 and by others since that date. This work has recently been extended and is discussed by Bergrun. The treatment of heat transfer from a wetted surface as examined initially by Hardy (reference 3) has also been investigated for the cases of the wing and windshield and these studies are presented by Neel and Holdaway, respectively.

Obtaining data on the characteristics of an icing cloud has been most difficult. Research on instruments whereby the liquid-water content and droplet size may be measured has been initiated in our laboratories and sponsored at universities. Without extensive data on the problem that nature presents, the design of the thermal system can only be approached in an empirical manner. During flights conducted the past several years, considerable meteorological data have been collected. The Weather Bureau has collaborated with the NACA in this phase on the research by providing meteorologists and special services of their weather stations in the areas of operation. The results of this work is presented in the following section by Lewis.

CONCLUSION

The results of NACA research on the thermal ice-prevention system have shown that all entering surfaces of aircraft intended for all-weather operation must be protected and that protection can be provided by the use of heat without significant penalties to the usefulness of the airplane.

REFERENCES

1. Theodorsen, Theodore, and Clay, William C.: Ice Prevention on Aircraft by Means of Engine Exhaust Heat and a Technical Study of Heat Transmission from a Clark Y Airfoil. NACA Rep. No. 403, 1932.

2. Kantrowitz, Arthur: Aerodynamic Heating and the Deflection of Drops by an Obstacle in an Air Stream in Relation to Aircraft Icing. NACA TN No. 779, 1940.

3. Hardy, J. K.: Kinetic Temperature of Wet Surfaces. A Method of Calculating the Amount of Alcohol Required to Prevent Ice, and the Derivation of the Psychrometric Equation. NACA ARR No. 5G13, 1945.

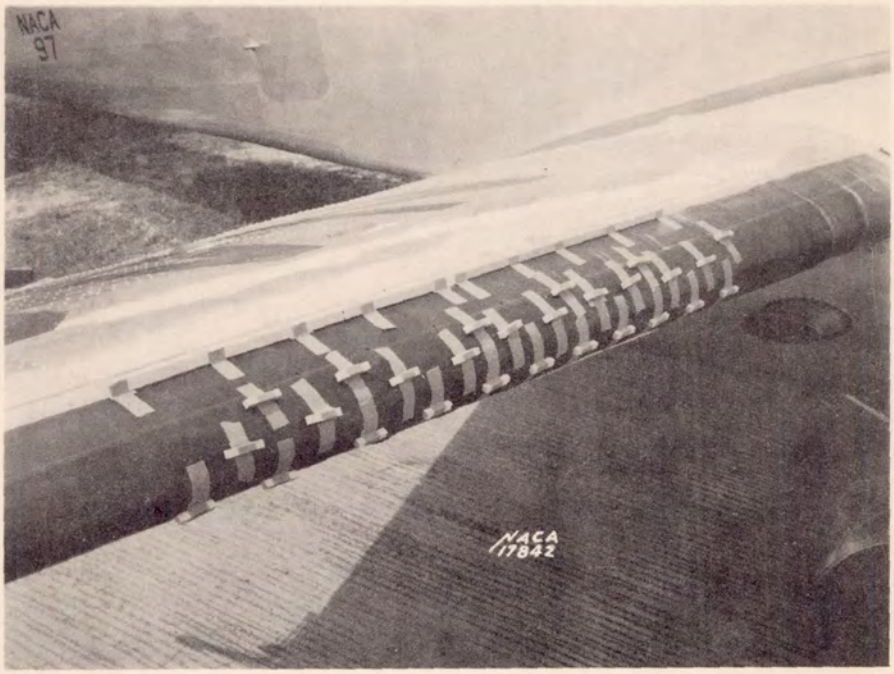

PROTUBERANCES ON WING LEADING EDGE
SIMULATIONS OF ICE
FIGURE 1.

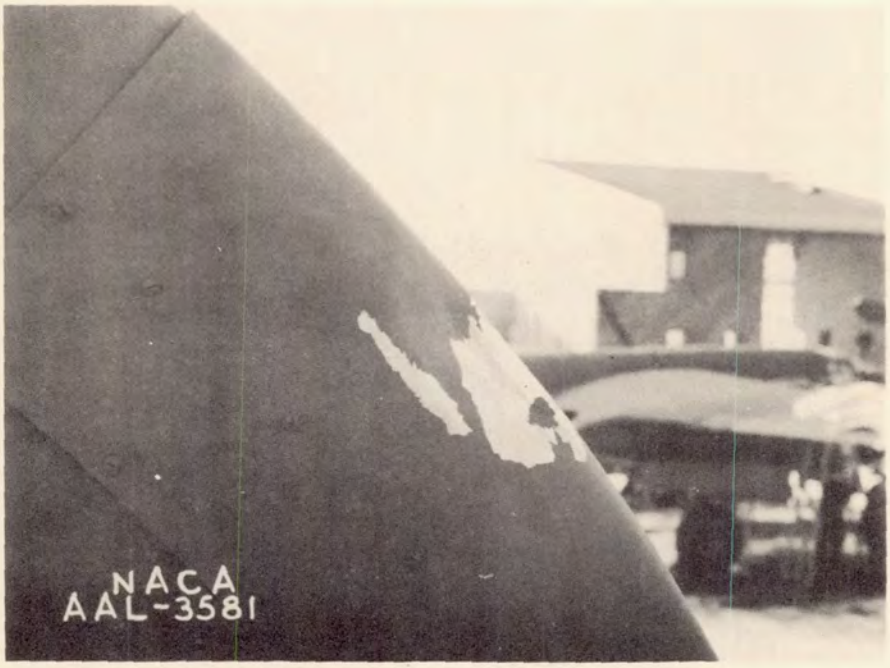

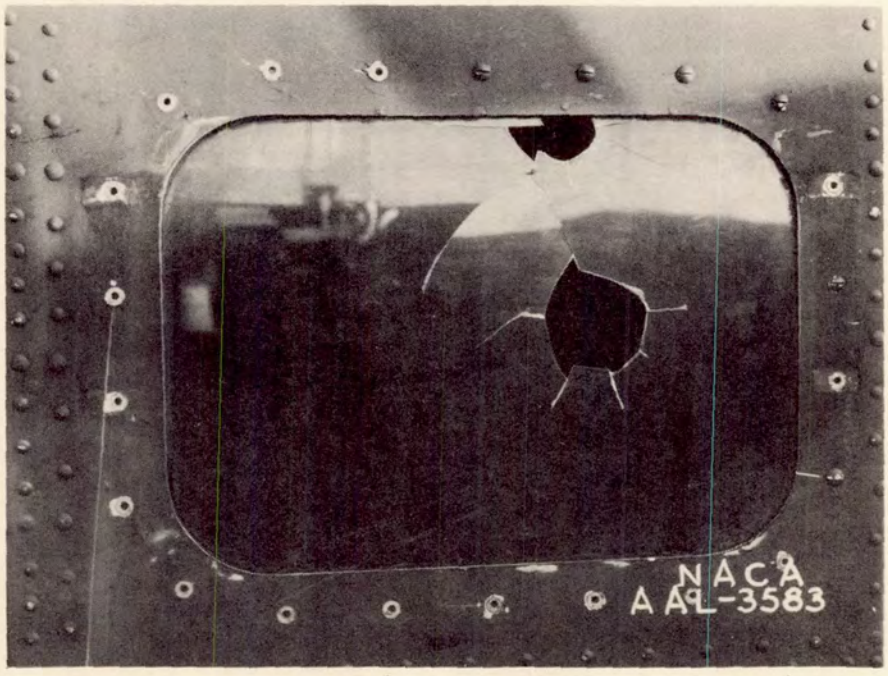

DAMAGE CAUSED BY SHEDDING OF ICE FRAGMENTS
FIGURE 2.

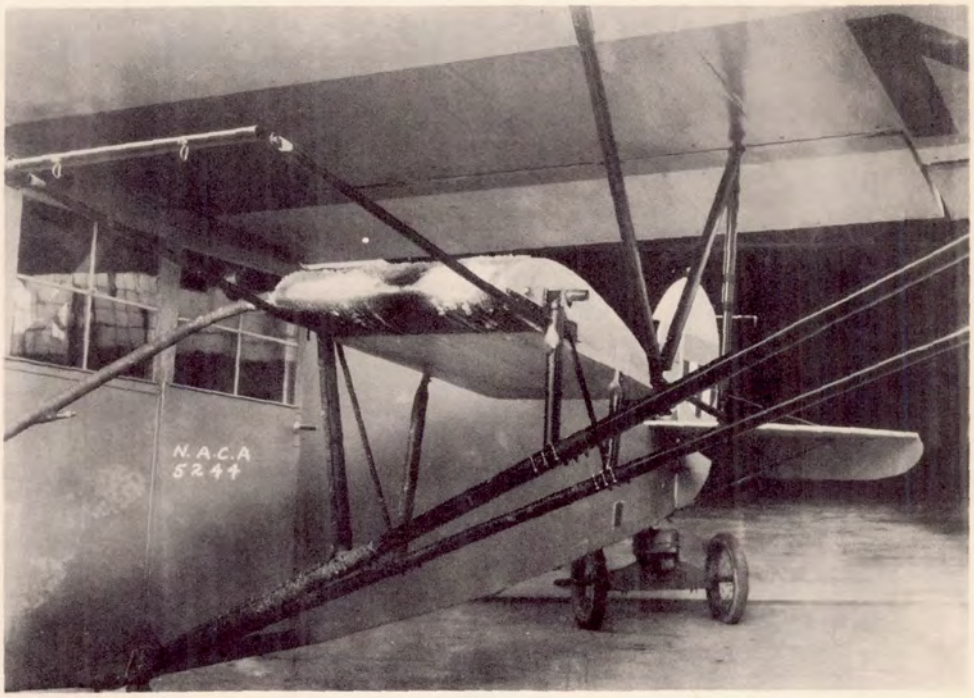

AIRFOIL MODEL WING HEATED BY STEAM
FIGURE 3.

WING LEADING-EDGE HEATING ARRANGEMENTS

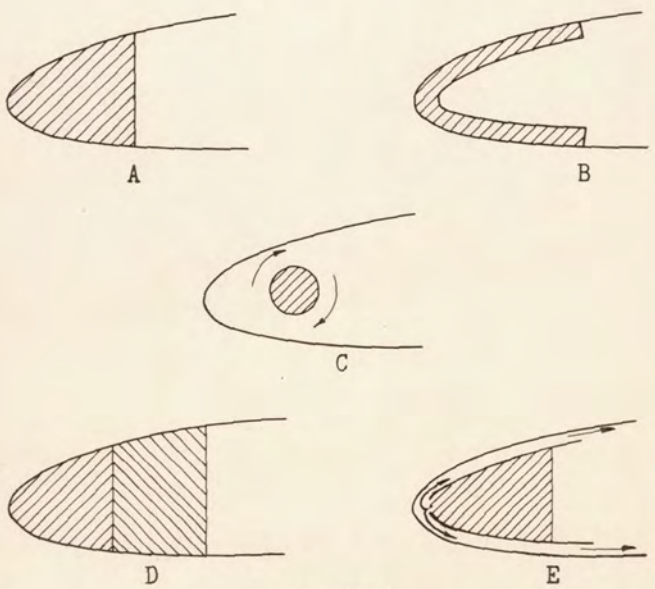

FIGURE 4.

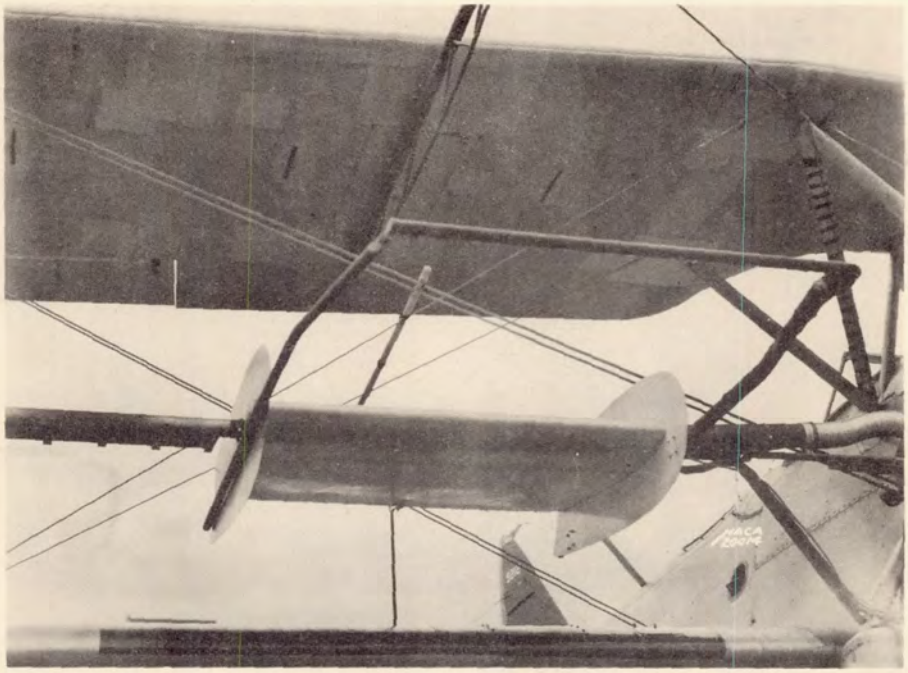

AIR-HEATED MODEL WING MOUNTED ON XBM AIRPLANE
FIGURE 5.

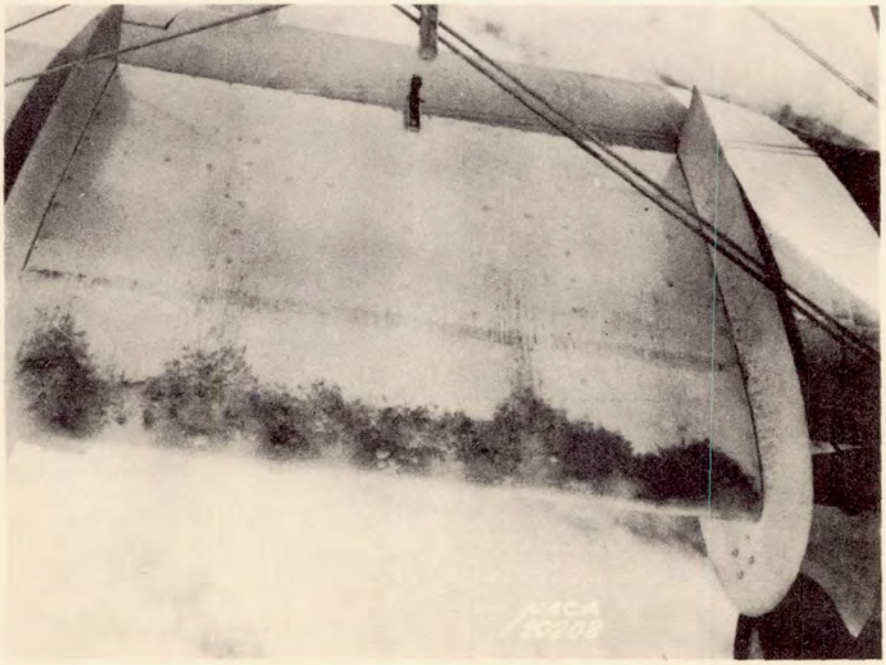

ICE FORMATION ON MODEL WING BEFORE
APPLYING HEAT
FIGURE 6.

LOCKHEED 12A USED FOR FULL-SCALE APPLICATION
OF THERMAL DE-ICING
FIGURE 7.

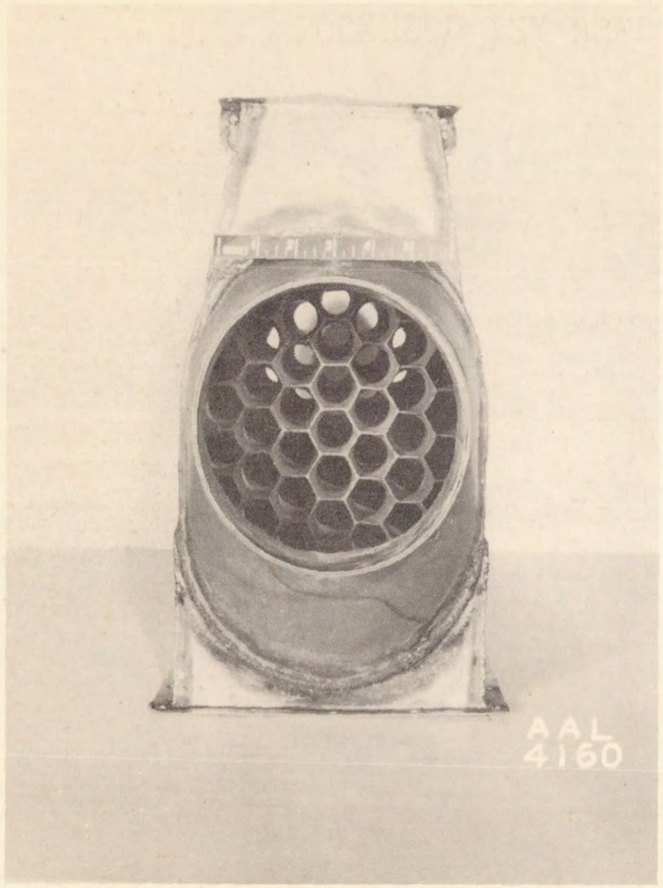

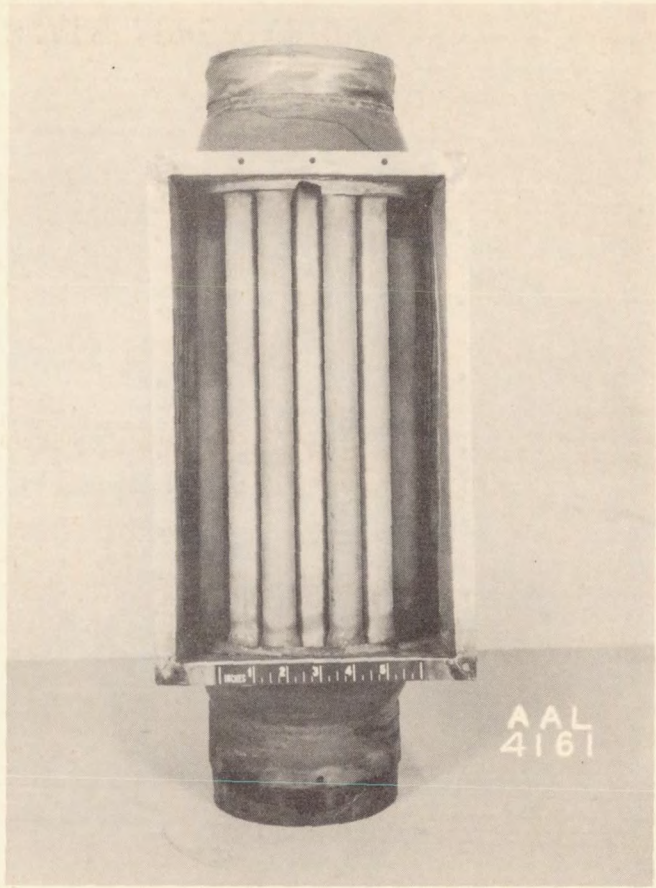

TUBE-BUNDLE TYPE EXHAUST-AIR HEAT EXCHANGER
FIGURE 8.

XB24 IN WHICH FIRST FULL-SCALE SERVICE INSTALLATION WAS MADE

FIGURE 9.

NACA
C. 15314
7.9.46

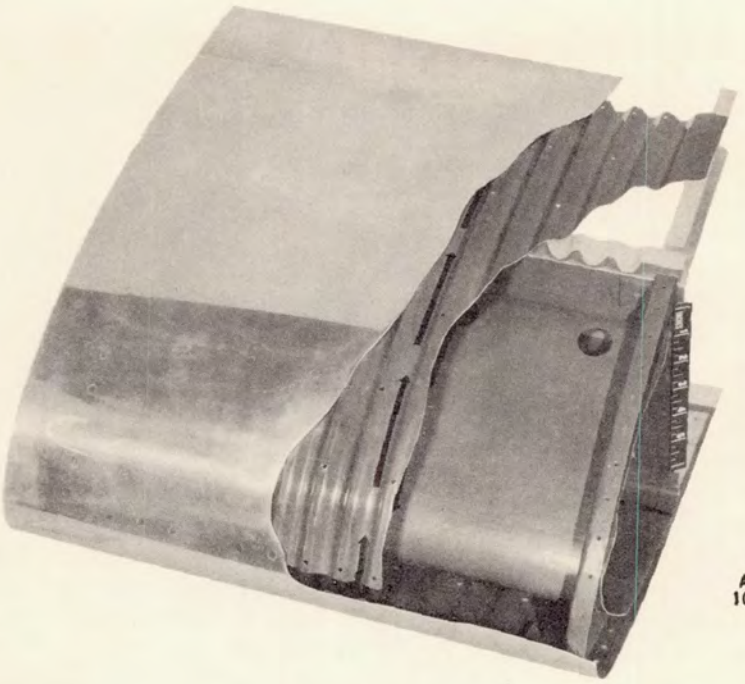

CONSTRUCTION OF AIR-HEATED WING LEADING EDGE
FIGURE 10.

HEATED SECTION ON AIRPLANE WINDSHIELD
FIGURE 11.

FLIGHT INVESTIGATION OF METEOROLOGICAL FACTORS CONDUCIVE TO AIRCRAFT ICING

By William Lewis[1]

U.S. Weather Bureau

INTRODUCTION

The NACA is currently engaged in a fundamental research investigation of aircraft-icing problems. The meteorological phase of this investigation consists of the development of instruments required for the evaluation of the critical factors responsible for the formation of ice on aircraft, and the actual measurement of these factors during flight in icing conditions. These measurements furnish data establishing, for the pertinent meteorological variables, the range of values commonly encountered in icing conditions. These data are required as a basis for the definition of the physical characteristics of the maximum icing conditions in which ice-prevention equipment will be expected to provide adequate protection. As a result of this investigation, some progress is also being made toward a solution of some of the problems associated with the forecasting of icing conditions. This paper is directed chiefly to the problem of design conditions, the problems of instrumentation and forecasting are treated only incidentally. In the conduct of this project, a Curtiss-Wright C-46 airplane operated by the Ames Aeronautical Laboratory has been flown in natural icing conditions during the last three winters and a considerable amount of data have been collected. Results of the investigation have been presented in references 1 through 5. During the 1946-47 season, measurements in icing conditions were also made with two airplanes operated by the NACA Flight Propulsion Research Laboratory.

METHODS OF COLLECTING DATA

During the 1944-45 season, the dew-point method was used to obtain data on liquid-water content. Because of various difficulties in the use of this method, the use of rotating cylinders was initiated early in 1946 and has been relied upon since that time for all measurements of liquid-water content and average drop size. The

---

[1]Mr. Lewis, U.S. Weather Bureau, has been assigned to the Ames Aeronautical Laboratory to participate in the icing research program.

value of average drop diameter obtained by the use of rotating cylinders, which is called the mean-effective diameter is approximately the median of a volume distribution, characterized by the property that equal volumes of water are present in drops larger and smaller than the mean-effective diameter. Values of maximum drop diameter were calculated from the width of the area of drop impingement upon a stationary cylinder. The calculations of maximum diameter, mean-effective diameter, and liquid-water content were based on the theoretical data for drop impingement on cylinders presented by Langmuir and Blodgett of the General Electric Co. (See reference 6.)

Efforts to develop other methods for measuring liquid-water content and drop size have been continued, but the results thus far have not been as satisfactory as the rotating-cylinder measurements.

DISCUSSION

Meteorological Factors Determining the Distribution of Liquid Water in Clouds

The major cause of condensation of water vapor in the free air is cooling of the air by expansion due to vertical motion. Cloud-forming processes may be divided into three general classes according to the factors responsible for the vertical motion.

Convection. - The relatively rapid rising of individual masses of potentially warmer air with respect to the air mass as a whole produces clouds of considerable vertical development but limited horizontal extent.

Turbulence. - Mixing of entire layers by turbulence produces a condition approaching constant mixing ratio and adiabatic lapse rates throughout the layers involved. Condensation frequently occurs in the upper portions of such layers, giving rise to extensive horizontal cloud layers limited in vertical extent.

Horizontal convergence. - Gradual lifting of large masses of air at middle levels is produced by horizontal convergence in the velocity field at lower levels. This results in the formation of very extensive cloud systems. Frontal and orographic lifting are important special cases of this process.

In the case of clouds formed by convection or turbulence, the liquid-water content can be calculated if it is assumed that a condition of constant ratio of water (liquid plus vapor) to air and moist-adiabatic lapse rate prevails throughout the cloud mass. The liquid-water content calculated on this basis is shown in figure 1 in terms of temperature at the cloud base and vertical distance above the cloud base. In most actual cloud layers, the assumptions upon which the calculated curves of figure 1 are based are not completely fulfilled, because of downward mixing of dry air from above and other factors. The actual liquid-water content is most likely to be about one-half the calculated value and is sometimes much less. The calculated value, however, does represent an upper limit which is unlikely to be exceeded.

In the case of clouds formed by convergence or frontal or upslope action, the liquid-water content cannot be readily calculated, since it depends upon the initial humidity distribution as well as the amount of lifting. The limited amount of observational data from clouds of this type indicates that the liquid-water content is ordinarily much less than the value which would be calculated on the basis of adiabatic lifting from the actual cloud base. Thus the calculated value of liquid-water content may be regarded as a practical upper limit which is unlikely to be exceeded in clouds of any type.

Since high values of liquid-water content can only occur in clouds of considerable vertical extent, it is useful in a study of icing conditions to divide clouds into two general classes: (1) cumulus clouds, which may have very great vertical development and are relatively small in horizontal extent, and (2) layer clouds, which are generally limited in vertical extent but may cover a very large area. Altostratus clouds are included as layer clouds even though they are sometimes several thousand feet in vertical extent, since, during winter, the thicker portions are usually composed of ice crystals, the existence of water drops being confined to the thinner portions near the edges of the cloud systems.

The effect of snow upon liquid-water content. - The effect of snow is always a reduction of the liquid-water content due to the difference in saturation vapor pressure over water and ice at temperatures below freezing. When snowflakes form within a cloud layer, the dissipation of the cloud proceeds upward from the bottom of the layer. When snow falls into a cloud layer from above, as when a precipitating altostratus cloud overlies a stratocumulus layer, the liquid-water content of the lower layer is depleted quite rapidly. In the case of widespread precipitation areas, the cloud systems

above the freezing level are ordinarily composed almost entirely of snow, the only supercooled liquid water being in a thin layer just above the freezing level and in patches near the edges of the precipitation areas. The transformation of cumulus clouds caused by the formation of snowflakes in the upper portions usually progresses quite rapidly, resulting in a very marked reduction of the liquid-water content.

The resultant effect of all these factors is shown in figure 2, which gives the frequency of various values of liquid water in layer clouds and cumulus clouds, with and without precipitation. It is noted that the highest liquid-water content is much less for layer clouds than for cumulus clouds, and that the presence of snow results in a higher frequency of low values of water content for both cloud types. The high values of water content observed in cumulus clouds with precipitation occurred in cases in which precipitation had just begun at the time the observations were made. It should also be noted that as cumulus clouds become taller, they are more likely to contain precipitation; hence, on the average, the observations in cumulus clouds with precipitation were made in larger and more fully developed clouds.

The Problem of Design Conditions

For the design of thermal ice-prevention systems on a wet-air basis, information is required concerning the significant properties of the icing conditions in which the equipment is expected to provide protection. Information is required particularly in answer to the following questions: (1) What is the largest value of liquid-water content which will be encountered without regard to extent or duration, and what are the probable concurrent values of temperature and drop size? (2) What is the probable extent of conditions of very high liquid-water content, and the approximate relation between maximum liquid-water content and the extent of the conditions? (3) What is the relation between maximum water content and mean-effective drop diameter for icing conditions in which continuous flight may be required? (4) What is the relation between temperature and maximum water content in icing conditions? (5) What are the largest drop diameters likely to be encountered and the corresponding values of water content? And (6) what are the most frequent or typical values of liquid-water content and mean-effective diameter and what are the relative frequencies of various values?

Tentative answers to these questions will be presented, as applied to conditions to be expected in the course of all-weather transport operations in the United States during winter.

Maximum liquid-water content. - Figure 3 presents the range of values of liquid-water content and mean-effective drop diameter as observed in flight in cumulus clouds and layer clouds, and as measured at the Mt. Washington Observatory (reference 7). The highest value of liquid-water content measured in the flight investigation was 1.9 grams per cubic meter. This value, which was observed in the upper portion of a tall cumulus cloud in western Oregon, is much higher than any observed in layer clouds. Theoretical calculations indicate that much higher values may occur near the tops of tall summer cumulus clouds in warm moist climates. Such occurrences, however, have no practical importance in connection with aircraft operations, since flight at subfreezing temperatures can be avoided in the summer time. If consideration is limited to conditions in which the condensation temperature is 32° F or lower, the theoretical maximum liquid-water content is about 2.5 grams per cubic meter. Since these conditions are sharply limited both in space and time, it is considered very unlikely that values exceeding 2.0 grams per cubic meter would ever be encountered in the course of normal operations. This value, 2.0 grams per cubic meter, is therefore proposed as the estimated maximum liquid-water content to be expected in all-weather transport operations in the United States during winter. It was noted that for the seven observations of water content greater than 1.2 grams per cubic meter, the corresponding values of mean-effective diameter were all in the range from 17 to 23 microns. The average of these values, 20 microns, was chosen as the probable value of mean-effective diameter corresponding to a maximum liquid-water content of 2.0 grams per cubic meter. Considerations of cloud height, condensation temperature, and lapse rates led to the conclusion that the corresponding temperature is likely to be as low as 0° F.

The relation between maximum liquid-water content and extent of icing conditions. - Because of the facts that heavy icing conditions were observed only in cumulus clouds and that cumulus clouds are always rather limited in horizontal extent, a study of the data was made in an effort to define a relation between the extent and intensity of icing conditions. Unfortunately, data on the linear dimensions of the icing conditions were not obtained. The duration of continuous flight in icing was therefore used as a measure of the extent of the conditions, although in several cases the airplane was flown back and forth in a single cloud formation, thus giving rise to longer duration than would have been required for a straight flight. Figure 4 shows the relation between the duration of periods

of flight in continuous icing conditions and the average liquid-water content during the periods. The plotted points are for individual observations, only the extreme cases being reproduced here, and the line represents the estimated relation between average water content and the greatest duration to be expected at a true airspeed of 160 miles per hour, the approximate average speed of the airplane during the tests. In the application of these results it should be remembered that on the research flights during which these data were collected, the flight path was chosen with the object of maximizing the severity and duration of the icing conditions. For this reason it is believed that the line in the diagram represents a conservative estimate of the relation between the intensity and duration of icing conditions as they would be encountered in all-weather transport operations in the United States.

Maximum continuous icing conditions. - The results of the foregoing discussion of the extent of icing conditions as related to their intensity suggest a need to define the most severe icing conditions likely to occur over an area large enough to require continuous operation in such conditions. These conditions will occur in layer-type clouds, since cumulus clouds are by their nature discontinuous. Sufficient data are available from layer clouds to provide the basis for what are believed to be fairly reliable estimates of the relation between maximum liquid-water content and mean-effective diameter and between maximum liquid-water content and temperature. No reliable relationship between drop size and temperature is indicated by the data.

The relation between maximum liquid-water content and mean-effective diameter in layer clouds can best be illustrated with reference to figure 5, which includes a curve showing maximum observed liquid-water content in layer clouds as a function of mean-effective drop diameter. The range of values most frequently encountered is indicated in the diagram by the rectangle which contains 50 percent of the observations. The fact that large values of mean-effective diameter are infrequent is indicated by the vertical line which limits an area to the right containing 5 percent of the observations. The greatest observed values of liquid-water content were 0.7 gram per cubic meter at 11 and 12 microns. The maximum observed liquid-water content decreases with increasing drop diameter to 0.17 at 50 microns and 0.04 at 150 microns. There is considerable uncertainty in the position of the curve beyond about 35 microns because of the small number of observations. On the basis of these data it is estimated that the maximum icing conditions likely to be encountered in layer clouds are 0.8 gram per cubic meter at

15 microns or 0.5 gram per cubic meter at 25 microns. The temperature corresponding to these conditions is estimated to be 20° F or higher.

Temperature and maximum liquid-water content. - The relation between temperature and maximum liquid-water content is considered. In the case of cumulus clouds, very low-temperature icing conditions can be associated with relatively high condensation temperature, due to the great vertical extent of such clouds. The maximum liquid-water content is therefore not directly related to the temperature. In layer-type clouds, on the other hand, the maximum liquid-water content is a function of temperature; the temperature within such clouds is closely related to the condensation temperature due to their limited vertical extent. The relation between maximum liquid-water content and temperature in layer clouds is shown in figure 6. As pointed out previously, the maximum liquid-water content is related to the water content that would be produced by adiabatic lifting from the cloud base. Since a cloud layer thickness of 3000 feet appears to represent the maximum ordinarily encountered, and the water content is likely to be about one-half the adiabatic value, the curve A in the diagram was drawn to represent one-half the liquid-water content which would be obtained by adiabatic lifting through a pressure altitude interval of 3000 feet from the condensation level. This curve falls very close to the points representing the highest observed values of liquid-water content in layer-type clouds. Since it is reasonable to expect that a larger sample of data would include higher values of water content, the curve B, which represents two-thirds of the liquid-water content produced by adiabatic lifting through 3000 feet, is presented as an estimate of the highest values of liquid-water content to be expected in layer clouds. This curve indicates a maximum liquid-water content of 0.8 gram per cubic meter at 20° F; 0.5 gram per cubic meter at 0° F, and 0.25 gram per cubic meter at -20° F.

Icing conditions with very large drops. - Another important aspect of the problem of the description of maximum icing conditions concerns the largest drop diameter likely to be encountered and the probable corresponding values of water content. Figure 7 shows the relative frequency of observation of various values of mean-effective diameter and maximum diameter as observed during the 1946-47 season. It is noted that 2 percent of the observations of mean-effective diameter are 35 microns or over. The largest observed value of mean-effective diameter was 150 microns or more. The exact value is unknown as it was beyond the effective range of the rotating-cylinder instrument. The value of liquid-water content

in this case was 0.04 gram per cubic meter. For three observations of mean-effective diameter of 48 microns or more, the highest value of liquid-water content was 0.17 gram per cubic meter.

Although the curve for maximum diameter is based upon a smaller number of observations than that for mean-effective diameter, it should give a fairly representative indication of relative frequencies. This curve shows that the maximum diameter is less than 30 microns in 93 percent of the cases. This indicates that the presence of appreciable amounts of water in drops of 30 microns or more diameter is unusual.

The spread between the mean-effective diameter and maximum diameter is not as great as would be expected from the size distributions usually indicated by the rotating-cylinder data. It is believed that the size-distribution data obtained in flight by the rotating-cylinder method are subject to serious errors caused by the acceleration of the air as it flows around the fuselage. If the maximum drop-size data, which were calculated from the area of impingement on a fixed cylinder, and the mean-effective diameter from the rotating cylinders are accepted as correct, the size distributions ordinarily encountered in clouds are fairly uniform and the distributions obtained from the rotating-cylinder technique are sometimes in error. The ratio of maximum diameter to mean-effective diameter is less than 1.33 for 75 percent of 92 simultaneous observations and is less than 1.75 for 90 percent of these observations.

Typical icing conditions. - The estimated maximum conditions given in the foregoing discussion are encountered only rarely. Consideration is given to the relative frequencies of the values of drop size and liquid-water content more commonly encountered. It is noted that 50 percent of the observations of mean-effective diameter fall in the relatively narrow range from 11.2 to 16.2 microns and that 90 percent are less than 22 microns. Fifty percent of the observations of maximum diameter are between 12.6 and 20 microns and 90 percent are below 28 microns.

The highest values of liquid-water content measured during each of 21 flights in cumulus clouds and 51 flights in layer clouds are presented in figure 8. The median value of maximum liquid-water content per flight is 0.76 gram per cubic meter for cumulus clouds and 0.28 gram per cubic meter for layer clouds. It is also noted that 90 percent of the flights in cumulus clouds encountered less than 1.2 grams per cubic meter and 90 percent of the flights in layer clouds encountered less than 0.5 gram per cubic meter.

These distribution curves indicate that the icing conditions most commonly encountered are much less severe than the estimated maximum conditions. Thus if it were assumed that most cumulus clouds and the most severe 10 percent of icing conditions in layer clouds can be avoided by proper meteorological navigation, it would only be necessary to protect against 0.5 gram per cubic meter at 13 microns or 0.3 gram per cubic meter at 20 microns. The extent to which meteorological navigation can be relied upon, however, can be determined only by an extensive study of the distribution of icing conditions in various weather situations and an analysis of air traffic control procedures.

CONCLUSIONS

The meteorological conditions conducive to aircraft icing which are considered to be of most interest to the designer of thermal ice-prevention equipment are summarized in table I. The two cases are selected of "most probable maximum" and "typical or normal" icing conditions. The drop-size distribution has not been specified in the table but may be considered uniform for these conditions. In addition to the two conditions specified in the table, however, the designer should give consideration to the possibility of encountering drop sizes larger than 35 microns, although with corresponding low liquid-water content.

As a general conclusion, it is believed that the meteorological factors of icing conditions have been sufficiently defined to allow the design of thermal ice-prevention equipment on a fundamental wet-air basis.

REFERENCES

1. Hardy, J. K.: Measurement of Free Water in Cloud Under Conditions of Icing. NACA ARR No. 4I11, 1944.

2. Lewis, William: Icing Properties of Noncyclonic Winter Stratus Clouds. NACA TN (to be pub.).

3. Lewis, William: Icing Zones in a Warm-Front System with General Precipitation. NACA TN (to be pub.).

4. Lewis, William: A Flight Investigation of the Meteorological Conditions Conducive to the Formation of Ice on Airplanes. NACA TN (to be pub.).

5. Lewis, William, Kline, Dwight B., and Steinmetz, Charles P.: A Further Flight Investigation of the Meteorological Conditions Conducive to Aircraft Icing. NACA TN (to be pub.).

6. Langmuir, Irving, and Blodgett, Kathrine B.: A Mathematical Investigation of Water Droplet Trajectories. General Electric Co., July 1945.

7. Anon: Mt. Washington Observatory, New Hampshire Icing Reports, vol. I, no. 9 to vol. II, no. 4, Oct. 1945 to Apr. 1946.

TABLE I - ICING CONDITIONS ANTICIPATED

IN ALL-WEATHER OPERATIONS

Most probable maximum				
Cloud type	Duration	Liquid-water content (gm/m^3)	Drop diameter (microns)	Free-air temperature ($^{\circ}F$)
Cumulus	1 minute	2.0	20	0
Stratus or stratocumulus	Continuous	0.8	15	20
		0.5	25	
		0.5	15	0
		0.25	15	-20
Typical or normal				
Cumulus	1 minute	0.8	10 to 17	0 to 20
Stratus or stratocumulus	Continuous	0.3		10 to 25

National Advisory Committee
for Aeronautics

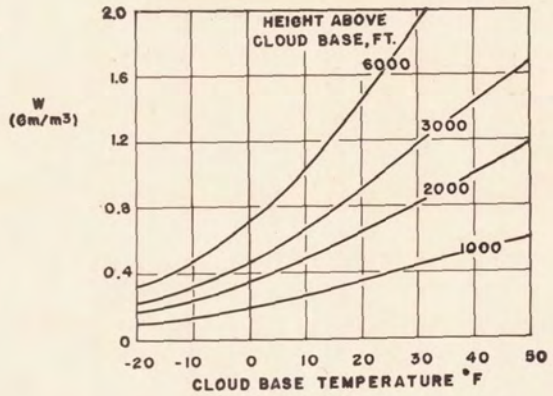

LIQUID-WATER CONTENT, W, IN ISENTROPIC CLOUDS

Figure 1.

NATIONAL ADVISORY
COMMITTEE FOR AERONAUTICS

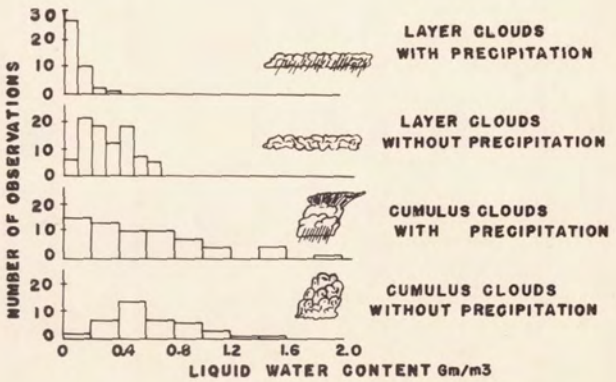

LIQUID-WATER CONTENT AS RELATED TO CLOUD FORMS AND PRECIPITATION

Figure 2.

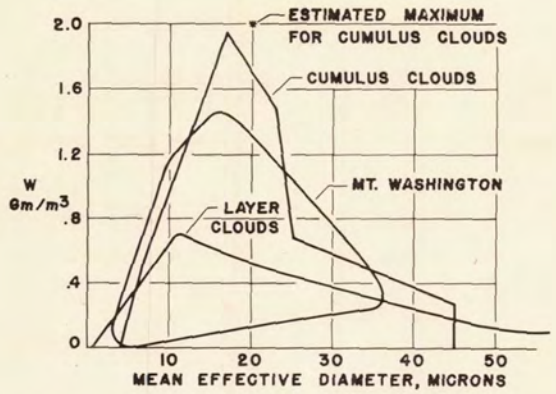

LIQUID-WATER CONTENT, W, AND AVERAGE DROP DIAMETER IN ICING CLOUDS

Figure 3.

NATIONAL ADVISORY
COMMITTEE FOR AERONAUTICS

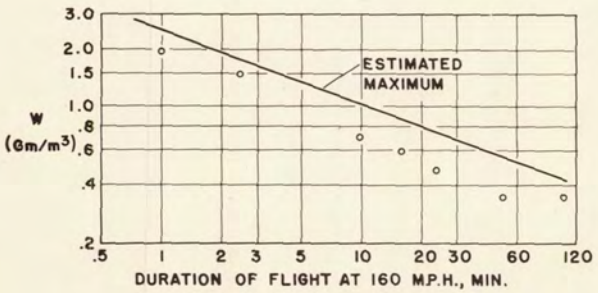

**LIQUID-WATER CONTENT, W,
AS RELATED TO EXTENT OF ICING CLOUDS**

Figure 4.

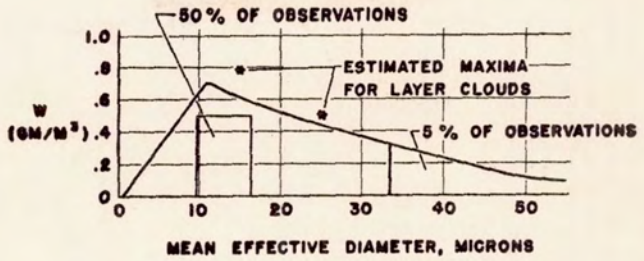

LIQUID-WATER CONTENT, W,
AND DROP SIZE IN LAYER-TYPE CLOUDS

Figure 5.

NATIONAL ADVISORY
COMMITTEE FOR AERONAUTICS

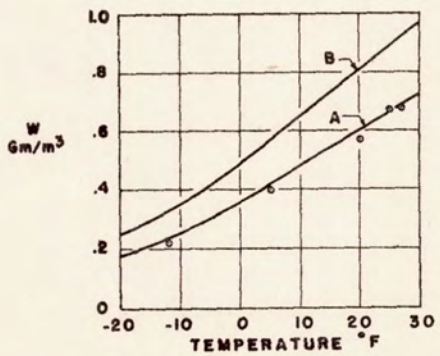

LIQUID-WATER CONTENT, W, AS RELATED
TO TEMPERATURE IN LAYER-TYPE CLOUDS

Figure 6.

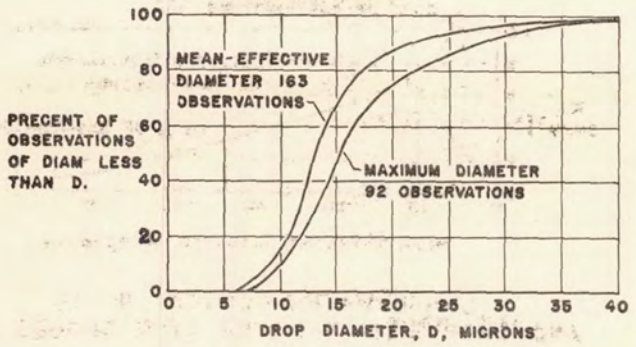

OGIVES OF MAXIMUM AND MEAN-EFFECTIVE DROP DIAMETER

Figure 7.

NATIONAL ADVISORY
COMMITTEE FOR AERONAUTICS

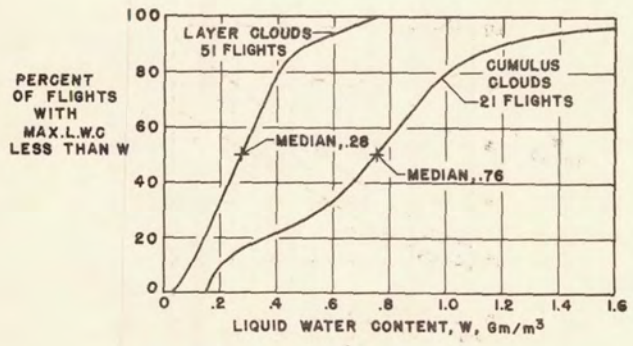

OGIVES OF MAXIMUM LIQUID-WATER CONTENT PER FLIGHT

Figure 8.

METHOD FOR NUMERICALLY CALCULATING AREA AND DISTRIBUTION OF WATER IMPINGEMENT ON LEADING EDGE OF AIRFOIL IN A CLOUD

By Norman R. Bergrun

Ames Aeronautical Laboratory

INTRODUCTION

As part of a comprehensive research program directed toward a fundamental understanding of the mechanism of thermal ice prevention for airplanes, the NACA has undertaken an investigation of the performance of a heated wing or empennage section in specified icing conditions. One of the first essentials of such an investigation is a method for estimating or calculating the area over which water will strike a wing section, and the distribution of water impingement over that area.

Previous investigations of this nature have considered the water-drop trajectories about cylinders (references 1 and 2) and about an airfoil (reference 2). In these studies, the assumption was made that the water drops were sufficiently small to obey Stokes' law of resistance. A more recent investigation on trajectories about cylinders, by Langmuir and Bladgett (reference 3), shows that, for velocities of airplanes and the drop sizes frequently present in clouds, Stokes' law no longer applies and the force acting on the drop can be determined only from a knowledge of the drag coefficient for spheres. Methods of previous investigators were therefore modified to include more accurate values of the drop drag coefficient, and differential equations were established for determining drop trajectories around cylinders, spheres, and ribbons. These equations were placed into forms suitable for use in a differential analyzer and, by utilizing an analyzer, the trajectories were calculated and plotted.

The designer of a heated wing, desiring to know the rate and area of water impingement on the leading edge in a specified icing cloud at a given flight speed, might assume that the impingement will be the same as that for a cylinder with radius equal to the wing leading-edge radius. However, there is some question as to the accuracy of this assumption for large drop diameters and for wing sections with small leading-edge radii. The designer is therefore confronted with the desirability of employing a computation

method, preferably without the necessity of a differential analyzer, which will provide some indication of the area and distribution of water impingement on airfoil sections. With this view in mind, the water-drop trajectory equations developed by Langmuir and Blodgett (reference 3) to include the effect of the variable drag coefficient for spheres have been modified to establish a step-by-step integration method applicable to any two-dimensional flow for which the streamline velocity components are known.

The step-by-step integration method permits the calculation of any desired number of water-drop trajectories; although if trajectories for a large range of airspeeds and drop diameters are required, the computation time is large and the desirability of access to a differential analyzer becomes evident. The method also provides a means for estimating the error that will be incurred by replacing the airfoil by a cylinder with a radius equal to the leading-edge radius of the airfoil; and in addition, water-impingement data over the entire airfoil surface can be obtained by the integration method.

ANALYSIS

In order to obtain area and concentration of water-drop impingement at the leading edge of an airfoil, the path of the drops, as affected by the airstream, must be traced. In order to compute these paths, or trajectories, it is necessary to define the motion of a drop through the air. The equations that depict this motion, which have been modified to include the effect of a drop departing from Stokes' law of resistance, take the following form:

$$\frac{dv_x}{dt} = -\frac{C_D R}{24K}(v_x - u_x) \tag{1}$$

$$\frac{dv_y}{dt} = -\frac{C_D R}{24K}(v_y - u_y) \tag{2}$$

$$\left(\frac{R}{R_U}\right)^2 = (v_x - u_x)^2 + (v_y - u_y)^2 \tag{3}$$

In these equations, the letter v designates the velocity of the drop and the letter u designates the velocity of the air, both velocities being relative to free-stream velocity. The subscripts x and y signify that the components C_D are in x-

and y- directions. The drag coefficient for spheres is C_D; K is a dimensionless water-frop inertia quantity; R is the Reynolds number of the drop relative to the air at a given point; and R_U is the Reynolds number of a drop traveling with free-stream velocity. Time is expressed by a time unit t.

Equations (1) and (2) show that the instantaneous deceleration of a drop is directly proportional to its drag coefficient, its local Reynolds number, the velocity difference between the air and the drop, and inversely proportional to its inertia. Equation (3) shows that the square of the ratio of local Reynolds number to the free-stream Reynolds number of a drop is related to the velocity difference between air and drop by the sums of the squares x- and y-component velocity differences.

Since equations (1), (2), and (3) relate the exact instantaneous values of the variables for infinitesimally small changes in velocity and time, they cannot be solved by treating algebraically the differential quantities dv_x/dt and dv_y/dt. However, for small increments in velocity and time, the two quantities $C_DR/24K\ (v_x-u_x)$ and $C_DR/24K\ (v_y-u_y)$ may be taken as the average acceleration over the increment of time selected. Then, by defining the average velocity of a drop over the time increment by one-half the sum of the drop velocity at the beginning and the end of the time interval, a new set of equations can be established, which lend themselves to step-by-step computations. These new equations, which are suitable for step-by-step computations, are given by:

$$v_{x_{n+1}} = v_{x_n} - \frac{C_DR}{24K}\,(v_{x_n}-u_{x_n})\Delta t \tag{4}$$

$$x_{(n+1)} = x_n + v_{x_n}\Delta t - \frac{1}{2}\left[\frac{C_DR}{24K}\,(v_{x_n}-u_{x_n})\right]\Delta t^2 \tag{5}$$

$$v_{y(n+1)} = v_{y_n} - \frac{C_DR}{24K}\,(v_{y_n}-u_{y_n})\Delta t \tag{6}$$

$$y_{(n+1)} = y_n + v_{y_n}\Delta t - \frac{1}{2}\left[\frac{C_DR}{24K}\,(v_{y_n}-u_{y_n})\right]\Delta t^2 \tag{7}$$

$$\left(\frac{R}{R_U}\right)^2 = (v_{x_n}-u_{x_n})^2 + (v_{y_n}-u_{y_n})^2 \tag{8}$$

Equation (4) shows that the velocity of the drop in the x-direction, at the end of any interval of time, is equal to the velocity of the drop at the beginning of the time interval minus the product of the average acceleration and the time interval.

Equation (5) shows that the x-coordinate of the drop at the end of any interval of time is given by the x coordinate of the drop at the beginning of the interval of time, plus the distance the drop travels during the time interval minus a correction term

$$\frac{1}{2}\left[\frac{C_D R}{24K}\left(v_{x_n}-u_{x_n}\right)\right]\Delta t^2$$

which compensates for the velocity of the drop not being of the value v_{x_n} over the entire time interval Δt. The same statements also apply to equations (6) and (7), which define the velocity and coordinate of a drop in the y-direction. Equation (8) is of the same form as equation (3), and connects the velocity components, the Reynolds numbers, the drag coefficient, and the drop-inertia parameter. In order to use these equations, it is necessary to define graphically the velocity components of the air u_x and u_y about the body under consideration for a number of selected streamlines. In addition, a plot of R against $C_D R/24$ is necessary for evaluating the latter function at the beginning of any time interval. Once the necessary graphic information is established, it is only necessary to evaluate for a trajectory the velocity differences between the air and the drop $v_{x_n}-u_{x_n}$ and $v_{y_n}-u_{y_n}$ at starting coordinates well forward of the body.

The following equations show the relationship that can be used to evaluate the initial velocity components of the drop at the beginning of a trajectory:

$$v_{x_1} = \frac{\left(u_{x_o}+B\Delta x\right) \pm \sqrt{\left(u_{x_o}+B\Delta x\right)^2 - 4Bu_{x_1}\Delta x}}{2} \qquad (9)$$

$$v_{y_1} = \frac{-\left(B\Delta y-u_{y_o}\right) \pm \sqrt{\left(B\Delta y-u_{y_o}\right)^2 + 4Bu_{y_1}\Delta y}}{2} \qquad (10)$$

Effectively, equations (9) and (10) perform the first step in the computation of a trajectory, but they must be solved by a trial-and-error procedure. These equations show that initial values of v_x

and v_y in the step-by-step computations can be obtained by a relatively simply relation involving the velocity of the air u_{x_o} and u_{y_o}, at the starting coordinate of the trajectories, the drag coefficient function $C_DR/24K$ given here as B, the first increment in the coordinate position of the trajectory Δx and Δy, and the velocity of the air u_{x_1} and u_{y_1} at the end of the first increment of time. Thus, in equations (4), (5), (6), (7), and (8) the differences between the velocity of the drop and the air $v_{x_n}-u_{x_n}$ and $v_{y_n}-u_{y_n}$ can be obtained for the first step in the successive computations; and with the aid of the graphic representations of the air-velocity components and the drag-coefficient function $C_DR/24$, the computation of a trajectory can be accomplished.

Water-drop trajectories are related to the area and rate of water impingement on a body by the equations

$$MLds = UwLdy_o \tag{11}$$

$$M = Uw\,\frac{dy_o}{ds} \tag{12}$$

$$M_T = \int_o^s Mds = Uwy_o \tag{13}$$

In equation (11), M is the rate per unit area, or intensity at which water impinges on the body, L is a unit length of span, ds is an increment in distance over which water impinges on the body, U is free-stream velocity, w is the liquid water content of the cloud, and dy_o is an increment in the ordinate of a trajectory at its starting point. The equation shows that, for a small increment, the weight of water impinging on the surface of a body is equal to the weight of water starting toward it well forward of the body. By rearranging equation (11), equation (12) shows that the intensity of drop deposition on the surface of a body is directly proportional to the velocity of the free air stream, the liquid water content of the cloud, and the rate of change of the starting ordinate of a trajectory with respect to a change in the distance included by the trajectories along the surface of the body. By integrating equation (11), the total rate of water impingement on the body is given by the summation of the rate of impingement per unit area over the distance on the

surface where drops hit, or more simply by the product of the velocity of the free stream, the liquid water content, and the starting ordinate of a trajectory.

If trajectories are computed for drops of the same inertia starting at different ordinates above a convenient reference line, results like those shown in figure 1 for a symmetrical Joukowski airfoil 12 percent thick at 0° angle of attack are obtained. Here it is seen that for larger and larger drop inertias, the area of drop interception on the airfoil also increases. The theoretical limit to which area of drop impingement can extend in the case of this airfoil at 0° angle of attack is back to the point of maximum thickness. This limit case corresponds to an infinitely large drop inertia, and means that the drop is so large or is traveling so fast that it is undeflected by forces acting on the drop in the air stream. Thus, to obtain the $K=\infty$ curve, trajectory equations do not have to be used because the problem reduces to one of plotting the ordinates of the body against the distance along the surface intercepted by these ordinates. The trajectories computed for a K value of 0.058 correspond to a drop 22 microns in diameter impinging upon a Joukowski airfoil of 8-foot chord at an altitude of 7000 feet and true airspeed of 170 miles per hour. The dotted line connecting the end points of the trajectories defines the maximum starting ordinate of a drop having a given inertia for which drops just impinge upon the airfoil. For example, a trajectoty having as a starting ordinate a distance greater than 1.9 percent chord for a K value of 0.2 will not hit the airfoil but will pass around it. Because of the limited time available for calculating trajectories, a set of these curves were computed only for a free-stream Reynolds number of a drop of 95.65. This value of Reynolds number was selected because it corresponded to the flight and meteorological conditions associated with a large amount of flight data obtained in natural icing conditions.

If the slopes of the K curves are obtained and plotted against the distance along the surface of the airfoil at which the slopes were determined, an indication of the distribution of water-drop impingement over a symmetrical Joukowski airfoil can be obtained (fig. 2). The concentration factor C denotes the slope of the K curves, and is given by dy_0/ds in equation (12). In order to illustrate how curves of this nature are used, an icing cloud at 7000 feet pressure altitude having a uniform drop-size diameter of 22 microns is assumed. If a symmetrical Joukowski airfoil of 8-foot chord were passing through the cloud at 0° angle of attack, the free-stream Reynolds number of the drop would be approximately 95.65 and the drop-inertia quantity K would be approximately 0.058. According to equation (12), the weight rate of water impingement on a body per

unit area is equal to the product of airspeed, liquid water content, and the concentration factor C, given by dy_o/ds.

Thus it is apparent by figure 2 that the weight rate of impingement per unit area on the Joukowski airfoil for the condition just specified is maximum at the stagnation point and diminishes to zero at an s/c value of a little more than 2 percent. It is interesting to observe that the area under this curve (K=0.058) is directly proportional to the total weight rate of water impingement per unit span.

Another method for determining the total rate of water impingement per unit span can be used when the distribution of impingement over the surface is not needed. This method requires a knowledge of the collection efficiency of the airfoil for different drop inertias. Such a relationship was obtained for the Joukowski airfoil and it is shown in figure 3. Efficiency of drop impingement is the ratio of the starting ordinate of a trajectory, which just hits the airfoil to the maximum ordinate of the airfoil.

In discussing errors involved in the use of a cylinder the radius of which is equal to the leading-edge radius of an airfoil, figure 4 is of interest. The curves shown in figure 4 compare the rate and area of water-drop impingement on a symmetrical Joukowski airfoil, 12 percent thick, with a cylinder the radius of which is equal to the airfoil leading-edge radius. For area of impingement, the equivalent cylinder can be used without much error up to a drop-size diameter of approximately 20 microns. However, for rate of impingement, appreciable difference is encountered for drop diameters of this magnitude. The range of drop diameters between 0 and 20 microns, where the impingement factor is nearly unity, corresponds to the region on the surfaces of the equivalent cylinder and the airfoil where their surfaces coincide. Values presented in figure 4 should not be taken as absolute ones, but rather as indicative of what can occur when an equivalent cylinder is used without full knowledge of its limitations. For airfoil sections having large leading-edge radii, the use of an equivalent cylinder would of course be more favorable than is shown here.

Figure 5 shows how water distributes itself over three different airfoils, one with a leading-edge radius, and two without leading-edge radii, for the case where drops are undeflected by forces in the air stream. By having all three airfoils the same maximum thickness and at the same angle of attack, the area under the distribution curve for each is the same and, therefore, the same amount of water would be intercepted by each airfoil. The

distribution of water impingement, however, would be different for each section as indicated by the shape of the curves. From these considerations, it can be seen that the effect of shifting the location of maximum thickness is to change the degree and position of water-drop impingement, and that by doing so, the limit water-drop impingement distribution for a given body at 0° angle of attack can be made to have any desired profile by the proper combination of contour and location of maximum thickness. If only the leading edge of an airfoil can be heated, the use of a leading-edge radius is indicated, since the water will distribute itself to impinge in the leading-edge area where the heating is located.

Attention is directed to the fact that the distribution curves for the circular-arc and wedge-shape airfoils in figure 5 are based on pure geometeric considerations, which dictate no leading-edge radius. In the practical case, some radius would exist and since curvature of the leading edge apparently has considerable influence on the rate of impingement in that area, the impingement concentration for actual airfoils of this type will be appreciably increased at the leading edge.

Although the method just discussed for computing water-drop trajectories applies to two-dimensional flow, with a few changes to the basic equations, trajectories in three-dimensional flow can be computed. The basic equations which define the flow in three dimensions are:

$$\frac{dv_x}{dt} = -\frac{C_D R}{24K}(v_x - u_x) \tag{14}$$

$$\frac{dv_y}{dt} = -\frac{C_D R}{24K}(v_y - u_y) \tag{15}$$

$$\frac{dv_z}{dt} = -\frac{C_D R}{24K}(v_z - u_z) \tag{16}$$

$$\left(\frac{R}{R_U}\right)^2 = (v_x - u_x)^2 + (v_y - u_y)^2 + (v_z - u_z)^2 \tag{17}$$

Equation (16) is the additional equation needed to define the path in the third dimension; equation (17) is the equation needed to connect Reynolds numbers, drag coefficient, the drop inertia parameter, and

the velocity components. An additional term $(v_z - u_z)^2$ takes into account deviation of the trajectory in the third dimension. These equations are written for the z-axis in the spanwise direction. When equations (14), (15), (16), and (17) are revised in a manner similar to that for the two-dimensional case, trajectories in three dimensions can be computed by a step-by-step process when the velocity components are known for the body considered. Application of trajectory computations for three-dimensional flow can be made to the case of windshield ice prevention where it is desirable to know the rate at which water impinges upon a windshield.

SUMMARY

A major difficulty in the solution of a trajectory problem in both two-and three-dimensional flow is one of obtaining accurate values of velocity components for streamlines about the body to be investigated. For two-dimensional flow, the analytic determination of the velocity components can be obtained readily for only a few airfoil sections; and for three-dimensional flow, the analytical problem is formidable. Therefore, in order to carry on extensive trajectory computations for families of airfoils and various windshield configurations, considerable research remains in establishing means for experimentally determining air-velocity components. It is believed, however, that the trajectory method that has been presented has merit in the fact that it provides a means for obtaining an indication of the rate and area of water impingement without resorting to a differential analyzer. In addition, the method exceeds the scope of previously available procedures by providing an indication of the distribution of water interception over the area of impingement.

(Editor's note: A complete discussion of the numerical method for calculating trajectories will be found in reference 4.)

REFERENCES

1. Kantrowitz, Arthur: Aerodynamic Heating and the Deflection of Drops by an Obstacle in an Airstream in Relation to Aircraft Icing. NACA TN No. 779, 1940.

2. Glauert, Muriel: A Method of Constructing the Paths of Raindrops of Different Diameters Moving in the Neighbourhood of (1) A Circular Cylinder, (2) An Aerofoil, Placed in a Uniform Stream of Air; and A Determination of the Rate of Deposit of the Drops on the Surface and the Percentage of Drops Caught. R. & M. No. 2025, British A.R.C., 1940.

3. Langmuir, Irving, and Blodgett, Katherine B: A Mathematical Investigation of Water Droplet Trajectories. General Electric Co., July 1945.

4. Bergrun, Norman R.: A Method for Numerically Calculating the Area and Distribution of Water Impingement on the Leading Edge of an Airfoil in a Cloud. NACA TN, May 1947. (To be pub.)

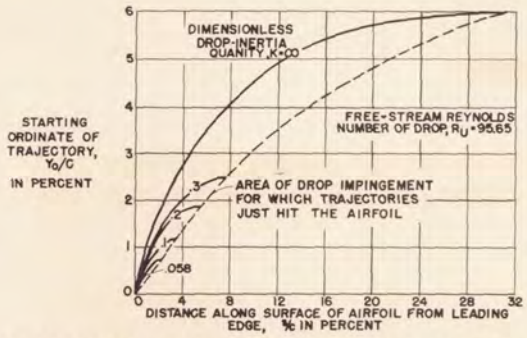

AREA OF DROP INTERCEPTION CORRESPONDING TO DROPS OF DIFFERENT INERTIA FOR A SYMMETRICAL JOUKOWSKI AIRFOIL.

Figure 1.

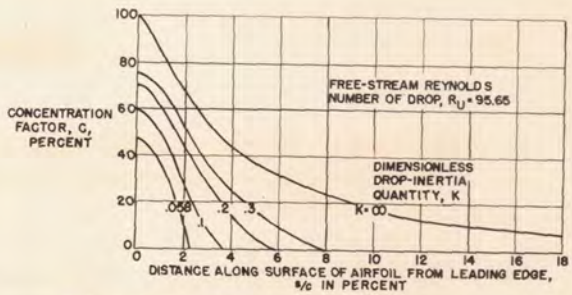

DISTRIBUTION OF WATER-DROP IMPINGEMENT OVER A SYMMETRICAL JOUKOWSKI AIRFOIL

Figure 2.

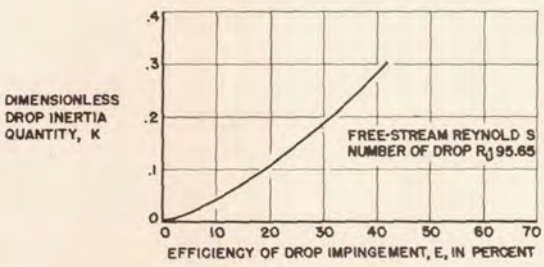

WATER-DROP-COLLECTION EFFICIENCY FOR A SYMMETRICAL JOUKOWSKI AIRFOIL

Figure 3.

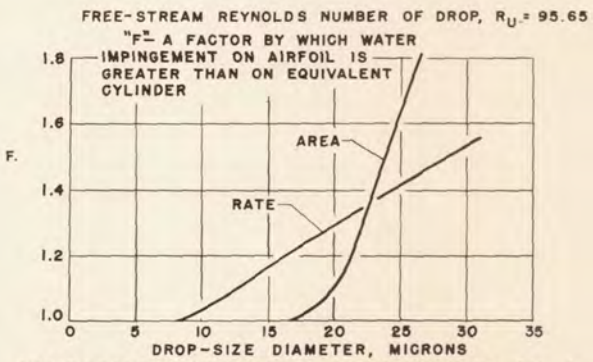

COMPARISON OF WATER IMPINGEMENT ON A SYMMETRICAL JOUKOWSKI AIRFOIL AND AN EQUIVALENT CYLINDER

Figure 4.

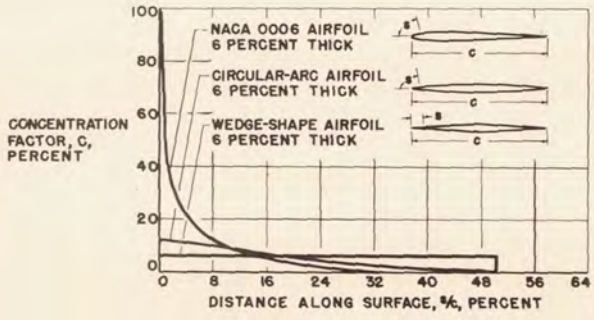

NATIONAL ADVISORY COMMITTEE FOR AERONAUTICS

DISTRIBUTION OF WATER DROPS ON THREE DIFFERENT AIRFOILS WHEN THE DROPS ARE UNDEFLECTED BY FORCES IN THE AIRSTREAM.

Figure 5.

CALCULATION OF HEAT REQUIRED FOR WING THERMAL ICE PREVENTION IN SPECIFIED ICING CONDITIONS

By Carr B. Neel, Jr. and Norman R. Bergrun

Ames Aeronautical Laboratory

INTRODUCTION

The efficient design of wing thermal ice-prevention equipment has been hampered greatly by lack of knowledge of the physical characteristics of the icing conditions upon which to base the design and the exact process by which water intercepted by a heated wing is dispersed.

The National Advisory Committee for Aeronautics at present is engaged in an investigation of the meteorological factors conducive to icing and a fundamental study of the heat-transfer processes which govern the operation of wing thermal ice-prevention equipment. During the winters of 1945-46 and 1946-47 a Curtiss-Wright C-46 airplane which had been provided with a thermal ice-prevention system (reference 1) was equipped with special meteorological and electrically heated test apparatus and flown in natural icing conditions along airline routes over most of the United States. The meteorological data recorded during the icing conditions encountered in the two seasons are presented and discussed in references 2 and 3.

The material of this paper was taken from reference 4, and presents an analysis of the data obtained during the 1945-46 and 1946-47 winter seasons with two electrically heated test airfoils. The data were analyzed using heat-transfer equations developed by Hardy of the Royal Aircraft Establishment, Farnborough, England (references 5 and 6). A discussion of the area and rate of water impingement on one of the airfoil sections based on an analytical study of water-drop trajectories (reference 7) is also presented.

APPARATUS AND METHOD

In order to study the process of heat transfer from airfoils in icing conditions, two electrically heated airfoils of 8-foot chord and 5-foot span were constructed to obtain test data. Each airfoil was mounted vertically on top of the fuselage of the C-46 airplane,

as shown in figure 1. The test airfoil installed during the winter of 1945-46 had an NACA 0012 section. For the tests in the winter of 1946-47 the airfoil had an NACA 65,2-016 section in order to provide data for low-drag as well as conventional sections. Each airfoil had a heated test section of 1-foot span located 2 feet above the top of the fuselage. The airfoils contained electrical heating elements which allowed a variety of chordwise heat-flow distributions. Thermocouples were installed on the test-section surfaces for the purpose of measuring surface temperature.

During flight in icing conditions, airfoil thermal data were recorded simultaneously with the measurement of meteorological factors. Rotating cylinders were used for the measurement of liquid-water concentration, drop size, and drop-size distribution.

RESULTS AND DISCUSSION

The process of airfoil thermal ice prevention and the analysis of the data obtained with the C-46 airplane are discussed. The ultimate in performance of a wing thermal ice-prevention system is one which prevents the accretion of ice on any portion of the wing. This ideal operation requires that any water on the wing surface must be maintained in a liquid state until it evaporates or flows off the wing at the trailing edge. In many wing designs, heating of the entire surface is not practicable because of such features as integral fuel tanks, and in these instances any water flowing aft of the heated region is apt to freeze and form the type of ice accretion normally termed "runback."

A study of the action of a heated wing requires the consideration of three factors: namely (1) the meteorological and flight conditions for which the wing must provide protection, (2) the area of water impingement and the rate and distribution of impingement over that area, and (3) the rate at which the water is evaporated from the wing surface. The two latter factors are important in the heat-transfer process, and are examined later.

Meteorological and Flight Conditions

The specification of a meteorological condition for the design of thermal ice-prevention equipment depends upon the geographical areas over which the airplane will fly, the seasons of operation, and other factors dictated by the intended service of the aircraft. Obviously, the establishment of design conditions for a specific area requires a knowledge of the conditions prevailing over the area.

If, on the other hand, the ice-prevention system is to provide protection for all-weather operation, general specifications of a meteorological condition must be established which will encompass all conditions likely to be encountered.

The most recent and extensive information in regard to the severity of icing conditions likely to be experienced in all-weather operation in the United States is contained in references 2 and 3. In these reports, estimates of the maximum continuous icing conditions, as well as the maximum probable icing conditions liable to be encountered, are presented. Since the duration of the maximum probable icing condition is quite short (1 to 2 minutes) and icing of this severity is entirely associated with cumulus clouds which can be avoided in daytime operations, the maximum continuous icing condition is believed to be of greater interest for design purposes. Two conditions of maximum continuous icing are presented based on a relationship of drop size and liquid-water content. These conditions are given in the following table:

Liquid-water concentration (gram/cubic meter)	Mean-effective drop size (microns)	Free-air temperature ($^{\circ}$F)
0.8	15	20
0.5	25	20

It is believed that the conditions in the above table form a good basis for the design of thermal ice-prevention equipment for all-weather operation. In addition to these values, however, the proposed wing thermal system should be analyzed for possible undesirable operation in other icing conditions. For example, reference 2 points out that drops of 35 to 50 microns diameter should not be regarded as exceptional. Although the amount of liquid water associated with such large drops is usually low (about 0.1 gram per cubic meter) the fact remains that the area of water impingement would be very large and would probably exceed the limits of the heated region if this region had been based only on a consideration of the data in the maximum continuous table. Finally, the possibility of encountering icing conditions at low temperatures (0° F) may be a critical condition for heated wings on some airplanes.

From the foregoing discussion it is evident that the analysis of a heated wing should give consideration to several possibly critical icing conditions in the same manner that several flight conditions are assumed for the wing structural analysis. The data of references 2 and 3, although somewhat limited in scope, are considered to be sufficiently indicative of icing conditions in the United States to form a meteorological basis for heated-wing design.

The problem of selecting a flight condition for the design of ice-prevention equipment is concerned with the airspeed and altitude at which the airplane will fly. The airspeed will depend upon the specific airplane, and, in general, a cruise condition should be selected. Choosing an altitude for design is dependent upon several factors, which are discussed later.

Rate of Water Impingement and Evaporation

During flight in icing conditions, a heated wing is cooled by convective heat transfer, by evaporation of the water on the surface, and, in the region of droplet interception, by the water striking the wing. The rate at which heat must be supplied in order to maintain the wing surface at a specified temperature is, therefore, a function of the rates of convection, evaporation, and water impingement.

The unit heat losses from a wetted surface in the area of water impingement and in the area aft of water impingement are expressed by the following equations:

$$q_A = M_a (t_s - t_o) + hX (t_s - t_{o_k}) \quad (1)$$

$$q_B = hX (t_s - t_{o_k}) \quad (2)$$

where

$$X = 1 + 3.75 \frac{e_s - e_{ok}}{t_s - t_{o_k}} \frac{P_{SL}}{P_l} \quad (3)$$

q_A unit heat loss in region of water impingement, Btu/(hr)(sq ft)

q_B unit heat loss in region aft of water impingement, Btu/(hr)(sq ft)

M_a rate of impingement of water at a particular point, lb/(hr)(sq ft)

h	convective heat-transfer coefficient, Btu/(hr)(sq ft)(^{o}F)
t_s	surface temperature, ^{o}F
t_o	free-air temperature, ^{o}F
t_{o_k}	kinetic temperature of the air, ^{o}F
e_s and e_{o_k}	saturation vapor pressures corresponding to the temperatures t_s and t_{o_k}, mm Hg
P_{SL}/P_l	ratio of standard sea-level pressure to the local pressure

Equation (1) denotes the heat loss in the region of water impingement. Aft of the area of water impingement, equation (2) applies. The term X is the evaporative factor, and as given in equation (3) it implies that the surface under consideration is fully wetted. If only partial wetness prevails, the value of X must be modified according to the degree of wetness.

The rate of water impingement on the wing, the area of impingement, and the distribution of the water over that area are important factors in the heat-transfer analysis. The evaluation of the rate of water interception determines the quantity of water which must be maintained in a liquid state until it either evaporates or runs off the trailing edge if runback is to be avoided. The area of impingement influences the extent of heated region to be provided at the leading edge, while knowledge of the distribution of water impingement is required in the calculation of the heating requirement in areas where water is striking.

The rate of water impingement is a function mainly of the number and size of water drops present in the icing cloud, the contour and size of the wing, and the speed of flight. Calculations have been made by Glauert (reference 8) for the trajectories of water drops about cylinders and airfoils. In this work the assumption was made that the drops obeyed Stokes' law of resistance. At the speeds of flight, however, Stokes' law no longer strictly holds, and Langmuir and Blodgett (reference 9) computed a series of drop trajectories about cylinders, spheres, and ribbons taking into consideration deviations from Stokes' law. These computations were undertaken on the assumption that the trajectories for cylinders would apply to airfoils if the leading edge of the airfoil were replaced by an "equivalent" cylinder (reference 10).

Preliminary calculations at the Ames laboratory based on references 8 and 9 indicated that for large values of drop size and airspeed the assumption of the equivalent cylinder would not hold for airfoils. Therefore, more extensive calculations were undertaken to determine the drop trajectories for an NACA 0012 airfoil at 0° angle of attack. These calculations have been described by Bergrun (reference 7), and were used in this paper for the computation of rate and area of impingement for the airfoils tested.

Although the method of reference 7 is considered to provide a complete and quite accurate prediction of the distribution of water impingement on the leading edge of an airfoil, it does have the disadvantages of requiring (1) a knowledge of the velocity components along a number of the airfoil streamlines, and (2) considerable computation. The difficulties associated with the computation of the water-drop trajectories for airfoils have encouraged the substitution of a cylinder with radius equal to the airfoil leading-edge radius in the determination of water impingement. The curves of reference 9, which have been calculated for a large range of drop sizes, airspeeds, altitudes, and cylinder diameters, are then used directly to evaluate the anticipated water impingement on the airfoil. This substitution procedure is a useful device, but should be employed with a full knowledge of its limitations. One of these limitations is the fact that the curves of reference 9 provide the area and total rate of water impingement, but give no direct indication of the distribution of impingement.

A second restriction of the cylinder-substitution method is concerned with the contour and size of the forward portion of the airfoil. To obtain an indication of this effect, the rate and area of water impingement on the NACA 0012 airfoil, at 0° angle of attack, and on the leading-edge cylinder of this airfoil are compared for the same flight conditions and various drop sizes in figure 2. This figure illustrates how much greater the rate and area of impingement are on the airfoil than on the cylinder. At the smaller drop diameters (10 to 15 microns) the areas of impingement on the airfoil and the cylinder are identical, although the rate of impingement on the airfoil ranges from 4 to 17 percent greater than the rate for the cylinder. At a drop diameter of 25 microns, which is not unusual and was presented previously as a possible maximum continuous condition, the rate of impingement on the airfoil is 40 percent greater than on the cylinder, while the area of impingement has increased to about 60 percent greater. It should be observed that the value of 25 microns for the maximum continuous condition is the mean-effective diameter, and that drops of a larger size probably will be present due to the existence of a distribution of sizes. Although these values provide an indication of the scale limitation of the cylinder-substitution method,

the fact should be noted that figure 2 applies to only one airfoil section, with an 8-foot chord, and at one flight condition. The leading-edge radius of the NACA 0012 section is small (1.5 in.) and the leading-edge cylinder does not match the section contour for any great extent above the chord line. This is shown graphically in figure 3 which presents a comparison of the forward portion of the NACA 0012 airfoil and its leading-edge cylinder. In the case of airfoil sections with the leading-edge radius a greater percentage of the chord than the NACA 0012 section, and also for airfoils of NACA 0012 section, or similar with chords greater than 8 feet, the cylinder-substitution method will present a better approximation than that indicated by figure 2 for the same speed range.

For airfoil sections with a leading-edge radius, which represents a small percentage of the chord, the substitution of an equivalent cylinder (reference 10) with a radius larger than the leading-edge radius would probably provide a better indication of the rate and area of water impingement on the airfoil than would be obtained for the leading-edge cylinder. At the present time there is not sufficient information on water-drop trajectories about airfoils to provide a basis for selecting the proper cylinder in each instance; therefore, the designer must utilize the more complicated, but more accurate, method of reference 7 or assume some cylinder diameter based on his experience and ingenuity. The possibility that the rate and area of impingement on an ellipse would more closely approximate the rate and area of impingement on a series of similar airfoils has been suggested and is worthy of future consideration.

The ability to select a proper drop size for the design of wing ice-prevention equipment is a factor of considerable importance to the designer, as can be illustrated by figure 4. In this figure the area and total rate of impingement are presented for the NACA 0012 airfoils as a function of drop size. The rate of impingement was calculated for a liquid-water concentration of 1.0 gram per cubic meter. Consider, then, a change in design drop diameter from 10 microns to 20 microns. The resultant increase in rate of water impingement is 1.75 pounds per hour per foot of span or an increase of 175 percent, although the actual amount of water present per unit volume of cloud has not been changed at all. The same increase in drop size will cause an increase in area of impingement from 1.5 to 4 percent s/c.

In contrast, consider the effect on the rate of water impingement produced by an increase in the quantity of liquid water present assuming the drop size to remain constant. The area of impingement will remain unchanged, while the rate of impingement will increase only in direct proportion to the increase in water concentration.

This example clearly illustrates the fact that the amount of free water present in an icing cloud is only one factor influencing the quantity of water which will actually strike the wing in a specified time interval, and that the size of the cloud drops is a factor of at least equal importance.

After presenting the problem of area and rate of water interception, the next step is to establish the rate at which the intercepted water is evaporated from the wing surface and the validity of the equations presented previously for determining the rate of heat dissipation during the process of evaporation. The problem of rate of evaporation is particularly important, because all of the water intercepted by a wing heated only in the region of the leading edge must be dispersed by evaporation if the formation of runback is to be avoided.

From a superficial study of the mechanism by which water is deposited on the surface of a wing, it would be expected that in the area of water impingement the surface is completely wetted, and that equation (1) for calculating the heat loss from a heated wing is valid. Aft of the area of impingement, it would be anticipated that the surface may not be fully wetted, since water does not reach this region directly, but instead must flow back from the area of impingement. If the surface aft of the area of impingement is only partially wetted, the expression for X (equation (3)) must be modified for use in equation (2) to calculate heat requirements.

A picture of the conditions of wetness which actually exist on a wing during flight in clouds can be seen in figure 5. This figure, which shows typical records obtained with strips of blueprint paper wrapped around the leading edge of the NACA 65,2-016 airfoil model during flight in icing conditions, illustrates the pattern formed by the water in striking the airfoil leading edge and flowing aft. It appears from the patterns that the area of impingement, which is clearly defined, is completely wetted, while back of this area the water collects and forms rivulets, creating a partiallly wetted surface. A study of the patterns obtained in this manner revealed a variation in the fraction of surface area wetted aft of impingement with rate of impingement of water. Figure 6 presents the relation between calculated values of the rate of water flow rearward from the area of drop impingement and the degree of surface wetness as obtained from the rivulet patterns. Values of the rate of water flow are given in pounds per hour per foot span. Another factor which undoubtedly influences the amount of surface area wetted aft of the region of impingment is the condition of the surface. It should be noted that the values shown in this figure were calculated from data obtained with blueprint paper strips mounted on the NACA

65-series airfoil. The maximum probable degree of surface wetness is not definitely known. There is evidence, however, indicating that the degree of surface wetness aft of the area of impingement reaches a maximum which is not exceeded, regardless of the rate at which water is intercepted. It is believed that the limit of surface wetness for surfaces not specially treated is about 40 percent.

With the information gained so far, it should be possible to analyze the data obtained with the two electrically heated airfoil models and to establish the validity of the equations previously presented. Figure 7 shows typical values of surface temperature, heat flow, and resulting heat-transfer coefficient measured with the heated airfoils during flight in icing conditions. The values shown are for the NACA 65,2-016 section. The heat-flow distribution was set during flight in clear air to provide a uniform surface temperature over the entire surface. However, during icing conditions, the curve of surface temperature took the form shown in this figure. The curve of measured heat-flow distribution was faired to produce a form more suitable for comparison with heat-flow curves calculated using equations (1) and (2). A comparison of the measured heat flow and the heat flow calculated to produce the measured surface temperatures, assuming the entire surface to be completely wetted, is shown in figure 8. These curves are also compared to the calculated heat loss due to convection only, that is, assuming the surface to be completely dry. A study of the measured and calculated heat-flow curves shows that in the area of water impingement good agreement is obtained between measured values and the values calculated for a completely wetted surface, indicating that, in the region where it is reasonable to assume a fully wetted surface, the equations for calculating heat flow are valid. Aft of this area in the region of low heat flow, the calculated values are considerably lower than the measured values. Since the calculated values are based on full evaporation, partial evaporation would cause the calculated curve to be even lower. The most reasonable possible explanation of the discrepancy between the measured and calculated curves is that the values of convective heat-transfer coefficient used for calculating values of heat flow (equation (2)) are too low. The values of convective heat-transfer coefficient which were used in the calculations are those measured during flight in clear air. The most obvious conclusion, therefore, is that during flight in icing conditions the presence of water on the airfoil surface caused movement of the location of transition from its position in clear air to a point close to the leading edge. The exact values of the convective heat-transfer coefficient in this region in icing conditions are unknown, but it is believed the values fluctuate due to changes in the location of transition during flight.

In the region of high heat flow where the convective heat-transfer coefficients are known, the measured heat-flow curve and the calculated curve of convective heat transfer come together, indicating that at the point where the curves coincide all the water on the surface has been evaporated.

Since the equations for calculating heat flow have been shown to be valid in the area where the surface is completely wetted, it is reasonable to assume that the equations hold in regions where the surface is only partly wetted, provided the correct modifications are made to the evaporative factor X. Fairly accurate modifications to the factor X are believed to be possible by using the curve of surface wetness shown in figure 6. Using this curve it should be possible to calculate the rate of evaporation of water from the surface aft of the region of water impingement. In the region of impingement the calculation of rate of evaporation is strainghtforward, since full evaporation occurs.

Calculations of the rates of evaporation from the surfaces of the two test airfoils for a large number of test conditions were made, using the curve of wetness fraction (fig. 6) to modify values of X in the region aft of water impingement. The rates of evaporation were compared with the rates of water impingement which were calculated from results of the trajectory calculations of reference 7 using measured values of water concentration and drop size. An average agreement of 13 percent for all of the 14 conditions analyzed (reference 4) was obtained, indicating the reliability of the method for calculating the rate of evaporation of water from a heated wing. Since the rate of evaporation can be calculated with reasonable certainty, the rate of heat flow required to produce a particular rate of evaporation can be determined with equal dependability, provided the coefficients of convective heat transfer are known.

Using the equations and method presented for calculating the rate of evaporation of water from a heated airfoil surface in conditions of icing, several calculations were made for the NACA 0012 test airfoil at 0° angle of attack to determine the effects of altitude, air temperature, and location of transition on the requirements of heat flow and extent of heated area necessary to evaporate all of the intercepted water. The meteorological conditions used in the calculations are the maximum continuous conditions expressed previously in this paper of 0.5 gram per cubic meter, liquid-water concentration, 25 microns, mean-effective drop size, and 20° F, free-air temperature. An E-type drop-size distribution was assumed (reference 9). The flight conditions taken were pressure altitude, 12,000 feet, and true airspeed, 170 miles per hour. It was assumed that transition occurrred near the leading edge. To determine the effect of altitude on the heat

requirement, a comparative calculation was made for sea-level conditions, with all other flight conditions as previously specified and with the area and rate of water impingement the same as at the 12,000-foot condition. The method of calculation employed was to assume a reasonable intensity and distribution of total heat flow and then calculate the extent of heated area required to evaporate all the intercepted water for each condition. The results of this calculation are shown in figure 9, which compares the relative convective heat losses at sea level and 12,000 feet. It should be noted that the rate of evaporation of water, which is the determining factor in the requirements of total heat flow and extent of heated area, is denoted by the area between the curves of total heat flow and convective heat loss, except in the region of water impingement. In the region of impingement, the rate of evaporation is given by the area between the curve of heat loss due to warming the intercepted water and the curves of heat loss due to convection.

For the conditions at 12,000 feet, extension of the heated area to 18 percent s/c would be adequate to ensure evaporation of all of the water intercepted. At sea level it would be necessary to extend the heated area to 26 percent s/c for evaporation of all of the water intercepted.

The curves of figure 9 can also be used to determine the amount of increase necessary in the total heat flow if all of the water is to be evaporated in an area forward of a specified chord point. For example, assume that the extent of heated region for the curves of figure 9 is limited to 18 percent s/c. At 12,000 feet all of the water would be evaporated, as has been previously mentioned. At sea level, however, some of the water would not have been evaporated. By measurement of the areas of figure 9, it can be shown that the total heat flow required to evaporate all the water within the area from 0 to 18 percent s/c at sea level is approximately 10 percent greater than the amount required at 12,000 feet. The increase in heat requirement with decrease in altitude is due to the fact that the rate of evaporation of water decreases as altitude is decreased, because of the decrease in the evaporative factor X (equation (3)). Apparently, then, airfoil thermal ice-prevention equipment in which the heat flow is fixed, such as electrical systems, should be designed for the minimum altitude at which the airplane is expected to encounter icing. However, if the airplane is designed to utilize some form of air-heated system, the performance of which probably will decrease with increase in altitude, the maximum altitude at which icing is expected to be encountered should also be investigated.

To determine the effect of air temperature on the heat requirement, a calculation was made of the convective heat loss at 0° F free-air temperature and is compared in figure 10 with the convective heat loss at 20° F. The procedure of assuming a fixed total heat flow used in the previous calculation was again employed. In the calculation with the free-air temperature at 0° F, it was determined that the surface temperature dropped to freezing at 24 percent s/c. However, the total heat flow required to evaporate all the water within the area from 0 to 18 percent s/c with the air temperature at 0° F is approximately only 15 percent greater than the amount required at 20° F. Although this is an appreciable increase in the heat requirement, it is considerably less than that necessary for a similar change in conditions for ice-prevention equipment designed on the basis of maintaining the surface temperature just above freezing, such as for the case of windshields. It appears, then, that a wing thermal system which has been designed for a relatively high air temperature will be capable of ice prevention at low air temperatures in icing conditions nearly as severe as those upon which the design was based. Of course, the system is more subject to failure through the possibility of the surface temperature falling below freezing in the low air-temperature conditions, but, in general, the surface temperatures required for evaporation of all impinging water in the relatively small heated area of the leading edge will be sufficiently high to obviate this possibility.

To establish the effect of the location of transition on the heat requirement, a calculation was made of the convective heat loss, assuming laminar flow exists throughout the heated area. This is compared in figure 11 with the convective heat loss, assuming transition started at 5 percent s/c. In the case of complete laminar flow, it would be necessary to heat only to 14 percent s/c to obtain evaporation of all the water. The total heat flow required to evaporate all the water within the area from 0 to 14 percent s/c with transition at 5 percent s/c is approximately 10 percent greater than the amount of heat required if laminar flow prevails. Apparently, the location of transition moves forward in conditions of icing, even in the presence of a favorable pressure gradient, to a point where a strong favorable pressure gradient is encountered. As was stated previously, the location of transition is believed to fluctuate, probably over a considerable distance. It is suggested that forward movement of transition to a point close to the leading edge of the wing be assumed in the design of thermal ice-prevention equipment, especially in view of the fact that such an assumption tends to be more conservative in the thermal design.

From a study of the results shown in figures 9, 10, and 11, some general conclusions can be reached. It is apparent that aft of the

area of droplet impingement, the efficiency of removal of water, by evaporation, decreases rapidly. The reason for the decrease in efficiency is that only partial wetness prevails aft of the area of impingement, while the area of impingement is entirely wet. This indicates that the more of the total amount of water intercepted that is evaporated in the area of interception, the greater becomes the efficiency of the thermal system. The rate of evaporation of water is the determining factor in the efficiency of a wing thermal ice-prevention system. Only the heat that is dissipated in evaporation is used to advantage. The heat lost by convection only warms the air. Thus, the conclusion is drawn that the heating should be concentrated as much as possible in the leading edge of a wing, in the area of drop impingement, if an efficient thermal system is to be obtained.

From the foregoing discussion, it appears that the extent of knowledge of the meteorology of icing, the impingement of water drops on airfoil surfaces, and the processes of heat transfer and evaporation from a wetted airfoil surface has been increased to a point where the design of heated wings on a fundamental, wet-air basis now can be undertaken with reasonable certainty.

REFERENCES

1. Jones, Alun R., and Spies, Ray J., Jr.: An Investigation of a Thermal Ice-Prevention System for a C-46 Cargo Airplane. III - Description of Thermal Ice-Prevention Equipment for Wings, Empennage, and Windshield. NACA ARR No. 5A03b, 1945.

2. Lewis, William: A Flight Investigation of the Meteorological Conditions Conducive to the Formation of Ice on Airplanes. NACA TN (to be pub.).

3. Lewis, William, Kline, Dwight B., and Steinmetz, Charles P.: A Further Flight Investigation of the Meteorological Conditions Conducive to Aircraft Icing. NACA TN (to be pub.).

4. Neel, Carr B., Jr., Bergrun, Norman R., Jukoff, David, and Schlaff, Bernard A.: The Calculation of the Heat Required for Wing Thermal Ice Prevention in Specified Icing Conditions. NACA TN (to be pub.).

5. Hardy, J. K.: An Analysis of the Dissipation of Heat in Conditions of Icing from a Section of the Wing of the C-46 Airplane. NACA ARR No. 4Illa, Oct. 1944.

6. Hardy, J. K.: Protection of Aircraft against Ice. S.M.E. Rep. No. 3380, R.A.E., (British), July 1946.

7. Bergrun, Norman R.: A Method for Numerically Calculating the Area and Distribution of Water Impingement on the Leading Edge of an Airfoil in a Cloud. NACA TN (to be pub.).

8. Glauert, Muriel: A Method of Constructing the Paths of Raindrops of Different Diameters Moving in the Neighbourhood of (1) A Circular Cylinder, (2) An Aerofoil, Placed in a Uniform Stream of Air: and A Determination of the Rate of Deposit of the Drops on the Surface and the Percentage of Drops Caught. R. & M. No. 2025, British A.R.C., 1940.

9. Langmuir, Irving, and Blodgett, Katharine B.: A Mathematical Investigation of Water Droplet Trajectories. General Electric Co., July 1945.

10. Tribus, Myron, and Tessman, J. R.: Report on the Development and Application of Heated Wings, Addendum I. A.A.F Tech. Rep. 4972, Jan. 1946.

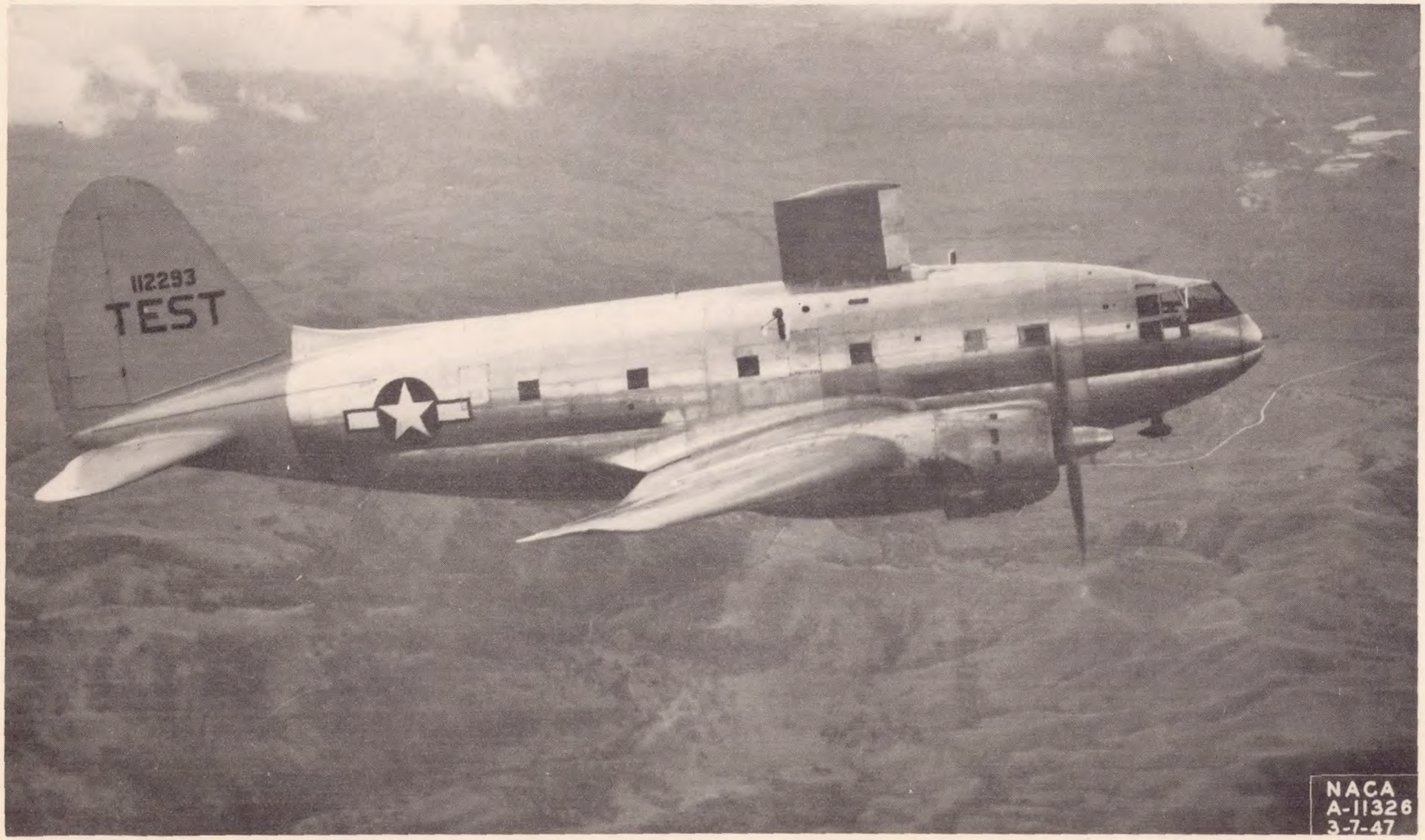

Figure 1.- C-46 test airplane showing the manner in which the test airfoils were mounted.

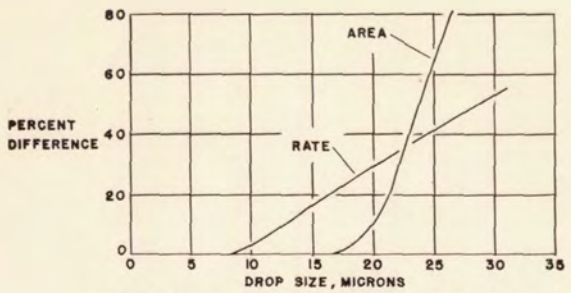

COMPARISON OF AREA AND RATE OF IMPINGEMENT ON AN AIRFOIL AND THE LEADING-EDGE CYLINDER

Figure 2.– Comparison of area and rate of water impingement on an NACA 0012 airfoil and the leading-edge cylinder.

NATIONAL ADVISORY
COMMITTEE FOR AERONAUTICS

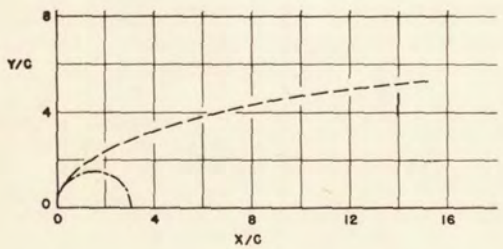

COMPARISON OF CONTOURS OF AN NACA 0012 AIRFOIL SECTION AND THE LEADING-EDGE CYLINDER

Figure 3.– Comparison of contours of an NACA 0012 airfoil section and the leading-edge cylinder.

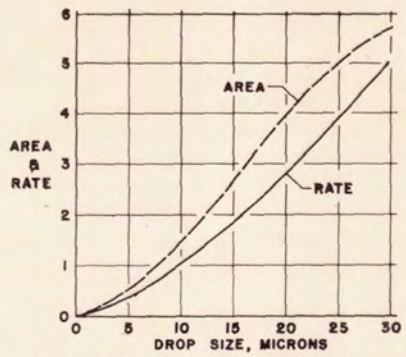

AREA AND RATE OF WATER IMPINGEMENT AS A FUNCTION OF DROP SIZE

Figure 4.- Area and rate of water impingement on an NACA 0012 airfoil as a function of mean-effective drop size. Liquid-water concentration, 1.0 gram per cubic meter; drop-size distribution, type C; true airspeed, 170 mph; chord length, 8 feet. Area values in s/c percent for 1-foot span; rate values in pounds per hour, foot span for one side of airfoil.

NATIONAL ADVISORY
COMMITTEE FOR AERONAUTICS

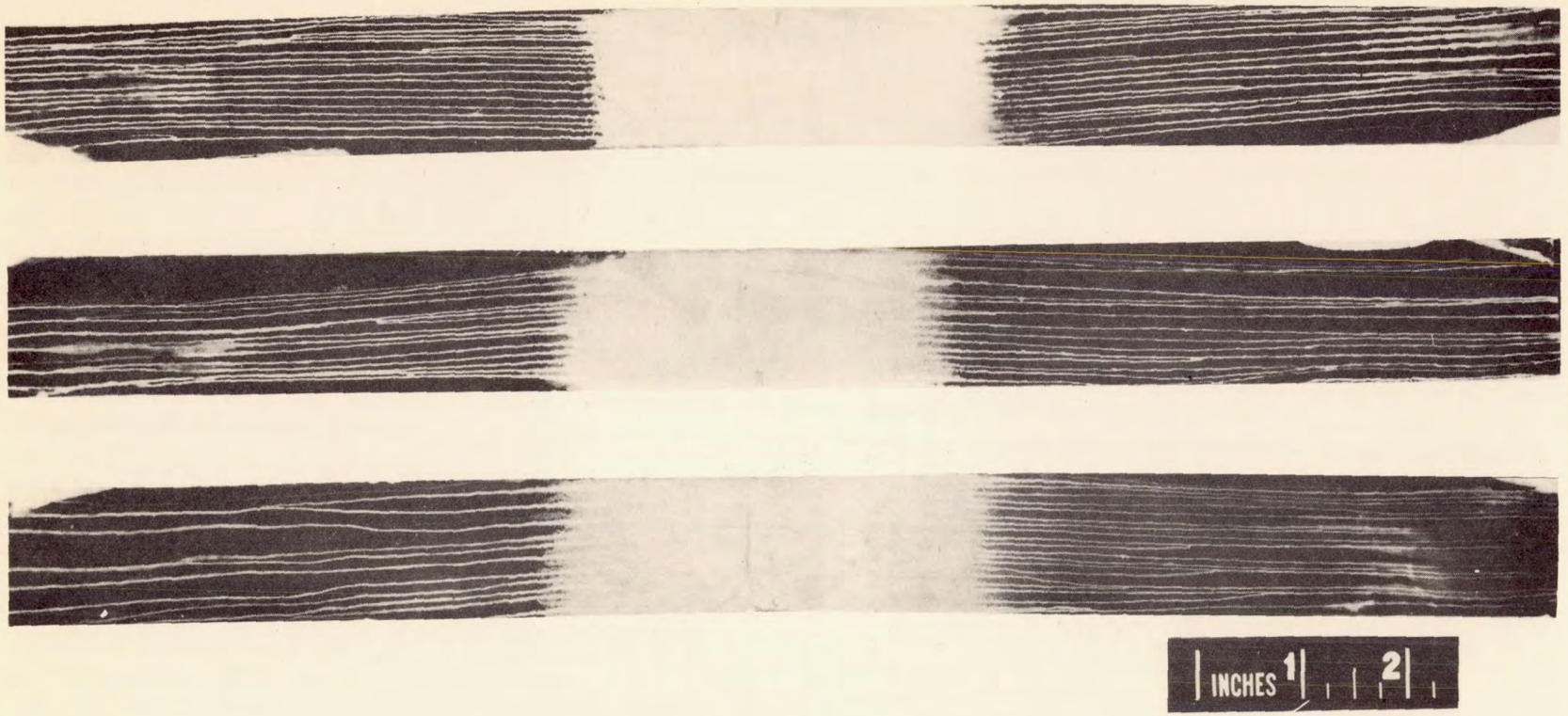

NACA
A-11533
5-12-47

Figure 5.- Typical records obtained with blueprint paper strips on the NACA 65, 2-016 airfoil model showing pattern formed by water in striking the leading edge and flowing aft.

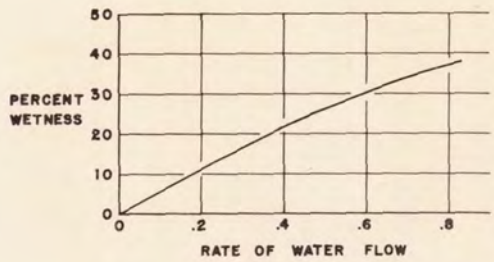

DEGREE OF SURFACE WETNESS AS
A FUNCTION OF RATE OF FLOW
OF WATER FROM AREA OF IMPINGEMENT

Figure 6.– Degree of surface wetness as a function of rate of water flow from area of impingement. Rate of water-flow values in pounds per hour, foot span for one side of airfoil.

NATIONAL ADVISORY
COMMITTEE FOR AERONAUTICS

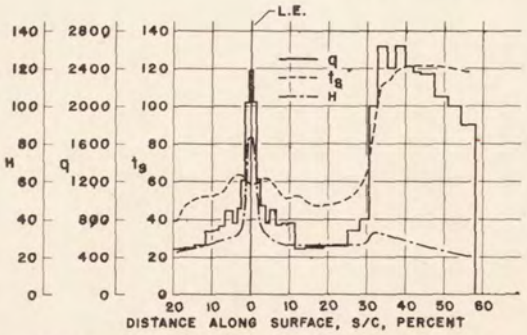

THERMAL DATA OBTAINED WITH HEATED
AIRFOIL MODEL DURING FLIGHT
IN ICING CONDITIONS

Figure 7.– Typical thermal data obtained with NACA 65,2-016 heated airfoil model during flight in natural-icing conditions. Values of surface temperature t_s in $^{\circ}F$; values of heat flow q in Btu per hour, square foot; values of heat-transfer coefficient H in Btu per hour, square foot, $^{\circ}F$.

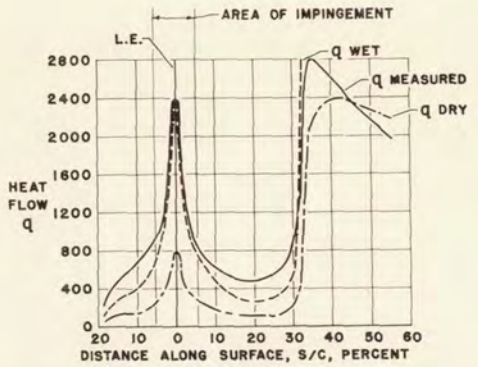

MEASURED HEAT FLOW COMPARED WITH HEAT FLOWS CALCULATED FOR COMPLETELY WET AND COMPLETELY DRY SURFACE

Figure 8.– Comparison of measured heat flow and calculated heat flows for completely wet and completely dry surface on NACA 65,2–016 heated airfoil model. Heat–flow values in Btu per hour, square foot.

NATIONAL ADVISORY
COMMITTEE FOR AERONAUTICS

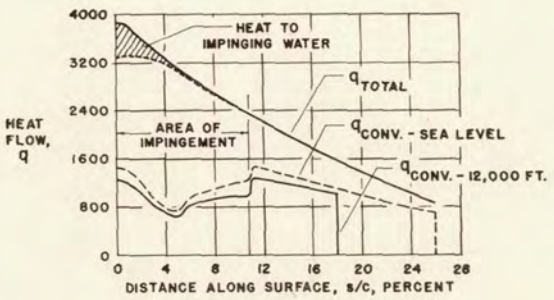

CALCULATED HEAT LOSSES AT TWO ALTITUDES

Figure 9.– Comparison of calculated convective heat losses from an NACA 0012 heated airfoil at different altitudes. Heat–flow values in Btu per hour, square foot.

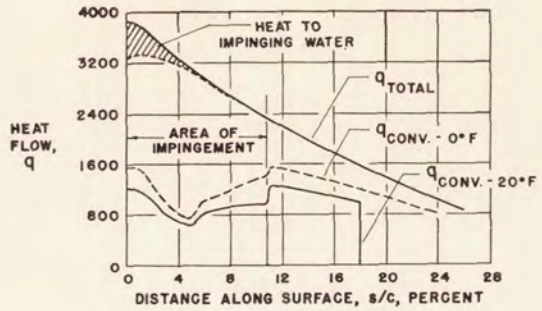

CALCULATED HEAT LOSSES AT TWO AIR TEMPERATURES

Figure 10.– Comparison of calculated convective heat losses from an NACA 0012 heated airfoil at different free-air temperatures. Heat-flow values in Btu per hour, square foot.

NATIONAL ADVISORY
COMMITTEE FOR AERONAUTICS

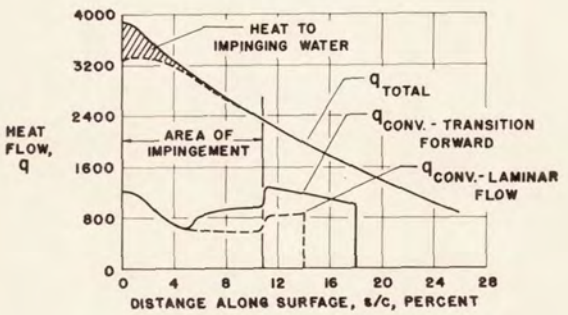

CALCULATED HEAT LOSSES AT TWO LOCATIONS OF TRANSITION

Figure 11.– Comparison of calculated convective heat losses from an NACA 0012 heated airfoil at two locations of transition. Heat-flow values in Btu per hour, square foot.

TENSION IN RADIO ANTENNA WIRES RESULTING FROM ICE FORMATION

By William L. Kepple

Flight Propulsion Research Laboratory

INTRODUCTION

The collection of ice on aircraft radio antennas necessitates an investigation to determine (1) the effect of ice formations on the electrical properties of the antenna, (2) the effect of ice formations on the tension occurring in the antenna, and (3) the decrease in aircraft performance due to antenna ice formations. Information is also needed concerning the prevention and removal of ice on radio antennas and the installation of the radio antennas in the wings or fuselage.

A flight investigation was conducted at the NACA Cleveland laboratory during the winter of 1946-47 to determine the tension occurring in aircraft antennas while flying in natural icing conditions. This investigation was conducted at true airspeeds from 155 to 215 miles per hour and at altitudes at which icing conditions occurred. The effect of the following factors upon antenna tension were investigated: (1) distance flown in the icing region; (2) included angle between the antenna and the thrust axis of the airplane; (3) antenna length; and (4) meteorological variables pertinent to ice accretion.

APPARATUS AND PROCEDURE

The location of the seven experimental antennas and the two service antennas are presented in figure 1. The antenna angles varied from 0° to 64° and the antenna lengths varied from 15 to 43 feet. It was anticipated that the tension that would be imposed upon the antennas would exceed the breaking strength of the various antenna wires in general use at the present time. In consideration of this factor, the antennas used were 1/16-inch diameter, 7 by 7 aircraft control cable. The breaking strength of the antenna cable was 540 pounds. Turnbuckles and spring-tension units were mounted on the rearward end of the antennas to impose a 30-pound static tension.

The tension in the seven experimental antennas was measured by strain gages located at the forward end of the antennas as shown

in figure 2. The strain gages were temperature compensating and sealed by means of electrical de-icing boots so as to be moisture free. A recording galvanometer registered the tension in the antennas. Multirotating cylinders were used to determine the average droplet diameter and the liquid-water content.

RESULTS AND DISCUSSION

Figure 3 shows the ice formation on the 15°, 32-foot antenna. The typical ice formation resembles a cup and saucer. The direction of the air flow is from left to right at a 15° angle with the antenna. The maximum diameter of the ice formations averaged $2\frac{1}{2}$ inches.

Figure 4 shows the ice formations on the 8°, 41-foot antenna. The ice formation generally is in the form of a cone with the base of the cone facing upstream. The diameter of the bases averaged $1\frac{1}{2}$ inches. The air flow is from left to right at an 8° angle with the antenna.

Figure 5 is a photograph taken in flight of a service antenna; the 15°, 32-foot antenna; and the 64°, 40-foot antenna. The ice configurations on the 64°, 40-foot antenna are illustrative of the configurations incurred on the 64° and the 44° antennas during most of the flight operations.

A typical plot of the variation of the antenna tension with distance flown in the icing region is presented in figure 6. Distance flown in the icing region is used as the abscissa because it represents the volume of air swept by the antennas. The vertical distance between the upper and lower curve for the 64°, 40-foot antenna and the 44°, 42-foot antenna represents the maximum and minimum tension produced by whipping of the antenna. The variations in tension for the 0° to 15° antennas were small. This figure shows that for the 44° and the 64° antennas there is considerable increase in antenna tension with distance traversed in the icing region while for antennas of 15° and less, the variation in tension with distance is small.

Figure 7, which is similar to figure 6, presents the variation of antenna tension with distance traversed in the icing region. However, figure 7 shows the effect of whipping of the antenna upon antenna tension. At the 139-mile point, the whipping of the 64° antenna produced a variation in tension of 120 pounds. Shortly after this point, the whipping caused considerable quantities of ice to break off and thus temporarily reduced the tension.

Figure 8 presents the variation of antenna tension with antenna angle at a constant length of 41 feet. The tension values presented in this figure were obtained from figures 6 and 7 at the 115-mile point and from similar figures in reference 1. This figure shows that at constant length the antenna tension increased with increasing antenna angle. With increasing angle, the antenna tension increased eight times faster in the 44° to 64° range than in the 0° to 15° range. The slope of the curve begins to change appreciably above 15°, indicating that the required strength of the antennas will be small when the antenna angle is 15° or less. The maximum tension measured was 438 pounds.

The variation of antenna tension with antenna length at a constant antenna angle of 15° is presented in figure 9. Distance traversed in the icing region was 115 miles. These data indicate that tension increased at a nearly uniform rate with antenna length.

Insufficient data were obtained during the investigation to establish a correlation between antenna tension and the meteorological variables.

The meteorological conditions encountered produced icing of only moderate intensity and consequently the antenna tension recorded while in these icing regions would not be as great as could be encountered in high-intensity icing regions.

REFERENCE

1. Kepple, William L.: Determination of Aircraft Antenna Loads Produced by Natural Icing Conditions. NACA RM (to be pub.).

SERVICE AND EXPERIMENTAL ANTENNAS

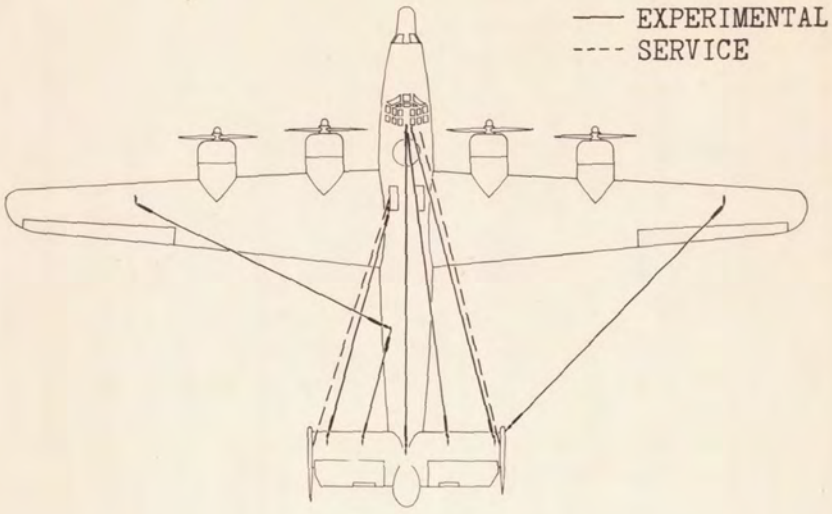

FIGURE 1.

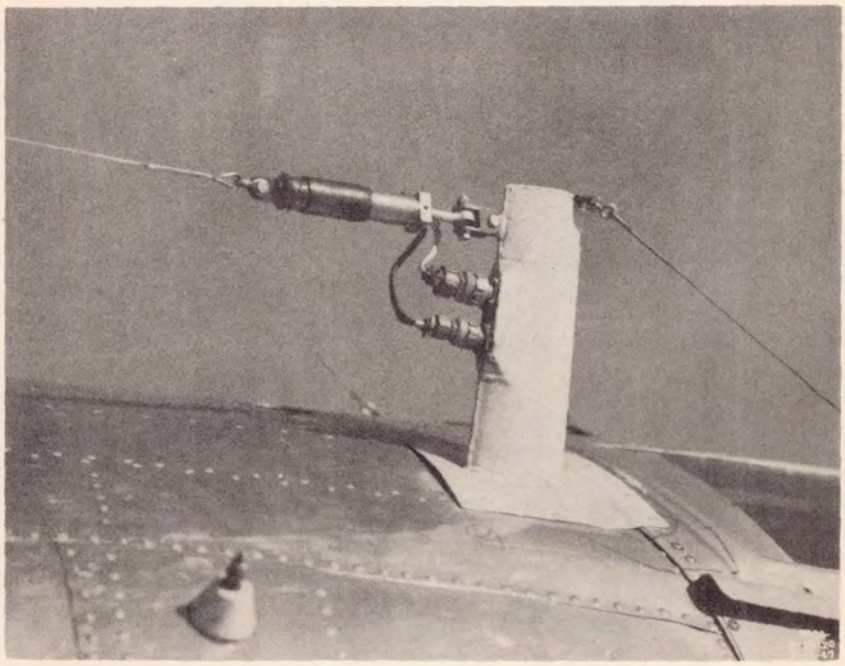

ANTENNA-TENSION STRAIN GAGE
FIGURE 2.

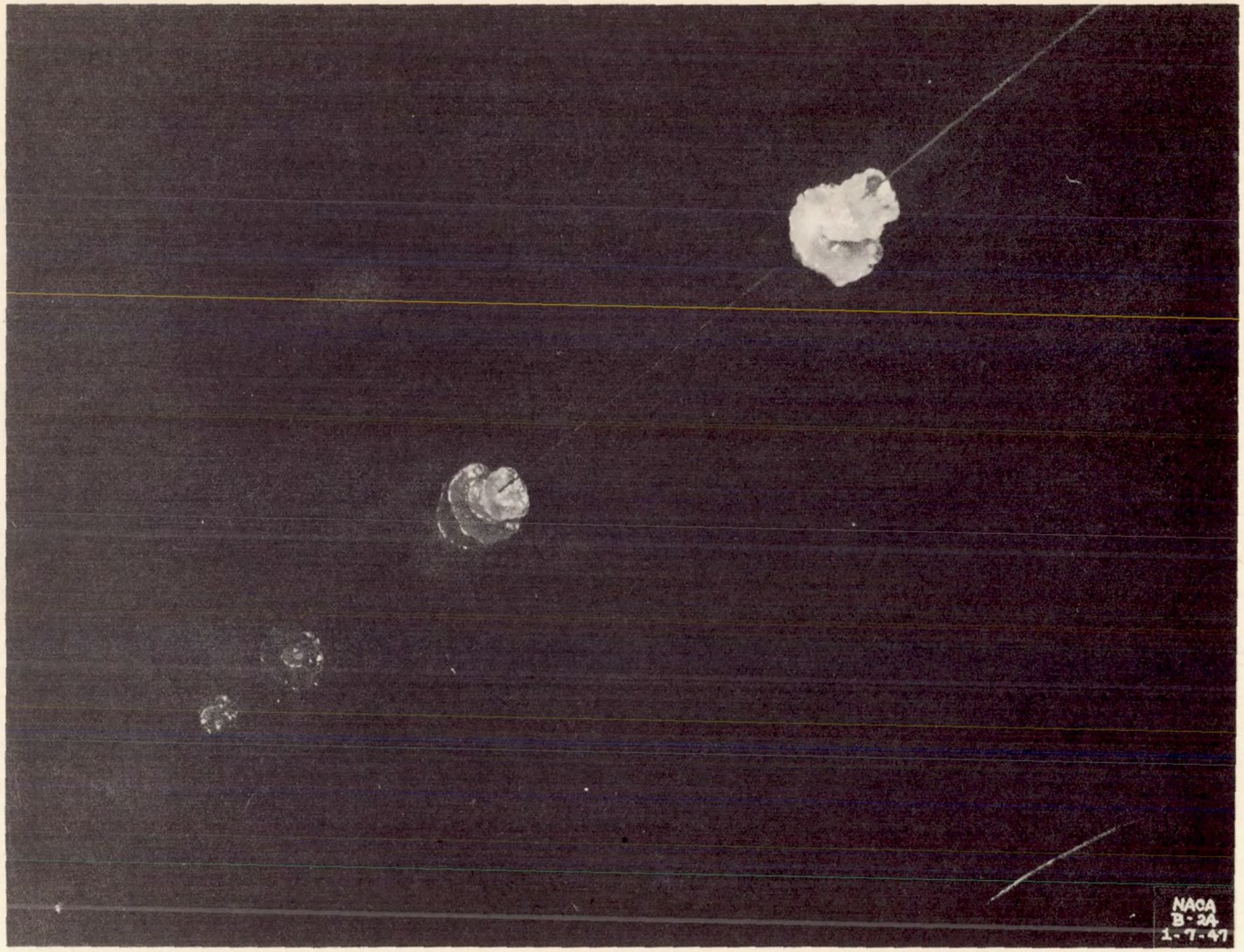

ICE FORMATION ON 15°, 32-FT ANTENNA
FIGURE 3.

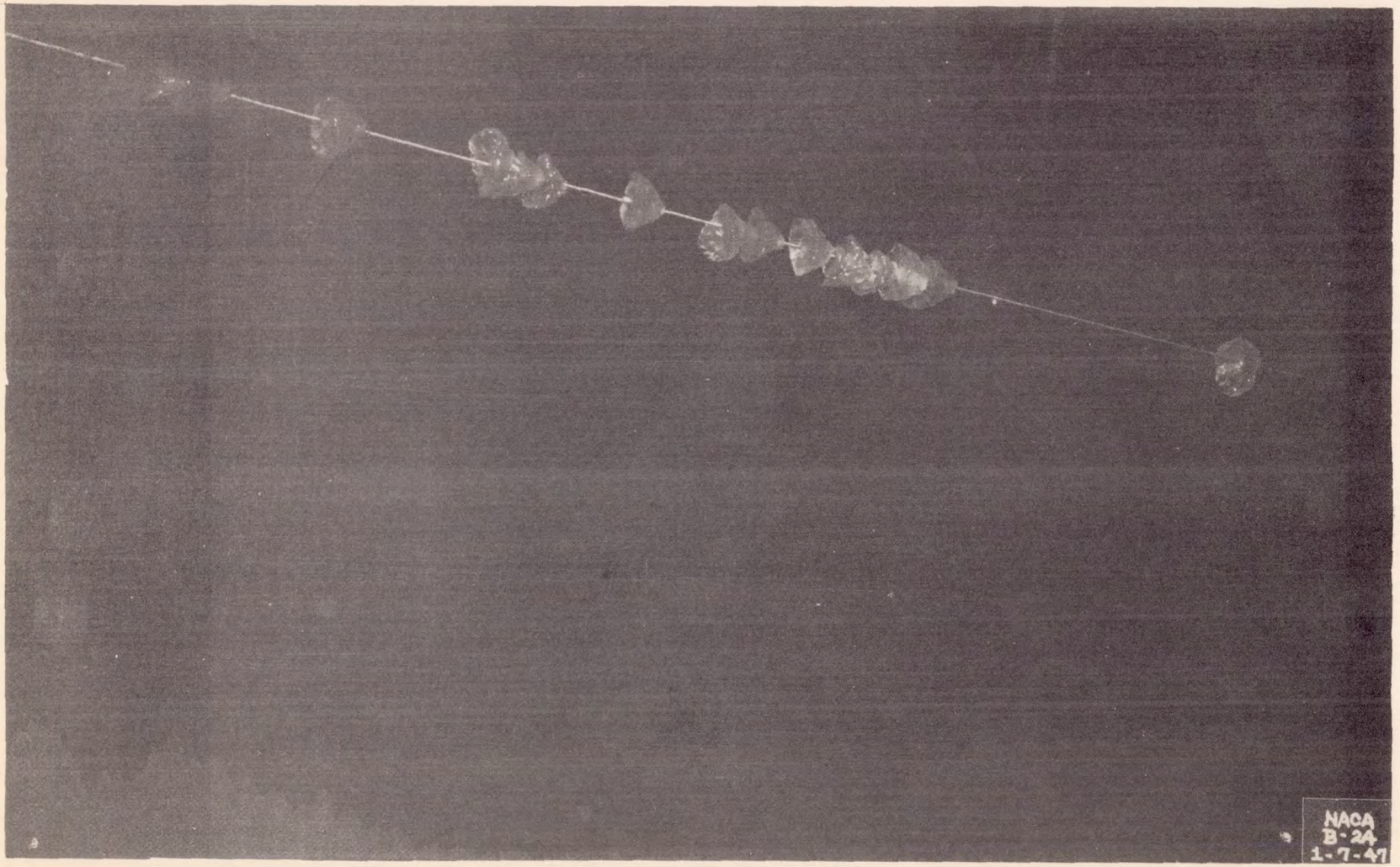

ICE FORMATION ON 8°, 41-FT ANTENNA
FIGURE 4.

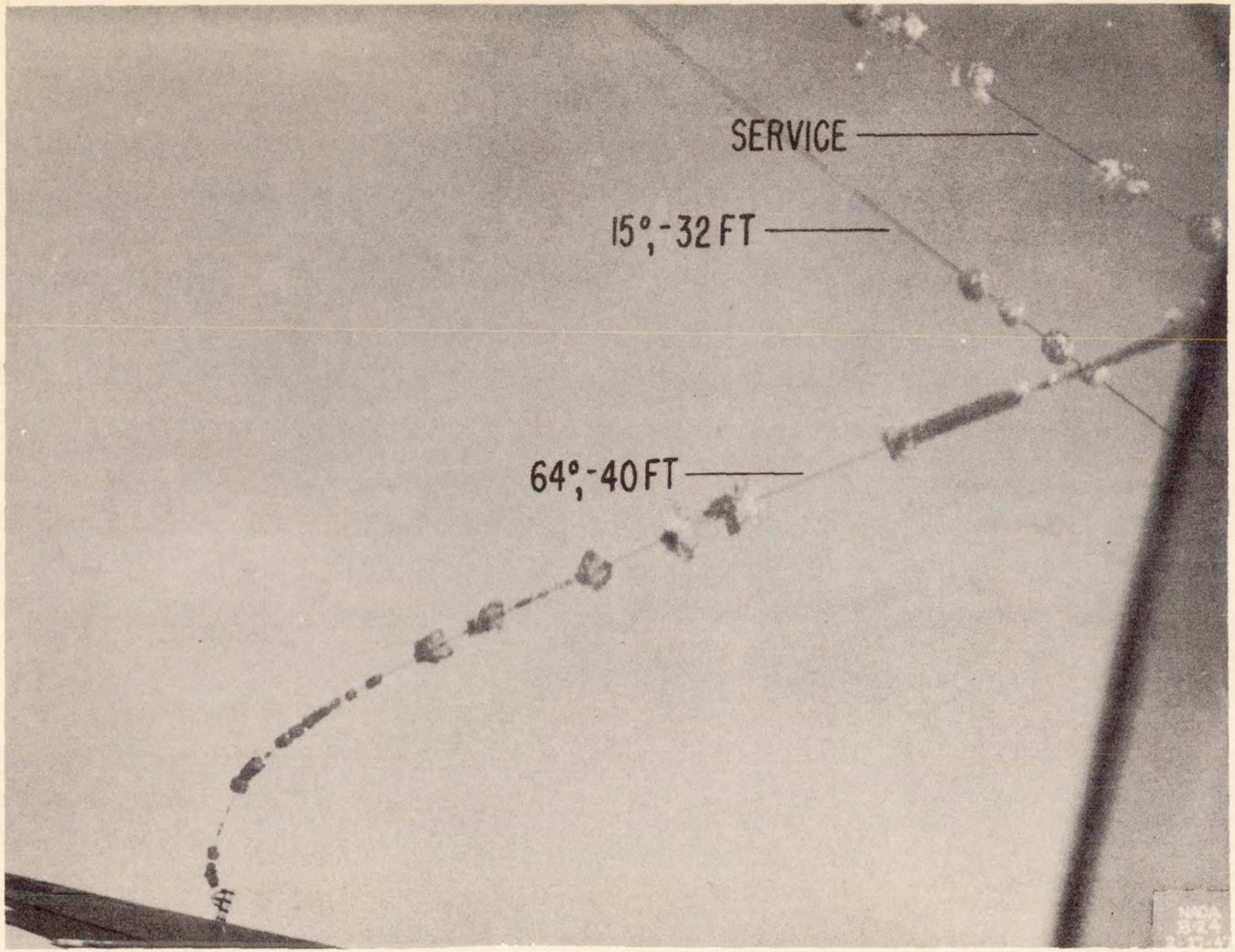

ANTENNA ICE FORMATION
FIGURE 5.

VARIATION OF ANTENNA TENSION WITH DISTANCE TRAVERSED IN ICING REGION FOR EXPERIMENTAL ANTENNAS

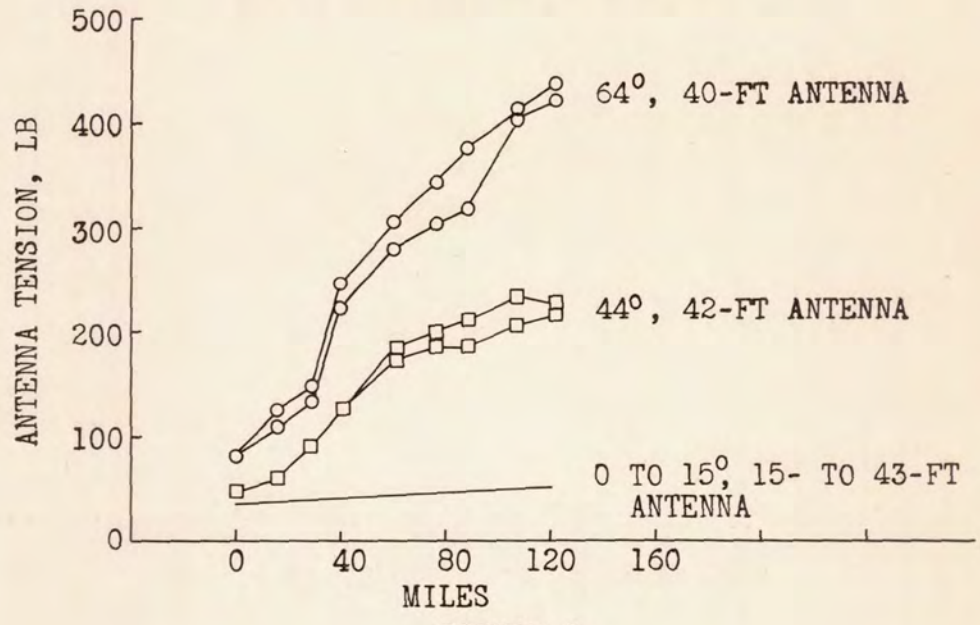

FIGURE 6.

VARIATION OF ANTENNA TENSION WITH DISTANCE TRAVERSED IN ICING REGION FOR EXPERIMENTAL ANTENNAS

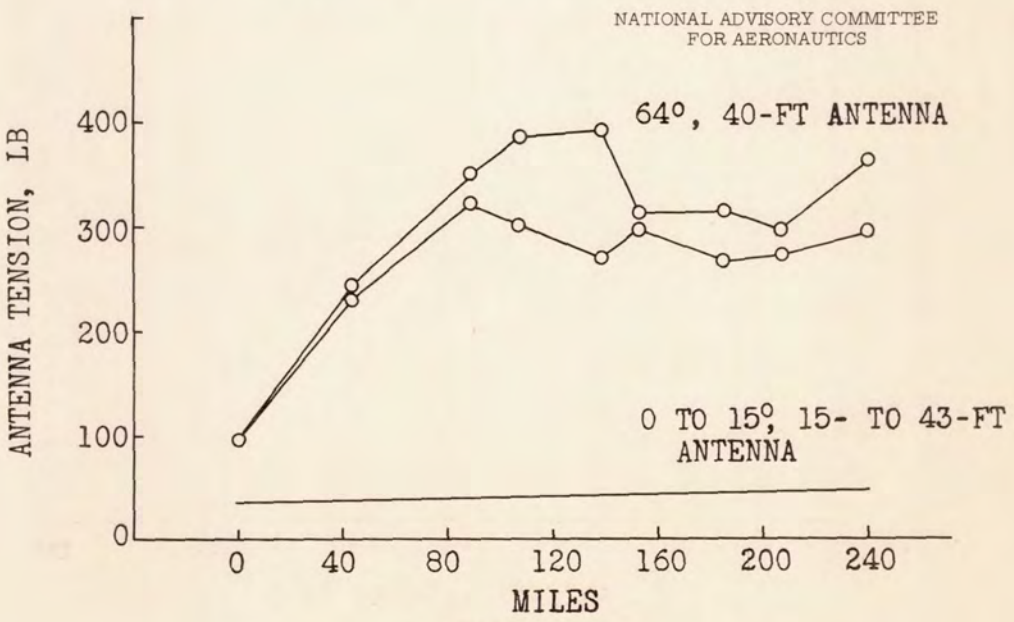

FIGURE 7.

VARIATION OF ANTENNA TENSION WITH ANTENNA ANGLE
ANTENNA LENGTH, 41 FT
DISTANCE TRAVERSED, 115 MILES

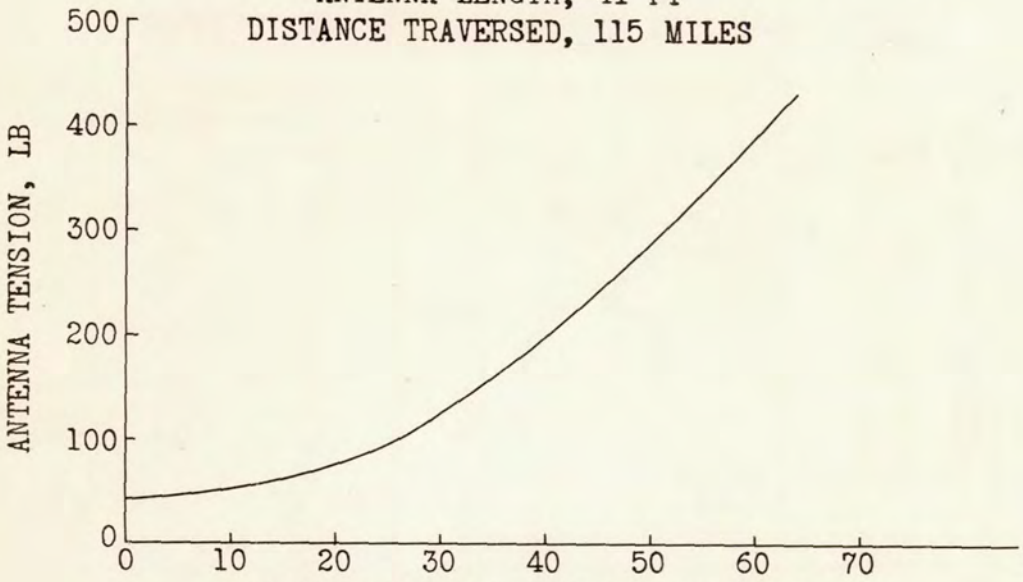

FIGURE 8.

VARIATION OF ANTENNA TENSION WITH ANTENNA LENGTH
ANTENNA ANGLE, 15°
DISTANCE TRAVERSED, 115 MILES

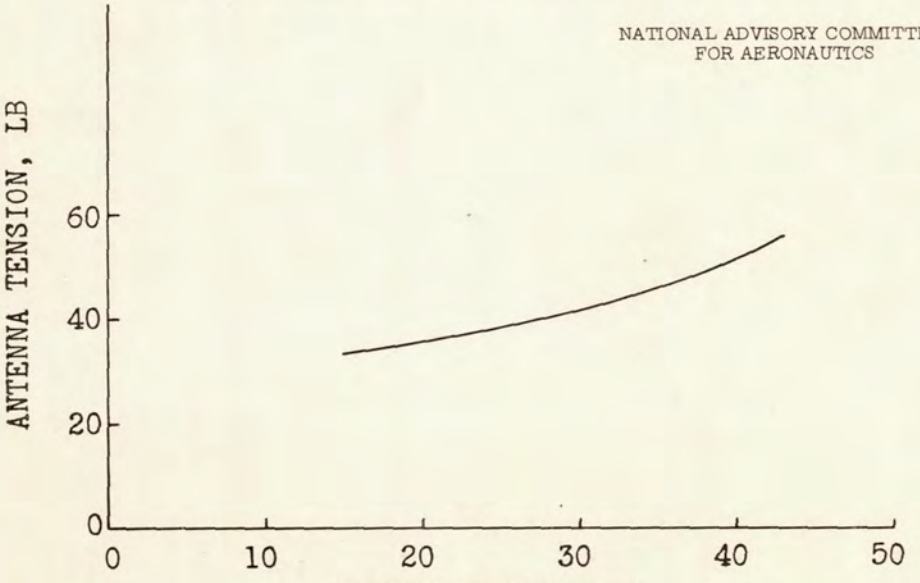

FIGURE 9.

ANALYTICAL STUDY OF THERMAL ICE-PREVENTION SYSTEMS APPLIED TO LIGHT AIRCRAFT

By James G. Thompson

Flight Propulsion Research Laboratory

INTRODUCTION

The thermal ice-prevention system has been adopted for use on commercial transports and large military aircraft and consideration is now given to its practicability on smaller aircraft having a smaller useful load and greater need for economy and simplicity than the larger aircraft. Conveniences and equipment that have long been in use on larger aircraft are today being incorporated in small privately operated aircraft which heretofore were without such advantages. It is therefore anticipated that a serious effort will be made to provide ice protection for small aircraft in the future.

An analytical study was made to determine the thermal requirements of ice-prevention systems for application on three small aircraft with dimensions and specifications covering the range of sizes commonly found in private operation as follows: wing areas of 140, 184, and 250 square feet; sea-level horsepower ratings of 75, 185, and 450 brake horsepower; and cruising speeds of 105, 150, and 205 miles per hour, respectively.

The quantity of heat required for ice prevention on small aircraft has been determined in order that operators may evaluate the penalties in weight, cost, and complications, which must be compensated by the advantages derived from the application of a thermal ice-prevention system. Future industrial progress and research will probably reduce these penalties.

METHOD OF ANALYSIS

The wet-air analysis as developed by Hardy (reference 1) and discussed by Neel in a paper presented previously was used in this investigation. For this analysis, the rate of water impingement was evaluated by a simplified method as developed by Glauert (reference 2), a more rigorous solution is possible by using the method presented previously by Bergrun.

DISCUSSION OF METHOD

Justification for using such a method can be established by comparing heat requirements (which are calculated by use of wet-air method) with the thermal properties of the C-46 ice-research airplane wing section, which has been successfully protected in a wide variety of icing conditions. Sample calculations were made for comparison purposes with the data obtained on the C-46 airplane at the Ames laboratory. The calculations were made for station 159 of the outer wing panel for several icing conditions. The following icing conditions gave results comparable to the heat employed in the C-46 airplane:

Liquid-water content, q_w, gram/cu meter	1
Droplet diameter, d_d, micron	20
Ambient-air temperature, t_o, ^oF	0
Surface temperature, t_s, ^oF	35

These values, which represent very severe icing conditions in light of the data presented by Lewis, gave the average heat required as 1900 Btu per hour per square foot. This quantity compares favorably with the average heat provided for the C-46 airplane wing, which was 1830 Btu per hour per square foot during full heat tests conducted in flight.

The equipment on the C-46 airplane has prevented ice from forming on the wing surfaces when operated in a wide variety of icing conditions, including an extreme case when the liquid-water content was 1.90 grams per cubic meter and the droplet size was 20 microns; therefore, if design conditions of a liquid-water content of 1 gram per cubic meter, droplet size of 20 microns, ambient-air temperature of 0^o F, and a surface temperature of 35^o F are chosen, the calculated heat required should be satisfactory for design purposes and will also be conservative enough to provide a satisfactory factor of safety. These conditions were chosen as the design basis for the calculations in this analysis.

RESULTS AND DISCUSSION

The total heat required in Btu per hour for the fixed lifting surfaces of three typical airplanes is presented in the following table:

Fixed lifting surface	Airplane		
	1	2	3
Wings	48,600	72,300	97,000
Horizontal stabilizer	10,800	28,800	27,000
Vertical fin	4,600	5,400	6,400
Total	64,000	106,500	130,400

The heat required may be obtained from the engine exhaust gases, combustion heaters, or electric generators. By mixing the exhaust gases with air in an air-ejector-cooling and muffling system, a mixture is obtained that possesses heat far in excess of the quantity required for ice prevention. If it is adaptable for reasons of engine cooling and muffling action, this system appears to present desirable characteristics. The required heat may also be obtained from small compact combustion heaters that are available on the commercial market. The leading-edge structure of the airfoil can be altered and the necessary ducting installed for the hot-air heating systems without any appreciable increase in the total weight of the airplane. The use of electric generators on large military or commercial airplanes may be practical but the weight, costs, and loss in engine power involved appear to make its application on small airplanes impractical at this time.

A thermal ice-prevention system designed by wet-air method and values of important parameters assumed in this text will probably provide protection in the most adverse conditions that may be encountered in flight; however, it may not be practical to give all types of airplane this maximum protection. Therefore, with the proper selection of the meteorological variables and the degree of protection desired, which are dictated by the airplane's operating schedule, the total amount of heat required can be significantly reduced. By intermittently heating the components, that is, cycling, the amount of heat that must be supplied at any time can be greatly reduced, thus reducing the large quantities of heat required for protecting all of the components simultaneously.

By limiting the operations to conditions of lesser severity than those for which larger scheduled aircraft must be designed and by taking advantage of savings that may accrue from intermittently heating the various components, it appears that the thermal ice-prevention system may find practical application on small non-scheduled aircraft.

REFERENCES

1. Hardy, J. K.: Protection of Aircraft against Ice. S.M.E. Rep. no. 3380, R.A.E. (British), July 1946.

2. Glauert, Muriel: A Method of Constructing the Paths of Raindrops of Different Diameters Moving in the Neighbourhood of (1) A Circular Cylinder, (2) An Aerofoil, Placed in a Uniform Stream of Air: and a Determination of the Rate of Deposit of the Drops on the Surface and the Percentage of Drops Caught. R. & M. No. 2025, British A.R.C., 1940.

CALCULATION OF HEAT REQUIRED FOR WINDSHIELD THERMAL ICE PREVENTION IN SPECIFIED ICING CONDITIONS

By George H. Holdaway

Ames Aeronautical Laboratory

INTRODUCTION

One part of a broad icing research program conducted by the NACA has been concerned with the investigation of thermal means of windshield ice prevention. The first satisfactory windshield heating system investigated was the double-panel heated-air type of system tested on a Lockheed 12-A airplane, and described by Rodert and others in reference 1. The tests of reference 1 resulted in the tentative specification of a heat-flow requirement of 1000 Btu per hour per square foot through the windshield outer surface. This value was based on data obtained for a flat-pane, V-type windshield at flight speeds up to 150 miles per hour, and applied to internally heated windshields.

Although this initial research provided some information on windshield heat requirements, the results were empirical in nature and could not serve as a fundamental basis for the prediction of the internal heating requirements for windshield configurations and flight conditions different than those investigated. Accordingly, a fundamental investigation was undertaken to establish equations for calculating the heat dissipation from the surface of an internally heated windshield in conditions of icing. By measuring the heat flow from various test windshield surfaces during measured icing conditions and comparing these flows with calculated values, the validity of proposed design equations was investigated and design procedures suitable for the prediction of general windshield heating requirements were established.

In addition to the research directed towards the establishment of the heat requirement in the case where the heating was supplied internally, a secondary investigation conducted at the same time was concerned with the practicability of ice prevention by the means of discharging a jet of heated air into the windshield boundary layer. This device was initially installed in the C-46 airplane (reference 2) as a means of augmenting the internal, double-panel windshield system. The test results with this initial installation were sufficiently promising to warrant further investigation.

The windshield flight investigations conducted by the NACA Ames Aeronautical Laboratory at Moffett Field, Calif., during the winters of 1945-46 and 1946-47 were made in clear air and in natural icing conditions with a twin-engine, C-46 cargo airplane. (See fig. 1.) A detailed report of the windshield data obtained, its analysis, and a method for calculating the heat required for windshield thermal ice prevention are presented in reference 3.

Additional windshields were tested on a four-engine, B-24 bomber-type airplane operated by the NACA Flight Propulsion Research Laboratory at Cleveland, Ohio, during the winter of 1946-47. (See fig. 2.) The detailed results of this latter investigation are presented in reference 4 by Kleinknecht.

DESCRIPTION OF APPARATUS

Both the test airplanes incorporated an NACA thermal ice-prevention system, which permitted continuous operations in natural icing conditions. Meteorological equipment was installed to measure the free-stream air temperature, the water drop size, drop-size distribution, and liquid water content. A description of the meteorological instruments and their use, and typical meteorological data are presented by Lewis in reference 5.

Internally Heated Windshields

Three general types of aircraft windshield were tested to provide fundamental heat-transfer data: flat-plate, flush, and V-type. Figure 3 shows the electrically heated flat-plate and flush test windshields installed on the C-46 airplane during the winter of 1945-46. The flat-plate windshield was intended to supply heat-transfer data for two-dimensional flow over a flat-plate inclined at different angles to the air stream. Provision was made to fix the panel in one of three positions: 30°, 45°, and 60° measured from the tangent to the fuselage at the panel hinge line.

The electrically heated flush windshield was installed in the copilot's panel which, at that time, was flush with the fuselage contours. Construction of the panel consisted of three sheets of glass and two of plastic bonded together. Heating elements of very fine resistance wires were embedded between the outer glass layer and the adjacent plastic layer.

All the windshields tested were instrumented with thermocouples on both the inner and outer surfaces. The temperatures were recorded by a self-balancing automatic-recording potentiometer with an over-all accuracy of ±3° F.

For the 1946-47 operations with the C-46 airplane, the flush windshield was replaced by a V-type windshield. A top view of this windshield installation is shown in figure 4. The windshield center post was sloped at an angle of 57° (measured from the horizontal during cruising flight) and the included angle of the V was 86° measured in the horizontal plane. The fabrication of the pilot's and copilot's panels was the same and consisted of three sheets of glass and interposed sheets of plastic bonded together. One of these special panels is shown in figure 5. Heating of the panels was attained through a transparent electrically conductive surface coated on the outer sheet of glass on the surface adjacent to the plastic inner layer. The panels were purchased commercially. Although the panels were trapezoidal in shape, the heated area was rectangular to insure uniformity of heat distribution.

Figure 6 shows the special forebody section of the B-24 airplane as tested by the Flight Propulsion Research Laboratory. This section incorporated seven windshield panels mounted at angles of 30°, 45°, and 60° to the thrust axis. Several of the windshields were electrically heated and fabricated in a manner similar to the C-46 airplane windshield panels.

External Air-Heated Windshields

Figure 7 shows the external air-heated windshield, thermal ice-prevention system tested on the flush pilot's windshield of the C-46 airplane during the winter of 1945-46. For the 1946-47 operations with the V-type windshield, one 3/16-inch external discharge slot was located along the bottom edge of the pilot's windshield and another along the center post between the windshields with the heated air directed over the pilot's windshield. Each slot was 1 foot in length.

ANALYSIS AND RESULTS

Heating Requirement for Internally Heated Windshields

Inasmuch as the main objective of this investigation was to establish fundamental design equations for the calculation of

windshield heat requirements in specified icing conditions, such equations are presented and are discussed in the light of the test data to establish their usefulness for this purpose.

The unit heat flow from the outer surface of a windshield during flight in icing conditions can be considered as the sum of four individual heat losses, or

$$q = q_1 + q_2 + q_3 + q_4 \tag{1}$$

where

q_1 heat loss due to forced convection

q_2 heat loss due to evaporation

q_3 heat loss due to warming water

q_4 heat loss due to radiation

The values of q represent heat flows per unit of windshield surface area expressed in Btu per hour per square foot. Each of the individual heat losses will be discussed separately and then combined to form a general design equation. (For convenience, all symbols are defined in the appendix.)

Heat loss due to convection. - The following equation expresses the heat loss due to convection from the windshield surface to the free-stream air, including the correction for the kinetic temperature rise:

$$q_1 = h(t_s - t_o - \Delta t_{k,a}) \tag{2}$$

where the temperature rise is obtained from references 6 and 7,

$$\Delta t_{k,a} = \frac{U_o^2 - U_1^2}{2gJc_p} + \frac{rU_1^2}{2gJc_p} \tag{3}$$

or approximately,

$$\Delta t_{k,a} = 0.832r\left(\frac{U_o}{100}\right)^2 \tag{4}$$

The subscript o refers to ambient or free-stream air conditions whereas the subscript 1 refers to local conditions just

outside the boundary layer. Theoretically, the recovery factor r equals Prandtl number to the 1/3 power, for turbulent flow, but the flight data indicated values of r for the test windshields ranging from 0.8 to 0.9.

Several equations for calculating the coefficient of convective heat transfer h from a flat plate have been developed, and a comparison of these equations has been made in reference 6 by the University of California. For a turbulent boundary layer, the general form of the coefficient was presented in the following form:

$$h = 0.0296 \times 3600 \frac{U_1 \gamma c_p}{Pr^{2/3} R^{0.2}} \qquad (5)$$

Following the presentation of equation (5) in reference 6, various specific forms of the equation are derived by expressing the properties of air as a function of the average temperature in the boundary layer. The coefficient at any distance s from the leading edge of a flat plate, for the region of turbulent flow, is given as

$$h = 0.51 \, T_{av}^{0.3} \left(\frac{U_1 \gamma}{s^{0.25}} \right)^{0.8} \qquad (6)$$

For a turbulent boundary layer extending from $s = o$ to $s = l$ on a flat plate, the average coefficient is presented as

$$h = 0.64 \, T_{av}^{0.3} \left(\frac{U_1 \gamma}{l^{0.25}} \right)^{0.8} \qquad (7)$$

In order to evaluate the accuracy of these equations for the calculation of the convective heat-transfer coefficient, a comparison was made of measured and calculated values. Because measured values of the local velocity just outside the boundary layer U_1 were available only at the center of the test panels, the equation for calculating the value of the heat-transfer coefficient at a point, rather than the average equation, was used in the computations. A comparison of measured values of the coefficient with values calculated by equation (6), for the 45° position of the flat-plate panel, is presented in figure 8. Two widely different values of s were used in the calculations: s_1 representing the distance from the panel hinge to the center of the panel, and s_2 the distance from the center of the panel

to the stagnation point at the nose of the airplane fuselage. The two computed curves bracket the experimental curve with the lower value of s providing the larger values of h. The curves presented are typical of the results obtained for other panel angles and for the flush windshield, and the agreement is considered to be satisfactory for design purposes. In the case of the V-type windshield installation, the local velocity over the windshield was not measured and hence calculation of the local heat-transfer coefficient was not attempted. For design application, the lower value of s should provide heat-transfer coefficients that would probably be somewhat larger than the true case, but would be conservative. Although comparisons were not made between measured values of the average heat-transfer coefficient and values calculated by equation (7), it is considered that the order of accuracy would be the same as that associated with equation (6).

In an attempt to establish the accuracy of the equations for the prediction of the heat requirement, it is desirable to utilize the most accurate available values of h. The test values obtained in clear air were not applicable in most cases, because corresponding clear-air data were not available for all the icing tests. The alternative employed was to determine the value of s that would provide the best average agreement between calculated and measured values of h at the center of the windshields, and then multiply that coefficient by a factor to give the average convective coefficient for the entire windshield. Consideration of the two equations, which have been presented for the average coefficient and the coefficient at a point on the surface, indicates that the average value can be taken as approximately 1.1 times the value at the center of the panel.

Heat loss due to evaporation. - The heat loss due to evaporation may be calculated by the equation

$$q_2 = 0.622hL_s \left(\frac{e_s - e_o}{c_p P_o}\right) \qquad (8)$$

This equation is presented in the analysis by Hardy in reference 7. It is based on the assumption that the windshield surface is fully wetted, and inasmuch as this condition requires the maximum heat supply to maintain a given surface temperature, it is chosen for design. Because water runback from the heated windshield area is of little consequence, no effort was made in the calculations to evaporate all the water intercepted by the windshield. In addition, such a requirement would impose an exorbitant heating load in some cases.

Heat loss due to warming impinging water. - The heat loss due to warming the impinging water is expressed by the equation

$$q_3 = Mc_{p,w} (t_s - t_o - \Delta t_{k,w}) \tag{9}$$

where

$$\Delta t_{k,w} = \frac{U_o^2}{2gJc_{p,w}} = 0.198 \left(\frac{U_o}{100}\right)^2$$

and M is the average weight rate of water impingement per unit area of windshield and is given for flat-plate windshields as

$$M = 0.225 \frac{\eta}{100} U_o m \frac{A_p}{A} \tag{10}$$

where $\frac{A_p}{A}$ is the ratio of the projected area of a windshield to its actual area, and m is the liquid water content of the air in grams per cubic meter.

The determination of the amount of water striking a windshield in a given time interval is a problem regarding which very little information is available. The most recent and extensive treatment of water-drop trajectories around several generalized objects is presented by Langmuir and Blodgett in reference 8. Although this investigation was undertaken primarily to estimate the rate of water impingement on an airfoil, some trajectory calculations are presented for the cases of a ribbon (or flat plate normal to the direction of air flow) and a sphere. These calculations were used herein to approximate the efficiency of water impingement η on the flat-plate windshield (using ribbon data) and the flush windshield (using sphere data).

By considering first the case of the flat-plate panel, the assumption was made that the rate of water impingement on the panel would be equal to the rate of impingement on the projected area of the panel considered as one-half of a ribbon, as shown in figure 9. The efficiency of water impingement η and the weight rate of water impingement w for various drop sizes have been approximated for the three positions of the flat-plate panel from the ribbon data by Langmuir and Blodgett (reference 8) and are presented in table I. It is of interest to note that, for drop diameters greater than 30 microns, as the panel angle is reduced (panel becoming more flush with the fuselage) the

impingement efficiency is increased but the weight rate of water interception is decreased. A second item of interest is the fact that the maximum calculated efficiency of water impingement was 80 percent, and this value corresponds to exceedingly large drops for most icing conditions. This result is somewhat surprising, and possibly in error, because it would appear that the presence of the fuselage forward of the windshield would cause a concentration of drops near the surface and produce impingement efficiency values of possibly greater than 100 percent.

To obtain an estimation of the rate of water impingement on the flush windshield, the assumption was made that the impingement would be the same as that on a portion of a sphere having a diameter equal to the fuselage maximum diameter. (See fig. 10.) The flush test panel was located between the angles A (13.5°) and B (27.5°). The assumption was made that, for water drop sizes of sufficient diameter to cause the area of impingement to include the flush test panel, the water intercepted per unit area of the panel would be approximately equal to the average weight rate of water intercepted over the entire area of impingement on the nose of the airplane. On the basis of this assumption, the previous equation for the weight rate of water impingement used for flat-plate windshields was modified to become

$$M = 0.225 \frac{\eta}{100} \frac{U_o m}{C(1 - \cos \theta_M)} \qquad (11)$$

where θ_M is half of the central angle of the total area of impingement on a spherical surface, and C is the radius of the sphere. Calculated values of water impingement on the flush windshield tested on the C-46 airplane for one flight condition are presented in table II. An interesting conclusion resulting from an inspection of table II is that, for the conditions presented, drop diameters of 50 microns are required in order to give a value of θ_M of sufficient magnitude to reach the test panel, which is in agreement with the observations of water impingement on the C-46 flush windshield in icing conditions. The drops were observed to strike the windshield only during flights for which the meteorological data indicated the presence of a mean effective drop size of 30 microns in diameter or larger. The maximum drop diameter in these clouds was probably in the range of 40 to 50 microns, or greater.

Heat loss due to radiation. - The heat loss due to radiation from the windshield surface to the surrounding atmosphere can be calculated from the Stefan-Boltzman equation

$$q_4 = 0.173\epsilon\left[\left(\frac{T_s}{100}\right)^4 - \left(\frac{T_o}{100}\right)^4\right] \quad (12)$$

Although a windshield radiates heat to the atmosphere, the amount is small for the temperatures associated with windshield thermal ice prevention and can usually be neglected.

Summation of heat losses. - Combining equations (1) to (12), the complete equation for the dissipation of heat from a windshield surface is written as

$$q = h\left[t_s - t_o - 0.832r\left(\frac{U_o}{100}\right)^2\right] + 0.622hL_s\left(\frac{e_s-e_o}{c_p P_o}\right)$$

$$+ Mc_{p,w}\left[t_s-t_o-0.198\left(\frac{U_o}{100}\right)^2\right] + 0.173\epsilon\left[\left(\frac{T_s}{100}\right)^4 - \left(\frac{T_o}{100}\right)^4\right] \quad (13)$$

Equation (13) was simplified by neglecting the heat loss due to radiation and the kinetic temperature rise of the impinging water. This latter factor is not effective for flight speeds under 200 miles per hour. A regrouping of the remaining terms was made to segregate the primary heat losses, which are due to convective heat transfer and evaporation, from the secondary effects of heating the impinging water and kinetic heating of the air. Thus, the simplified form of equation (13) becomes

$$q = hX(t_s-t_o) + M(t_s-t_o) - 0.832hr\left(\frac{U_o}{100}\right)^2 \quad (14)$$

where

$$X = 1 + \frac{0.622L_s}{c_p P_o}\left(\frac{e_s-e_o}{t_s-t_o}\right) \quad (15)$$

A grouping similar to equation (15) was used by Hardy in reference 9.

Comparison of calculated and measured heat flows from surface of internally heated windshield. - The applicability of equation (14) for the determination of windshield heating requirements can be evaluated best by a comparison of calculated and measured values of heat flow from a windshield surface, for the same surface temperature, and for specific flight and icing conditions.

Table III presents some representative data for each angle of the flat-plate panel and for the V-type windshield, as tested on the C-46 airplane. The drop sizes listed are the mean-effective water-drop diameters expressed in microns, with the exception for the 45° position of the flat plate; for this case the value is for the maximum drop size. For purposes of calculation, the drop-size distribution was assumed to be uniform. The surface temperatures are the arithmetical average of the recorded values for the several thermocouples on the surfaces. The quantity q_c is the calculated heat flow to the outer surface of the windshield required to produce the indicated average surface temperature, and q_E is the measured heat flow. The difference between these values divided by the calculated heat flow gives a percentage indication of the validity of the design equation for predicting windshield heat requirements. The fact that the calculated values of q for the V-type windshield are considerably higher than the experimental values may be attributed, in part, to the fact that the local velocity over the windshield was not measured and therefore the free-stream velocity was used to calculate the average convective heat-transfer coefficient.

The few instances in which icing of the flush test panel occurred provided very limited data for a comparison of the calculated and measured values of the heat requirement. Only for one case was the surface sufficiently wetted to give reliable data, and the calculated heat flow was 12 percent greater than the measured heat flow.

In order to obtain further verification of the accuracy of the general design equation for the prediction of windshield heating requirements, a comparison was made between measured and calculated heat flows for the 60° windshield on the B-24 airplane. In the calculations, the values of convective heat-transfer coefficient derived for the 60° flat panel on the C-46 airplane were used. The results of this comparison are shown in table IV. The experimental data were obtained from reference 4. The values of measured heat flow q_E presented in table IV represent the net heat supplied to the outer surface of the test windshield, and were obtained by calculating the inward heat flow to the windshield compartment and subtracting this value from the total heat input listed in table I of reference 4.

Greater accuracy in the calculated heat flows could be attained if the drop-size distribution were used, but the distribution was not always known and the inaccuracy of other experimental factors did not warrant this refinement.

Prediction of minimum requirements for internally heated windshields. - Having shown that the general design equation is applicable for the calculation of windshield heating requirements, provided various components of the equation can be evaluated, it is of interest to utilize the equation to investigate the heat requirements for various windshield configurations in icing conditions that might be selected as design requirements. An indication of the meteorological conditions corresponding to typical icing and to the most probable maximum icing to be expected in all weather transport operations was obtained from a report by Lewis (reference 5). For each of the two general cloud types (cumulus and stratus), factors were selected that corresponded to a moderate icing condition. A water drop-size distribution E was chosen to allow for the variation in the size of the drops existing in many moderate icing conditions. Table V presents the calculated minimum requirements for ice prevention on three types of internally heated windshield for the selected moderate icing condition. The heat flows are minimum values required to keep the windshield surface temperature just at 32° F.

From this table, the previous empirical heating requirement of 1000 Btu per hour per square foot of windshield surface (reference 1) is seen to provide adequate protection for V-type windshields in moderate stratus for flight speeds as great as 300 miles per hour. In the case of the moderate cumulus cloud, however, this quantity of heat flow would not be adequate for complete and continuous protection even at a speed of 150 miles per hour. There is some question as to whether complete and continuous windshield ice protection is required in cumulus clouds, because such formations can usually be avoided and are not a problem to the same extent as extensive, thick banks of stratus at low altitudes. For military flying, however, the desirability of complete visibility at all times is evident.

In considering the individual contribution to the total heat requirement of each of the meteorological factors that constitute icing conditions, the powerful effect of changes in the value of free-stream air temperature is noted. As an illustration of this effect, consider the increase in heating requirement shown in table V for the flat-plate windshield from 540 to 1040 Btu per hour per square foot as a result of (1) increasing the mean drop diameter by 5 microns, (2) doubling the liquid water content, and (3) decreasing the free-stream air temperature by 15° F. By utilization of the design equations, it can be shown that the 500-Btu-per-hour-per-square-foot increase is composed of 13 percent increase due to increased drop size and liquid water content,

and 87 percent due to the change in the free-air temperature. This fact leads to the conclusion that once the windshield heat requirement has been established for a specified icing condition, and assuming the condition is severe enough to completely wet the windshield surface, changes in drop size and liquid water content will not change the heating requirement appreciably. A change in free-air temperature, however, will have a very noticeable effect on the heating requirement.

Heating Requirement of External-Discharge Windshields

An analytical approach to the external-discharge type of windshield thermal ice-prevention system was attempted, but the unknowns involved, such as the mixing of the heated jet with the boundary-layer air, precluded a reasonable prediction of the action of this system. The next approach involved measurements of the velocity and temperature profiles during flight tests in the hope that a basis for the establishment of empirical design equations would result. Unfortunately, a review of the data did not reveal any basis for a rational analysis of the mixing of the jet with the boundary-layer air and the prediction of the resultant surface-temperature rise.

A few items of interest, however, were noted during the investigation. One of these items was the large amount of heat supply required for ice protection by the external-discharge method in comparison with internal heating of the surface. For example, figure 11, which is a photograph of the flush windshields of the C-46 airplane from inside the cockpit, illustrates a flight in which the windshield area under the discharge jet was maintained clear with a heat supply of 20,000 Btu per hour, which is an approximate unit heat flow of 10,000 Btu per hour per square foot of cleared surface. In the same icing condition, ice accretions were removed from the electrically heated flush panel with a heat flow to the outer surface of 545 Btu per hour per square foot. Thus the external-discharge system required a heat supply approximately 20 times that required for the internally heated system, for the same degree of protection in the same icing condition.

Figure 12 shows that the thermal inefficiency of the external-discharge system is apparently the result of rapid mixing of the discharge jet with the cold boundary layer, with a resultant rapid decrease in the jet and windshield surface temperature. The data were obtained during flight tests of the flush windshields on the C-46 airplane, and y represents the distance measured from the surface into the boundary layer or heated-air jet. The surface-

temperature data in this figure indicate a decrease of the surface temperature from 160° F at the discharge slot to a value of 42° F at a distance of only 6 inches from the point of discharge.

Satisfactory operation of the external-discharge system for the V-type windshield was not obtained because of failure of the jet to flow across the entire surface. Figure 13 illustrates a typical ice-removal attempt, with a heat supply of 18,000 Btu per hour through the heated-air jets. A small area along the bottom of the pilot's windshield, and also at the center post, has been cleared by the jet, but the rest of the panel is covered by an ice formation. Attempts to remove the ice by increasing the flow rate and temperature of the heated air were limited by the temperature restrictions of the vinyl plastic at the lower edge of the windshield.

The external-discharge system of windshield ice prevention appears to be a desirable installation only in those instances where (1) internal heating is not possible, (2) a large supply of heated air is available in the region of the windshield to be protected, and (3) the discharged air will flow over the windshield without the additional weight penalty of blowers.

CONCLUSIONS

The following conclusions are based on the analytical studies and test data of this research and should be applicable to windshield configurations and icing conditions similar to those investigated:

1. The coefficient of convective heat transfer for the external surface of flat-plate, V-type, or flush windshields can be approximated with an accuracy suitable for design purposes by the use of the established equations for turbulent flow on a flat plate.

2. The heat requirement for ice prevention on a flush or flat-plate airplane windshield during flight in specified icing conditions can be calculated to an accuracy of 20 percent.

3. The complete and continuous prevention of ice accretions on the surface of a flat-plate or V-type airplane windshield, for flight in moderate cumulus icing conditions at speeds up to 300 miles per hour, will require a heat flow from the surface of from 2000 to 2500 Btu per hour per square foot of surface. In

the case of continuous flight for the same speed range, in moderate stratus conditions, a heat flow of 1000 Btu per hour per square foot should prove adequate.

4. The complete and continuous prevention of ice accretions on the surface of a flush-type airplane windshield located well aft of the fuselage stagnation region, for a speed range up to 300 miles per hour in stratus and moderate cumulus conditions, can be obtained with a heat flow of 1000 Btu per hour per square foot of surface.

5. The tendency of ice to accrete on windshields that are installed flush with the fuselage contours is considerably less than for V-type windshields.

6. The external-discharge system of windshield thermal ice prevention is thermally inefficient and requires a heat supply approximately 20 times that required for an internal system having the same performance.

7. Windshield installations that conform to the fuselage contours are more adaptable to the use of the external-discharge system than V-type installations, because the heated jet will flow naturally over the windshield surface.

APPENDIX - SYMBOLS

The following nomenclature is used throughout this report:

A	windshield surface area, sq ft
A_p	projected windshield area, sq ft
C	radius of sphere, ft
c_p	specific heat of air, Btu/(lb)($^\circ$F)
$c_{p,w}$	specific heat of water, Btu/(lb)($^\circ$F)
D	characteristic length used in calculating Reynolds number, ft
e	water vapor pressure, in. Hg
g	acceleration due to gravity, ft/sec^2
h	convective heat-transfer coefficient, Btu/(hr)(sq ft)($^\circ$F)
J	mechanical equivalent of heat, ft-lb/Btu
L_s	latent heat of evaporation at surface temperature, Btu/lb water
l	length of windshield panel or flat plate in direction of local air flow, ft
M	weight rate of water impingement per unit area, lb/(hr)(sq ft)
m	liquid water content of air, grams/cu meter
P	barometric pressure, in. Hg
Pr	Prandtl number $\left(\frac{3600 c_p \mu g}{k}\right)$
q	unit rate of heat flow, Btu/hr/sq ft
R	Reynolds number $\left(\frac{\gamma UD}{\mu g}\right)$
r	recovery factor equal to $Pr^{1/3}$ for turbulent flow

s distance from region of air stagnation, ft

T temperature, ^{o}F absolute

t temperature, ^{o}F

U velocity, ft/sec

w weight rate of water impingement, lb/hr

X evaporation factor, $1 + \frac{0.622L_s}{c_p P_o}\left(\frac{e_s - e_o}{t_s - t_o}\right)$

y distance normal to the windshield surface, in.

α angle between plane of a flat-plate windshield and plane normal to streamlines around forebody of windshield, deg

γ specific weight of air, lb/cu ft

$\Delta t_{k,a}$ kinetic temperature rise of air, ^{o}F

$\Delta t_{k,w}$ kinetic temperature rise of water droplets, ^{o}F

ϵ emissivity of windshield panel

η efficiency of water impingement, percent

θ_M one-half the central angle of total area of impingement on spherical surface, deg

μ viscosity of air, (lb-sec)/sq ft

Subscripts:

av average conditions

c calculated values

E measured or experimental values

o ambient or free-stream air conditions

l local conditions just outside boundary layer

s windshield external-surface conditions

REFERENCES

1. Rodert, Lewis A., Clousing, Lawrence A., and McAvoy, William H.: Recent Flight Research on Ice Prevention. NACA ARR Jan. 1942.

2. Selna, James, Neel, Carr B., Jr., and Zeiller, E. Lewis: An Investigation of a Thermal Ice-Prevention System for a C-46 Cargo Airplane. IV - Results of Flight Tests in Dry-Air and Natural-Icing Conditions. NACA ARR No. 5A03c, 1945.

3. Jones, Alun R., Holdaway, George H., and Steinmetz, Charles P.: A Method for Calculating the Heat Required for Windshield Thermal Ice Prevention Based on Extensive Flight Tests in Natural Icing Conditions. NACA TN (to be pub.).

4. Kleinknecht, Kenneth S.: A Flight Investigation of the Prevention of Ice on Aircraft Windshields. NACA RM (to be pub.).

5. Lewis, William: A Flight Investigation of the Meteorological Conditions Conducive to the Formation of Ice on Airplanes. NACA TN (to be pub.).

6. Boelter, L. M. K., Grossman, L. M., Martinelli, R. C., and Morrin, E. H.: Comparison of Several Methods of Calculating Heat Losses from Airfoils. XXIX - An Investigation of Aircraft Heaters. Univ. Calif., August 1944.

7. Hardy, J. K.: Protection of Aircraft against Ice. Rep. No. SME 3380., R.A.E., July 1946.

8. Langmuir, Irving, and Blodgett, Katherine B.: A Mathematical Investigation of Water Droplet Trajectories. General Electric Co., 1945.

9. Hardy, J. K.: An Analysis of the Dissipation of Heat in Conditions of Icing from a Section of the Wing of the C-46 Airplane. NACA ARR No. 4I11a, 1944.

TABLE I - CALCULATED VALUES OF WATER IMPINGEMENT ON A FLAT-PLATE PANEL, BASED ON DATA CALCULATED FOR RIBBONS

Drop diameter (microns)	Panel angle 60°		Panel angle 45°		Panel angle 30°	
	η, (percent)	w, (lb/hr)	η, (percent)	w, (lb/hr)	η, (percent)	w, (lb/hr)
10	0	0	0	0	0	0
20	1	0.64	2	1.04	5	1.84
30	15	9.6	20	10.4	32	11.8
50	45	28.8	50	26.1	60	22.1
100	73	46.6	75	39.0	80	29.5

Pressure altitude, 10,000 ft Ambient-air temperature, 0° F

True airspeed, 150 mph Area of panel, 1.49 sq ft

NATIONAL ADVISORY COMMITTEE
FOR AERONAUTICS

TABLE II - CALCULATED VALUES OF WATER IMPINGEMENT ON A FLUSH WINDSHIELD PANEL, BASED ON DATA CALCULATED FOR SPHERES

Drop diameter (microns)	η, (percent)	θ_M (deg)	Sphere w (lb/hr)	Flush panel w (lb/hr)	Flush panel M (lb/hr)/(sq ft)
20	0	0	0	0	0
30	<1	3	<18	0	0
50	3	16	54	8.4	7.2
70	8	28	144	7.4	6.4
100	15	45	270	5.5	4.8

Pressure altitude, 10,000 ft

True airspeed, 150 mph

Ambient-air temperature, 0° F

NATIONAL ADVISORY COMMITTEE
FOR AERONAUTICS

TABLE III - COMPARISON OF CALCULATED AND MEASURED HEAT FLOW, FROM THE OUTER SURFACE OF THE TEST WINDSHIELDS, C-46 AIRPLANE

Item	Altitude (ft)	True air-speed (mph)	t_o (^oF)	m (gm/m^3)	Drop size (micron)	t_s (^oF)	q_c (Btu/(hr)(sq ft))	q_E (Btu/(hr)(sq ft))	$\frac{q_c - q_E}{q_c} \times 100$
30	11,650	180	17	0.5	18	39	1210	1240	-3
45	12,700	140	-2	1.0	44	37	1580	1720	-9
60	10,300	170	20	0.2	48	53	1250	1205	4
V	5,000	156	21	0.37	19	39	830	670	19
V	19,500	150	-12	0.22	24	27	1340	1030	23

NATIONAL ADVISORY COMMITTEE
FOR AERONAUTICS

TABLE IV - COMPARISON OF CALCULATED AND MEASURED HEAT FLOW, FROM THE OUTER SURFACE OF THE TEST WINDSHIELDS, B-24 AIRPLANE

Item	Altitude (ft)	True air-speed (mph)	t_o (^oF)	m (gm/m^3)	Drop size (micron)	t_s (^oF)	q_c (Btu/(hr)(sq ft))	q_E (Btu/(hr)(sq ft))	$\frac{q_c - q_E}{q_c} \times 100$
60	3200	157	16	0.28	8.5	51	1175	1165	1
60	2800	152	26	0.20	11	62	1420	1140	20
60	4000	155	24	0.51	10	42	540	500	7
60	9700	225	19	0.24	18	36	525	510	3
60	9900	191	20	0.12	18	48	990	990	0

NATIONAL ADVISORY COMMITTEE
FOR AERONAUTICS

TABLE V - CALCULATED MINIMUM WINDSHIELD HEAT REQUIREMENTS FOR A MODERATE ICING CONDITION IN TWO TYPES OF ICING CLOUD, BASED ON AN ASSUMED DROP-SIZE DISTRIBUTION E

Condition	Cloud type	t_o (^oF)	m (gm/m^3)	Drop size (micron)	True air-speed (mph)	q, (Btu/hr)(sq ft)		
						Flush panel	Flat panel	V-type panel
I	Stratus	15	0.5	15	150	0	540	675
I	Stratus	15	0.5	15	300	410	560	700
II	Cumulus	0	1.0	20	150	800	1040	1440
II	Cumulus	0	1.0	20	300	1120	1630	2100

Pressure altitude, 10,000 ft

Surface temperature, 32^o F

Flat-plate angle, 45^o

NATIONAL ADVISORY COMMITTEE
FOR AERONAUTICS

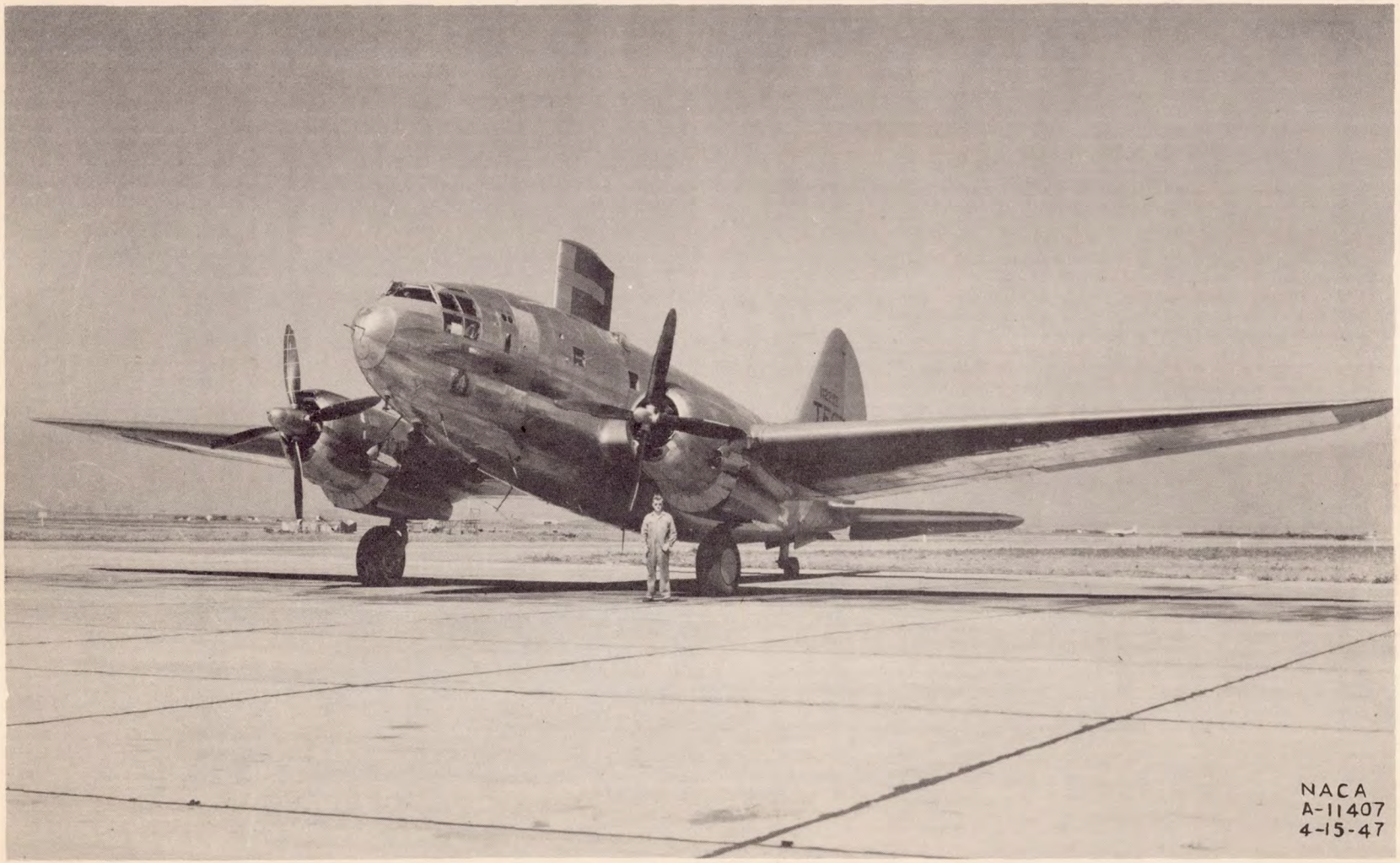

Figure 1.- The C-46 airplane as equipped for icing flight research and operated by the Ames Aeronautical Laboratory during the winter of 1946-47.

Figure 2.- The B-24 airplane as equipped for icing flight research and operated by the Flight Propulsion Research Laboratory during the winter of 1946-47.

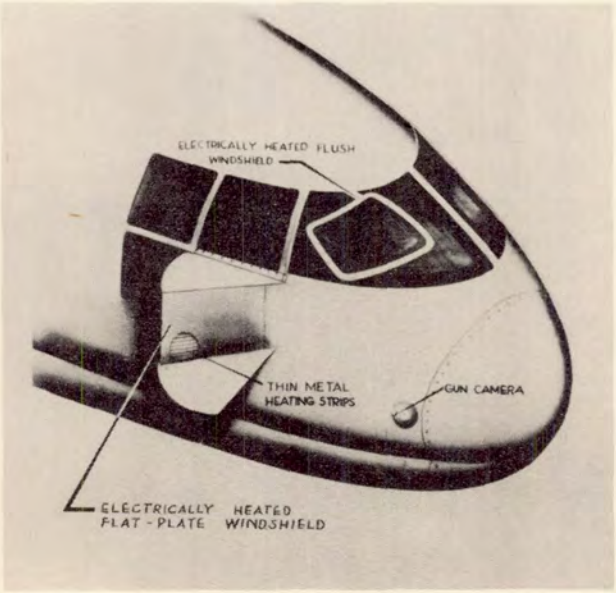

Figure 3.- Adjustable flat-plate and flush windshield test panels as installed on the C-46 airplane for the winter of 1945-46.

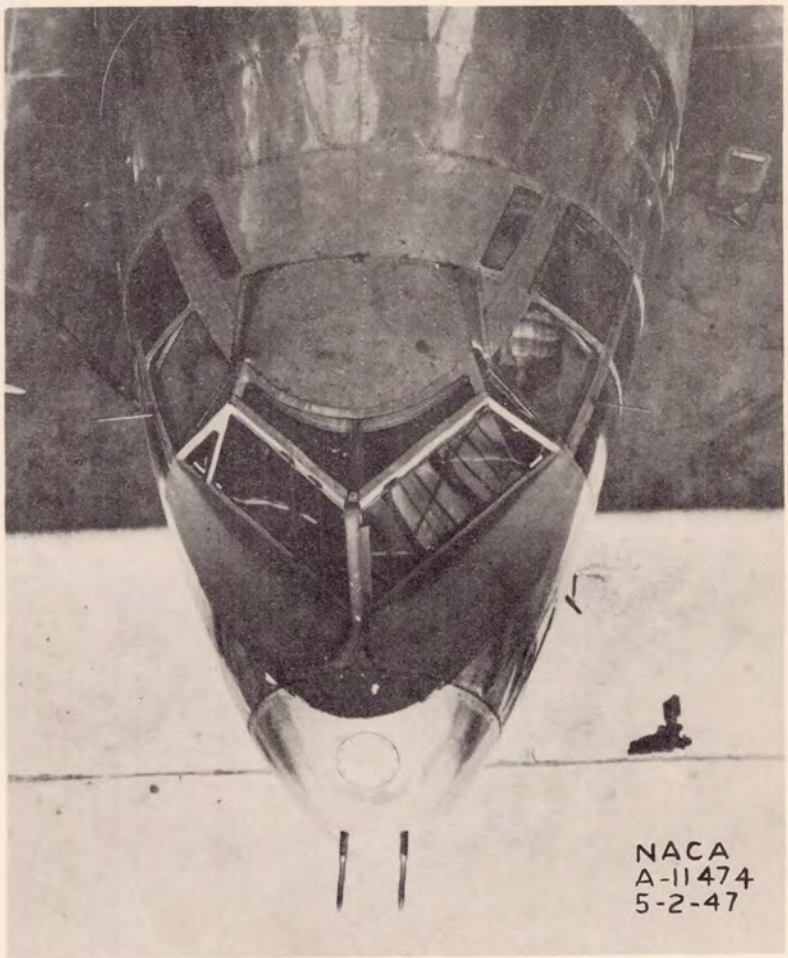

Figure 4.- A top view of the V-type electrically heated windshield installed on the C-46 airplane during the winter of 1946-47.

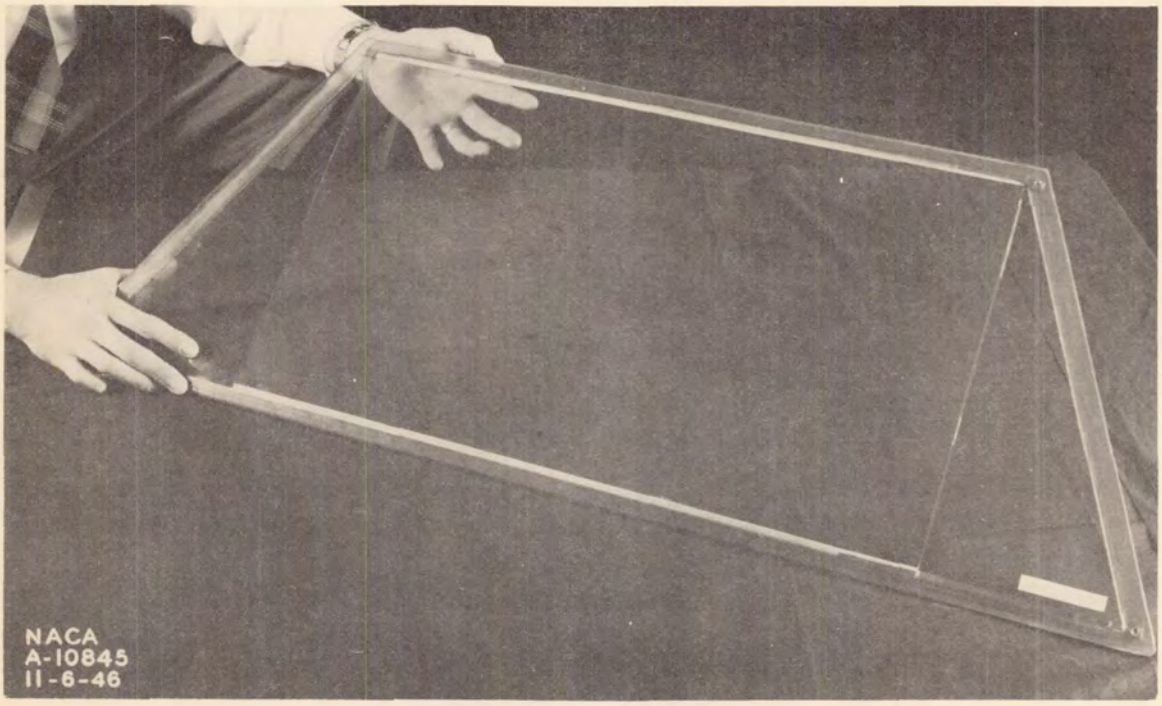

Figure 5.- Single panel from the V-type windshield installation. Heating was provided by a transparent, electrical conducting film under the outer glass layer.

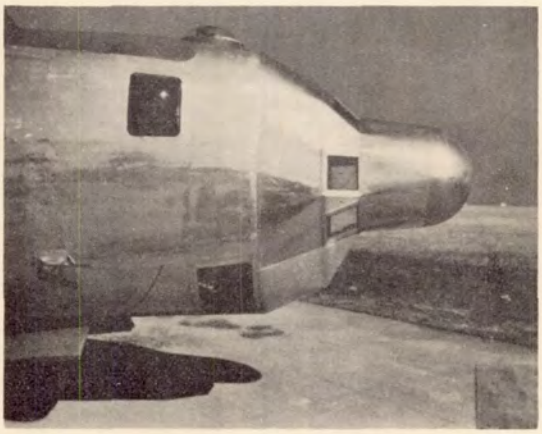

Figure 6.- General arrangement of windshield panels as tested on the B-24 airplane during the winter of 1946-47.

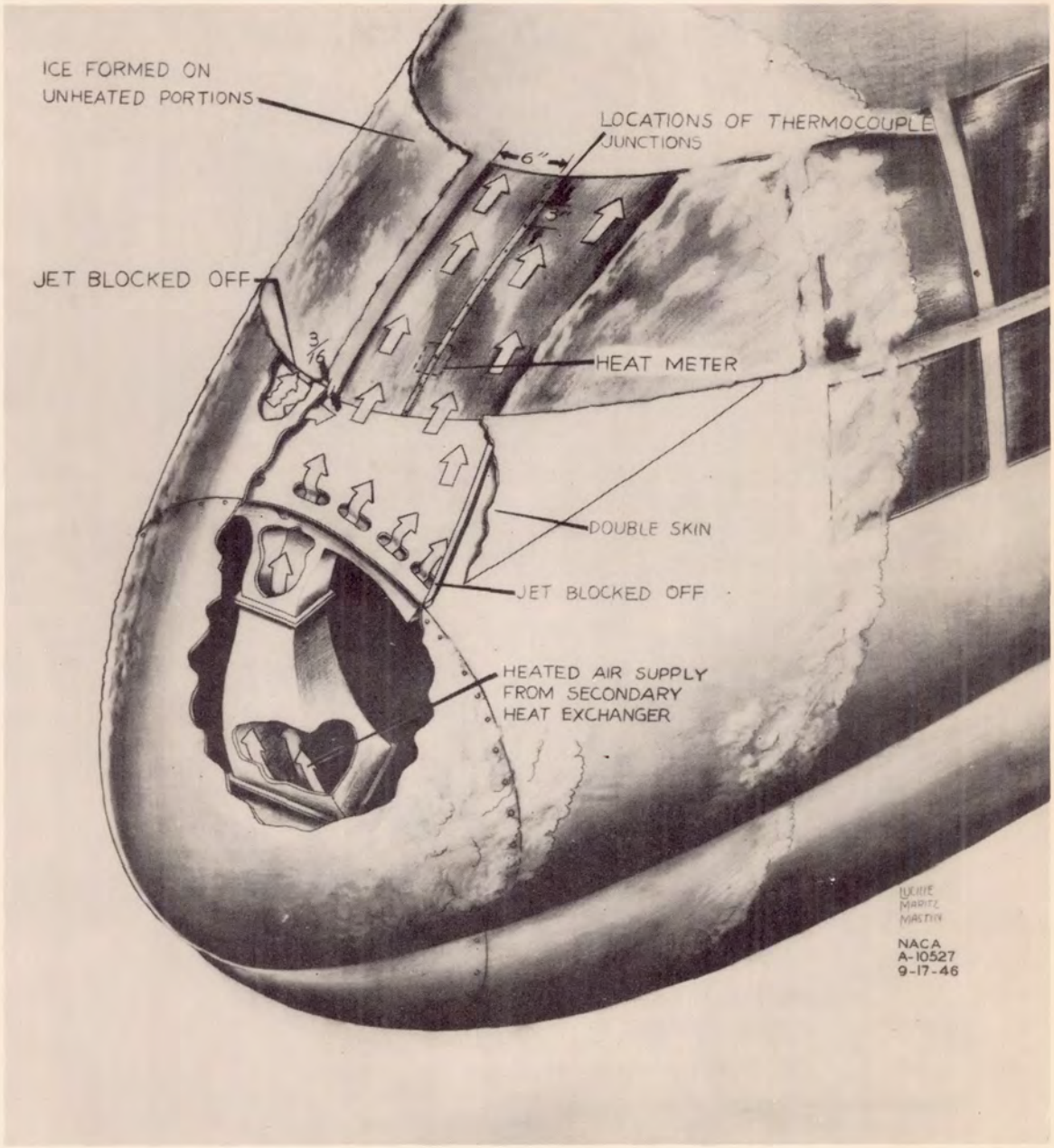

Figure 7.- Details of external discharge heated-air ice-prevention system for the flush windshield of the C-46 airplane.

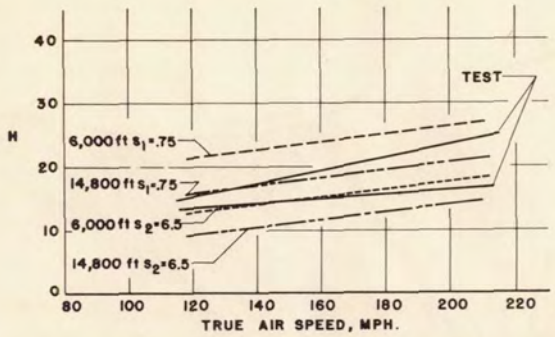

VARIATION OF HEAT TRANSFER COEFFICIENT, H, WITH AIR SPEED

Figure 8.- Comparison of measured and calculated convective heat-transfer coefficients for the flat-plate panel set 45° from the tangent to the fuselage. C-46 airplane, winter 1945-46.

NATIONAL ADVISORY
COMMITTEE FOR AERONAUTICS

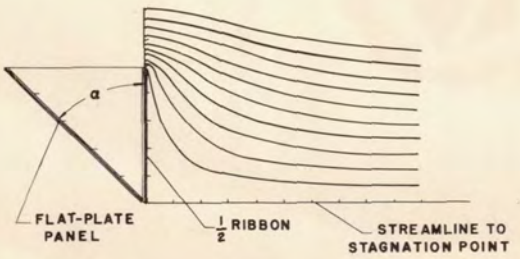

FLOW LINES AROUND PROJECTED AREA OF FLAT-PLATE PANEL USED IN COMPUTING RATE OF IMPINGEMENT

Figure 9.

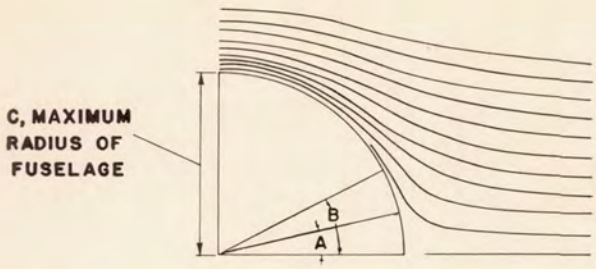

FLOW LINES AROUND A SPHERE, SHOWING INTERNAL ANGLE USED IN COMPUTING RATE OF IMPINGEMENT ON THE FLUSH PANEL

Figure 10.

Figure 11.- Flush windshield of C-46 airplane showing ice protection afforded by the external heated-air jet, left side, and the electrically heated flush panel, right side.

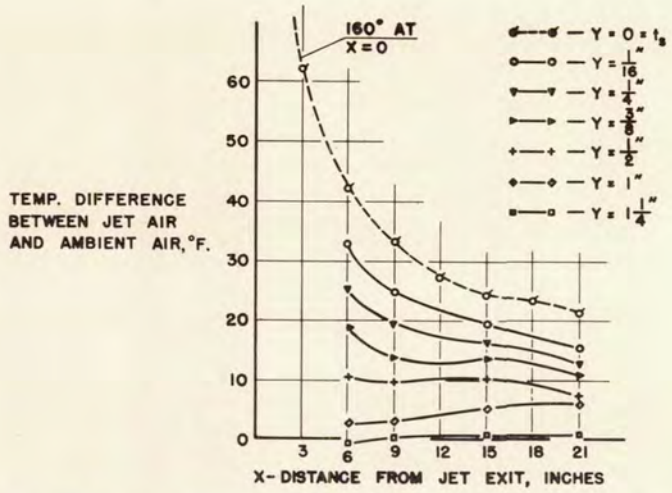

Figure 12.- Temperature gradients in the heated boundary layer over the flush windshield of the C-46 airplane. Pressure altitude 12,000 feet, true airspeed 155 miles per hour, and heated air supplied 13,000 Btu per hour. Winter 1945-46.

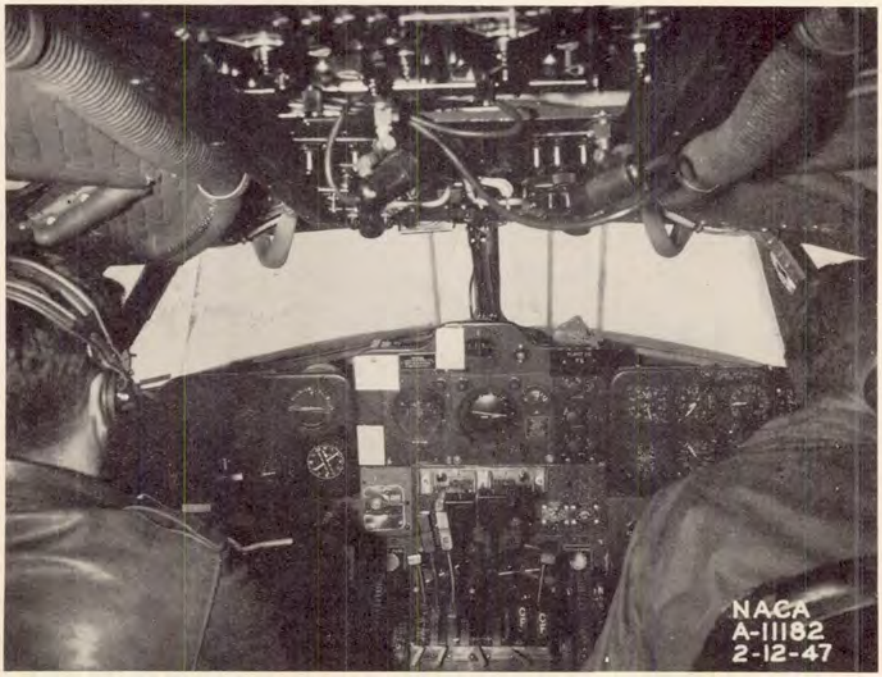

Figure 13.- V-type windshield of C-46 airplane during flight in icing conditions showing unsuccessful ice-removal operation of external discharge jets over pilot's panel, with heat supply of 18,000 Btu per hour.

SUMMARY OF INDUCTION-SYSTEM ICING-PROTECTION REQUIREMENTS FOR RECIPROCATING-ENGINE POWER PLANTS

By Willson H. Hunter

Flight Propulsion Research Laboratory

INTRODUCTION

The purpose of this paper is to summarize NACA research in the field of induction-system icing and to review recommendations that should result in inherently ice-free induction systems.

The formation of ice in engine air-intake systems has been a recognized hazard since 1921 when ice was rated as a predominant cause of power failure resulting in airplane crashes. Induction-system icing has remained a serious hazard despite the development of relatively ice-free carburetors and despite rigid civil and military regulations requiring alternate or heated-air intakes and alcohol sprays for emergency de-icing. The Civil Aeronautics Administration report of 195 accidents in 1945 involving personal aircraft clearly emphasizes the need for aggressive action in the elimination of this hazard. In 1940, as operations through inclement weather began to increase, the Air Transport Association recognized the need for a better understanding of the causes, effects, and prevention of induction-system icing and requested the NACA to study the problem.

Research was started in 1941 under the direction of a special NACA subcommittee in the Altitude Engine Testing Laboratory of the National Bureau of Standards. In 1943 the work was transferred to newly completed research facilities at the NACA Cleveland laboratory with a more comprehensive program under Army sponsorship. The NACA research program included laboratory determination of icing characteristics and de-icing requirements for representative carburetor-supercharger combinations, dynamometer measurements of the effects of ice on engine operation, icing-research-tunnel studies of several protected air-intake scoops, altitude air-box experiments with alcohol de-icing systems, and flight research under natural and simulated icing conditions. The detection of ice by means of special ice-warning instruments was investigated and a study was made of methods for eliminating the icing problem by suitable design of the air entrance, the throttles, and the fuel-injection device.

Research is now in progress to determine the icing characteristics of light-airplane induction systems in order to determine the criterions for an inherently ice-free system.

Appreciation is extended to the participating airlines, manufacturers, and government agencies for the excellent cooperation and material support throughout this research program.

DESCRIPTION OF REPRESENTATIVE INDUCTION SYSTEMS

The induction system of an aircraft engine includes all elements and accessories of the air duct from the main air-intake scoop to the intake valve on the engine cylinder. The possible combinations of these elements is increased by variations in the design and the size of each component and by the use of several different groups of components on a single model aircraft. Each configuration exhibits somewhat different icing characteristics and must be studied individually.

A conventional light-airplane induction system for a small tractor airplane with a flat engine is shown in figure 1. The main air duct contains a ram-air filter, a selector valve, an updraft suction-type carburetor, a fuel nozzle below the throttle, and a mixture-distributing manifold. Warm air from the engine compartment is drawn through a heating shroud surrounding the exhaust manifold when the selector valve closes the ram-air inlet and the hot-air bypass. This type of system operated by inexperienced pilots has been responsible for a large number of light-airplane accidents due to carburetor icing; however, the icing characteristics and the methods of improving the ice protection differ little from those required for larger aircraft.

Figure 2 shows a typical induction system for a large high-performance aircraft and illustrates two types of air intake commonly used with NACA radial-engine cowlings. The top diagram shows an articulated scoop with boundary-layer bypass, a hot-air selector valve, a protective screen, a pressure-injection type downdraft carburetor, a fuel-injection nozzle in the carburetor adaptor, turning vanes in the supercharger-inlet elbow, and an engine-stage supercharger. Warm air from behind the engine cylinders may be drawn into the system through a heating shroud surrounding the exhaust collector when the hot-air valve closes the cold ram-air inlet. The leading-edge scoop in the lower diagram is an alternate design used to secure better ram-pressure recovery during climb and at full throttle above critical engine altitude; other components of this system are the same as for the articulated-scoop system.

The several important differences in the air intakes are shown in figures 1 and 2. The bluntness of the light-airplane fuselage nose near the air intake, the inclination of the filter, and the relatively low flight speed all aid appreciably in deflecting most cloud droplets and in minimizing the impingement of rain and wet snow. The articulated scoop, because of its rear location, low contour, and boundary-layer bypass, prevents the intake of high concentrations of water that are deflected from the front of the nacelle and bypasses the runback of rain on the top of the nacelle. The leading-edge scoop, on the other hand, receives abnormal concentrations of deflected water, contains a great internal-surface area against which water will impinge, and the water, which strikes the nacelle surface, is carried aft into the hot-air valve. Because of these inherent differences in water-scooping rate, ram-pressure recovery, and temperature rises in various systems, a system of rating the icing characteristics of a carburetor and an engine on the basis of the air conditions at the entrance to the carburetor has been adopted.

THREE INDUCTION-SYSTEM ICING PROCESSES

Unlike the icing of other aircraft components, induction-system icing presents additional hazards because its occurrence is nonseasonal and much of the ice forms without warning where it is never seen by the pilot. Three distinct icing processes, impact, throttling, and fuel-evaporation, can occur in the induction systems that have just been described; the names are descriptive of the location and cause of formation, and provide immediate clues as to methods for their elimination.

Impact icing. - Typical impact icing (fig. 3) occurs when freezing rain, wet snow, or super-cooled cloud droplets strike surfaces that are below freezing. The rate of impact icing in the system increases with airspeed and the amount of water gaining entrance. Impact icing is most prevalent above 15° F but may be encountered at temperatures as low as -50° F. Except at night, the pilot is usually warned of the occurrence of impact icing by the formation of ice elsewhere on the aircraft and can take remedial action by switching to the alternate hot-air intake.

In addition to coating the forward surfaces of the airplane, impact icing forms at the scoop entrance and duct walls, on the carburetor-inlet screen, on the carburetor air-metering elements, on the top surfaces of the throttle plates, and on internal

obstructions such as hot-air valves, air-temperature bulbs, and turning vanes. Air filters or screens in the main duct block the most rapidly, causing sudden reduction in engine power, disturbing fuel metering and mixture distribution, and, in some cases, causing engine stoppage. Dry snow and sleet at low temperature may block some types of filter but generally these forms of precipitation are not serious unless induction systems are heated sufficiently to turn dry snow into an impact-icing condition.

Impact-ice formations and rain may also enter the small air-metering passages of the carburetor and disturb fuel metering. Some carburetors were found to be more sensitive than others in this respect, but generally the effects of water in the carburetor are unpredictable. Sluggishness in restoring proper fuel-air ratio after completely de-icing the system is an indication of this trouble. New forms of fuel-metering systems that avoid the use of exposed pressure-sensing and flow-circulating air passages can eliminate this problem. It should also be evident that the exclusion of cloud droplets and precipitation from the induction system will prevent impact icing and its related problems.

Throttling icing. - The second form of icing, throttling icing, occurs when expansion cooling of the air through the throttles lowers the air temperature and that of surrounding surfaces below 32° F, provided sufficient liquid water is present or the dew point is above the final temperature so that condensation takes place. Under some conditions, the acceleration of air through the metering venturi lowers the air temperature enough to start condensation, which then increases the rate of icing at the throttles. Air must be nearly saturated or must contain some liquid water and the throttling pressure drop must be quite high before throttling icing becomes a serious hazard.

Theoretically, it is possible to form ice in an insulated passage with normal amounts of throttling at an inlet-air temperature of approximately 42° F with about 80 percent relative humidity; but experimentally, serious throttling icing has not been observed above 39° F or with air that is unsaturated. Throttling ice occurs at the edges of the throttle plates and the adjacent walls at low power settings and, in addition to restricting air flows, may freeze the throttle in a partly closed position and prevent closure for landing. The throttling process, however, is most important for its contribution at all temperatures to the more prevalent and serious fuel-evaporation icing process.

Double-opposed throttles or variable-venturi throttles in rectangular carburetors were found to be relatively free from throttling ice as compared with the single butterfly type of throttle. Most British carburetors and throttle bodies of the butterfly type are automatically protected from icing by the forced circulation of hot engine oil through carburetor jackets and hollow throttle plates - a practice that appears to have been suggested originally in this country but never adopted. It should be possible to eliminate throttling ice, without resorting to special heating, by using variable-venturi throttles in a warm region of the engine.

Fuel-evaporation icing. - Fuel-evaporation icing occurs when the air stream and surrounding metal parts are cooled below freezing by the refrigerating effect of fuel vaporization and water is present or is condensed from the cooled air. The fuel-air mixture temperature has been observed to drop more than 80° F lower than the carburetor-inlet temperature. Inasmuch as a finite time is required to evaporate fuel, it is to be expected that serious refrigeration would not develop in the rapidly moving air stream in the immediate vicinity of the fuel spray. However, this is actually the case in a well-designed system operating at full throttle but at low-power settings; fuel droplets eddy back into the turbulent wake of the partly-closed throttles or are splashed back by the supercharger impeller in a manner that increases the refrigeration effect. This effect is even more pronounced in suction carburetors where the throttles are continually bathed with evaporating fuel and become focal points of icing, which quickly blocks air flow.

At extremely low air flow or high water concentrations, ice may so form on the fuel nozzle of some pressure carburetors as to obstruct the fuel flow and lean the mixture; whereas, in suction carburetors ice has been observed to enrich the mixture. In either case loss of power or rough running results.

The icing shown in figure 4 occurred at low cruise-power conditions. The top picture was taken looking down into the inlet elbow of the engine with the carburetor removed; the bottom row shows the under side of the carburetor, which was removed from the inlet elbow, with throttles in the operating position. The two left views show ice that caused a 40-percent reduction in air flow in 6 minutes whereas the ice in the center pictures reduced air flow 34 percent in only 1 minute in simulated rain of nearly double intensity. The right-hand pictures were taken after simulating automatic regulation of manifold pressure by slowly opening the throttles during icing in clear-air conditions. After 80 minutes of operation, the throttles

had been opened from 26° to 87°, where they became frozen. The throttles remained locked for 1 hour with air flow fluctuating widely, and at times exceeding that for cruise power, as ice formed and sloughed off. The Navy has reported several similar cases where, in very long over-water patrols at fixed throttle with power maintained constant by means of electronic control of the turbosupercharger waste gate, icing suddenly and severely reduced power without warning after 7 hours in clear-air conditions.

A comparison of the effects of pressure-carburetor configuration on fuel-evaporation icing is shown in figure 5 for twin-barrel and variable-venturi carburetors. The top pictures show the under side of the carburetor with the throttles in the operating position and the lower pictures are of the supercharger-inlet elbow. In the left-hand pictures, ice coated the entire throttle plates and inlet elbow thereby causing a serious loss in air flow; on the other hand, the variable-venturi type throttles are almost entirely free from ice although sufficient ice formed on the central fuel-spray bar and on the sloping adapter walls to seriously affect air flows.

The results of the investigations indicate that fuel-evaporation icing is not significantly affected by changes in fuel-air ratio or by normal variations in fuel temperature. Fuel volatility, however, was determined to be a distinct factor in the rapidity with which icing occurs. A low volatility safety fuel could greatly reduce icing tendencies.

The most promising and functional prevention of fuel-evaporation icing is, of course, to move the point of fuel injection to a location that is automatically maintained above 32° F, which may be accomplished by injecting fuel (1) through a rotating spinner at the entrance to the supercharger, (2) through holes in the impeller itself, (3) into a warm portion of the manifold, (4) near the intake valve, or (5) directly into the cylinder.

ICING CHARACTERISTICS OF CARBURETOR AND ENGINE

Figure 6 shows the icing characteristics for low cruise power of the variable-venturi carburetor and engine (fig. 5). Carburetor inlet-air dry-bulb temperature is here plotted against inlet-air water-air ratio for the limits below which nonserious icing was observed to be present somewhere in the system and the limits below which serious icing occurred. Serious icing was arbitrarily considered to be that which caused more than a 2-percent reduction of air flow or 6-percent

change in fuel-air ratio within 15 minutes. All conditions to the left of the saturation line are in clear air; all conditions to the right are in clouds or precipitation. The area between the top and bottom limits represents potentially serious icing conditions for times varying from infinity to 15 minutes, respectively. Icing occurred when the inlet-air temperature was 110° F and the relative humidity was less than 20 percent, but serious icing occurred only with saturated or wet air at a maximum temperature of 65° F.

The effect of engine size on icing characteristics is indicated by the fact that the same type carburetor on a similar engine of 1820 cubic-inch displacement had almost identical icing limits at the same fraction of rated power as this engine of 2600 cubic-inch displacement.

The effect on icing limits of two power settings for a twin-barrel pressure carburetor on a liquid-cooled V-type engine is shown in figure 7. The limits of nonserious icing are higher than for serious icing at both normal rated and 60-percent rated power. A reduction of approximately 25° F in maximum values can be noted for both nonserious and serious icing when the power is increased from cruise to normal rated power. At nearly full throttle such low throttle pressure drops and such high velocities occurred that the serious-icing limits at rated power recede almost to the limits for impact icing, that is, to 32° F. The effect of an increase in altitude is similar to that for an increase in power; wider throttle openings lower the icing limits.

Reasonable correlation was found between these results obtained in the laboratory with 65-octane fuel and those obtained with the complete engine on a dynamometer stand with the less volatile grade 130 fuel. In the engine tests, the icing limits were found to be about 5° F lower than those shown in figure 7 for cruise power. Reductions in air flow and changes in fuel metering that were greater than those arbitrarily chosen as criterions for serious icing actually resulted in rough operation and rapid losses of power, which confirmed the validity of the initial assumptions.

The recent trend toward use of water injection for increased take-off and climb power suggested the possibility that icing would become a problem when water was introduced with the fuel. This condition was found to be true at the war emergency power rating because the total water-air ratio represented rain conditions even though the inlet conditions were those of clear air. All traces of icing above the impact-icing level disappeared, however, when 50-50 water-alcohol mixtures were injected with the fuel at the war emergency power rating.

Figure 8 shows the benefits of an improved method of fuel injection and warm inlet-elbow surfaces in lowering the icing tendencies of a carburetor-engine combination at cruise power. In this case a three-barrel pressure carburetor on an inlet elbow containing three turning vanes and other protuberances would be expected to show icing limits higher than those in figures 6 and 7. However, injection of fuel from a rotating spinner at the entrance to the supercharger and submergence of the supercharger-inlet elbow into the oil-warmed accessory section reduced the icing limits below the theoretical limits for throttling and impact icing. Operation at temperatures slightly below freezing with slightly more than saturation water contents for a 3-hour period was possible without serious effects.

It is apparent from figure 8 that if free water could be excluded from the induction system, that is, if all conditions to the right of the saturation line were eliminated, this particular carburetor and engine combination would be inherently ice-free at cruise power. These same results for spinner fuel injection were obtained earlier in laboratory tests elsewhere for a smaller model of the same engine. Extensive investigations at this laboratory with another type of engine have also conclusively confirmed the fact that in a supercharged engine fuel must be injected from a rotating device at the entrance to the supercharger or at a point further downstream to eliminate completely fuel-evaporation icing. The icing limits shown in figure 7 were reduced by spinner injection to almost identical values presented in figure 8. Cylinder fuel injection would not further lower the icing limits but does offer the advantage of requiring no air-preheat system for cold-weather operation and eliminates the backfiring, which occasionally damages induction systems. Unsupercharged engines for light airplanes can be as effectively protected from fuel-evaporation icing by injecting fuel in the individual manifold pipes near the intake valves.

Greater freedom from impact icing and erratic metering caused by rain entering the air-metering system of the carburetor can be achieved by adopting a fuel-metering system, which in its simplest form is based on engine speed and throttle opening, and in its most accurate form is based upon engine speed, manifold-pressure and temperature, and exhaust back pressure. If the induction system has a water-excluding air intake, a heated throttle assembly, a speed-density fuel-metering device, and cylinder fuel injection, the ultimate simplicity and reliability with respect to freedom from icing is attained without attention from the pilot except to regulate power.

In summarizing the investigation of icing characteristics, figure 9 presents six carburetor-supercharger combinations with

twin-barrel carburetors for which icing limits were determined. Figure 10 then summarizes the serious-icing limits of the six configurations shown in figure 9. It may be noted that in four combinations serious icing can occur at high temperatures and low relative humidities in clear air. The impressive reduction of icing limits from curve 4, which were dropped to curve 1 by the use of spinner fuel injection, should be noted in figure 10.

Figure 10 represents icing tendencies of most of our present transport airplanes and it must be apparent that the accident potential is still present for pilots who lack training or relax vigilance. When it is realized that in one new four-engine transport there are 635 items for the pilot to watch or control in the cockpit, it can be appreciated that the pilot will find it increasingly difficult to "fly" the induction system while he is so thoroughly busy flying the airplane. Despite this situation the commercial air transports are singularly free from accidents caused by induction-system icing, but only by virtue of intensive pilot training, provision of multiple systems of ice protection, and excellent instruments for checking airplane and engine performance. It would be unreasonable to expect most current types of private aircraft to be operated as safely with this same equipment because of the relative inexperience of the average private pilot. It is evident then that an inherently ice-free induction system is needed.

ICE-PROTECTION METHODS

Throughout this discussion, the benefits to be derived from exclusion of water from the induction system have been presented. Figure 11 presents an historical progression of some of the proposals for reducing impact icing, for reducing the intake of various types of precipitation, and for approaching the goal of complete water elimination with negligible loss of ram. The British type of gapped ice guard A was intended to block rapidly in impact-icing conditions; air without freezing water would then be drawn in through the gap behind the guard. This device was discontinued because of its high drag in nonicing conditions and because it produced negative ram in icing conditions. In a later version of the ice guard, the screen was tightly fitted to the air intake and a spring-loaded valve automatically admitted air from behind the engine cylinders during icing conditions. Arrangement B is a streamlined deflection body placed ahead of the inlet to deflect rain and snow and to catch most of the impact ice. This device has not been adopted because it is excessively bulky, causes some ram-pressure losses at all times, and does not adequately cope with impact-icing conditions.

Design C, which has met with some current favor, is a simple articulated scoop modified so as to provide a plenum chamber and water drain to separate some water and ice from the air stream and to prevent dislodging of large sheets of ice onto the carburetor when hot air is applied. Design D is the conventional leading-edge scoop previously discussed, and E is the undercowl scoop derived from D, which is intended to exclude the entry of water from the system by means of inertia separation. Icing-tunnel research on the undercowl scoop showed that it excluded approximately 95 percent of the water that normally enters the conventional scoop and maintained equal or better ram-pressure recovery for climb and ceiling cruise conditions. This design is being applied to new aircraft and is expected to help appreciably in rendering induction systems inherently ice-free.

In most transport airplanes, emergency alcohol de-icing is mandatory to avoid the possibility that exhaust heat will not be available in case of inadvertent engine stoppage due to ice or to hasten the recovery of power when heat is applied. However, figure 12 indicates that the value of alcohol de-icing is debatable. Typical results of alcohol de-icing experiments are presented here for cruise-power conditions at sea level, 10,000, and 20,000 feet when 95 pounds per hour of isopropyl alcohol were sprayed from six nozzles located around the periphery of the duct several inches above the screen for 10 minutes during impact-icing conditions. The induction system is one with a leading-edge scoop. The first three photographs were taken through an observation hatch above the carburetor looking directly down on the carburetor screen; the photograph at 20,000 feet was taken looking directly upstream toward the inlet at the severe impact icing in the horizontal duct. It may be seen that de-icing was not effective below the alcohol nozzles and, of course, did not touch the ice upstream of the nozzles.

Hot-air de-icing systems are similarly ineffective in removing ice upstream of the hot-air valve and may cause large sheets of ice to be dislodged and fall on the carburetor screen. The trend to remove carburetor screens, which provide the most serious impact-icing hazard in induction systems, should be encouraged because the absence of screens will improve the icing tolerance of most installations.

Typical results of hot-air de-icing are presented in figure 13. The time in minutes to recover 95 percent of the maximum possible air flow after icing the system a predetermined amount is plotted against dry-bulb and wet-bulb temperatures for three different relative humidities. Dry-bulb temperature alone is obviously no true

criterion of de-icing effectiveness but the correlation is good on a wet-bulb basis. At a dry-bulb temperature of 60° F, for example, a de-icing time of 5 minutes is required for dry air as against only 1/2 minute for saturated air. The effect of engine configuration, engine size, initial icing temperature, and air-flow reduction did not disclose significant differences in de-icing requirements on a wet-bulb basis. The de-icing rate below a wet-bulb temperature of approximately 60° F was generally unsatisfactory and an increase in the wet-bulb temperature above 60° F resulted in little improvement in recovery time. Excessive air temperature should be avoided because it seriously reduces engine power by reducing charge-air density, increases the hazard of detonation, and causes excessive leaning of the mixture through overcompensation of the automatic mixture regulator when applied at high altitude.

CONCLUSIONS

In summarizing the results of NACA research, the following generalizations can be stated with respect to the icing characteristics of existing systems, the remedial action required to protect these systems, cautions to be observed, and desirable fundamental improvements that can be made in new designs and perhaps retroactively.

1. The icing characteristics of conventional carburetors of both the suction and pressure type with fuel injected near the throttles present a serious icing hazard in clear air at inlet-air temperatures as high as 70° F.

2. Fuel-air ratio and mixture distribution are adversely affected by icing and by the trapping of water in the air-metering passages of the carburetor and can cause rough running and engine stoppage.

3. Throttles may freeze at a given power setting or when an automatic pressure regulator compensates for the effects of icing and may lead to forced landings with no control over power setting.

4. Hot-air valves may also freeze in the full-cold or full-hot position.

5. Throttles and hot-air selector valves should be of sturdy design and with low control forces to permit mechanically breaking them free when frozen with ice.

6. Duct inlet, carburetor and engine configuration, water injection, power setting, and fuel volatility significantly affected the icing characteristics, but engine size, fuel temperature, fuel-air ratio, and water-alcohol injection did not.

7. Screens and air filters in the main air duct without bypass constitute an unwarranted icing hazard and should be removed where possible.

8. Exposed fuel nozzles in severe-icing regions may cause leaning out in some pressure carburetors and excessive enrichment in suction carburetors.

9. Remedial ice protection may be provided by means of selecting an alternate air intake, by warming the surfaces, by applying hot air or alcohol, and by changing the power settings; however, none of these methods fully removes ice formations that occur upstream of the point of protection.

10. A wet-bulb temperature of 60° F affords prompt de-icing of serious-ice formation below the carburetor but may cause icing if applied in dry snow or sleet conditions, and may dislodge sheets of ice that will fall onto the carburetor and disturb operation. Hot-air should be applied when icing begins.

11. Excessive temperatures should be avoided in the hot-air de-icing system to avoid detonation, overcompensation of the fuel-air mixture, and excessive loss of power.

12. A protected ram-air intake can be provided that will automatically exclude most serious impact-icing particles without appreciable loss in ram-pressure recovery.

13. The speed-density metering system with oil-heated throttle assembly automatically eliminates throttling icing and water fouling of the metering system.

14. Spinner fuel injection, manifold injection, or cylinder injection have satisfactorily eliminated fuel-evaporation icing.

15. Inherent ice elimination from the entire induction system may be provided by excluding water from the system, by locating well-designed throttles in warm locations, by making the induction system aerodynamically clean, by injecting fuel where the metal temperatures will remain above freezing, and by adopting a fuel-metering system that does not rely on exposed air-metering passages in potential icing regions.

It may therefore safely be concluded that a suitable combination of known induction-system components can now achieve the goal of an efficient and ice-free induction system for all-weather aircraft that will not require pilot control of heating nor need alcohol for emergency de-icing.

BIBLIOGRAPHY

Sparrow, Stanwood W.: "Airplane Crashes: Engine Trouble." A Possible Explanation. NACA TN No. 55, 1921.

Chandler, H. C., Jr.: Survey of Aircraft Anti-Icing Equipment. NACA OCR, Feb. 27, 1942.

Kimball, Leo B.: Icing Tests of Aircraft-Engine Induction Systems. NACA ARR, Jan. 1943.

Essex, Henry A.: De-Icing of an Aircraft-Engine Induction System. NACA ARR 3H13, 1943.

Essex, Henry A., and Galvin, Herman B.: A Laboratory Investigation of Icing and Heated-Air De-Icing of a Chandler-Evans 1900 CPB-3 Carburetor Mounted on a Pratt & Whitney R-1830-C4 Intermediate Rear Engine Section. NACA ARR No. E4J03, 1944.

Galvin, Herman B., and Essex, Henry A.: Fluid De-Icing Tests on a Chandler-Evans 1900 CPB-3 Carburetor Mounted on a Pratt & Whitney R-1830-C4 Intermediate Rear Engine Section. NACA ARR No. E4J06, 1944.

Galvin, Herman B., and Essex, Henry A.: A Laboratory Investigation of the Icing Characteristics of the Bendix-Stromberg Carburetor Model PD-12F5 with the Pratt & Whitney R-1830-C4 Intermediate Rear Engine Section. NACA ARR No. E4J18, 1944.

Wadleigh, Kenneth R.: Flight Tests to Determine the Effectiveness of Fluid-Spray Systems in Removing Ice Formations in the C-46 Airplane Engine Induction System. NACA MR No. A5E15, Army Air Forces, 1945.

Mulholland, Donald R., Rollin, Vern G., and Galvin, Herman B.: Laboratory Investigation of Icing in the Carburetor and Supercharger Inlet Elbow of an Aircraft Engine. I - Description of Setup and Testing Technique. NACA MR No. E5L13, 1945.

Essex, Henry A., Keith, Wayne C., and Mulholland, Donald R.: Laboratory Investigation of Icing in the Carburetor and Supercharger Inlet Elbow of an Aircraft Engine. II - Determination of the Limiting-Icing Conditions. NACA MR No. E5L18a, 1945.

Lyons, Richard E., and Coles, Willard D.: Laboratory Investigation of Icing in the Carburetor and Supercharger Inlet Elbow of an Aircraft Engine. III - Heated Air as a Means of De-Icing the Carburetor and Inlet Elbow. NACA MR No. E5L19, 1945.

Renner, Clark E.: Laboratory Investigation of Icing in the Carburetor and Supercharger Inlet Elbow of an Aircraft Engine. V - Effect of Injection of Water-Fuel Mixtures and Water-Ethanol - Fuel Mixtures on the Icing Characteristics. NACA MR No. E5L28, 1945.

Chapman, G. E., and Zlotowski, E. D.: Laboratory Investigation of Icing in the Carburetor and Supercharger Inlet Elbow of an Aircraft Engine. IV - Effect of Throttle Design and Method of Throttle Operation on Induction-System Icing Characteristics. NACA MR No. E5L27, 1946.

Mulholland, Donald R., and Chapman, Gilbert E.: Laboratory Investigation of Icing in the Carburetor and Supercharger Inlet Elbow of an Aircraft Engine. VI - Effect of Modifications to Fuel-Spray Nozzle on Icing Characteristics. NACA MR No. E6A23, 1946.

Essex, Henry A., Zlotowski, Edward D., and Ellisman, Carl: Investigation of Ice Formation in the Induction System of an Aircraft Engine. I - Ground Tests. NACA MR No. E6B28, 1946.

Essex, Henry A., Ellisman, Carl, and Zlotowski, Edward D.: Investigation of Ice Formation in the Induction System of an Aircraft Engine. II - Flight Tests. NACA MR No. E6E16, 1946.

Chapman, Gilbert E.: A Preliminary Investigation of the Icing Characteristics of the Chandler-Evans 58 CPB-4 Carburetor. NACA MR No. E6G11, Army Air Forces, 1946.

von Glahn, Uwe, and Renner, Clark E.: Development of a Protected Air Scoop for the Reduction of Induction-System Icing. NACA TN No. 1134, 1946.

Chapman, Gilbert E.: An Investigation of the Icing and Heated-Air De-Icing Characteristics of the R-2600-13 Induction System. NACA RM No. E6K11, Army Air Forces, 1946.

Mulholland, Donald R., and Zlotowski, Edward D.: Investigation of Operating Characteristics of an Engine Equipped with Modifications to Eliminate Fuel-Evaporation Icing. NACA RM No. E6L04a, Army Air Forces, 1946.

Stevens, Howard C., Jr.: Effects of Induction-System Icing on Aircraft-Engine Operation Characteristics. NACA RM No. E6L24, Army Air Forces, 1947.

Coles, Willard D.: Laboratory Investigation of Ice Formation and Elimination in the Induction System of a Large Twin-Engine Cargo Aircraft. NACA TN (to be pub.).

Essex, Henry A., Chapman, Gilbert E., and Hunter, Willson H.: Icing Protection Requirements for Reciprocating Engine Induction Systems. NACA TN (to be pub.).

CONVENTIONAL LIGHT-AIRPLANE INDUCTION SYSTEM

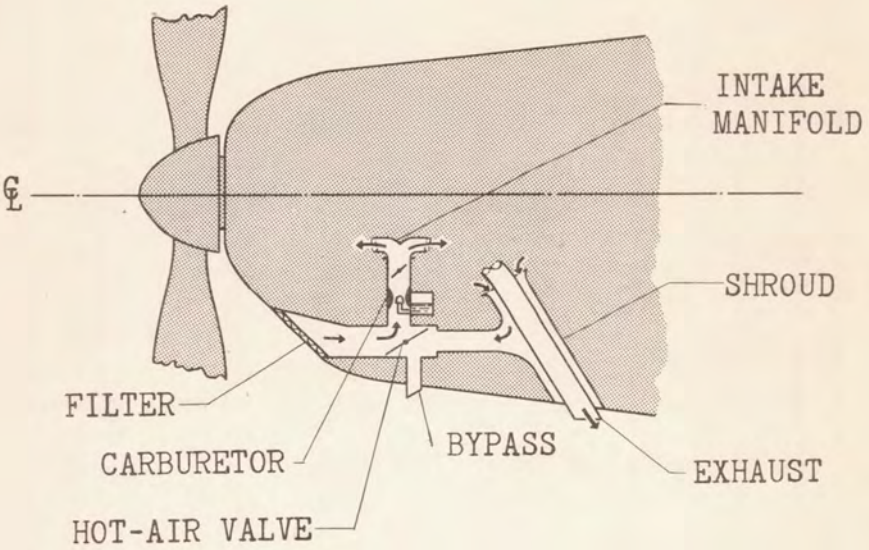

FIGURE 1.

TYPICAL INDUCTION SYSTEMS WITH NACA COWLINGS

NATIONAL ADVISORY COMMITTEE FOR AERONAUTICS

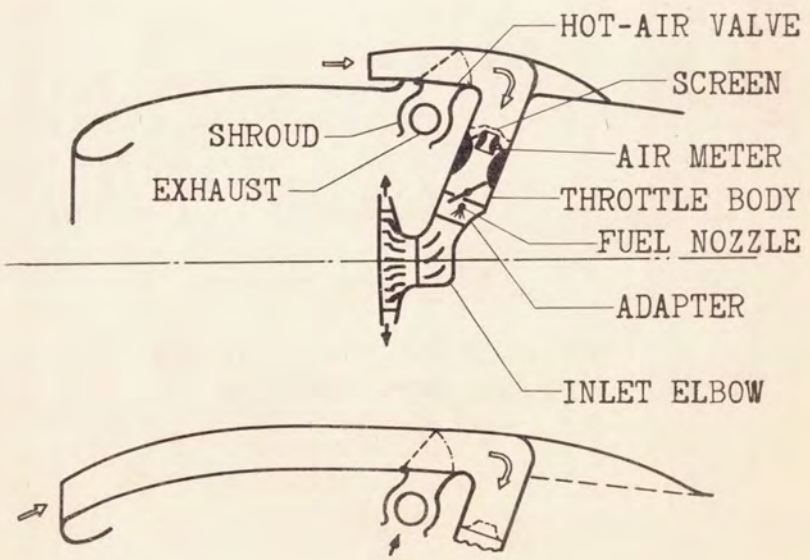

FIGURE 2.

AIR INTAKE

CARBURETOR SCREEN

AIR-METERING PARTS

THROTTLES

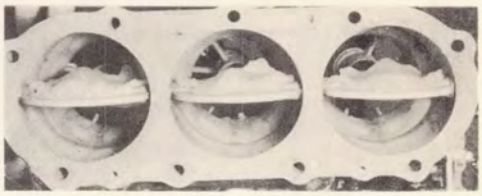

IMPACT ICING

FIGURE 3.

NATIONAL ADVISORY COMMITTEE
FOR AERONAUTICS

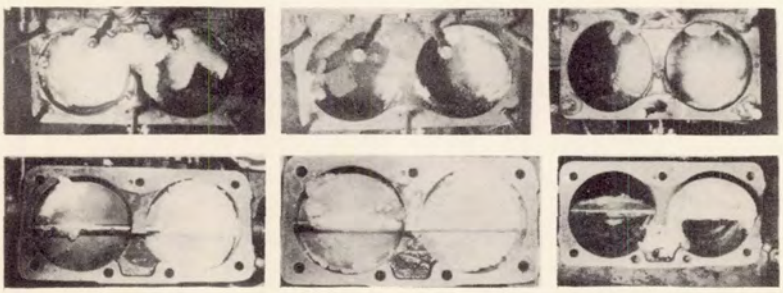

C.A.T. 40°F
R.H. 100%
WATER 350 G/M

C.A.T. 37°F
R.H. 100%
WATER 650 G/M

C.A.T. 40°F
R.H. 100%
WATER 0 G/M

60% CRUISE POWER

TYPICAL ICING IN V-1710-89
INDUCTION SYSTEM

FIGURE 4.

TWIN-BARREL CARBURETOR

VARIABLE-VENTURI CARBURETOR

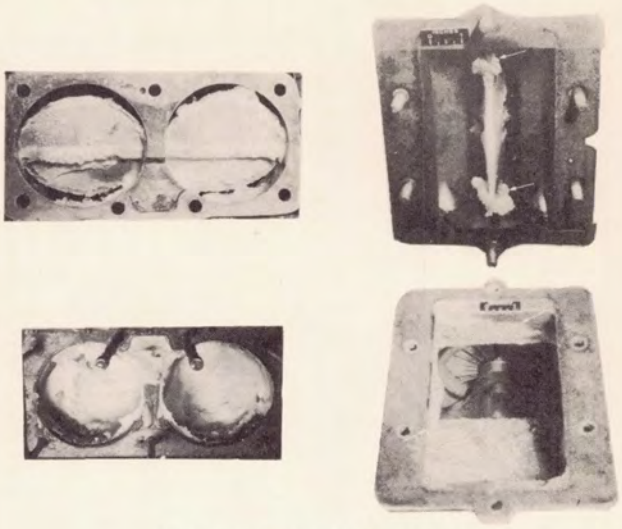

FUEL-EVAPORATION ICING
FIGURE 5.

ICING LIMITS AT LOW CRUISE POWER WITH VARIABLE-VENTURI CARBURETOR

NATIONAL ADVISORY COMMITTEE FOR AERONAUTICS

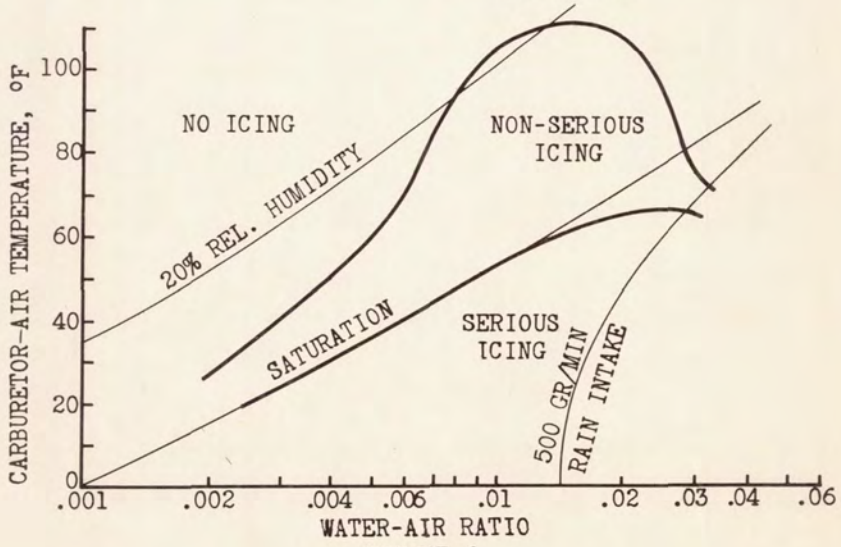

FIGURE 6.

TYPICAL ICING LIMITS AT TWO POWER SETTINGS

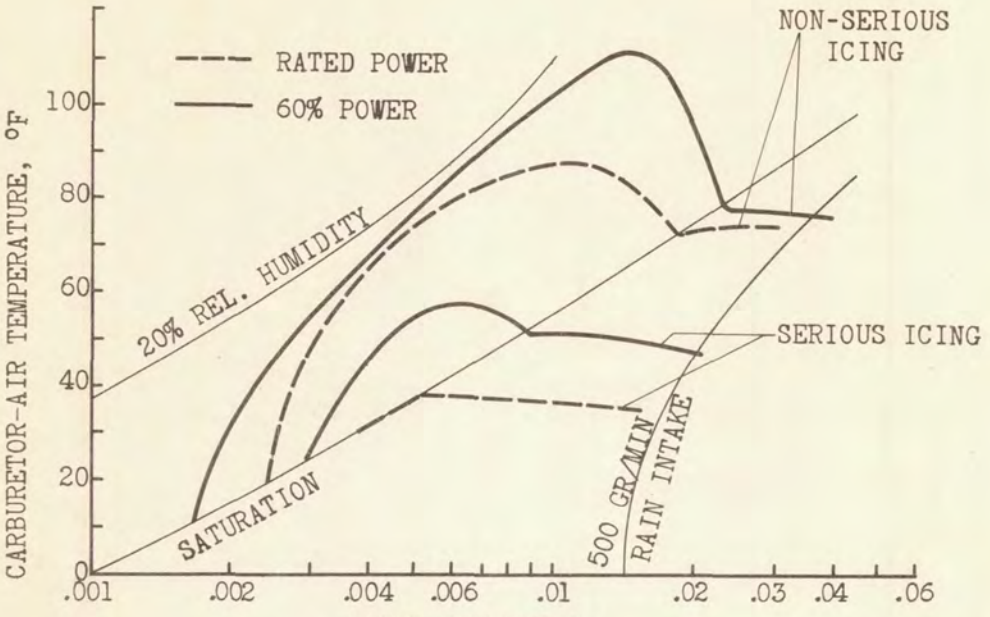

FIGURE 7.

ICING LIMITS WITH SPINNER FUEL INJECTION

NATIONAL ADVISORY COMMITTEE FOR AERONAUTICS

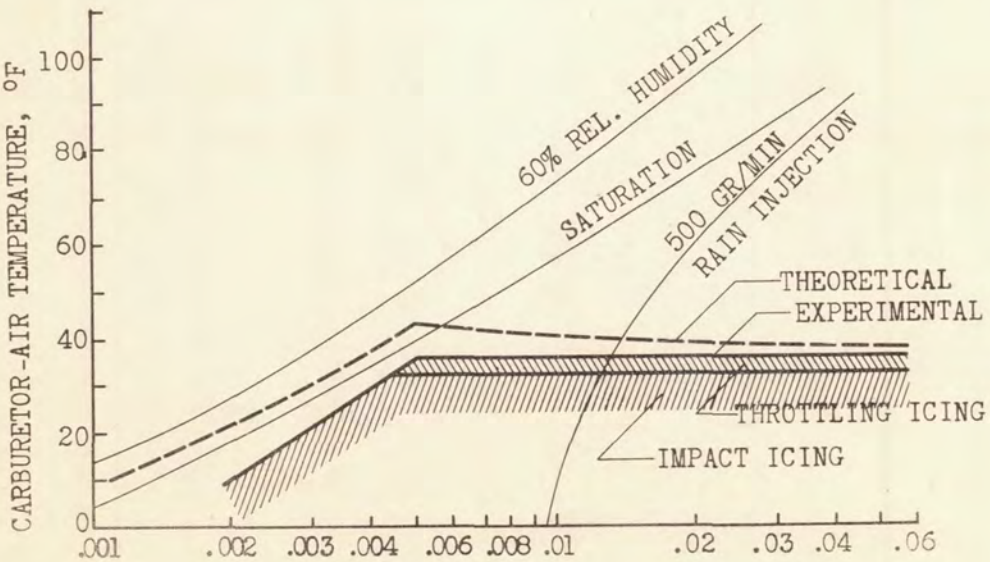

FIGURE 8.

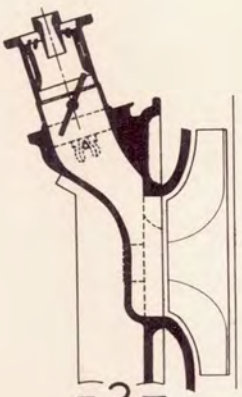

-3-
R-1830-C4 ENG.
BENDIX-STROMBERG
PD-12F3 CARB.

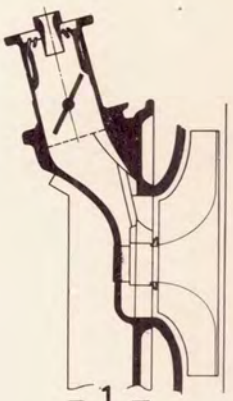

-1-
R-2000-D ENG.
BENDIX-STROMBERG
PD-12F3 CARB.

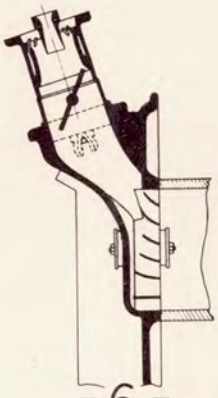

-6-
R-1830-C4 ENG.
BENDIX-STROMBERG PD-12F5

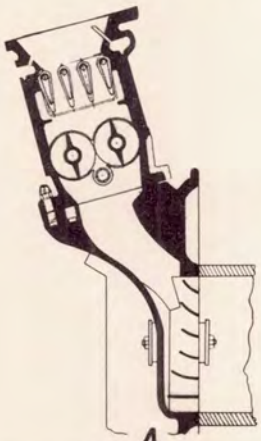

-4-
R-1830-C4 ENG.
CHANDLER-EVANS
1900 CPB-3 CARB

NATIONAL ADVISORY COMMITTEE
FOR AERONAUTICS

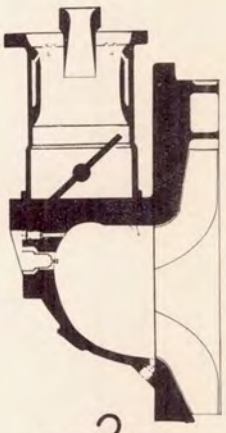

-2-
V-1710-89 ENG.
BENDIX-STROMBERG
PD-12K7

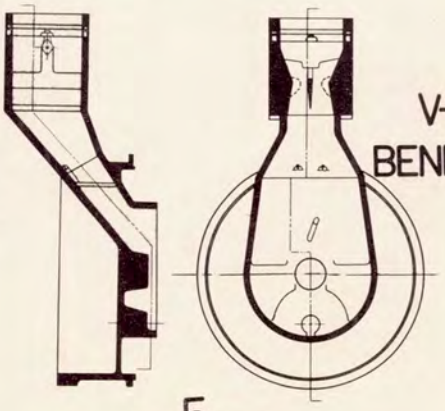

-5-
R-1820-G200 ENG
HOLLEY 1375-F CARB

FIGURE 9.

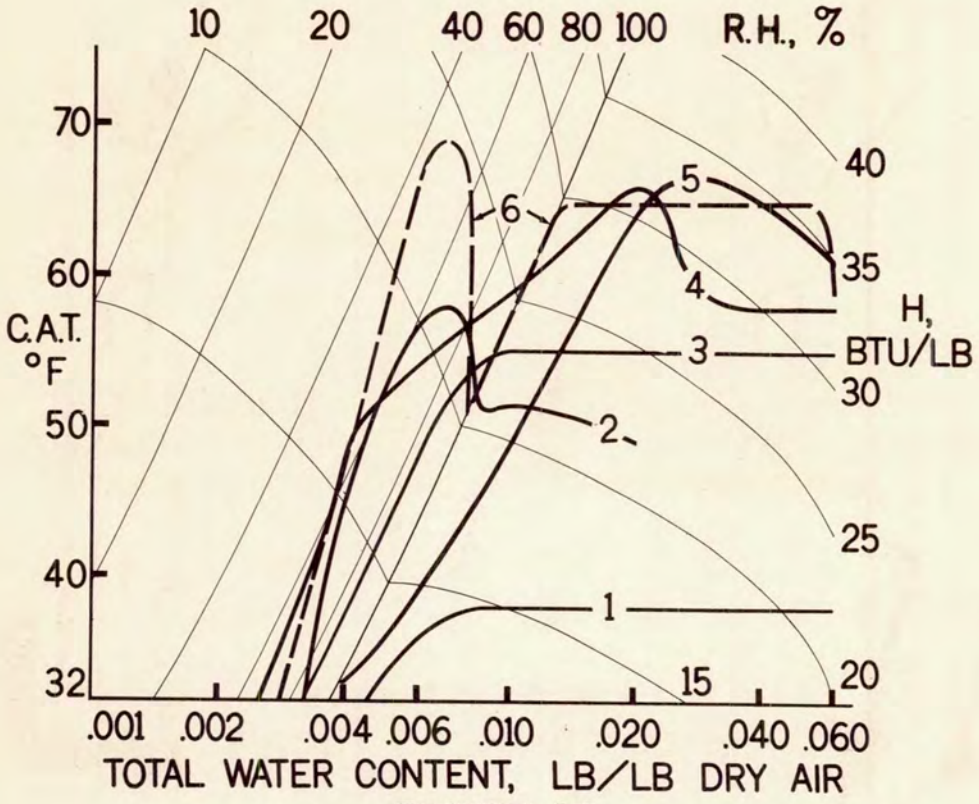

FIGURE 10.

NATIONAL ADVISORY COMMITTEE
FOR AERONAUTICS

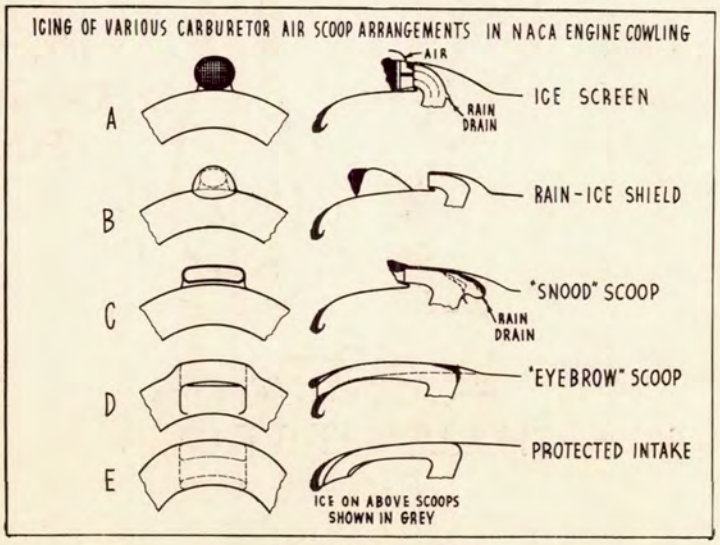

FIGURE 11.

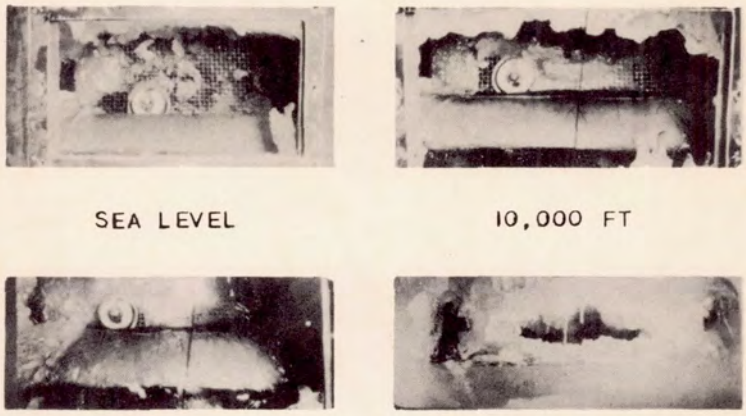

SEA LEVEL 10,000 FT

20,000 FT 20,000 FT

IMPACT ICE PROTECTION WITH ALCOHOL

LOW CRUISE POWER; AIR TEMP, 25° F; RAIN, 2 G/M^3
ALCOHOL RATE, 95LB/HR FOR 10 MIN.

FIGURE 12

EFFECT OF HUMIDITY ON DE-ICING TIME

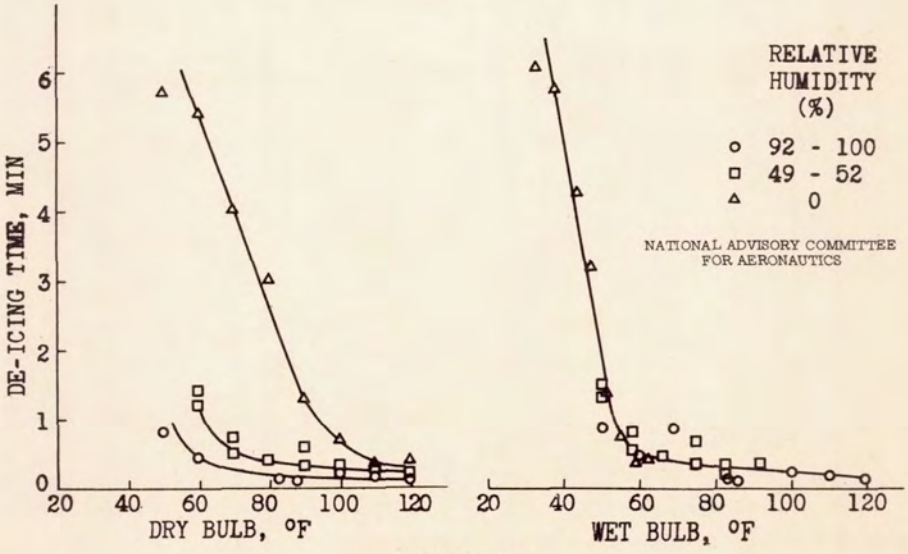

FIGURE 13.

HOT-GAS BLEEDBACK FOR JET-ENGINE ICE PROTECTION

By William A. Fleming

Flight Propulsion Research Laboratory

INTRODUCTION

Ice formation on the inlet of a turbojet engine in flight will result in a reduction in thrust and, if icing becomes serious, will render the engine inoperative as a result of high tail-pipe temperatures. Such conditions, particularly with axial-flow compressor engines, make flight in icing weather extremely hazardous without some type of equipment to protect the inlet of the engine from icing.

As part of a general program now being conducted at the Flight Propulsion Research Laboratory on ice prevention at the inlet of turbojet engines, an investigation has been conducted in the altitude wind tunnel on a 24C engine to study one phase of the ice-prevention work. The method of ice prevention studied consists of bleeding hot gas from the turbine inlet and injecting it into the air stream ahead of the compressor inlet in order to heat the air above the freezing temperature. This investigation was conducted at altitudes of 5000 and 20,000 feet with ambient-air temperatures from 0° to 35° F and over a range of engine speeds.

The turbine inlet was chosen as the station from which to bleed the gas, because at this station in the engine the gas is at the highest temperature and pressure. Because the temperature of the gas is high, a smaller amount is needed to heat the inlet air above the freezing temperature than would be required if the gas were bled from some other station in the engine. Inasmuch as the pressure at this station is also high, bleeding from the turbine inlet makes it possible to discharge the gas into the air stream at sonic velocity, thus affording better penetration of the hot air into the cold air.

INSTALLATION AND TEST PROCEDURE

The engine was mounted in a wing nacelle installed in the test section of the altitude wind tunnel. A photograph of the engine installation with the hot-gas bleedback system installed is shown in figure 1. Hot gas was bled from two points diametrically opposite at the turbine inlet. The gas was carried to the top of the engine through two 3-inch-diameter ducts and thence forward in a

single 4-inch-diameter duct, which carried the gas forward along the top of the engine. At the front of the engine, the hot gas was again divided into two 3-inch ducts that ran along either side of the inlet duct and discharged the hot gas into the cowl-inlet lip, which formed the manifold. Holes were drilled in the inlet lip to inject the gas into the air stream normal to the direction of air flow. At the rear of the engine in the 4-inch-diameter duct, a butterfly valve was installed to regulate the amount of gas flow bled to the inlet of the engine. At the forward end of this duct a survey rake was installed to obtain the measurements of temperature and pressure used in calculating the mass flow bled to the inlet. All hot-gas ducting was insulated with several layers of asbestos tape to prevent heat transfer. Another survey rake was mounted in the inlet duct $31\frac{1}{4}$ inches downstream from the plane at which the hot gas was injected in order to obtain the temperature distribution across the inlet. The ambient-air temperature was measured by two thermocouples installed upstream of the spray nozzles.

A spray tower on which five spray nozzles were mounted was installed in the tunnel test section 7 feet ahead of the duct inlet (fig. 2). These nozzles, which provide a homogeneous spray of fine drop size, injected water through small holes into a stream of air flowing at sonic velocity. In the photograph is shown a periscope lowered in front of the engine inlet. The periscope was mounted from the wall of the tunnel test section and could be raised above or lowered in front of the engine inlet from outside of the test section. A floodlight and a 16-millimeter motion picture camera were installed inside the fairing at the lower end of the periscope. Installation of the camera made it possible to photograph the inlet of the engine under icing conditions while the test was in progress.

A photograph of the spray nozzles in operation is shown in figure 3. This photograph was obtained with the engine inoperative and with zero velocity in the tunnel test section. Most of the tests were conducted at a tunnel airspeed of 140 miles per hour. At this airspeed in the tunnel test section and with the engine operating, the spray was not as homogeneous at the engine inlet as shown in figure 3. About 80 percent of the water went into the engine inlet when the tunnel was in operation.

Water concentrations used for the investigation were several times the normal amount of water encountered in natural icing conditions. The water concentrations varied from 3 to $5\frac{1}{2}$ grams per cubic meter. The water spray did not simulate natural icing conditions;

however, this method of injecting water into the air stream was adequate for this investigation. Because the spray tower was a distance of 12 feet from the compressor inlet, most of the water froze before reaching the engine inlet. It was therefore necessary to heat the water to a temperature of at least 100° F in order to obtain ice on the compressor-inlet guide vanes.

During the icing investigation the engine was operated at speeds below the rated engine speed of 12,500 rpm. The highest engine speed at which hot-gas bleedback was used was 12,000 rpm; at this speed the turbine-outlet temperature with no bleedback was 60° F below the limiting value. The highest engine speed at which inlet icing was investigated was 11,000 rpm; at this speed the turbine-outlet temperature with no ice on the inlet was 200° F below the limiting value.

CHARACTERISTICS OF INLET ICING

The first indication of inlet icing was observed when the tail-pipe temperatures began to rise. After the water spray was turned on, approximately 2 to 4 minutes elapsed before the temperature rise occurred. When the water spray was on and no effort was made to prevent ice from forming on the compressor-inlet guide vanes, it was necessary to shut the engine down within 1 to 2 minutes after the tail-pipe temperature first began to rise because the temperature became excessively high. A photograph of the engine inlet in a partly-iced condition is shown in figure 4. At this condition the turbine-outlet temperature had risen approximately 100° F above the temperature observed with no ice in the inlet. The photograph shows ice formation on the compressor-inlet guide vanes and also the heavy ice formation on the dome of the starter housing. A photograph of the inlet iced to such an extent as to render the engine inoperative is shown in figure 5. This figure shows that the air passage near the roots of the compressor-inlet guide vanes was almost completely blocked, a large percentage of the air passage near the tips of the guide vanes was blocked, and a very heavy coat of ice had formed on the dome of the starter housing.

A considerable decrease in net thrust resulted when the inlet of the engine was iced. Figure 6 presents the percent decrease in net thrust as a function of the percent decrease in air flow for an altitude of 20,000 feet, an airspeed of 140 miles per hour, and an ambient-air temperature of about 30° F. As the compressor-inlet guide vanes became iced and the air passage was reduced, the air

flow to the engine was similarly reduced. Reduction in this air flow resulted in a corresponding reduction in net thrust and, when the air flow had been reduced approximately 28 percent, it was no longer possible to operate the engine at any speed without exceeding the tail-pipe-temperature limits. With a 26-percent decrease in air flow, there was a 30.2-percent decrease in net thrust. Part of this decrease in thrust resulted from the fact that the pressure level through the entire engine was reduced as a result of the increased pressure drop across the compressor-inlet guide vanes when they were iced.

As the engine inlet iced, the specific fuel consumption based on net thrust increased very rapidly, as shown in figure 7. When the air flow was decreased 26 percent, the specific fuel consumption was increased 48.4 percent. The large increase in specific fuel consumption resulted from the fact that the net thrust had been reduced and that it was necessary to increase the engine fuel flow in order to maintain constant engine speed as the inlet became iced.

CHARACTERISTICS OF HOT-GAS BLEEDBACK

Three hole arrangements in the hot-gas manifold at the duct inlet were investigated. The physical characteristics of these three hole modifications are shown in the following table:

Configuration	Holes per row	Hole diameter (in.)	Total area (sq in.)	Percent bleedback
1	76	11/32	7.05	$4\frac{1}{2}$
2	19	1/2	3.74	$3\frac{1}{2}$
3	15 4	1/2 7/8	5.35	4

A large number of small holes were used in the first configuration in order to obtain a homogeneous mixture of hot gas around the inlet of the engine. The temperature profiles measured $31\frac{1}{4}$ inches downstream of the point where the hot gas was injected into the air stream are shown in figure 8 for configuration 1. These profiles were obtained with the hot-gas bleedback valve wide open and with

approximately $4\frac{1}{2}$ percent of the total gas flow being bled to the engine inlet. The temperature close to the outer wall of the duct was excessively high; the temperature at 10,000 rpm reached a maximum of 175° F. The gas penetrated only about 6 inches into the air stream and the entire central portion of the inlet duct was at ambient-air temperature. It was not possible to bleed $4\frac{1}{2}$ percent of the total gas flow to the engine inlet at an engine speed of 12,000 rpm without exceeding the tail-pipe-temperature limit.

An investigation of jet penetration conducted in a 2- by 20-inch wind tunnel showed that the depth of penetration was a linear function of the diameter of the hole from which the jet was discharged (fig. 9). The data shown in figure 9 are for fixed flow conditions in the air stream and the jet, the hole diameter being the only variable.

In view of these results, the diameter of the holes was increased from 11/32 to 1/2 inch and the total hole area was reduced from 7.05 to 3.74 square inches for configuration 2. This modification was intended to increase the penetration and reduce the average compressor-inlet air temperature. Reducing the compressor-inlet air temperature increased the compressor Mach number, thereby increasing the compressor-outlet and turbine-inlet pressure. This increase in pressure resulted in a higher pressure in the hot-gas manifold, which raised the jet velocity and further improved the penetration.

The temperature profiles presented in figure 10 for configuration 2 show that the temperature was approximately constant for a distance of 4 inches from the outer wall of the duct and then dropped off approximately linearly. The hot-gas jets penetrated about $7\frac{1}{2}$ inches from the outer wall of the inlet duct. These data were obtained with the hot-gas bleedback valve in the wide open position, giving a bleedback of approximately $3\frac{1}{2}$ percent of the total gas flow. It should be noted that as the engine speed was increased, the temperature profile was raised. This resulted from the fact that, at the higher engine speeds, the temperature of the hot gas bled to the inlet was higher than at low engine speeds.

Several attempts were made to prevent ice formation at the engine inlet and also to de-ice the engine inlet with configuration 2. A photograph of the compressor inlet being de-iced with configuration 2 is shown in figure 11. The inlet was iced until the tail-pipe temperatures were slightly below the limiting value.

The water spray was then turned off and the hot gas was bled to the inlet. This photograph was obtained after approximately 10 minutes of de-icing the inlet with configuration 2. It should be noticed that there is a large cap of ice on the starter housing and several large formations of ice on the compressor-inlet guide vanes. After a period of 20 minutes de-icing with configuration 2, some ice still remained on the engine inlet, as shown in figure 12. The large cap of ice remained on the starter housing as a result of no penetration of the hot gas to that region and a few small pieces of ice remained on some of the compressor-inlet guide vanes.

In order to further improve the penetration, four of the 19 holes drilled in the hot-gas manifold were enlarged from 1/2- to 7/8-inch diameter. These holes were approximately 90° apart. Enlarging the four holes in this manner gave penetration to the center of the duct, as shown in figure 13. The survey rake that measured the temperature profiles was located directly behind one of the holes that had been enlarged. There was undoubtedly some stratification of hot gas at the center of the duct; however, it was believed that sufficient hot gas would penetrate to the center portion of the duct to prevent ice from forming on the starter housing. The profiles shown in figure 13 for configuration 3 indicate a fairly uniform temperature from the duct wall to a point about $5\frac{1}{2}$ inches from the wall of the duct. Beyond this point the temperature fell off gradually and, at the center line of the duct, the temperature for 9000 and 11,000 rpm was approximately 30° F higher than the ambient-air temperature. At an engine speed of 6000 rpm, it was not possible to obtain sufficient penetration to get hot gas to the center of the duct. However, the hot gas penetrated to within less than 1 inch from the duct center line.

When the hot gas was turned on and then the water spray was turned on, it was possible to prevent ice formation on the compressor-inlet guide vanes. Such investigations were conducted with both configurations 2 and 3. A number of attempts were made to de-ice the engine inlet and to prevent further ice from forming on the inlet with the water spray on and considerable ice already formed. When the ice began to form on the inlet and the tail-pipe temperature approached the limiting value, it was not possible to de-ice the inlet or to prevent further ice from forming on the inlet by bleeding hot gas from the turbine. When trying to de-ice in this manner, it was necessary to shut the engine down because of excessively high turbine temperatures. If the inlet was iced until the turbine temperatures reached approximately their limiting value and then the water spray was shut off, it was possible to de-ice the engine

inlet, except for the dome of the starter housing, with configuration 2 in a period of 15 to 30 minutes. These long periods of time for de-icing, however, are unsatisfactory.

It should, therefore, be emphasized that the purpose of the hot-gas bleedback system is to prevent the formation of ice on the engine inlet. This system is not adequate for de-icing the inlet of the engine once the ice has formed. When a turbojet engine inlet begins to ice, the tail-pipe temperatures rise rapidly and the engine is in extreme danger of becoming inoperative within a short period of time. It is therefore necessary to anticipate such icing conditions in flight and to operate the hot-gas bleedback system when such conditions exist.

Bleeding the hot gas to the inlet of the engine resulted in a reduction of net thrust. The percent decrease in net thrust is presented as a function of the percent gas flow bled to the inlet in figure 14 for an altitude of 20,000 feet, an airspeed of 140 miles per hour, and an ambient-air temperature of 30° F. These data show for three different engine speeds, that as the gas flow bled to the inlet was increased, the net thrust decreased and a linear relation exists between the gas flow bled to the inlet and the change in net thrust. The percent decrease in thrust also became greater at higher engine speeds. With 4 percent of the gas flow bled to the inlet of the engine, the net thrust was reduced 7.4 percent at an engine speed of 8000 rpm, 14.3 percent at 10,000 rpm, and 18.8 percent at 12,000 rpm. The reduction in thrust became greater as the engine speed was increased because the temperature of the hot gas bled to the inlet was also raised, which therefore resulted in a rise in the average compressor-inlet temperature with engine speed. The rise in inlet-air temperature due to bleeding hot gas to the inlet accounts for approximately 75 percent of the reduction in net thrust. The remainder of the reduction in net thrust resulted from bleeding gas from the turbine inlet.

Bleeding hot gas to the engine inlet also resulted in an increase in the specific fuel consumption. The percent increase in specific fuel consumption is presented in figure 15 as a function of the percent gas flow bled to the inlet. With 4 percent gas flow bled to the engine inlet, the specific fuel consumption was increased 16 percent for an engine speed of 8000 rpm, 27.2 percent at 10,000 rpm, and 21.2 percent at 12,000 rpm. The change in specific fuel consumption was also linear with respect to the percent gas flow bled to the engine inlet. It should be noted that the increase in specific fuel consumption for 12,000 rpm was less than for 10,000 rpm.

WIND TUNNEL PROGRAM

The investigation of inlet ice prevention in the altitude wind tunnel with the 24C engine using the hot-gas bleedback system is being continued. In this program the dome of the starter housing will be heated directly with hot gas. A dome will be installed over the present one and hot gas bled from one of the lines running forward alongside the inlet duct will be injected in the passage between the two shells. It is hoped in this way to prevent ice from forming on the starter housing. A single row of holes will be used in the inlet manifold. Nine of the holes will be 5/8 inch in diameter and three holes, spaced 120° apart, will be 7/8 inch in diameter. This will give a total hole area of 4.55 square inches and, with the hot gas being bled to the starter housing, there will be a total bleedback of about 4 percent, which was the same amount of hot-gas bleedback used with configuration 3.

In order to afford better control of icing at the inlet, the water spray tower will be so installed that it can be moved axially along the test section and thus may be positioned at different stations ahead of the engine inlet. This procedure will make it possible to ice the inlet while regulating the water quantity over a wider range of water concentration than has been investigated thus far.

An icing rate meter will be installed at the compressor inlet to make possible the determination of the rate of ice formation that occurs on the compressor-inlet guide vanes. The icing rate meter consists of a small disk that rotates slowly, with the edge of the disk placed normal to the direction of air flow. Ice formation on the disk will be measured by a cam riding along the surface of the ice and a scraper, mounted immediately behind the cam, will scrape the disk clear of ice on each revolution.

The range of conditions over which it is possible to prevent ice formation at the engine inlet will be determined more thoroughly. Ice prevention will be investigated at ambient-air temperatures down to 0° F and water flow rates that give water concentrations comparable to those found in actual icing conditions. If necessary, various modifications will be made to the hole arrangement in the cowl-inlet manifold in order to obtain adequate ice prevention over the entire range of icing conditions that may be encountered in flight.

CONCLUSIONS

Ice forms rapidly at the compressor inlet under severe icing conditions and is extremely dangerous, inasmuch as the engine may be rendered inoperative within 1 or 2 minutes after icing begins. The hot-gas bleedback system should be used to prevent ice formation at the engine inlet. With configuration 2, 15 to 30 minutes were required to de-ice the engine inlet with the water spray turned off and once ice had formed, the system was not adequate to de-ice the inlet with the water spray remaining on. With 4 percent of the gas being bled to the engine inlet, the net thrust was reduced 18.8 percent at an engine speed of 12,000 rpm. Raising the inlet-air temperature accounts for approximately three-fourths of this decrease in thrust. At similar operating conditions, the specific fuel consumption based on net thrust was increased $16\frac{1}{2}$ percent.

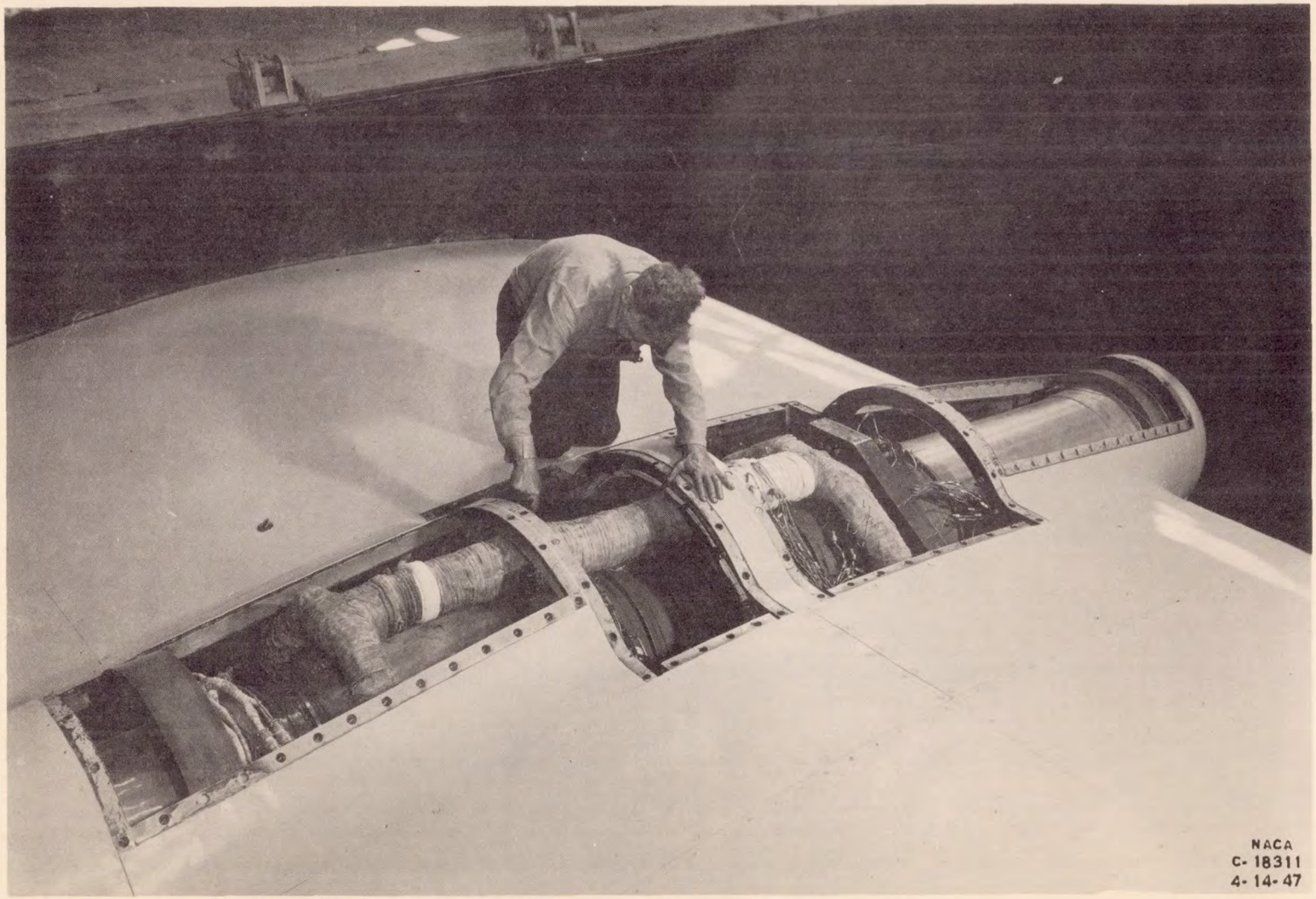

HOT-GAS BLEEDBACK SYSTEM
FIGURE 1.

INSTALLATION FOR ICING INVESTIGATION
FIGURE 2.

INLET ICING SPRAY
FIGURE 3.

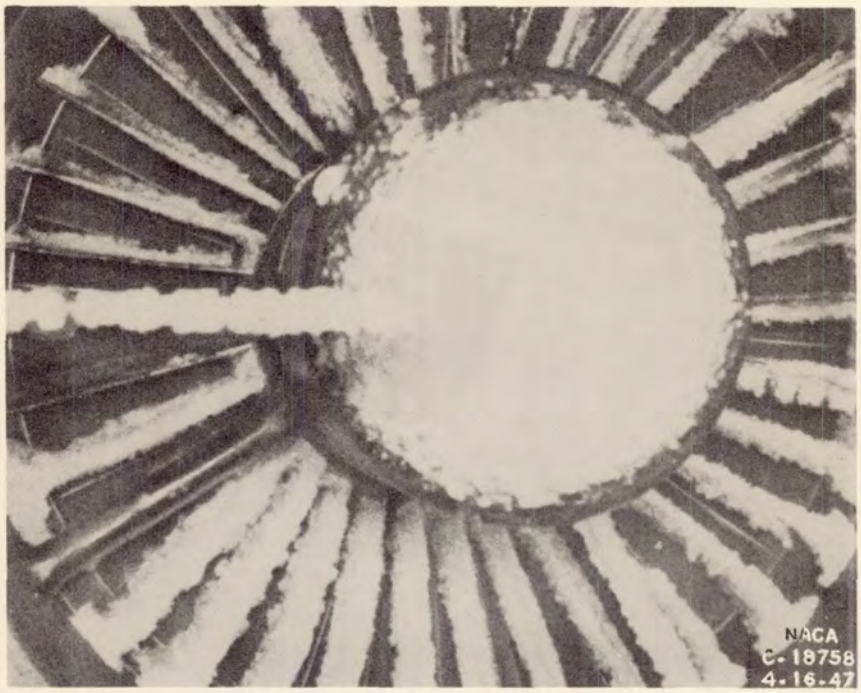

ENGINE INLET PARTLY ICED
FIGURE 4.

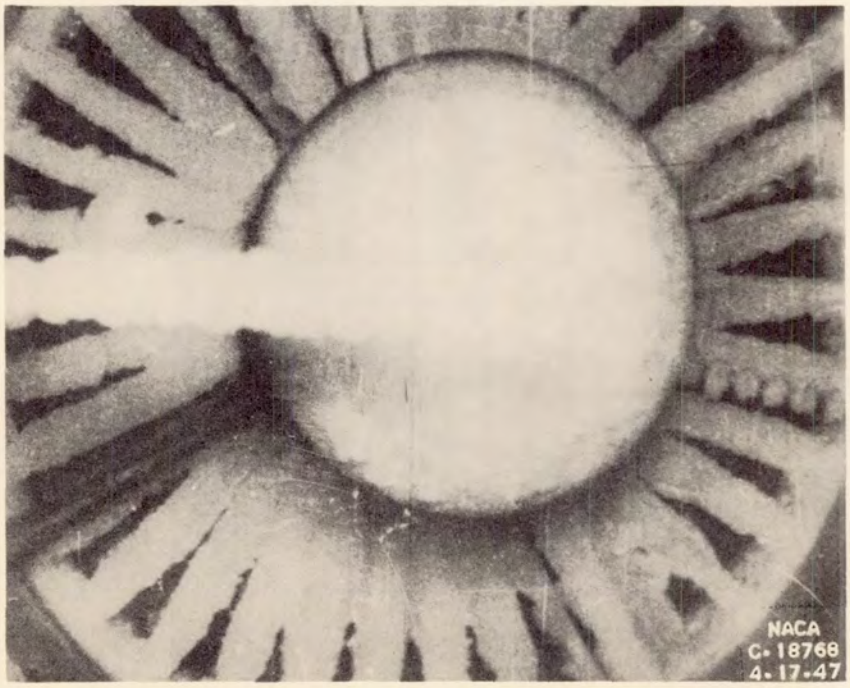

ENGINE INLET COMPLETELY ICED
FIGURE 5.

DECREASE IN THRUST WITH INLET ICED

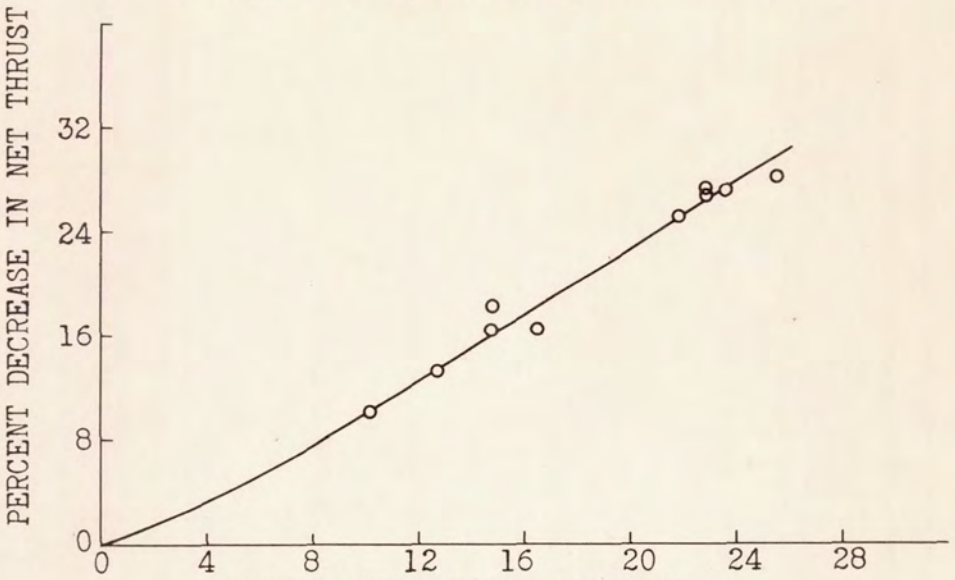

FIGURE 6.

INCREASE IN SPECIFIC FUEL CONSUMPTION
WITH INLET ICED

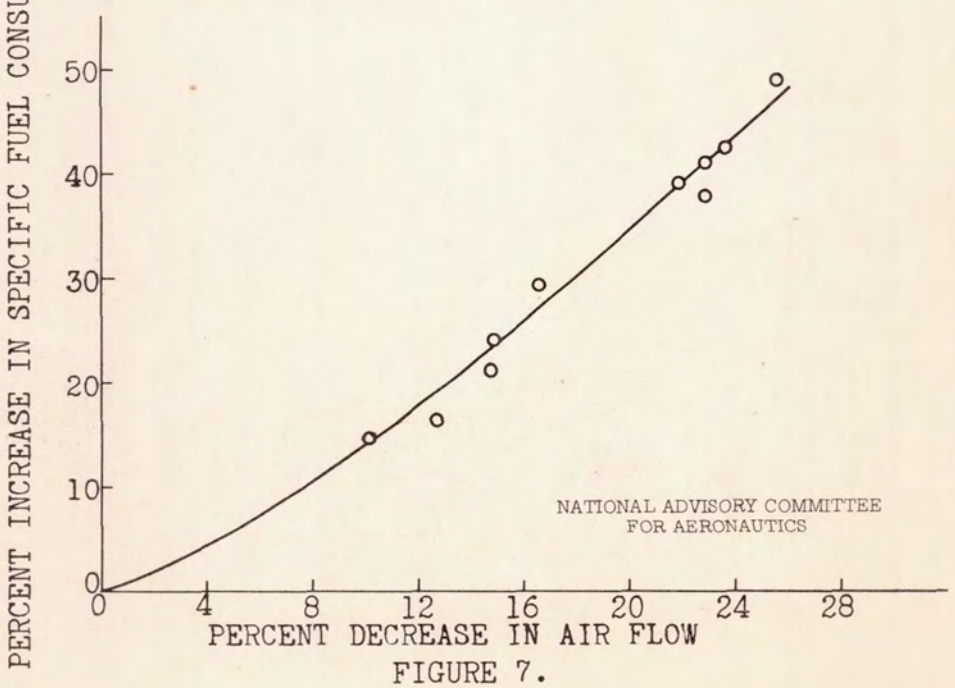

FIGURE 7.

INLET TEMPERATURE PROFILE
CONFIGURATION 1

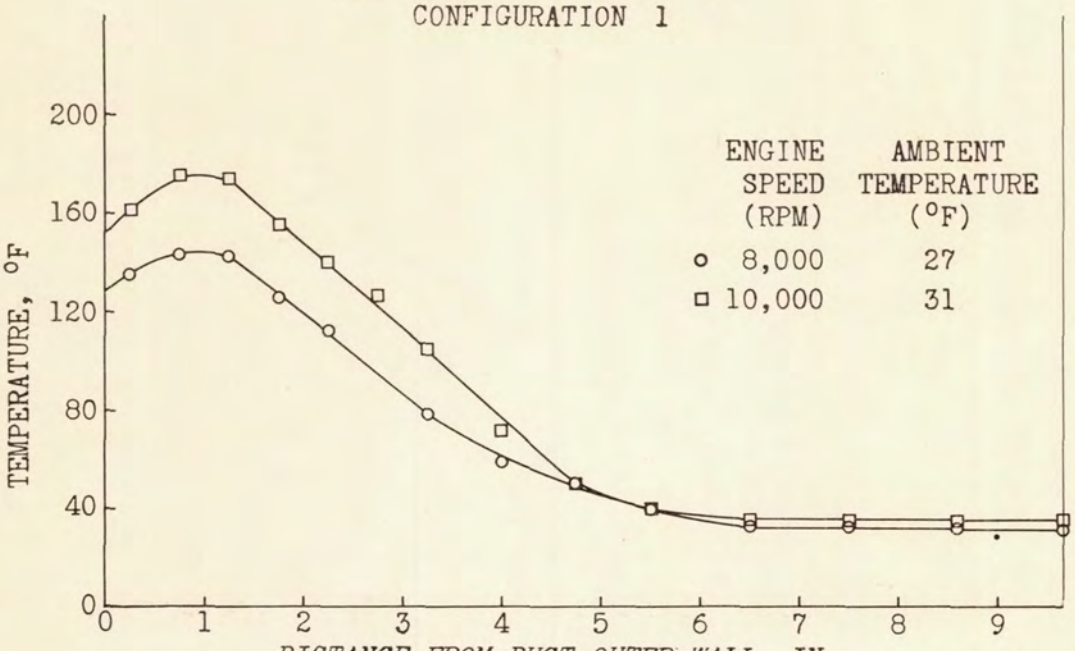

FIGURE 8.

EFFECT OF HOLE DIAMETER ON PENETRATION

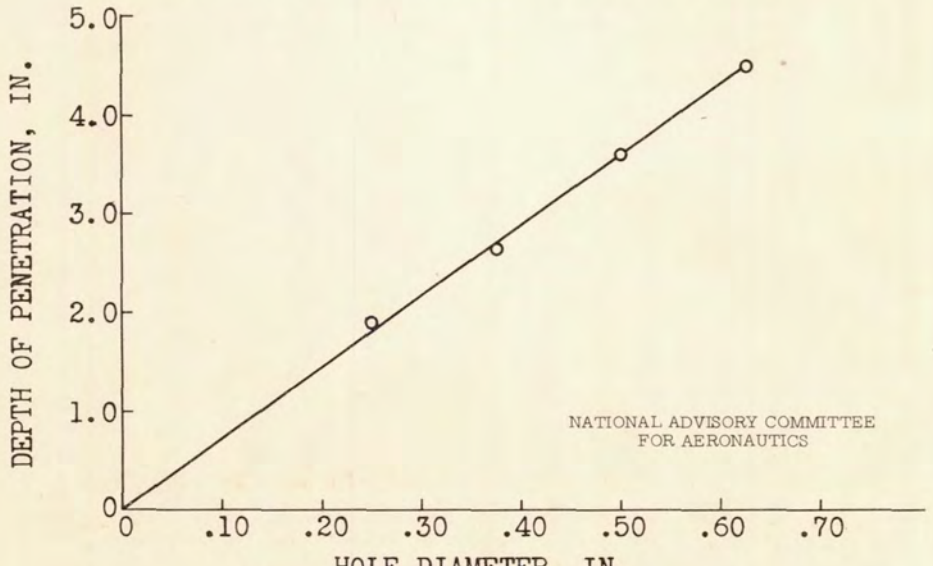

FIGURE 9.

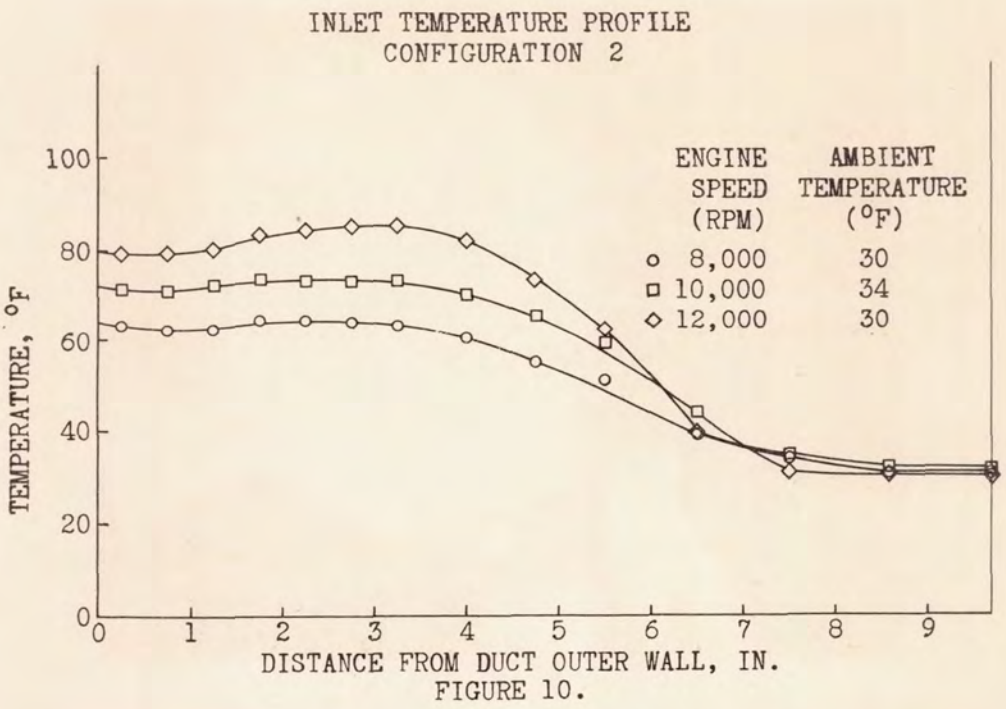

FIGURE 10.

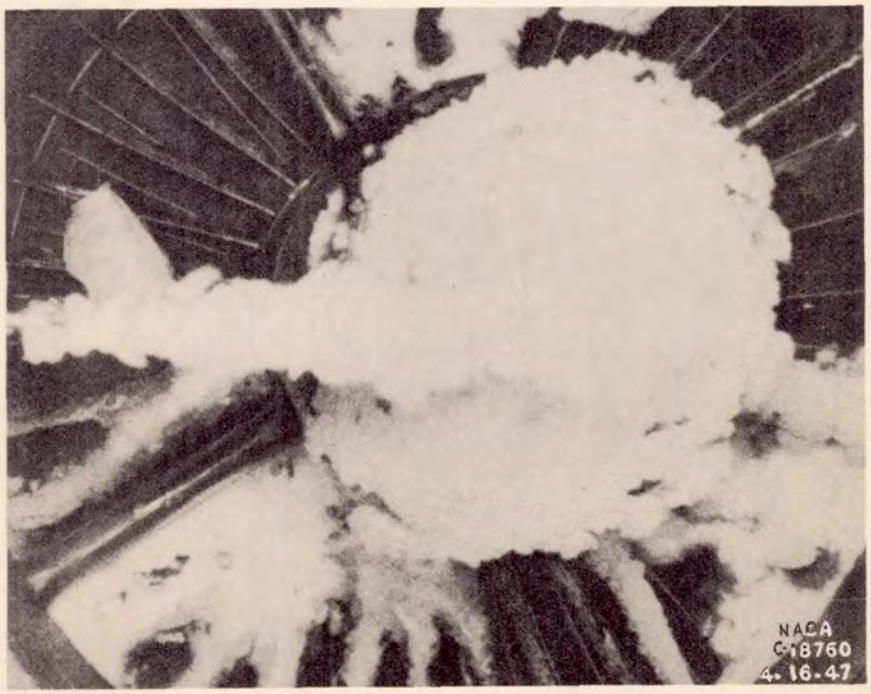

ENGINE INLET AFTER 10 MINUTES DE-ICING
FIGURE 11.

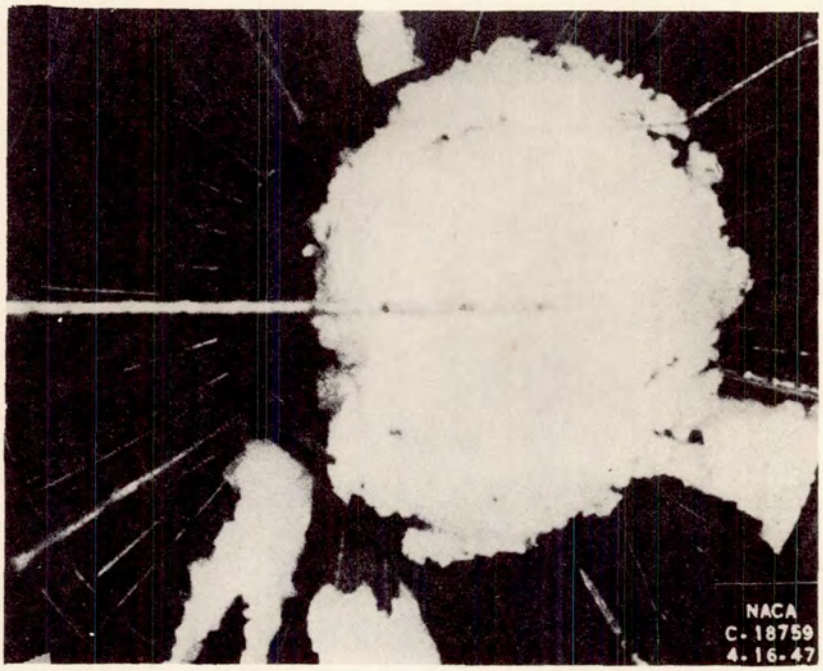

ENGINE INLET AFTER 20 MINUTES DE-ICING
FIGURE 12.

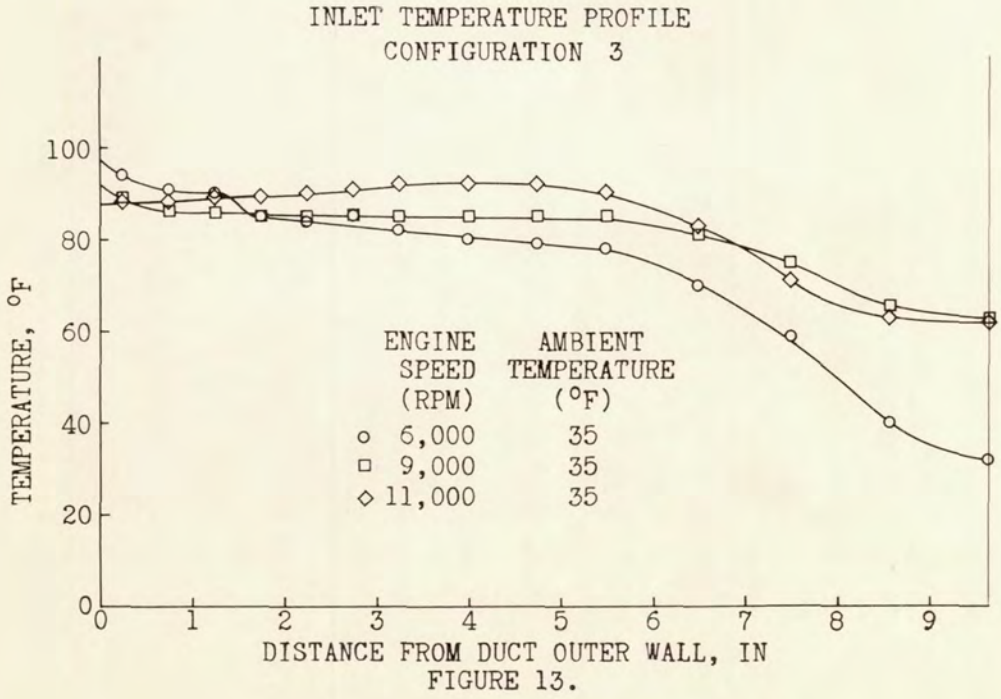

FIGURE 13.

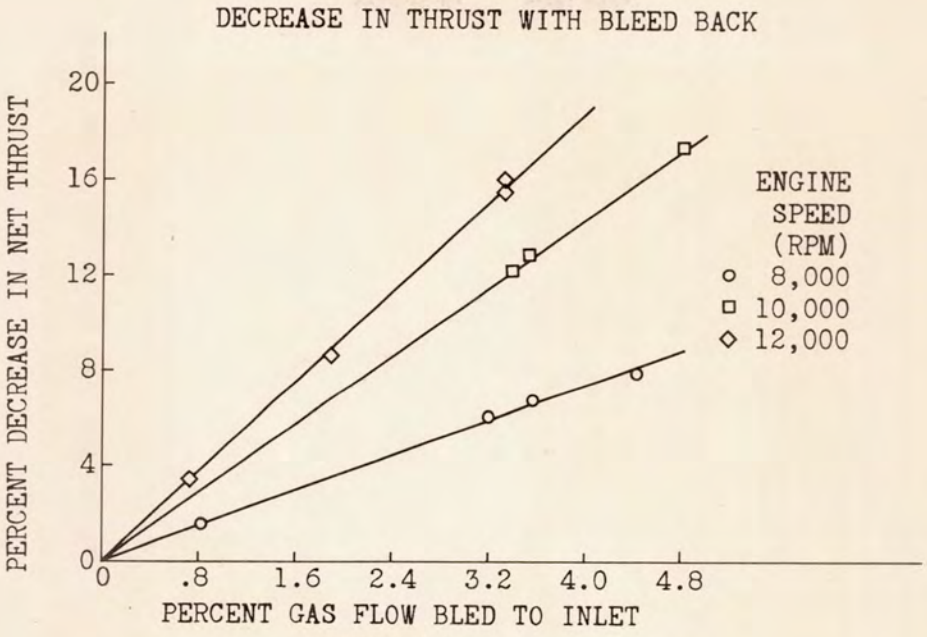

FIGURE 14.

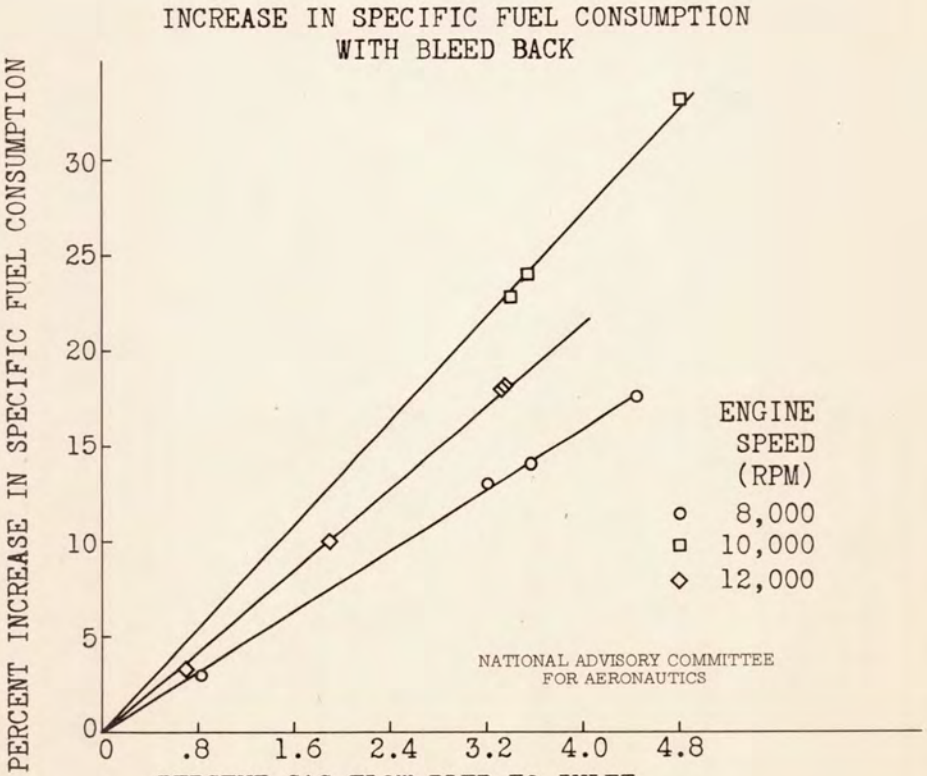

FIGURE 15.

PROTECTION OF JET-ENGINE INLETS BY MEANS OF INERTIA SEPARATION OF FREE-WATER PARTICLES

By Uwe von Glahn

Flight Propulsion Research Laboratory

INTRODUCTION

In endeavoring to protect turbojet engines from impact icing, it would appear that the following methods may provide the solution of the icing problem:

1. Bleedback of hot gases from some point in the engine and injecting the gases into the air stream ahead of the compressor inlet, thus raising the air and water-droplet temperatures above 32° F.

2. Heating all the surfaces subject to icing above 32° F.

3. Water-inertia separation from the air stream inside the nacelle by suitable inlet design.

4. External water exclusion by suitable inlet design.

After a study of the four methods which might be utilized to reduce the icing hazard to a minimum, the conclusion is that no one system can be applied to all aircraft. The methods presented can be applied only at the expense of aerodynamic performance, air frame weight, compressor design, or cabin pressurization.

This paper presents methods 3 and 4 for the ice protection of turbojet engines.

The design criterions for the turbojet engine inlet must include the following:

1. The rate of free-water ingestion must be reduced to a minimum.

2. Ram-pressure recovery must be maintained as high as possible in order not to reduce the engine performance.

3. The inlet shall be automatic in its operation throughout an icing condition.

With these conditions in mind, aerodynamic and preliminary icing tests were conducted in the NACA Cleveland icing research tunnel on experimental nonicing inlets for use with axial-flow turbojet engines.

TWO CONCENTRIC DUCT SYSTEM

The elimination of free water from induction systems at its source is an effective means of preventing impact icing (reference 1). With a good design, most droplets above 20 microns, wet snow, and sleet particles can be eliminated from the inlet air with a progressively increasing percentage of smaller droplets remaining in the air as the droplet size decreases.

A proposed design which eliminates water droplets from the air by inertia separation inside a nacelle, shown in figure 1, consists of two concentric annular ducts. During normal operation, air will enter the engine unit through the main (inner) duct. In an icing condition, the screen at the rear of the inner duct will block with ice rapidly and the inlet air will then enter only through the outer duct. Inasmuch as the air makes a sharp turn to enter the outer annular duct, the water droplets because of their greater inertia cannot follow and will accumulate in the inner duct where then can cause no harm to engine operation. In icing conditions the operation time of this inlet is limited by the icing rate in the main duct which in turn depends on the liquid-water content of the air, the droplet size, and the airspeed.

When the ice in the inner duct melts, the water may be drained off harmlessly through the engine. For large formations of ice in the inner duct, special drainage facilities may be required.

The design of a water-inertia separation induction system depends primarily upon three configuration variables, shown in figure 1; namely, the inlet gap or distance between the duct surfaces, the radial offset of the inner lip above the inlet opening, and the curvature of the duct surfaces. The greater the offset and the smaller the gap, the less tendency there will be for water droplets to enter the duct; however, the ram-pressure recovery must also be considered in the induction system and will influence the location of the duct members. A simplified analytical method, which can be applied to the designs investigated, is presented later. This analysis can be extended to all types of inertia-separation designs within its assumed limitations.

The models were instrumented to obtain mass flow variations circumferentially around the model, velocity profiles and ram-pressure recovery at the compressor inlet. Screens at the compressor-inlet section were used to determine the effectiveness of the water-inertia separation characteristics of the inlets by a measure of the amount of ice collected on the screens.

The droplet size, determined by the rotating-cylinder method developed by Langmuir (reference 2), was approximately 12 to 15 microns by volume maximum and the total temperature varied from 18° to 27° F for the icing tests. The ram-pressure recovery η was calculated as $1 - \left(\frac{P_0 - P_2}{q_0}\right)$

where

P_2 integrated average total pressure at the compressor inlet

P_0 free-stream total pressure

q_0 free-stream dynamic pressure

The integrated average ram recovery of all the aerodynamic-rake stations in the compressor-inlet section was chosen as the configuration ram-pressure recovery value. As a basis for comparison in figure 2, the alternate duct was sealed as a direct-ram installation and the nacelle was investigated for ram-pressure recovery. The ram-pressure recovery did not vary more than 1.5 percent at angles of attack up to 8° from the values attained at zero angle of attack. Losses were due to the sudden area expansion from the inlet section to the greater area surrounding the accessory housing. The final pressure losses for the direct-ram inlets were due to the wakes from the struts supporting the duct-splitter ring.

From total- and static-pressure measurements obtained in the rear part of the alternate duct, it was found that little or no air passes through the alternate duct for normal flight operation.

High local velocities were prevalent in the duct elbow when the air passed only through the alternate duct. This was especially true for configurations that had a small alternate duct cross-sectional area and was favorable to secondary water-inertia separation in the elbow. The variation of ram-pressure recovery with inlet velocity ratio for normal flight operation is also shown in figure 2.

With the main duct blocked, as would be the case for an icing condition, the ram-pressure recovery decreased rapidly with an increase in the inlet velocity ratio. Seven types of duct-splitter rings, varying in alternate duct-inlet area, radial offset above the inlet surface, and diffusion in the alternate duct, were investigated. In general the configurations having the largest alternate duct inlet show a higher ram recovery than the small-gap designs; however, the larger alternate duct inlets were also subject to rather severe screen icing.

The effect of ram-pressure recovery on the net thrust obtained with a typical turbojet engine is of considerable importance. The performance of an axial-flow engine was calculated to include the usual operations range. As the free stream Mach number M_0 increases, the effect of a high ram-pressure recovery becomes increasingly more important. It was found that a M_0 value of 0.2, which is representative of take-off conditions, the net thrust is little affected by a ram-pressure recovery as low as 50 percent. At a cruise condition of $M_0 = 0.6$ in an icing condition, a recovery of 75 percent will maintain 90 percent of the net thrust. For normal cruise operation, 3 percent or less of the maximum net thrust need be sacrificed with a good internal water-inertia separation inlet.

Typical velocity profiles for the compressor-inlet section are shown in figure 3 for the direct-ram inlets and for the inertia-separation inlets. The profiles are relatively uniform for all configurations at $\alpha = 0^\circ$; while at $\alpha = 8^\circ$, the nonuniformity increases slightly. Screens in the duct had some effect in making the distribution more uniform. With the main duct blocked, the velocity profiles are even more nonuniform at zero degrees angle of attack, as shown in figure 3.

Four nacelle nose designs shown in figure 4 were investigated in the course of the internal water-inertia separation program in an effort to improve the ram-pressure recovery and mass flow stability of the duct system at angles of attack. The original nacelle nose N-1 was designed for an inlet velocity ratio of 0.77. The second nacelle nose N-2 consisted of the nacelle nose N-1 arbitrarily redesigned to provide a faired inlet with a larger leading-edge radius. The entry velocity ratio for the N-3 inlet was 0.65 and converged to an effective ratio of 0.77 just ahead of the alternate duct inlet. Nacelle nose N-4 was a converging design with an entry velocity ratio of 0.60 and an effective velocity ratio ahead of the alternate duct inlet of 0.63. The N-3 and N-4 nose designs were investigated with nacelle-wall radius of 2 and 3 inches.

The effect of the redesigned nose sections on the ram-pressure recovery for normal operation and for operation with the main duct blocked is shown in figure 5. It can be seen that for normal operation an inlet (N-4) with a lower inlet velocity ratio will improve the ram-pressure recovery by as much as 10 percent above that obtained with high velocity ratio inlets (N-1, N-2, and N-3). An increase in ram-pressure recovery is also observed when the main duct is blocked. The change in nacelle-wall radius from 3 inches to 2 inches did not affect the aerodynamic performance of the duct system.

In the icing tests, typical cowl icing was observed on the nose itself. All icing runs were made near the design inlet velocity ratio.

At angles of attack, the upper portion of the nacelle-nose inlet surface was subjected to direct water impingement and severe icing occurred. No ice accreted on the duct-splitter ring surface in the alternate duct aft of the inlet. The main duct and accessory housing surfaces were coated with moderate-to-heavy formations of ice.

In general, the higher the ram-pressure recovery for the flight condition in which the main duct is blocked, the more ice was deposited on the screen and on the alternate duct nacelle wall. With a small inlet area and high velocities in the alternate duct, no screen icing was observed.

The validity of the data obtained from an icing investigation of a scaled-aircraft component depends primarily on whether or not the component collection efficiency and the angle of water interception on the model are identical to the full-scale values (reference 3). In the present investigations it was possible, by maintaining the air velocity at the compressor inlet at one-half the full-scale velocity, to obtain icing characteristics that can be applied to a full-scale model.

DESIGN ANALYSIS OF TWO CONCENTRIC DUCT SYSTEM

For a high critical Mach number nacelle design incorporating a straight section as part of the inlet, the curved surface into the alternate passage and the streamlines near that surface can be assumed to be a circular arc. The center of curvature for the nacelle radius is also the center of curvature for the streamlines. By starting at the surface point of tangency of the radius and

nacelle-inlet straight section, the departure of droplets (based on Stokes' law) can be computed by a method proposed by Stickley (reference 4).

The equations used apply only in the range of Stokes' law; however, on the basis of an investigation by Langmuir (reference 2), a Reynolds number correction for velocity has been made available. Thus, by choosing a true droplet diameter and velocity, the equivalent Stokes' diameter can readily be determined and used for droplet departure.

The droplet flow paths can be obtained from a graphical plot and then the location of the inner duct-splitter ring surface for a given design condition can be determined. The leading edge of the duct-splitter ring should be located at the inflection point of the nacelle-wall surface because at this point the droplet no longer departs from the streamlines in an advantageous manner. For a simple analysis, the velocity in the duct is considered constant. The analysis can be extended by calculating the secondary inertia separation in the other parts of the duct system by similar means.

The analytical method has been applied to a typical high inlet-velocity-ratio nacelle of the type investigated in the icing research tunnel. The data presented in figure 6 indicates that the variation of inlet gap with velocity is approximately a straight line for the assumed droplet sizes and arc angle θ, which is the turning angle into the alternate inlet.

The percentage of droplets of varying size that enter a configuration is determined by designing the installation to exclude all droplets above a predetermined size for a given velocity and nacelle-wall radius. The quantity of droplets of each size that enter the configuration can be determined on an inlet-area basis.

The largest droplet (fig. 7) that will enter an alternate inlet having a nacelle-wall radius of 4 inches at a velocity of 635 feet per second was determined. The critical droplet size is the maximum size that starts at the nacelle surface and is tangent to the outer surface of the splitter ring. The droplet-entry efficiency for a critical droplet is 0 percent. The term "droplet-entry efficiency" is defined as the ratio of the number of droplets of a given size that will enter the alternate duct to the number present in the inlet.

The analysis is then continued to determine the largest droplet that will enter the alternate inlet from a streamline below the inside

nacelle surface and is then continued for other streamlines, resulting in the curves shown in figure 7. For a given icing condition for which the droplet-size distribution is known, the volume percentage that will be ingested can easily be determined from figure 7.

The results of the investigation indicate that, over the usual range of operating conditions for an internal water-inertia separation inlet of the concentric-duct type, a relatively low ram-pressure recovery will result in an icing condition if the alternate duct screen is to remain ice free. An analysis of the effect of a low ram-pressure recovery on the net thrust obtained with a turbojet engine shows that for most conditions the engine would still maintain good performance; a recovery of 75 percent resulted in obtaining 90 percent of the available net thrust. For normal nonicing flight conditions only slightly greater losses, perhaps 3 percent, would be suffered than would be incurred with a direct-ram inlet.

It must also be considered that certain parts of the inlet such as the nose section and the areas in the alternate-duct elbow that are subject to severe icing due to secondary inertia separation must be protected by local surface heating.

SINGLE DUCT SYSTEM

A variation utilizing the water-inertia separation principle and based on the alternate-duct inlet is a design of a single duct entry that has several advantages over the two duct system provided that a high ram-pressure recovery can be attained. A single duct system, eliminates the rapid diffusion areas at the alternate-duct inlet and exit. The single duct system also does not depend on the main-duct screen icing characteristics to become effective in an icing condition.

Several configurations were investigated as single-duct inlets by blocking the main duct with a large plate near the alternate-duct inlet. A spike-nose design providing a constant-area passage from the nacelle-nose inlet to the duct elbow was also investigated.

The results, covering the investigation of a single-duct water-inertia separation inlet, were similar to those obtained for the condition in which air entered only the alternate duct. The spike-nose accessory housing did, however, improve the flow stability in the duct at angles of attack.

The single-duct inlets iced similarly to the previous designs, but the icing tolerance was considerably reduced by the lack of a suitable ice trap.

SUBMERGED-NOSE INLET SYSTEM

Recent research on the submerged entrance or the flush-inlet type of air intakes that are not subject to direct water impingement has shown that total-pressure recoveries of the order of 92 percent can be achieved with a nonramming inlet. The inlets were located in the sides of the fuselage and hence were not severly affected by angle of attack.

In the icing tunnel investigation, two basic submerged inlet configurations and modifications to each were investigated. The basic design, one of which is shown in figure 8, consisted of an annular submerged-nose inlet located in the nacelle nose just ahead of the maximum diameter in order to take advantage of the favorable pressure gradient along the surface. The ramp angles for the two models were 17° and 9° respectively. The inlet gap or area was purposely made small for the first design in order to provide a high inlet velocity and thus better water-inertia separation characteristics.

Modifications consisting of moving the forward body ahead, thus increasing the inlet area and reducing the duct velocities, were investigated.

In general, the aerodynamic and icing characteristics of the annular submerged-nose inlets investigated were unsatisfactory. The high ram-pressure recovery obtained in other investigations was not realized.

The rough model surfaces contributed excessive boundary-layer development at the inlet and had a great effect on the ram-pressure recovery. At $\alpha = 4^{\circ}$, the mass flow shifted to such an extent that almost no flow was passing through the top quarter of the nacelle. Velocity profiles for the annular submerged-nose inlet show that the flow has a pronounced tendency to separate from the ramp surface and consequently is extremely nonuniform. Increasing the inlet area had the effect of improving the aerodynamic characteristics of the inlet by both increasing the ram-pressure recovery and by making the velocity profiles more uniform.

In the icing tests at zero angle of attack, the nose section of the annular submerged-nose inlets iced heavily to about 5 inches from the stagnation point and light ice formations continued aft 3 inches

more. The configuration with the smallest inlet gap had the least screen icing. The screen ice was most noticeable on the screen brackets near the nacelle wall of the duct where the velocity was highest.

When the inlet area was increased, heavier screen icing was observed. No appreciable change in screen icing was observed when differently shaped nose sections were used on the forward body of the nacelle.

Therefore, unless extremely high inlet velocities are used, which is impractical and often impossible on a full-scale model, the inlet will ingest large quantities of water and, hence, is subject to severe icing. Inlets submerged in the sides of a nacelle or fuselage would eliminate the severe mass flow shifting associated with angle of attack, but would probably not improve the water ingestion characteristics of the inlet.

CONCLUSIONS

The results of the investigation of several types of nonicing inlet designs can be summarized as follows:

1. An internal water-inertia separation inlet composed of two concentric ducts can be designed to prevent the entry of most of the free droplets into the outer annular duct. The degree of water separation depends on the ram-pressure recovery that can be tolerated in an icing condition; the better the droplet separation characteristics, the lower the ram-pressure recovery. For normal flight operation, ram-pressure recovery values comparable to those obtained with direct-ram inlets can be obtained. The nacelle-nose inlet, duct-splitter ring leading edge, and alternate-duct elbow surfaces must be heated locally.

2. The single-duct inertia-separation inlets did not show improved performance characteristics over those of the two duct system for an icing condition and also had a low ram recovery for all flight conditions.

3. The annular submerged-nose inlets investigated excluded some of the droplets but were still subject to considerable screen icing. These inlets also exhibited undesirable aerodynamic characteristics.

REFERENCES

1. von Glahn, Uwe., and Renner, Clark E.: Development of a Protected Air Scoop for the Reduction of Induction-System Icing. NACA TN No. 1134, 1946.

2. Langmuir, Irving: Super-Cooled Water Droplets in Rising Currents of Cold Saturated Air. Parts I and II. General Electric Co., Res. Lab., April 1945.

3. Langmuir, Irving, and Blodgett, Katharine B.: A Mathematical Investigation of Water Droplet Trajectories. Army Contract W-33-038-ac-9151, General Electric Co., Dec. 1944 - July 1945.

4. Stickley, A. R.: Some Remarks on the Physical Aspects of the Aircraft Icing Problem. Jour. Aero. Sci., vol. 5, no. 11, Sept. 1938, pp. 442-446.

INTERNAL WATER-INERTIA SEPARATION INLET

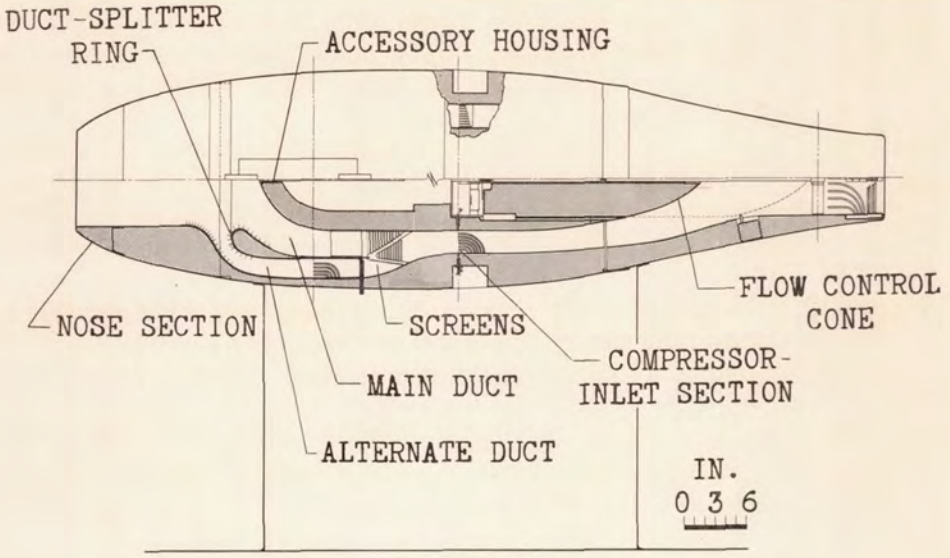

FIGURE 1.

EFFECT OF VELOCITY RATIO ON RECOVERY

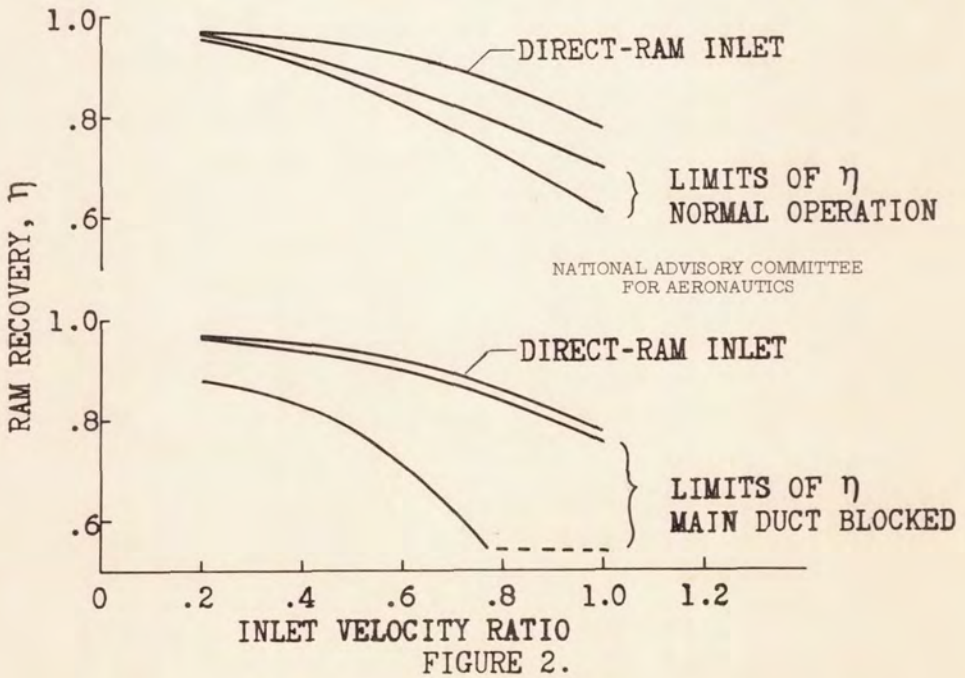

FIGURE 2.

AVERAGED RADIAL VELOCITY PROFILES
$\alpha = 0^\circ$

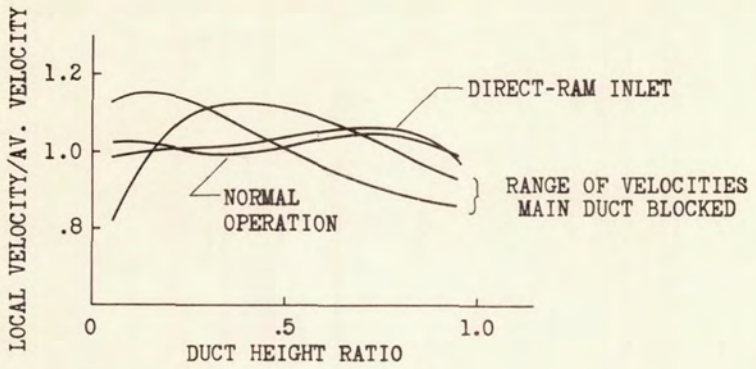

FIGURE 3.

NOSE CONTOURS

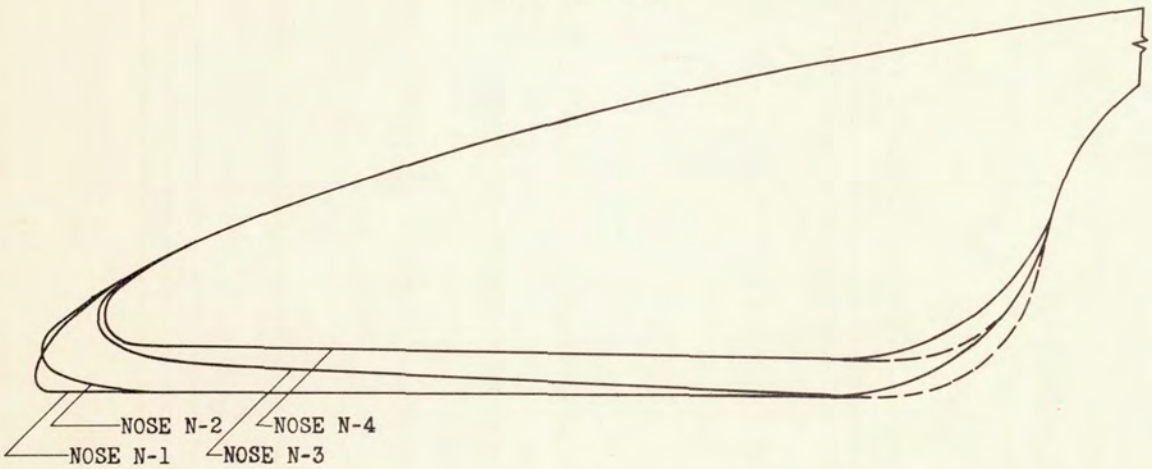

NATIONAL ADVISORY COMMITTEE FOR AERONAUTICS

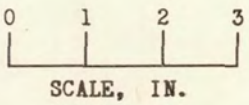

NACELLE CENTER LINE

FIGURE 4.

EFFECT OF NOSE INLET ON RAM RECOVERY

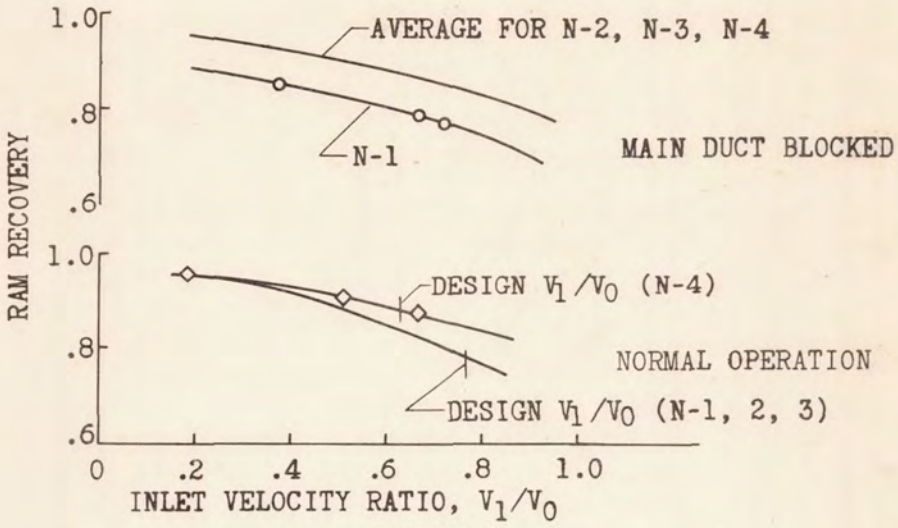

FIGURE 5.

VARIATION OF GAP WITH VELOCITY AND DROPLET SIZE

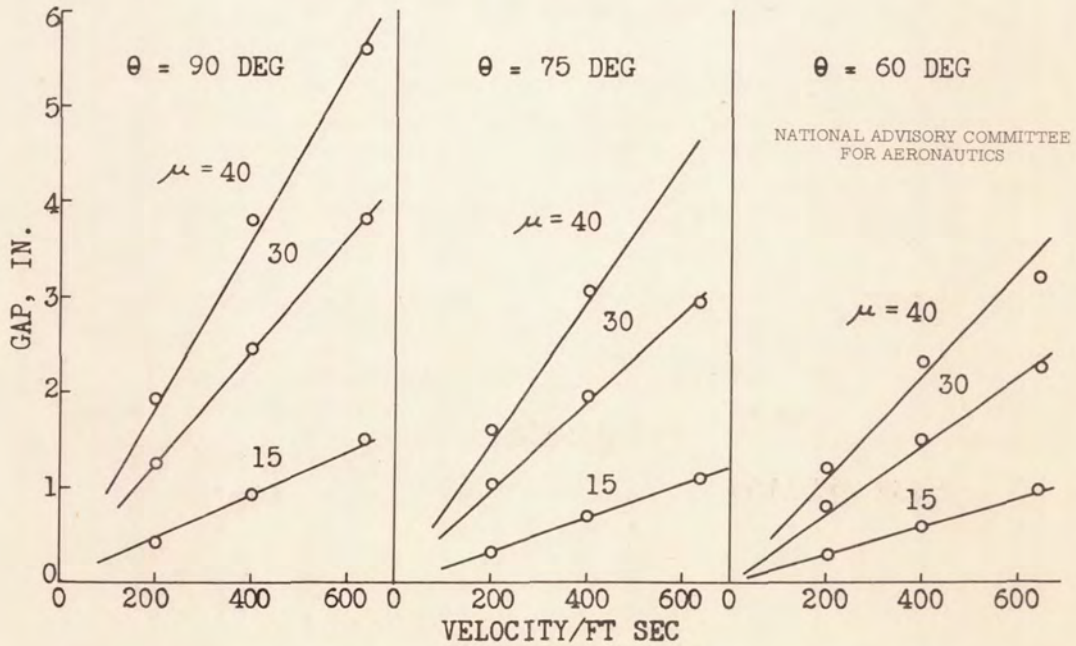

FIGURE 6.

DROPLETS ENTERING ALTERNATE DUCT

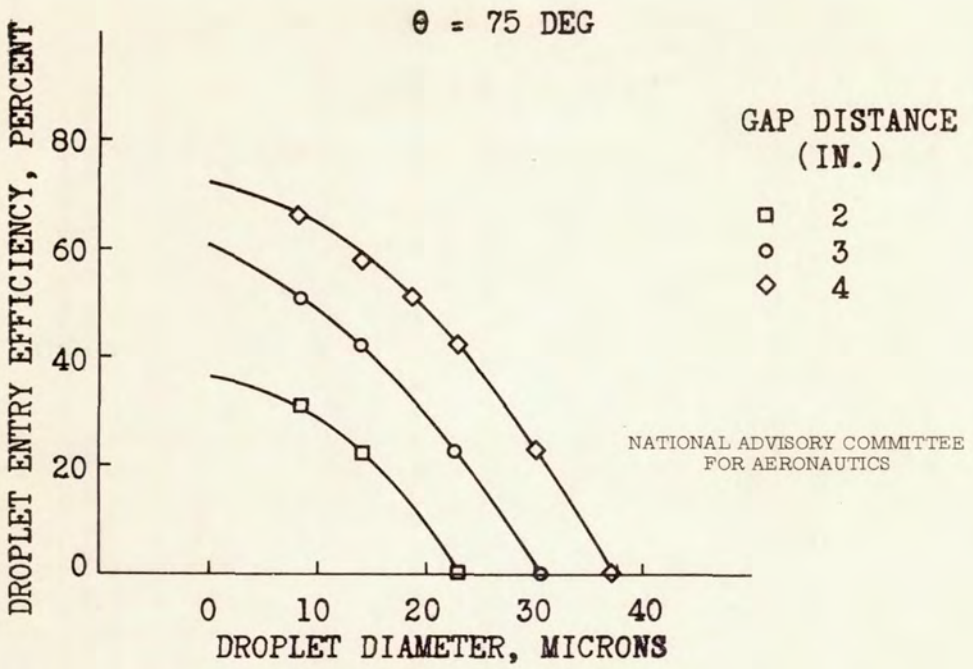

FIGURE 7.

ANNULAR SUBMERGED-NOSE INLET

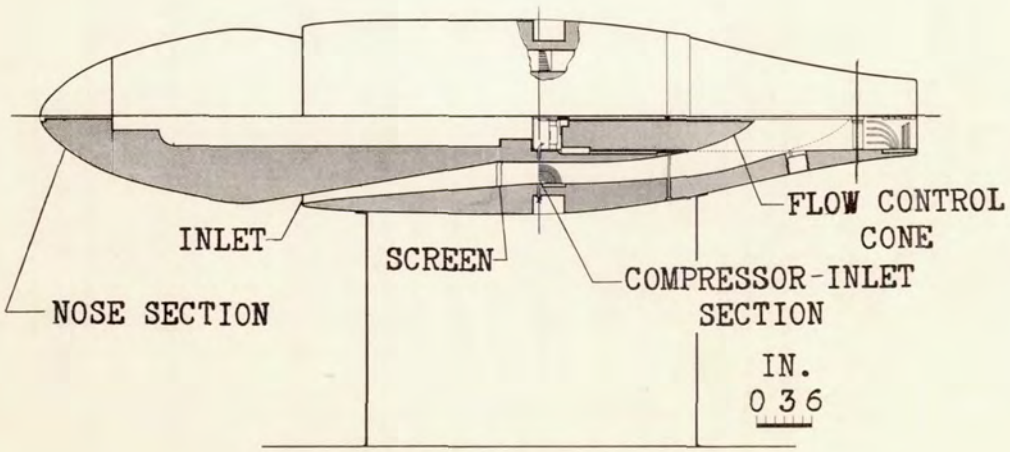

FIGURE 8.

ENGINE COOLING FAN AND PROPELLER SPINNER DE-ICING

By E. E. Callaghan

Flight Propulsion Research Laboratory

ENGINE COOLING FAN

In certain installations of high-powered radial engines in airplanes of large gross weights the problem of engine cooling is very difficult.

The use of an engine cooling fan, in either the submerged or nacelle type installation, has become the customary means of providing the additional cooling air that is necessary. Any blockage of the fan that would reduce the amount of cooling air must, of course, be prevented and anti-icing or de-icing of the fan is a problem of fundamental importance. Because of this expected loss in cooling air flow due to icing of the fan blades, an investigation of a typical cooling-fan installation was conducted in the icing research tunnel of the NACA Cleveland laboratory to determine the icing characteristics of the fan assembly components, to evaluate the effect of icing on fan performance, and to investigate the effectiveness of several systems of ice protection (reference 1).

Apparatus and procedure. - The cooling-fan assembly was mounted on the modified nose section of an airplane fuselage installed in the diffuser section of the icing research tunnel as shown in figure 1. The installation consisted of a typical propeller speed fan, a stator vane and diffuser assembly, a baffle plate located in a constant-area annular duct downstream of the fan to simulate the pressure drop across a radial engine, a standard radial-engine cowling, a three-bladed propeller and spinner, and necessary instrumentation.

The cooling-fan assembly was designed to be mounted at the front face of a radial engine and enclosed by the engine cowling with the fan rotor attached to the rear of the propeller hub and the stator vane assembly attached to the rear of the reduction-gear housing. The front fairing of the fan disk was of the "dishpan" type with a large forward bulge at the outer diameter of the dishpan. The fan had 72 cambered sheet-metal blades with a tip diameter of 43 inches and a tip clearance of $\frac{3}{16}$ inch. As part of the cooling-fan assembly, 49 cambered sheet-metal stator vanes were located behind the fan to remove the rotational component of the flow.

Total pressure in front of the fan and total and static pressure behind the stator vanes were measured by pressure-tube rakes as shown in figure 2. Four equally spaced rakes of shielded total-pressure tubes were located at the lip of the engine cowling between the fan and the propeller. These rakes were unheated because of the extreme difficulty in heating small shielded total-pressure tubes and hence, were used only in nonicing pressure-distribution studies. Electrically heated rakes consisting of four total-pressure tubes and one static-pressure tube were installed behind the stator vanes at four equally spaced positions corresponding to the positions of the front rake. In addition, static pressures were measured on the inner wall of the diffuser in the plane of the rear rakes.

The tunnel ambient-air temperature was measured by two shielded thermocouples located approximately 15 feet downstream of the cooling fan. A battery of four stroboscopic flash lamps permitted observations of the fan while operating.

The investigation was made at fan speeds and airspeeds corresponding to rated-power, cruise-power, and rated-power climb conditions of the airplane for which this particular fan was designed. The airplane thrust axis was at an angle of attack of 0° for the entire investigation.

Because of the difficulty of heating the shielded total-pressure tubes in front of the fan during the icing investigation, a calibration was made under nonicing conditions to determine the variation in air-flow total pressure at the fan inlet with tunnel airspeed, fan speed, and baffle pressure drop.

The general procedure for the icing investigation was as follows: After stabilizing the air temperature, tunnel airspeed, and fan speed at the desired conditions, the icing spray was started. All data were recorded at 1-minute intervals and visual observations of the icing were continuously made using the stroboscopic light system. The length of each icing experiment was determined by the severity of the icing of the cooling-fan assembly and the drop in the tunnel-air velocity due to icing. Upon completion of each experiment, photographs were taken of the residual ice formation on the component parts of the fan assembly. For all the experiments the drop size was approximately 55 microns and the water content varied from 0.3 gram per cubic meter to 1.1 grams per cubic meter.

Results and discussion. - Typical icing of the whole fan assembly under heavy icing conditions is shown in figure 3, the icing period was 5 minutes at an air temperature of 23° F and a liquid-water content of 0.9 gram per cubic meter. The fan speed was 872 rpm. A close-up showing the ice formations on the fan blades and stator vanes is

shown in figure 4. Although the fan blades are relatively free of ice, the stator vanes are completely blocked. A view looking upstream (fig. 5) showing the ice formations blocking the gaps between the vanes indicates the severity of the problem. In this case, complete blockage was accomplished in 5 minutes.

The results of the investigation are presented in the terms of the fan-performance coefficients C_p and C_q and by photographs of icing. The fan-pressure coefficient is defined as $C_p = \frac{P}{\rho/2\,(\pi nd)^2}$ and the air-flow coefficient as $C_q = \frac{Q}{nd^3}$

where

d fan-tip diameter, ft

n fan speed, rps

ΔP pressure rise through fan assembly $(P_2 - P_1)$, lb/sq ft

P_1 total pressure at front of fan, lb/sq ft

P_2 total pressure at rear of fan assembly, lb/sq ft

Q cooling-air flow, cu ft/sec

ρ cooling-air mass density, slugs/cu ft

The effects of icing on fan performance are shown in figures 6 and 7 where the ratios of the air flow and fan pressure of the iced fan to that of the fan before icing $\frac{C_q}{C_{q,0}}$ and $\frac{C_p}{C_{p,0}}$, respectively, are plotted against time. Although insufficient data were available to compare the effects of icing at all icing and performance conditions, the results shown are complete enough to define the effects of icing on fan performance throughout the normal range of icing and performance conditions.

Figure 6 shows that the only condition at which the air-flow coefficient ratio did not markedly decrease was at an air temperature of 2° F, liquid-water content of 0.3 gram per cubic meter, and fan speed of 872 rpm. At 16° F, 0.5 gram per cubic meter, and 897 rpm, the air-flow coefficient ratio decreased, approaching the minimum required value for engine cooling under these conditions in 5 minutes; whereas at 14° F, 0.5 gram per cubic meter, and 1060 rpm, the air-flow coefficient ratio fell to the minimum required value in $3\frac{3}{4}$ minutes, continued to decrease, and reached a fairly stable value

after 6 minutes. At approximately the same fan speeds as the experiments at 897 and 1060 rpm and at 23° F and 0.9 gram per cubic meter, the cooling air-flow coefficient fell off sharply, reaching the minimum required value in 2 to 3 minutes, and continued to decline with a complete stoppage of the flow occurring in 5 to 6 minutes.

The variation in the pressure-coefficient ratio at the same speed and icing conditions (fig. 7) exhibited similar trends, at 14° and 16° F the decrease in pressure coefficient was primarily due to icing at the fan blades.

In addition to the fan and stator blades, several other components of the fan assembly were subject to icing. The fan-disk dishpan accumulated ice in varying degrees. For most conditions, this icing was fairly light, never exceeding 3/8 inch in thickness. With the exception of runs at an air temperature below 5° F, this ice was periodically thrown off in irregular patterns. Although the dishpan is of small diameter, this irregular throw-off of ice could contribute to propeller unbalance in icing conditions particularly at higher fan speeds. Heavy icing of the engine cowling lip and the inlet duct at the fan-blade tips was obtained at several icing conditions. Icing of the dishpan, cowling lip, and inlet duct had no noticeable effect on the fan performance.

In the investigation of the use of isopropyl alcohol for de-icing, spray nozzle bars were mounted radially in front of the fan blades and also between the fan blades and the stator vanes as shown in figure 8. The spray nozzle bars, consisting of tubes having six small jets each 0.070 inch in diameter, were mounted so as to spray the alcohol forward in an attempt to obtain a good spray dispersion and at the same time to keep the spray tubes de-iced. For the first installation a single nozzle bar was mounted horizontally in front of the fan blades and one in a corresponding position was mounted at the leading edge of the stator vanes. For the second installation two spray nozzle bars located approximately 45 degrees apart were similarly mounted in front of the fan blades and two spray nozzle bars were also mounted at the leading edge of the stator vanes. This second configuration was used to obtain a greater coverage of alcohol on the stator vanes and to accomodate greater flows. A variable-control alcohol pump provided flow rates up to 2.5 pounds per minute.

For alcohol de-icing protection, the icing sprays and alcohol sprays were started simultaneously and the alcohol was turned off 30 seconds after the icing sprays. The investigation was made under various icing and performance conditions for different alcohol flows and spray configurations. Because only a part of the stator blades were de-iced, no pressure measurements were made. The water content for these experiments was varied from 0.5 gram per cubic meter to 1.2 grams per cubic meter.

Fairly good de-icing of the fan blades was accomplished for the conditions shown in figure 9; the air temperature was 25° F, the liquid-water content was 1.0 gram per cubic meter, the fan speed was 872 rpm, and the alcohol flow was 0.5 pound per minute. A heavy accumulation of slush was obtained on the leading edge of the stator vanes due to the ice washing off the blades. A view looking upstream (fig. 10) shows that much of the rear of the vanes that were concave upward retained deposits of slush. At an alcohol flow of 0.5 pound per minute, fairly good de-icing of the fan blades was obtained at an air temperature of 13° F and liquid-water content of 0.4 gram per cubic meter; again a relatively heavy accumulation of slush was retained, however, on several stator vanes that were concave upward. When the alcohol flow was increased to 1.2 pounds per minute at approximately the same icing and speed conditions, no improvement in de-icing was apparent. Although the convex face of the fan blades was almost completely clear of ice, heavy deposits of slush were as much as 3/4 inch thick at the concave-face trailing edge. The stator vanes again had large formations of wet ice and were approximately 50 percent blocked. At a medium icing condition (air temperature, 14° F, and liquid-water content, 0.5 gram/cu meter) and an alcohol flow of 1.5 pounds per minute, the fan blades were almost fully de-iced. Medium formations of wet ice were found on the stator vanes immediately behind the spray tubes and only a thin coating of ice was found on the rest of the stator blades. When the alcohol flow was increased to 2.3 pounds per minute, the fan blades were again almost completely de-iced. Large deposits accumlated, however, on all the stator vanes. As shown by the photographs of all the alcohol de-icing, the alcohol-diluted ice thrown off the fan blades impinged on the stator vanes where it remained and refroze. For all conditions, configurations, and flows investigated, the use of alcohol as a de-icing agent proved ineffective because of the marginal de-icing of the fan blades and the large ice deposits obtained on the stator vanes. It is estimated that no practical amount of alcohol would satisfactorily preserve fan performance under all icing conditions.

Because of the large number of blades and the anticipated large power requirement, only a few of the fan blades and stator vanes were heated. The blade heaters were similar to propeller blade de-icing heaters and consisted of parallel chordwise electrical resistance wires enclosed between two layers of neoprene cemented to cover the entire chord of both blade faces. Heaters were applied to twelve of the 72 fan blades, arranged in two groups of six consecutive blades diametrically opposite. Heaters were also applied to six consecutive stator vanes. The heated area on each fan blade was 21.3 square inches with a resistance of 12 ohms per blade; the heated area on a stator vane was 39 square inches with a resistance of 16 ohms per vane.

The power density of the heaters was uniform. Power to the blade heaters was metered through a variable resistance and transmitted to the fan through a slip ring mounted on the propeller hub behind the fan. An electronic cycle timer permitted the cyclical application of power to the blade heaters.

With the electrical blade heaters, only cyclical de-icing was investigated with heat-on and heat-off period of 30 seconds. Because of the anticipated large power requirements and the limitations of present aircraft generators, cyclical heating seemed to be the most practical method of electrical heating for the investigation. With cyclical heating, several groups of blades can be successively heated and the required generator capacity is considerably less than for simultaneous heating of all the blades. No pressure measurements were made because only a few of the blades were heated. The water-content range for these experiments was from 0.5 to 1.2 grams per cubic meter. The icing sprays and heat were started simultaneously.

As only a few of the fan blades and stator vanes were heated, no fan-performance data were obtained. With an air temperature of 15° F, liquid-water content of 0.5 gram per cubic meter, fan speed of 954 rpm, and a power density of 5 watts per square inch, fairly complete de-icing of the heated fan blades resulted. The de-icing of the stator vanes was only marginal with rough ice building up near the trailing edge. When the power density was increased to 6 watts per square inch under almost identical conditions, good de-icing of the fan blades was obtained (fig. 11), except at the root where insufficient heat was available. Fairly satisfactory de-icing of the stator vanes also resulted but rough ice still collected at the trailing edge (fig. 12). At a higher temperature and liquid-water content, complete de-icing of the heated-fan blades was obtained. At lower temperature, the de-icing of the stator vanes was marginal and at the higher temperature and liquid-water content, the de-icing of the stator vanes was completely ineffective.

From observation of the ice throw-off time, it is estimated that the heat-on time for the fan blades might be slightly reduced. Continuous anti-icing would probably provide the best means of protection for the stator vanes. The accumulation of rough ice at the trailing edge of the stator vanes indicates the occurrence of runback caused by the melted ice flowing toward the vanes and then refreezing during the heat-off period. Power requirements for the stator vanes may be even higher than indicated by this investigation as only one-sixth of the fan blades were heated, thus reducing the amount of ice that would be caught by the stator vanes with full protection of the fan blades. Power economies might be affected by increasing the cycle

time for the whole assembly but the icing runs indicate that a heat-off of more than 2 minutes would result in a serious loss in fan performance for the range of icing conditions investigated.

PROPELLER SPINNER

Incidental to the problem of ice protection for the cooling fan is the problem of protecting the propeller spinner. Protection is advisable in order to prevent damage by flying ice to the rest of the airplane such as the wing and tail surfaces, to eliminate aerodynamic disturbances, and to reduce unbalance of the rotating components. An analytical and experimental investigation to evaluate the ice protection requirements of a typical spinner was undertaken recently as a project separate from the cooling fan, because such work is also readily applicable to jet engine generator covers. The analytical investigation was based on the usual wet-air analysis and the optimum heat requirements were determined and compared with the experimental results.

Apparatus and procedure. - The contour of the spinner was the front 12 inches of a prolate spheroid of 64.1 inch major axis and 26 inch minor axis. An internal electric heating blanket of neoprene rubber, fabric, and resistance wires was cemented on the inner side of the spinner.

Surface temperatures for the nonrotating experiments were measured by thermocouples cemented to the outer skin at various chordwise stations.

The nonrotating experiments were conducted in the 6- by 9-foot test section of the icing research tunnel. The rotating experiments were conducted on the airplane mounted in the diffuser section of the icing research tunnel. The electrical power required for marginal anti-icing was measured for various icing conditions.

Results and discussion. - The analysis of the spinner for icing conditions, comparable to those existing in the tunnel (velocity of 200 ft/sec and 55 micron drop size at various tunnel temperatures and water-contents), for the laminar and fully turbulent cases are shown in figure 13. The results obtained for the nonrotating spinner are seen to fall along the turbulent curve. The fact that the data points fall along the turbulent rather than the laminar curve results from the high degree of turbulence introduced into the tunnel air stream by the water spray nozzles. In addition an optimum temperature distribution was not obtained and this would tend to raise the over-all heat requirements. The rotating spinner results are also

shown and are far above the expected requirements. The photographs (fig. 14) indicate that the icing tolerance at the indicated electrical powers was very small and hence the anti-icing was really marginal. The analysis of the spinner indicated that very little difference should be expected for the rotating and nonrotating cases. The large difference in the results is probably caused by the frozen water droplets in the air. These frozen droplets when mixed with the usual water droplets cause a large increase in the quantity of heat necessary, since the latent heat of fusion as well as the other usual quantities must be supplied.

CONCLUSIONS

The results of an icing investigation of a conventional radial-engine cooling-fan installation in the icing research tunnel indicate that:

1. The icing of the unprotected installation presents a serious operational problem. Reduction in air flow below the minimum value required for adequate engine cooling occurred within 2 minutes and complete stoppage of the cooling air flow through the fan assembly occurred within 5 minutes under normal icing conditions.

2. Alcohol de-icing of the fan proved to be ineffective and in some cases increased the icing problem by causing large ice formations on the stator vanes.

3. Electrical heat de-icing was the most promising method of de-icing the blades. The fan blades required a minimum power density of 6 watts per square inch but for the stator vanes this power density proved insufficient.

4. The spinner results show that good agreement between the analytical and experimental results are obtainable under known icing conditions.

REFERENCE

1. Lewis, James P.: Wind-Tunnel Investigation of Icing of an Engine Cooling-Fan Installation. NACA TN No. 1246, 1947.

ENGINE COOLING-FAN INSTALLATION

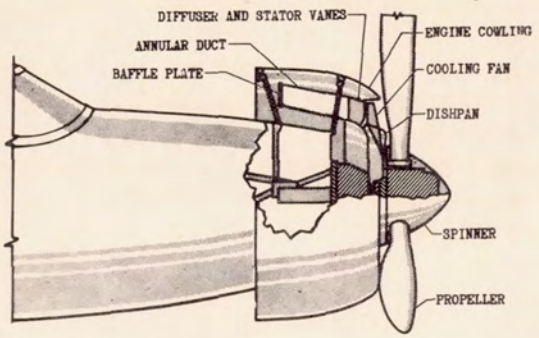

FIGURE 1.

NATIONAL ADVISORY
COMMITTEE FOR AERONAUTICS

PRESSURE-TUBE RAKES IN COOLING-FAN INSTALLATION

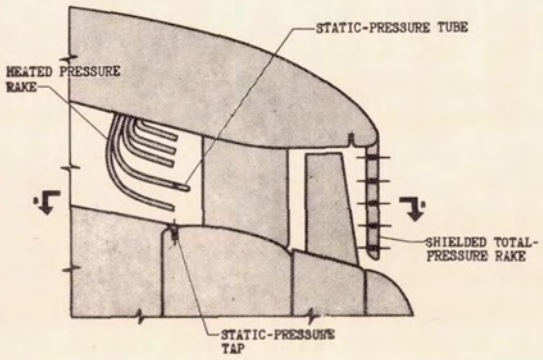

FIGURE 2.

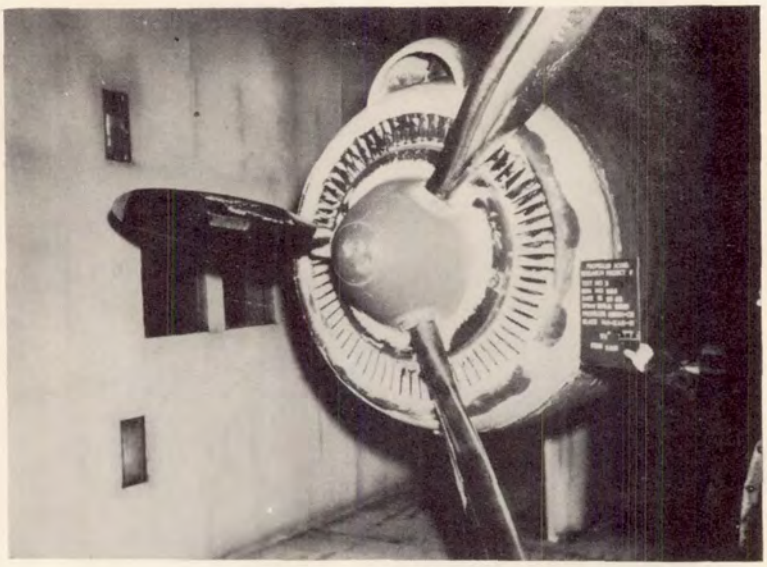

ICE ON COOLING-FAN INSTALLATION

ICING PERIOD, 5 MIN; AIR TEMPERATURE, 23° F; LIQUID-WATER CONTENT, 0.9 GRAM/CU M; FAN SPEED, 872 RPM

FIGURE 3.

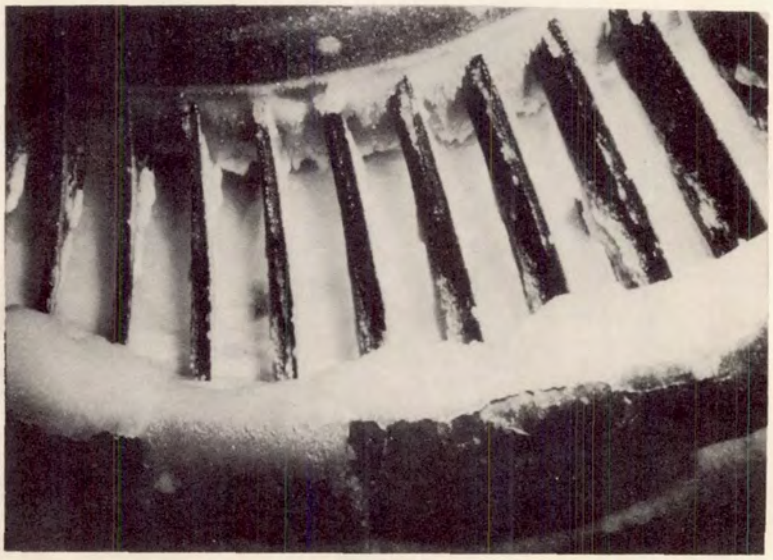

NACA
C-17158
11-7-46

ICE ON FAN BLADES

ICING PERIOD, 5 MIN; AIR TEMPERATURE, 23° F; LIQUID-WATER CONTENT, 0.9 GRAM/CU M; FAN SPEED, 872 RPM

FIGURE 4.

NACA
C-17158
1-7-46

ICE ON STATOR VANES

ICING PERIOD, 5 MIN; AIR TEMPERATURE, 23° F; LIQUID-WATER CONTENT, 0.9 GRAM/CU M; FAN SPEED, 872 RPM
FIGURE 5.

EFFECT OF ICING ON FLOW THROUGH FAN

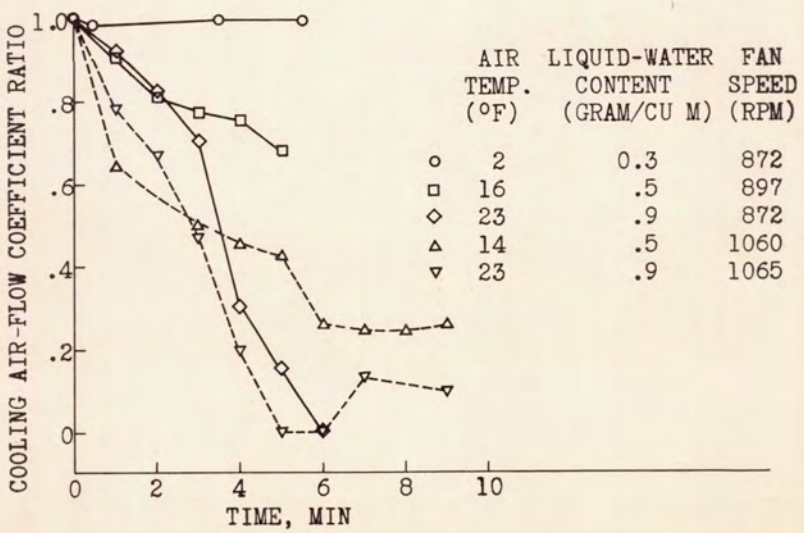

FIGURE 6.

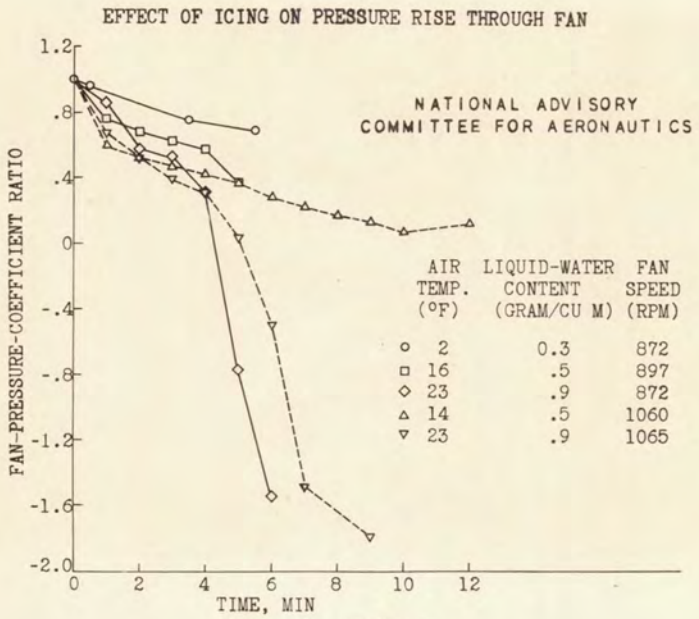

FIGURE 7.

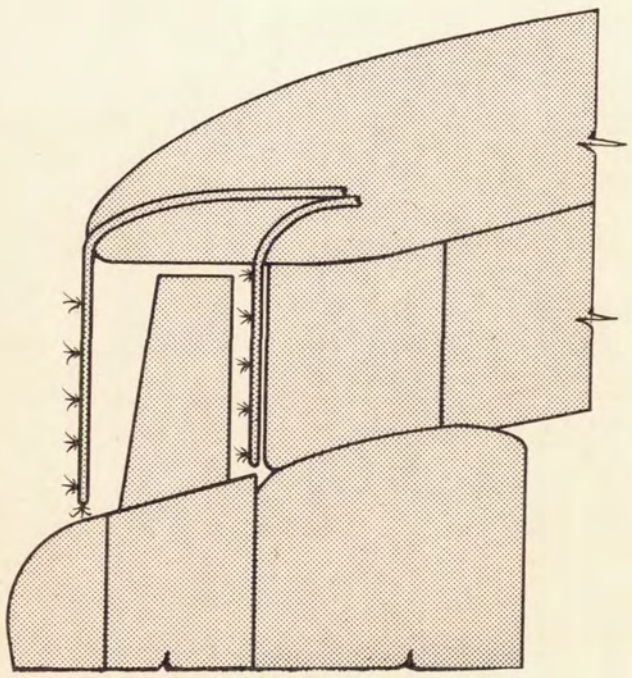

ALCOHOL SPRAY NOZZLE BARS IN COOLING-FAN INSTALLATION

FIGURE 8.

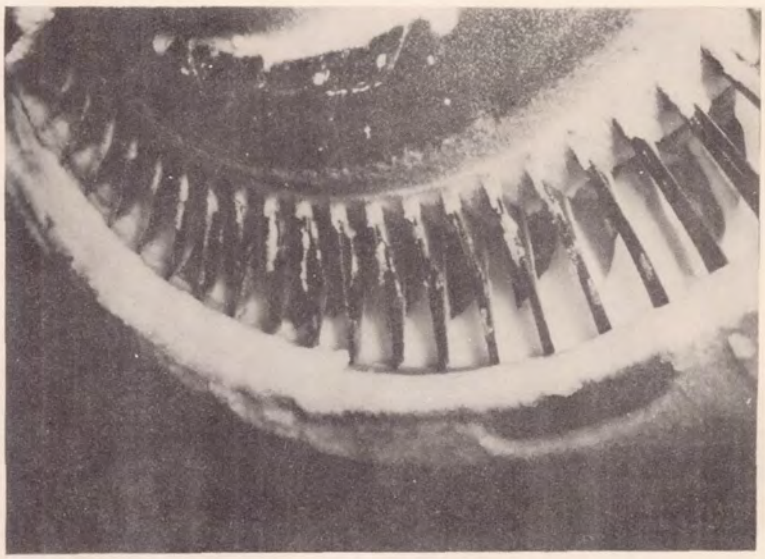

ICE ON LEADING EDGE OF STATOR VANES

AIR TEMPERATURE, 25° F; LIQUID-WATER CONTENT. 1.0 GRAM/CU M; FAN SPEED, 875 RPM; ALCOHOL FLOW, 0.5 LB/MIN
FIGURE 9.

NACA
C-17148
11.7.46

ICE ON STATOR VANES

AIR TEMPERATURE, 25° F; LIQUID-WATER CONTENT, 1.0 GRAM/CU M; FAN SPEED, 875 RPM; ALCOHOL FLOW, 0.5 LB/MIN
FIGURE 10.

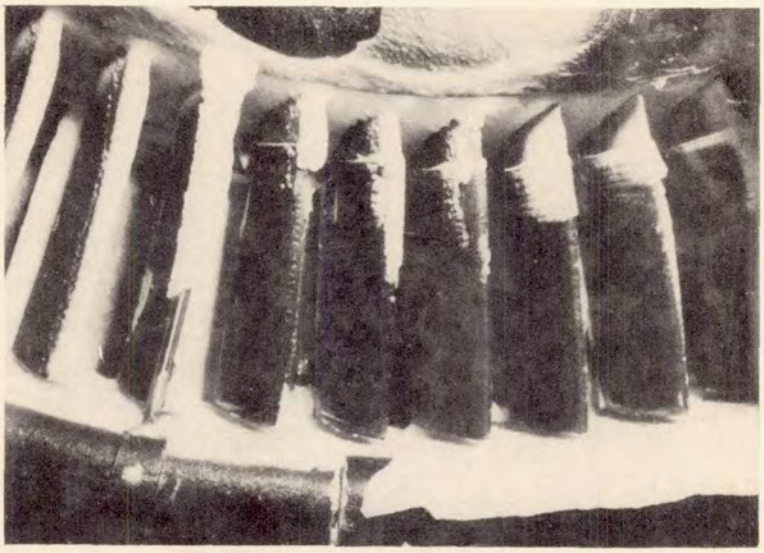

ICE ON HEATED FAN BLADES

ICING PERIOD, 5 MIN; AIR TEMPERATURE, 16° F; LIQUID-WATER CONTENT, 0.6 GRAM/CU M; FAN SPEED, 950 RPM POWER DENSITY, 6 WATTS/SQ IN.

FIGURE 11.

NACA
C-17153
11.7.46

ICE ON HEATED AND UNHEATED STATOR VANES

ICING PERIOD, 5 MIN; AIR TEMPERATURE, 16° F; LIQUID-WATER CONTENT, 0.6 GRAMS/CU M; FAN SPEED, 950 RPM POWER DENSITY, 6 WATTS/SQ IN.

FIGURE 12.

SPINNER POWER REQUIREMENTS

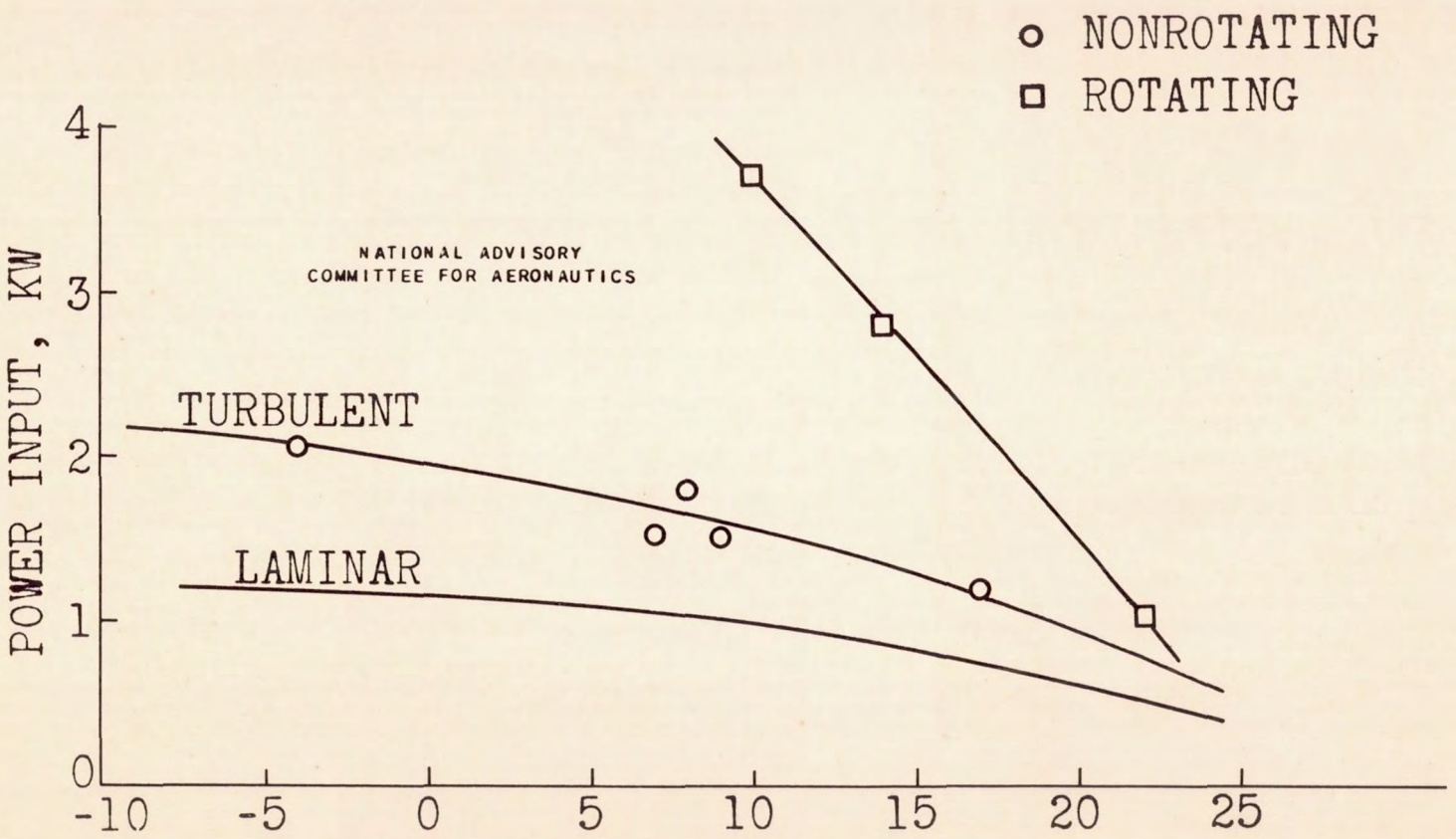

FIGURE 13.

CONFIDENTIAL

AIR TEMPERATURE, 0° F;
POWER INPUT, 4.5 KW

AIR TEMPERATURE, 21° F
POWER INPUT, 1.6 KW

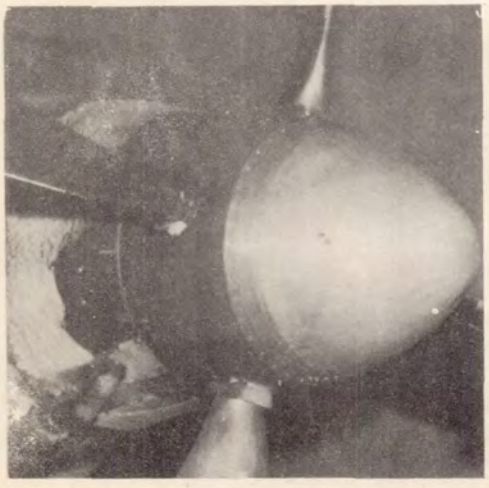

AIR TEMPERATURE, 14° F
POWER INPUT, 4.5 KW

AIR TEMPERATURE, 13° F
POWER INPUT, 2.5 KW

ICE PROTECTION OF INTERNALLY ELECTRICALLY
HEATED SPINNER

PROPELLER SPEED, 1050 RPM; TUNNEL VELOCITY, 200 FT/SEC
FIGURE 14.

NATIONAL ADVISORY
COMMITTEE FOR AERONAUTICS

EFFECT OF ICE FORMATIONS ON AIRPLANE PERFORMANCE

By G. Merritt Preston and W. V. Gough, Jr.

Flight Propulsion Research Laboratory

INTRODUCTION

A flight investigation has been conducted in nautral icing conditions by the NACA to determine the effect of ice formations on airplane performance.

The lack of quantitative evidence of the serious effect of ice formations on the aerodynamic performance of the propellers has tended to retard the adoption of new and improved systems of propeller ice protection. Numerous pilots have reported serious reduction in airplane performance attributed to inadequate propeller protection. The evidence was inconclusive inasmuch as the effect of ice on the remainder of the airplane and the accuracy of airspeed indication could not be evaluated.

Wind-tunnel tests employing simulated ice formations (reference 1) gave results that indicated a loss in propeller efficiency of 3 percent for level flight. Propeller-whirl tests, during which icing conditions were artificially created, indicated negligible losses (reference 2). Preliminary flight tests (reference 3) indicate a significant loss in performance of the propellers.

The results reported in references 1 and 2 are inconclusive inasmuch as the quantities of ice simulated or obtained are smaller than formations frequently observed during flight in natural icing conditions.

The results reported in reference 3 are also inconclusive inasmuch as they do not permit distinction between the effects of propeller ice and the effects of other ice formations on the performance of the airplane.

Formations of ice on propellers, in addition to deleteriously affecting the propeller performance, has been observed to cause serious unbalance. Also, the natural shedding of ice from the propeller commonly results in fuselage damage and passenger discomfort.

The present investigation was undertaken to determine the effect of ice formation on unprotected propellers by operating in natural icing conditions; by measuring the effects of the ice on the propellers independently of the effects of ice on other parts of the airplane;

and, conversely, to measure the effects of ice on other components independently of the effect of ice formations on the propellers. The degree of propeller unbalance that was experienced during flight with ice accretions on the blades was evaluated in the investigation. Photographs were taken in flight of natural ice formations on the airplane components to permit simulation for aerondynamic studies in wind tunnels.

APPARATUS

This investigation was conducted with the use of the twin-engine airplane shown in figure 1. This airplane was originally used by the Army in a preliminary investigation of icing of propellers (reference 3). The original anti-icing equipment provided by the manufacturer consisted of a thermal heated-air system protecting the outboard wings, horizontal and vertical tail surfaces, and the windshields. For the investigation the anti-icing system was considerably augmented by providing thermal electric anti-icing for the fuselage foresection, propellers, inboard wing, cowls, and antenna masts.

PROCEDURE

Flights were conducted in clear-air conditions to establish the performance of the airplane without ice accretion and the data were reduced by the V_{iw}, P_{iw} method described in reference 4. Flights were conducted in natural icing conditions to determine the effects of ice accretions on performance. Performance data were taken during the flight in natural icing conditions, allowing ice to collect on the propellers and on the miscellaneous protuberances of the airplane. Performance data were also taken in the icing condition with ice removed from the propeller blades, but with ice on the miscellaneous protuberances. Part of the performance data obtained in icing conditions was taken with a fixed-pitch propeller and part with a variable-pitch propeller while maintaining constant engine speed.

In order to determine the effect of icing on other components, the propellers were anti-iced and all other components were allowed to ice. The respective performance loss attributable to ice formations on the components was measured by selective de-icing of the components. The parasite-drag increments due to icing were computed for each component that was selectively de-iced. The derivation of these calculations are given in reference 4. Rotating-cylinder data were recorded for at least one 5-minute period of each run, and air temperature and rate of icing were recorded continuously during each run.

RESULTS AND DISCUSSION

In figures 2 and 3 propeller-efficiency-loss data are presented as a plot of brake horsepower against indicated airspeed. The dotted curves of efficiency loss were computed. The curve of zero efficiency loss was calculated to fair through the check point, which was determined after the icing run was completed. This point was established for the condition of propellers ice free and ice accretion only on the miscellaneous protuberances.

The maximum deleterious effect of ice formation on propeller performance experienced during this investigation for glaze-ice formations is also shown in figure 2. The heavy ice extends to 30 percent of the blade radius and some ice deposits extended to the 60-percent radius. This photograph was taken by a flash camera in clear air after the propeller performance data were taken and represents a condition which caused an efficiency loss of 8 percent. The data indicate a loss in propeller efficiency of 11 percent, which is equivalent to a decrease in airspeed from 185 miles per hour to 174 miles per hour at 1400 brake horsepower. After 12 minutes of flight in this case, a maximum propeller efficiency loss of 18 percent was obtained. Natural shedding of ice from the blades followed immediately. The airplane was then flown into clear subfreezing air and the 4 "above-icing" points were established to show the efficiency loss caused by the remaining propeller ice formation over a wide range of horsepower and airspeed. It was after this that the propellers were de-iced and the zero efficiency loss check point was established.

The maximum deleterious effect due to rime-ice formation on the propellers is shown in figure 3. The heavy rime-ice deposit is shown to extend to the 50-percent radius. Some small accretions remained beyond the 50-percent radius. A loss in propeller efficiency of 11 percent resulted from this formation.

The maximum propeller unbalance encountered during the investigation was 85 ounce-inches. The pilots and crew of the airplane were able to note slight objectionable vibration above 70-ounce-inches unbalance. Denting of the fuselage resulted from ice shedding; however, there was no serious damage to airplane structure.

The results of the investigation indicate that the formation of ice on an airplane propeller will cause a significant reduction in airplane performance when certain meteorological conditions exist. The investigation did not include a definition of the types of meteorological conditions that produced the most deleterious effect on

propeller performance. It was observed that many of the conditions encountered produced small loss in propeller performance.

Flight tests have also been conducted at the NACA Ames laboratory on a C-46 airplane to determine the effect of ice formation on propeller performance. The maximum loss in propeller efficiency encountered was 19 percent and is in agreement with results of the Cleveland investigation. However, on many of the flights insignificant losses in propeller efficiency were encountered. A statistical study was made of the Cleveland and Ames laboratory data to determine the most frequent loss in propeller efficiency that was encountered in the icing conditions. These data are presented in figure 4 and indicate that 50 percent of the time a loss of 5 to 10 percent was encountered and only $7\frac{1}{2}$ percent of the time losses from 15 to 20 percent of propeller efficiency were encountered.

In order to determine the effect of icing of other components, the propellers were anti-iced and the other components were not protected. A thick stratus cloud in the lee of Lake Erie was encountered in an area of cyclonic flow from the north that produced orographic lifting and mild turbulence. A time history of the icing condition shown in figure 5 indicates that the average icing rate was approximately 4 inches per hour and that a maximum rate of 12 inches per hour existed for a few minutes. The rotating-cylinder data, when compared with the icing-rate data for the corresponding period, indicate that the average liquid-water content was approximately 0.5 gram per cubic meter with an average drop size of 17 microns. These meteorological conditions are almost equal to the maximum conditions that would be encountered in a stratus cloud as determined by the Ames laboratory (reference 5).

The resulting ice formations were photographed and are presented in figures 6 to 13. Figure 6 is a front view of ice on the loop-antenna housing. The same ice formation is shown in profile in figure 7. This figure substantiates the 4-inch-per-hour icing rate. Equally heavy ice collected on the antenna mast and on the instrument-landing-system receiving antenna (fig. 8). Ice on the nose of the airplane was photographed on the ground after fifteen minutes of flight in above freezing temperature (fig. 9). Thin, rough, glaze-ice deposits extended well beyond the major ice accretion. Several large isolated pieces indicate that the total formation was much larger during the flight. Ice on the leading edge of the engine cowling is shown in figure 10. This formation is uniform but noticeably smaller than others. The ice formations on the inboard-wing panels were relatively small (fig. 11). The size of the formation can be judged by the 1-inch reference stripes on the wing surface.

Figure 12 shows that some of the ice was lost from the outboard-wing panels. This was probably caused by the air loads on the ice and wing flexure. Ice on the horizontal stabilizer, shown in figure 13, indicates the severity of the icing condition and the shape of the ice formation. It also shows that some ice was lost because of air loads and flexure

This flight was conducted by increasing power as required to maintain a constant speed of 205 miles per hour while the ice was being collected. After a good catch of ice, the airplane was flown into an area of clear subfreezing air and power was reduced to the values normally required for level flight cruising at 205 miles per hour. The airspeed stabilized at 164 miles per hour by holding constant altitude. Progressive de-icing was started and the airspeed was allowed to stabilize after each de-icing step. The components were de-iced in the following order and resulted in the increases in airspeed as shown in figure 14: inboard-wing panels, 3 miles per hour; tail surfaces, 4 miles per hour; outboard-wing panels, 12.5 miles per hour; and, engine cowlings, 4.5 miles per hour. The 17-mile per-hour-loss attributable to the ice formation on the miscellaneous components is determined by subtraction from clear-air performance of the airplane at the same power and flight conditions.

These data are interpreted in terms of parasite drag by the method given in reference 4. Figure 15 shows the percent drag increase based on the drag of the ice-free airplane. Ice on the inboard-wing panels accounted for an 8-percent drag increase; tail surfaces, 11-percent drag increase; and, the outboard-wing panels, 27-percent drag increase. Ice on the engine cowlings added 10 percent and the miscellaneous components, the second largest offender, were responsible for 25 percent of the airplane-drag increase.

This investigation did not include the determination of such factors as stalling speed, minimum single-engine speed, and low-speed flying qualities. It is significant to report that the control response of the airplane approached the point of being marginal when the entire airplane, except the propellers, was iced.

The data and results presented here are directly applicable only to the airplane type used in this investigation and under meteorologically similar conditions. However, by proper consideration of such factors as leading-edge radius, leading-edge lengths, and surface areas, the drag data can be used for estimating the effect of ice on the performance of other airplanes.

REFERENCES

1. Corson, Blake W., Jr., and Maynard, Julian D.: The Effect of Simulated Icing on Propeller Performance. NACA MR L4J21, Army Air Forces, Oct. 21, 1944.

2. Connor, Robert F.: Investigation of Propeller Icing Phenomena and Evaluation of Propeller Deicing Compounds. A.A.F. T.R. No. 5480, Air Materiel Command, Army Air Forces, April 4, 1946.

3. Kanter, M.: Flight Performance on XB-25E Airplane No. 42-32281 in Natural Ice During February, March and April 1945. A.A.F. T.R. No. 5403, Air Materiel Command, Army Air Forces Dec. 17, 1945.

4. Blackman, Calvin C.: The Effect of Ice Formations on Airplane Performance. NACA TN (to be pub.).

5. Lewis, William: A Flight Investigation of the Meteorological Conditions Conducive to the Formation of Ice on Airplanes. NACA TN (to be pub.).

XB-25E WITH THERMAL ANTI-ICING EQUIPMENT
FIGURE 1.

PROPELLER EFFICIENCY WITH GLAZE ICE

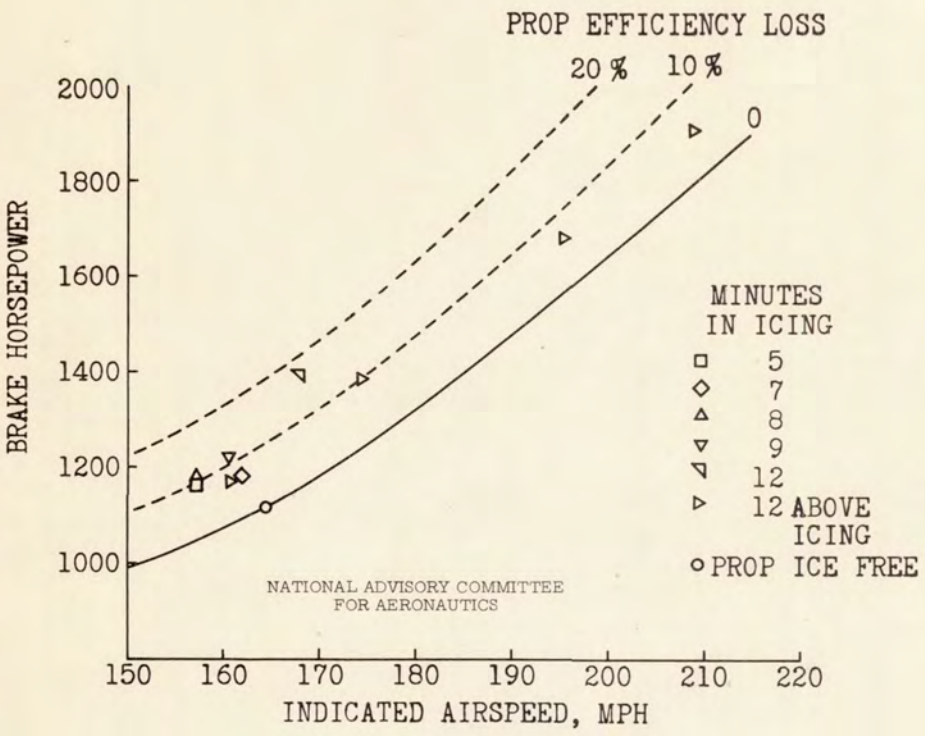

FIGURE 2.

PROPELLER EFFICIENCY WITH RIME ICE

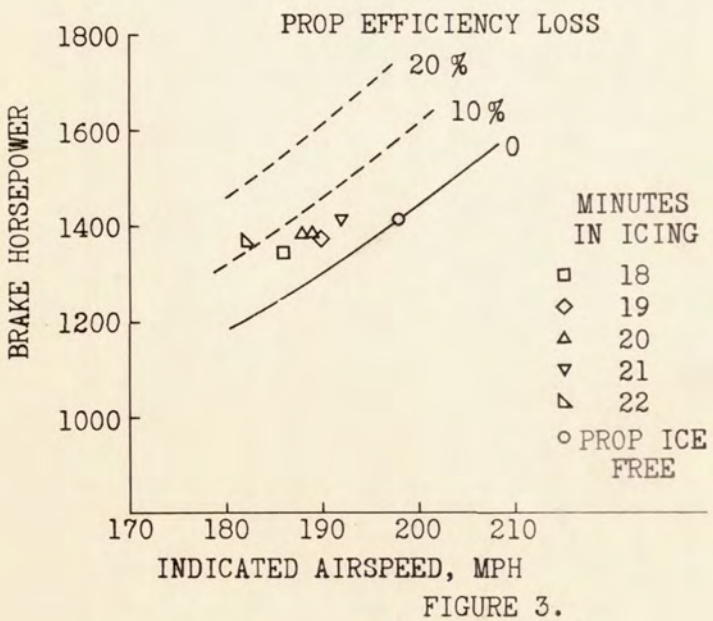

FIGURE 3.

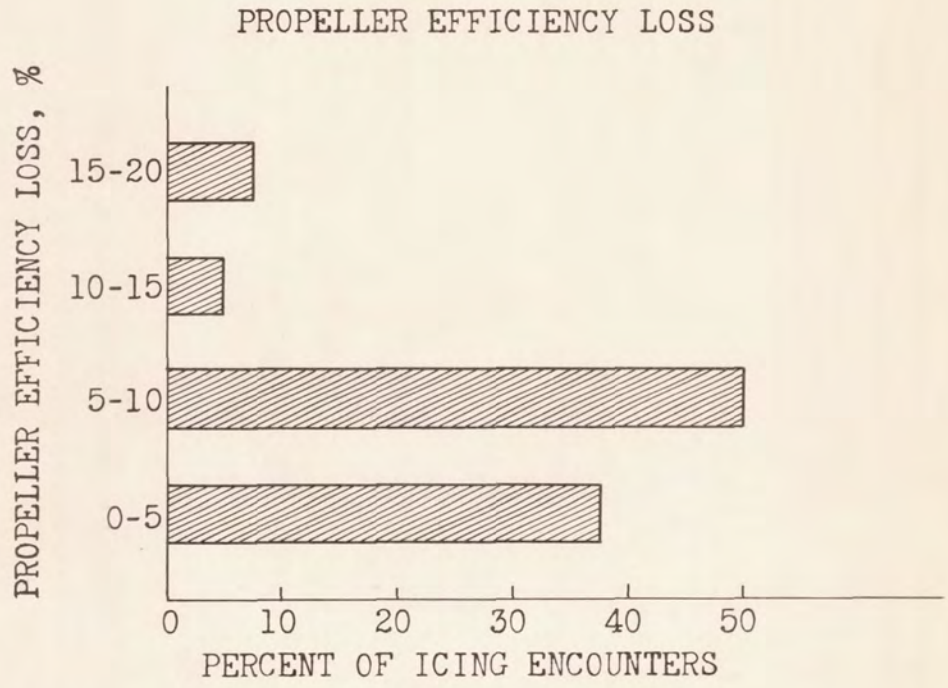

FIGURE 4.

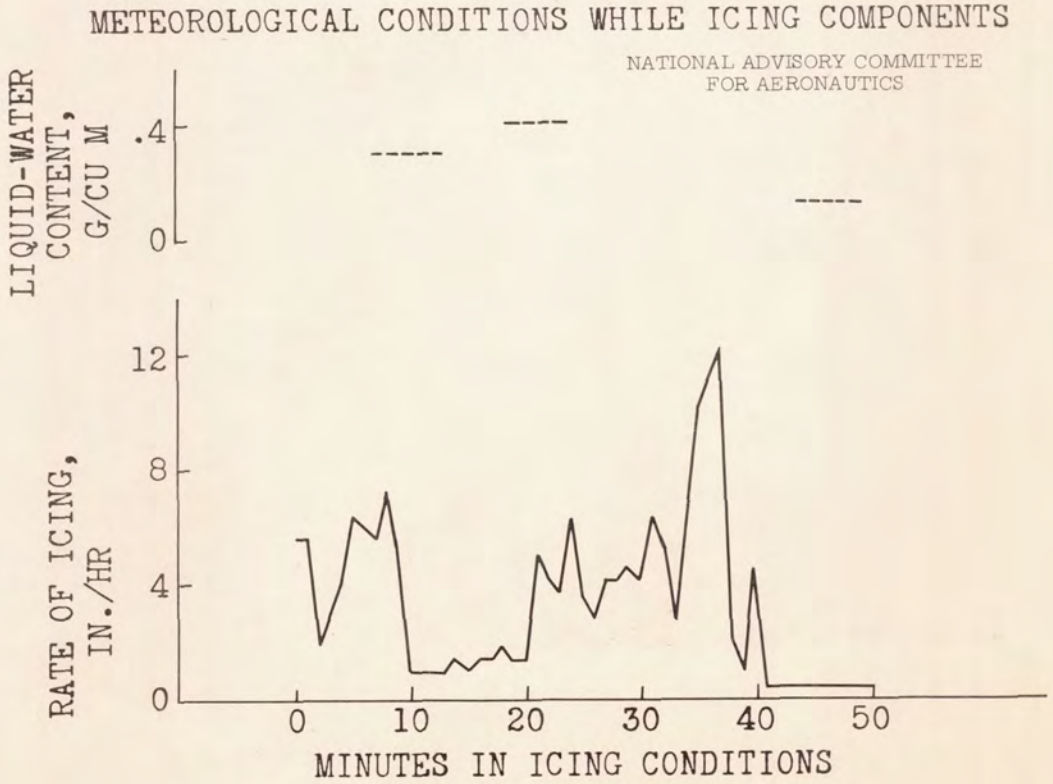

FIGURE 5.

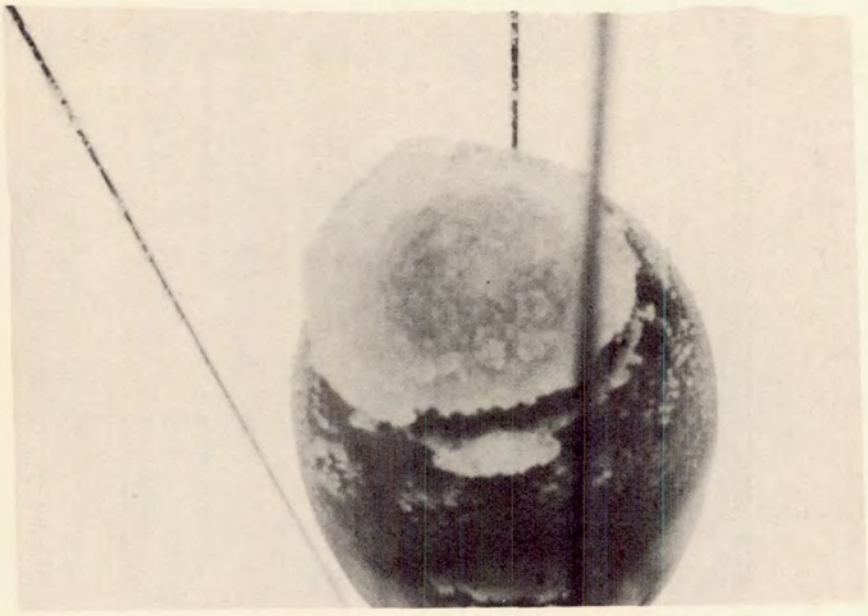

ICE ON LOOP-ANTENNA HOUSING
FIGURE 6.

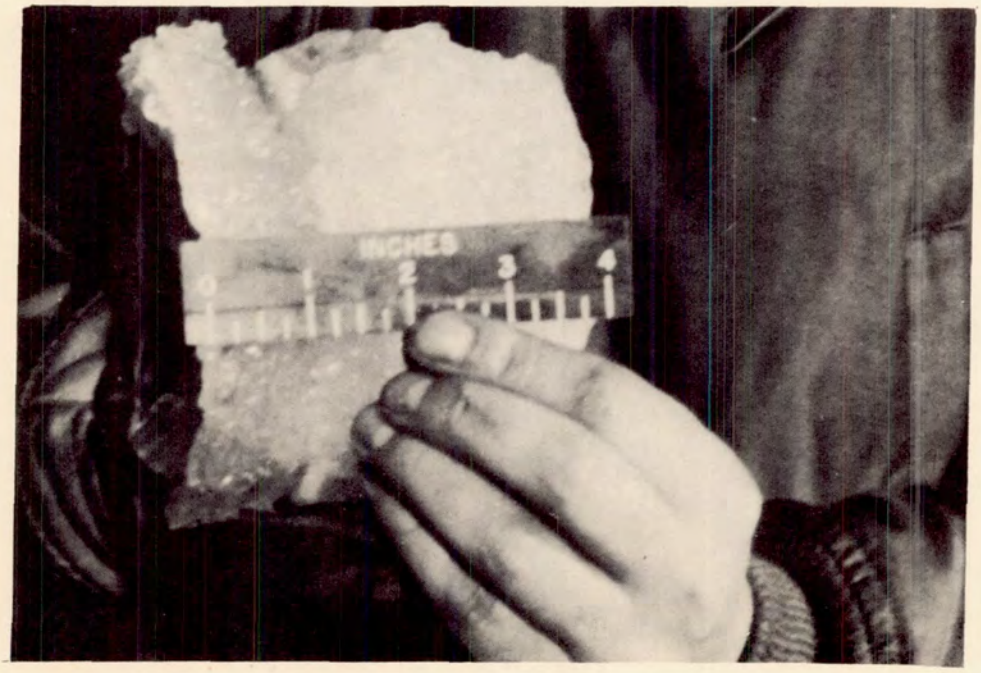

ICE ON LOOP, ANTENNA HOUSING
FIGURE 7.

NACA
C- 18586
5.7.47

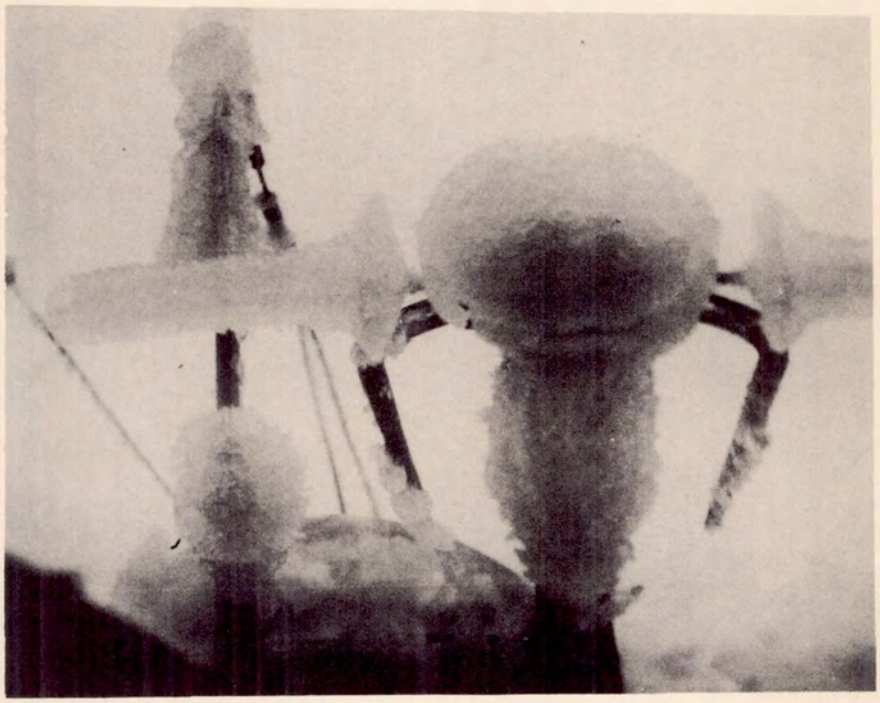

NATIONAL ADVISORY
COMMITTEE FOR AERONAUTICS

ICE ON ANTENNA MAST AND I.L.S.
RECEIVING ANTENNAS
FIGURE 8.

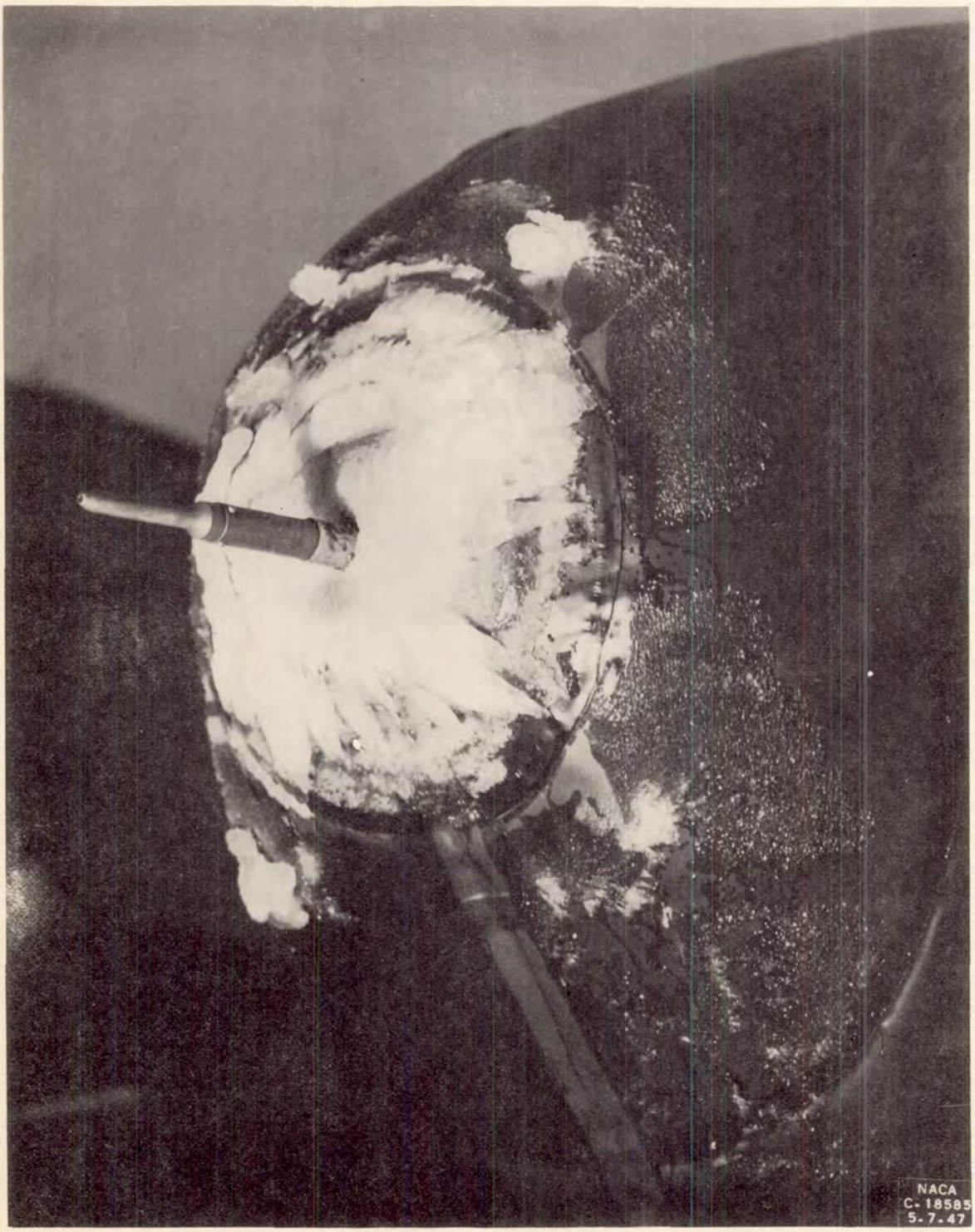

ICE ON NOSE OF FUSELAGE
FIGURE 9.

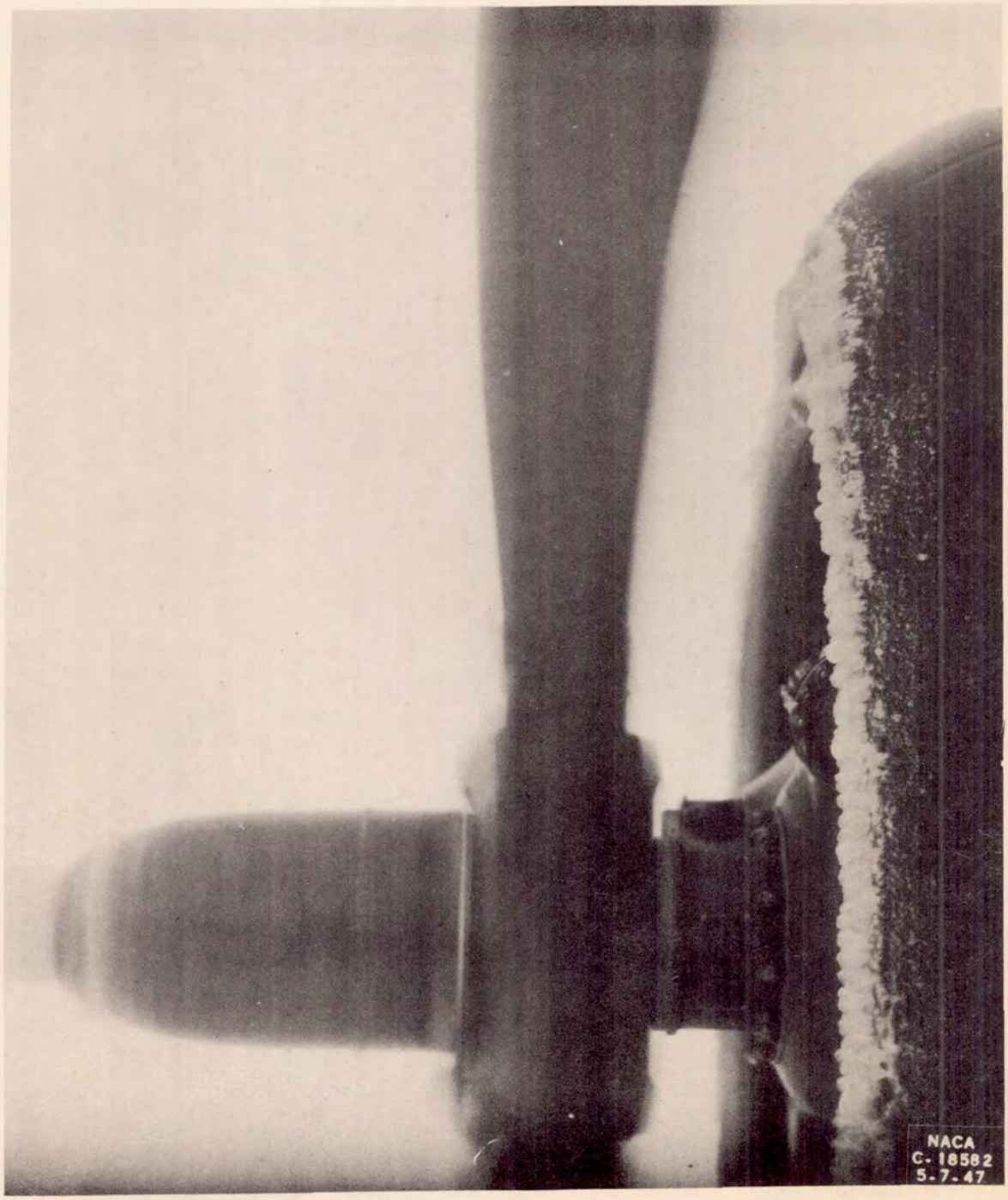

ICE ON LEADING EDGE OF ENGINE COWLING
FIGURE 10.

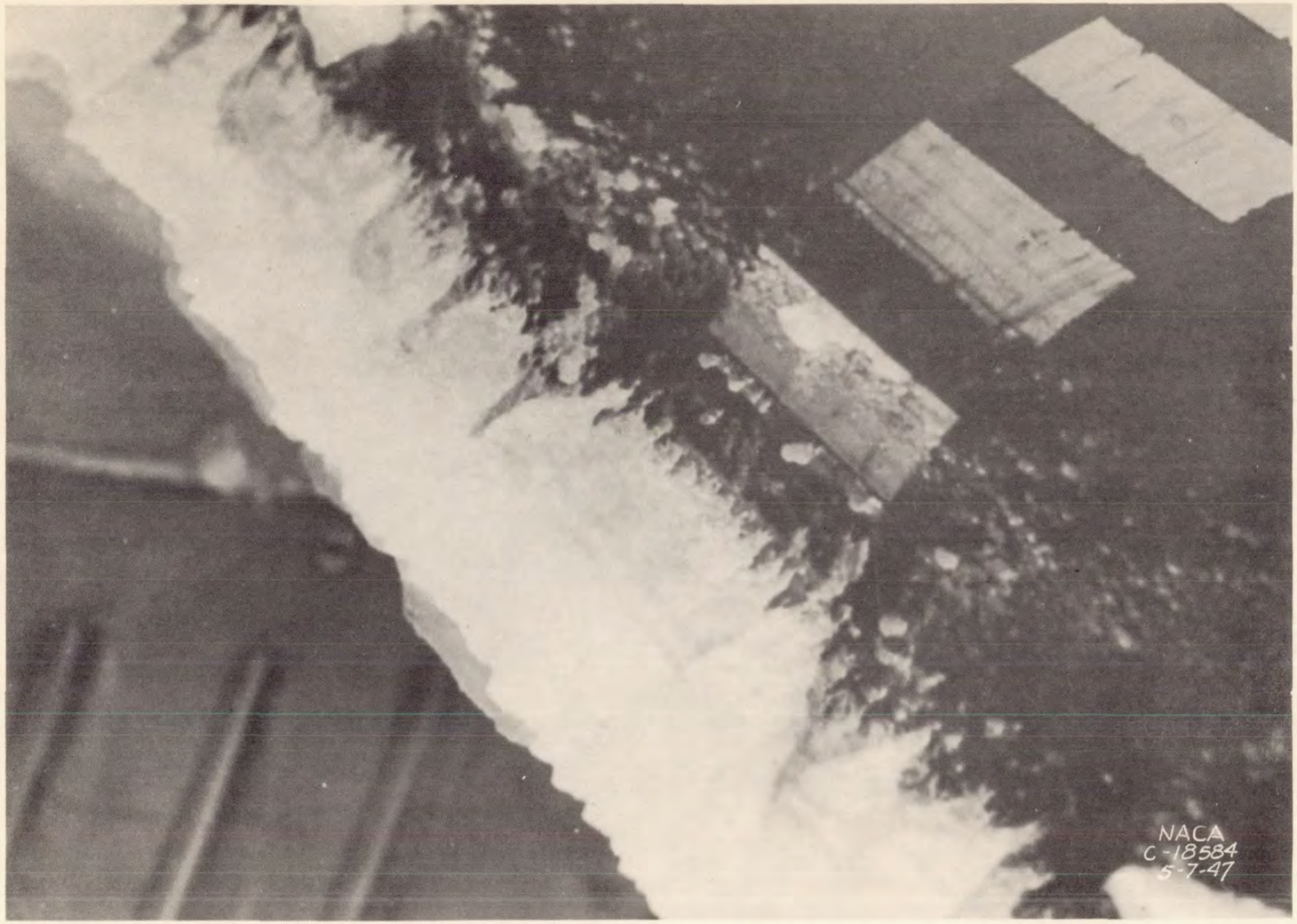

ICE ON INBOARD-WING PANEL
FIGURE 11.

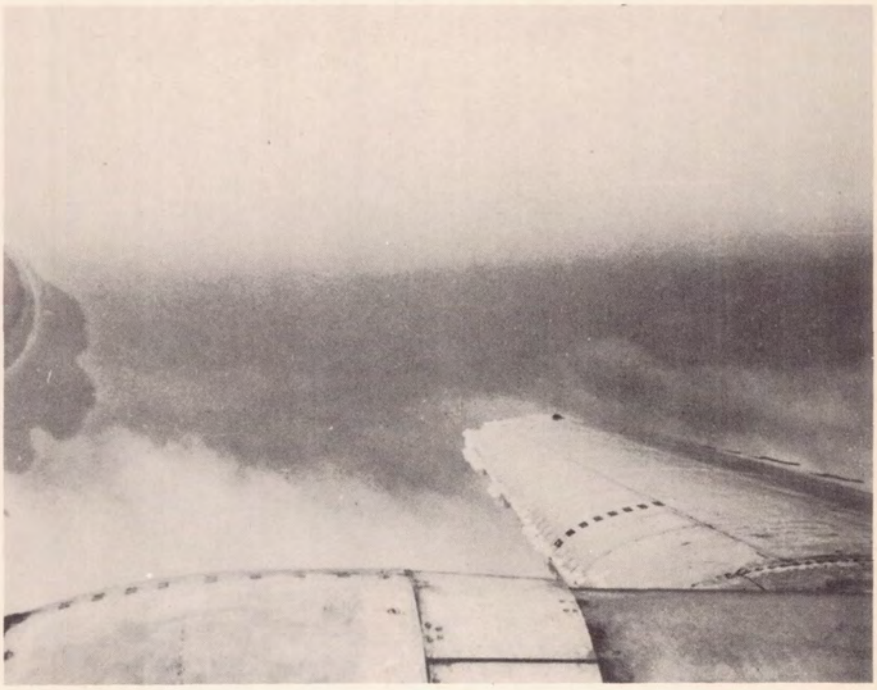

ICE ON OUTBOARD WING PANEL
FIGURE 12.

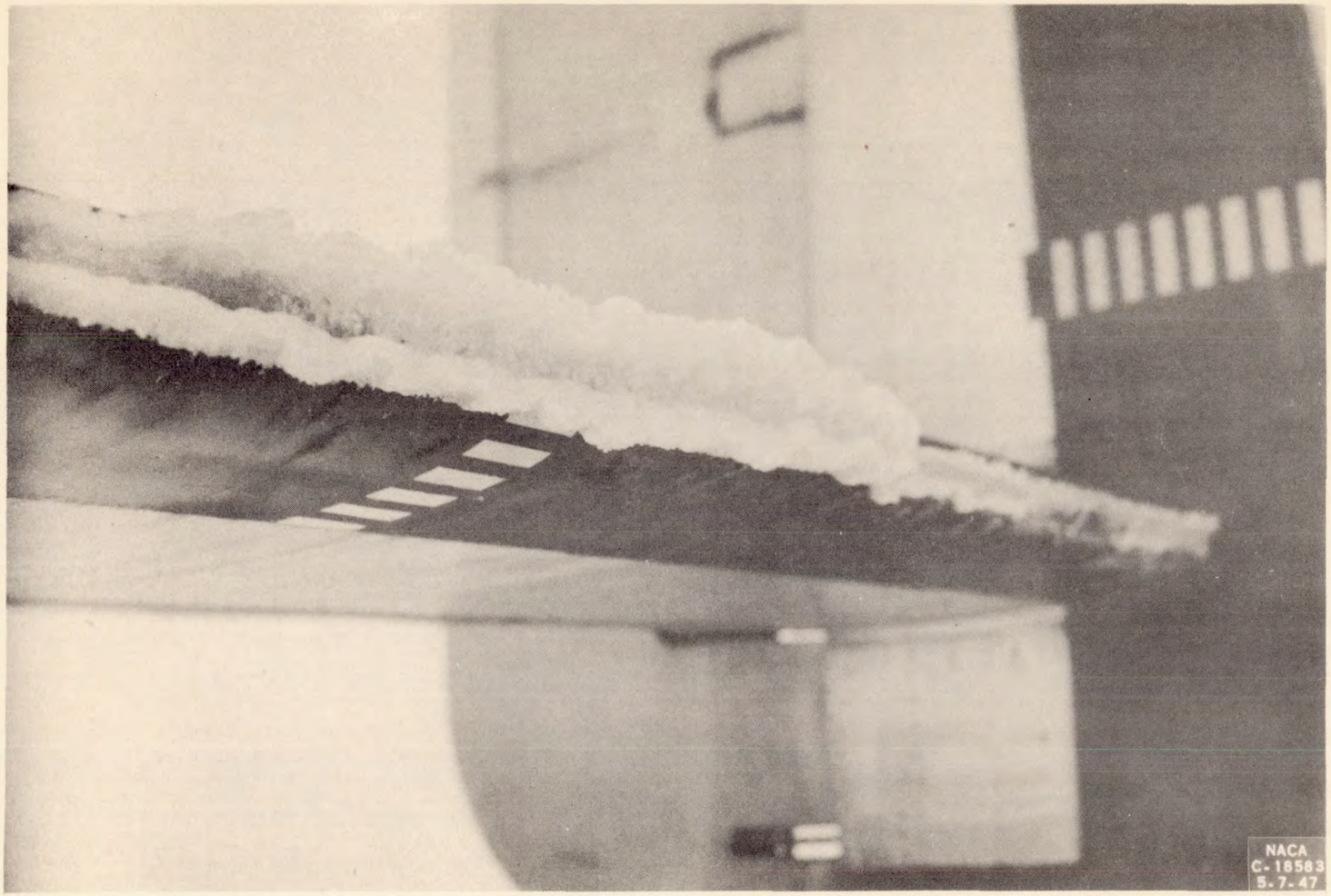

ICE ON HORIZONTAL STABILIZER
FIGURE 13.

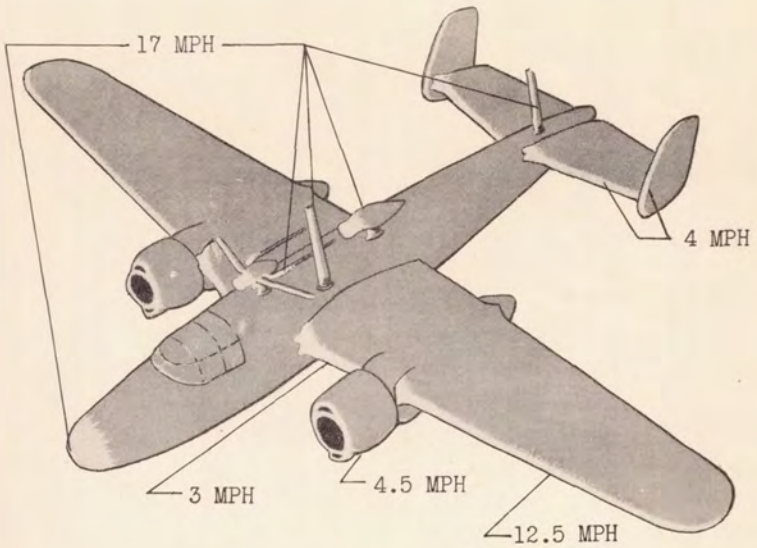

AIRSPEED LOSSES CAUSED BY ICE

AIRSPEED REDUCED FROM 205 TO 164 MPH

FIGURE 14.

DRAG INCREASE WITH COMPONENTS ICED

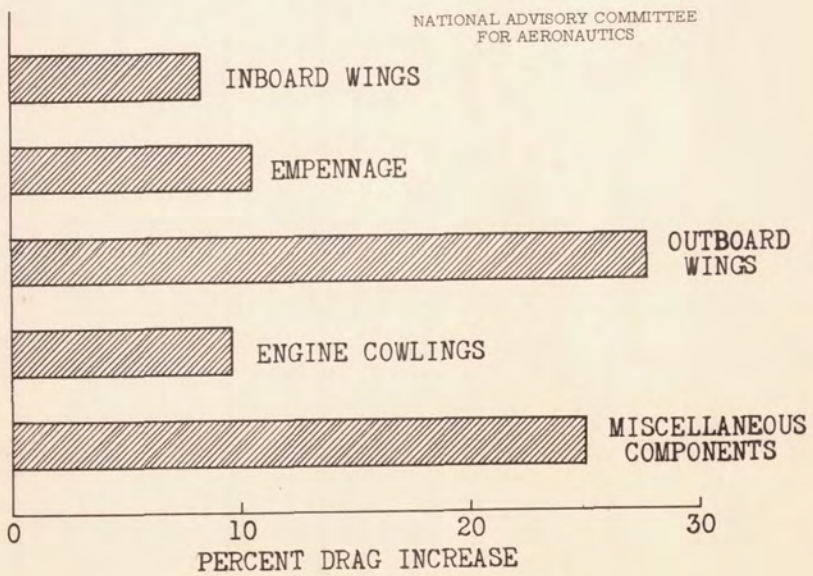

FIGURE 15.

PROPELLER ICE PROTECTION BY MEANS OF HOT GASES IN HOLLOW BLADES

By Vernon H. Gray

Flight Propulsion Research Laboratory

INTRODUCTION

Gas-heated hollow propellers have recently been investigated both analytically and experimentally (references 1 to 5) to determine the ice-prevention effectiveness of this method of blade heating. A typical schematic flow diagram for a gas-heated propeller is shown in figure 1.

The gas is first heated in a suitable heat source and passes through a manifold and a collector ring to cuffs located on the blade shanks. The gas then flows radially outward through the hollow blade, which may have internal partitions to confine the flow to the forward portion of the blade, as shown in the cross section (fig. 1). The gas leaves the blade through a discharge nozzle at the blade tip.

The analytical investigation developed a method for determining the required initial gas temperature and flow rate for maintaining surface temperatures on all parts of the heated blade area of at least 32° F. Two previous theoretical investigations upon which parts of this analysis are based are reported in references 6 and 7.

The experimental investigation obtained surface temperatures and icing data for three types of propeller blade subjected to icing conditions in the icing research tunnel. Three types of blade investigated were (1) hollow unpartitioned blades; (2) blades with radial partitions located at 50 percent of chord; and (3) blades with partitions at 25 percent of chord. The partitioned blades were investigated to determine the extent of heat flow savings.

ANALYTICAL INVESTIGATION

In analyzing the heat requirements for a gas-heated propeller, it is necessary to select several sets of flight and atmospheric conditions corresponding to take-off, climb, and cruise, and determine the set of conditions most critical from a heat requirement standpoint.

The present method of analysis assumes that the blade can be divided into an arbitrary number of successive, radially disposed segments, and that each segment may be treated as a separate cross-flow heat exchanger. Thus the heat transferred from the gas through the blade metal and into the air stream can be evaluated and subtracted from the heat content of the internal flow to determine the conditions of the gas as it leaves the segment.

In order to determine heat transfer through the blade metal, the equation developed in figure 2 must be considered. For a unit area of heated blade metal, the heat transfer can be expressed as heat into the metal and heat out of the metal, both of which consist fundamentally of a heat-transfer coefficient h and a temperature differential Δt. Assuming the metal to be thin enough to preclude surfacewise conduction in the metal and neglecting radiation, the heat into the metal area equals the heat out of the area and into the air stream. The heat into the metal from the hot gas consists of convective heat transfer only, whereas the heat out of the metal is of three kinds: the convective heat transfer, the evaporative heat transfer occasioned by evaporation of surface moisture, and the heat transfer to increase the sensible heat of the intercepted water from the ambient temperature up to the surface temperature.

The equation given in figure 2 is

$$h_g(t_{g,d} - t_s) = (h_a X + M)(t_s - t_{a,d})$$

where

h_g is the internal gas heat-transfer coefficient and depends mainly on the rate of gas flow divided by the flow area

$t_{g,d}$ is the datum gas temperature, or the static gas temperature plus the kinetic increment of temperature caused by friction in the boundary layer

t_s is the external surface temperature

h_a is the external air heat-transfer coefficient, and depends mainly on the boundary-layer thickness

X and M exist only when the surface becomes wetted, necessitating "wet-air analysis", which is presented in some detail by Neel. The evaporation factor X, as developed in reference 8, depends on the vapor pressures corresponding to the surface and air temperatures, multiplying h_a by as much as 6 in some conditions; M is the amount of water which intercepts the surface,

and depends on the liquid-water content of the ambient air, the resultant velocity and the angle of impingement of the water drops upon the surface

$t_{a,d}$ is the datum air temperature, or the ambient-air temperature plus the kinetic increment of temperature in the boundary layer. The kinetic increment is less for wet air than for dry air because of the evaporation process.

The equation is solved for several points around the blade surface, and thus a chordwise distribution of surface temperature is obtained. If the integrated average of the expression on either side of the equal sign is obtained and multiplied by the heated area of the segment, the total heat transfer from the segment will be determined. This value, when coupled with the thermodynamic effects of propeller rotation, permits evaluation of the gas conditions leaving the segment, and a progression, segment by segment, will determine the final conditions at the tip. In solving the equation, the initial gas temperature and flow rate are estimated and then adjusted by trial until the surface temperatures of the entire blade are above 32° F. When this is done the required heat-source input to the blade, as well as the nozzle area required to accomodate the flow, may be readily calculated.

In order to illustrate the nature of h_a, a typical distribution of the external heat-transfer coefficient h_a plotted against the chordwise distance from the stagnation point for the camber and thrust faces is presented in figure 3. The predominate feature of this variable is that it has a distinct maximum at the stagnation point and becomes much smaller a short distance away on either face. For complete laminar flow the heat transfer coefficient decreases from the high values at the leading edge and follows the dotted line through the laminar regime. If transition to turbulent flow is early, the distribution of temperature will be similar to the curve labeled turbulent flow to the left of the stagnation point in figure 3. The heat transfer accompanying turbulent flow is considerably greater than that for laminar flow. If the transition is late, the curve may follow the laminar case for a distance and then abruptly increase into the turbulent case. The proportions of the curves illustrated are typical of propeller operation conditions, and the effect of heat-transfer coefficient will be demonstrated subsequently in the surface temperature distributions.

Numerical example. - Calculations have been made by the wet-air analysis method for an hypothetical propeller having blades with radial partitions at 50 percent of chord. The assumed flight and

icing conditions for this example are: ambient-air temperature, 0° F; pressure altitude, 18,000 feet; flight speed, 325 miles per hour; propeller speed, 800 rpm; liquid-water content, 0.4 gram per cubic meter; propeller diameter, 11 feet, 3 inches. By assuming a minimum surface temperature of 32° F, the general results for these conditions were as follows: The required gas flow per blade was 750 pounds per hour for an assumed initial gas temperature of 500° F; the final gas temperature was 321° F. The heat-source input per blade was found to be 86,700 Btu per hour or 26 kw, of which 59,200 Btu per hour was discharged through the tip nozzle. This represents an overall blade heat exchanger effectiveness of 34 percent. The value of heat-source input required per blade appears high when compared with external electrically heated blade shoes, but it must be remembered that existing gas-heated propellers are equivalent to short, unfinned one-pass heat exchangers.

The surface temperatures, which resulted for the numerical example, are shown in figure 4. The temperatures are plotted for three radial stations, designated by the number of inches from the center of rotation; namely, the 24-, 48-, and 60-inch stations. The surface temperatures are seen to be approximately 32° F at the stagnation point and increase very rapidly on either face. The blade faces near the midpoint of chord are actually overheated from an economical heating standpoint, and some method of concentrating this heat at the leading edge would be desirable.

The effect of two factors mentioned previously is illustrated in figure 4. First, the two areas under assumed turbulent flow (for comparison purposes) are shown to have surface temperatures much less than the unmarked areas under assumed laminar flow, indicating that higher heat-transfer coefficients result in lower surface temperatures. Second, at two places on the thrust face the rate of evaporation from the surface became great enough to account for all of the water that intercepted the face, the surface became dry, and the surface temperatures aft of these points increased very markedly. This abrupt change in temperature indicates the difference between a wet and a dry surface because the latter has no additional heat losses due to evaporation.

The significant changes in the heat transfer variables along the propeller radius for the numerical example are shown in figure 5. Plotted against the propeller radius are the surface temperature at the stagnation point t_s, the internal heat-transfer coefficient h_g, and the internal gas temperature t_g. As expected, the internal gas temperature decreased steadily toward the tip because of the heat transfer through the metal, whereas the internal heat-transfer coefficient

increased steadily toward the tip, due to the decreasing flow area that accelerated the gas. Not shown in figure 5 are two external variables, the external heat-transfer coefficient and the datum air temperature, both of which increased because of the increase in resultant velocity toward the tip. The net result of these factors on the surface temperature at the stagnation point is a slight increase toward the tip. However, for lower airspeed, propeller speed, or ambient temperature, the surface temperature at the stagnation point would have decreased toward the tip.

Suggested Modification. - The analysis and the example presented has indicated that a primary problem in the design of a gas-heated propeller is getting enough heat to the leading-edge region without requiring an exorbitant amount of heat input to the blade. Accordingly, a modification has been suggested whereby the original blade section as shown in figure 6 has been modified to include the addition of metal fins attached to the leading edge and an additional partition as shown. The action of the fins is to increase the effective internal heat-transfer area, and to conduct heat into the leading-edge region where it is most needed. The action of the additional partition is to reduce the flow passage area and to confine the flow to the fore part of the blade, while permitting some heat transfer as far back as the midpoint of chord. An analysis has been made, based on the empirical formula for h_g, presented in reference 9, whereby the magnitude of the heat savings to be expected from such a modification can be demonstrated. For a blade that has an internal flow passage reduced to half its previous value, and that has a doubled effective heat-transfer area (fig. 6), the internal flow may be reduced to 15 percent of its original value and still maintain the same total heat transfer through the blade metal. This represents a saving in heat input of 85 percent, and can be accomplished along with a reduction in the gas velocity of 70 percent and a reduction of friction pressure loss of 20 percent. The amount of blade modification should be varied in the radial direction to balance the expected external heat losses, so that no area of the blade would have a temperature deficiency. It is felt that modified gas-heated propeller blades will provide complete ice protection with heat input values equivalent to external electrically heated blade shoes.

Experimental investigation. - Shown in figure 7 is a gas-heated propeller installed in the diffuser section of the icing research tunnel prior to icing runs. The propeller used was a production model, 10 feet, 2 inches in diameter, and modified with openings at the blade tips and shanks to permit the passage of the internal flow. Heated air was ducted from under the tunnel through the supply duct. Surface temperatures were obtained from thermocouples faired to the blade surface at two radial stations, 40 and 70 percent of radius.

The propeller speed was maintained at 1050 rpm, at which speed the maximum flow that was pumped through an unpartitioned blade was 450 pounds per hour. The maximum manifold temperature obtained was 450° F, which with the maximum flow produced a heat input of 40,000 Btu per hour for an unpartitioned blade. The average tunnel airspeed past the plane of the propeller was 200 feet per second, and the air temperature ranged from -9° to 23° F. Icing conditions were simulated in the tunnel by a ring of water spray nozzles located upstream of the contraction section of the tunnel. The spray produced an average liquid-water content at the propeller of 0.5 gram per cubic meter with an average drop diameter of 55 microns.

The blade heating results that were obtained in icing conditions during the investigations are shown in figure 8. The surface temperature rise above the ambient tunnel temperature is plotted against the chordwise distance from the stagnation point for the camber and thrust faces. The values shown are for the 70 percent radius station, which was chosen because it is in the center of the working area of the blade. The temperature rise for the unpartitioned blade was obtained with a heat input of 40,000 Btu per hour per blade. The rise in temperature for the 50 percent partitioned blade results from an input of 14,000 Btu per hour. The rise for the 25 percent partitioned blade corresponds to a maximum input of 10,000 Btu per hour. These heating values produced an average heat transfer through the heated area of the blades equivalent to 6, 5, and 9 watts per square inch, respectively.

Two significant results are evident in figure 8. First, the leading-edge temperature rises are much less than those a slight distance back from the leading edge on either face, which is especially true of the unpartitioned blade. The distribution is similar to that shown in the analytical example. Second, the level of heating, especially for the two partitioned blades, is much too low because a surface temperature of 32° F was maintained near the leading edge only at ambient temperatures above 20° F.

A comparison between the 70 percent station and the 40 percent station for both icing and nonicing conditions is shown in figure 9. The surface temperature rise above ambient is plotted against the chordwise distance from stagnation point for both faces. The comparison is for a 50 percent partitioned blade. The temperature rise for the 40 percent station is seen to be considerably greater than for the 70 percent station, indicating that the internal flow cooled down rapidly after leaving the blade shanks. The fact that the 40 percent station is within one foot of the spinner explains its more intensive heating. Also shown in figure 9 is a typical comparison between temperature rises in icing and nonicing conditions. The

rise, for both stations, when sprays are on is much less than that in clear air, and especially is this true on the camber face where the water interception and sensible heat requirement is maximum.

Icing Observations. - Surface temperatures alone cannot be taken as a measure of a heated propeller's ability to perform in icing conditions. The nature and effect of ice formations on the blades must also be considered. The aerodynamic losses associated with simulated propeller icing is discussed in reference 10. Observations of the icing characteristics of the blades indicated a much more favorable picture of the gas-heated propeller system than did the surface temperatures, either analytically or experimentally obtained. Figure 10 is a photograph of a propeller after an icing run in tunnel air at 20° F with no heat addition to the blades. A close-up of one of the blades is given in figure 11 showing that the ice obtained in the tunnel is broken and irregular and extends to the midchord on the camber face at several points. The ice that remained on an unpartitioned propeller after an icing run in air at 11° F with a heat input of 34,000 Btu per hour per blade is shown in figure 12 and figure 13 is a close-up of one of the blades. The ice is confined to the leading-edge region, indicating a need for more intensive heating along that area. The propeller with blades having 50 percent partitions (fig. 14) was subjected to icing in air at 22° F with a heat input of 14,000 Btu per hour. Only a trace of leading-edge ice is visible, indicating almost complete ice protection at 22° F. At lower temperatures the 50 percent partitioned blades were freed of leading-edge ice as well as or better than the unpartitioned blades and no freezing or runback moisture was observed. A propeller with 25 percent partitioned blades after an icing run in 16° F air with a heat input of 8000 Btu per hour is shown in figure 15. In addition to leading-edge ice there is apparent considerable ice in layers on the camber face, the result of intermittent freezing and throw-off of ice.

CONCLUSIONS

From the experimental investigation described, the following conclusions are made: Unpartitioned blades similar to those investigated will give adequate ice protection with a minimum heat input of 40,000 Btu per hour per blade; 50 percent partitioned blades with a heat input of 14,000 Btu per hour provide marginal ice protection, with an indicated need of 20,000 Btu per hour for adequate ice protection. The 25 percent partitioned blades investigated were underheated to an extent that no safe value of heat input was indicated that would with certainly preclude ice formations aft of the heated area.

From the analysis presented, it can be concluded that gas-heated propeller blades with carefully designed internal passages will provide better chordwise and radialwise ice protection than external blade shoes for comparable heat input values. In addition, gas-heated blades will not disturb the airfoil contour or be subject to damage by erosion.

REFERENCES

1. Gray, Vernon H., and Campbell, R. G.: A Method for Estimating Heat-Requirements for Ice Prevention on Gas-Heated Propeller Blades. NACA RM (to be pub.).

2. Mulholland, Donald R., and Perkins, Porter J.: An Investigation of the Effectiveness of Air-Heating a Hollow-Steel Propeller for Protection against Icing. I - Unpartitioned Propeller Blades. NACA TN (to be pub.).

3. Mulholland, Donald R., and Perkins, Porter J.: An Investigation of the Effectiveness of Air-Heating a Hollow-Steel Propeller for Protection against Icing. II - 50 Percent Partitioned Propeller Blades. NACA TN (to be pub.).

4. Mulholland, Donald R., and Perkins, Porter J.: An Investigation of the Effectiveness of Air-Heating a Hollow-Steel Propeller for Protection against Icing. III - 25 Percent Partitioned Propeller Blades. NACA TN (to be pub.).

5. Darsow, John F., and Selna, James: A Flight Investigation of the Thermal Performance of an Air-Heated Propeller. NACA TN 1178, 1947.

6. Scherrer, Richard: An Analytical Investigation of Thermal-Electric Means of Preventing Ice Formations on a Propeller Blade. NACA ACR No. 4H31, 1944.

7. Palmatier, E. P.: Thermal Propeller Anti-Icing Means. Analysis of the Heat Loss from a Hollow Steel Blade through which Hot Air is Directed. E.W.O. D-516-Project No. 1, Progress Rep. No. 3, Curtiss-Wright Corp., Curtiss Propeller Div., Oct. 31, 1942.

8. Hardy, J. K.: Kinetic Temperature of Wet Surfaces. A Method of Calculating the Amount of Alcohol Required to Prevent Ice, and the Derivation of the Psycrometric Equation. NACA ARR No. 5G13, 1945.

9. Boelter, L. M. K., Martinelli, R. C., Romie, F. E., and Morrin, E. H.: An Investigation of Aircraft Heaters. XVIII - A Design Manual for Exhaust Gas and Air Heat Exchangers. NACA ARR No. 5A06, 1945.

10. Corson, Blake W., Jr., and Maynard, Julian D.: The Effect of Simulated Icing on Propeller Performance. NACA TN 1084, 1946.

FLOW IN GAS-HEATED HOLLOW PROPELLER BLADE

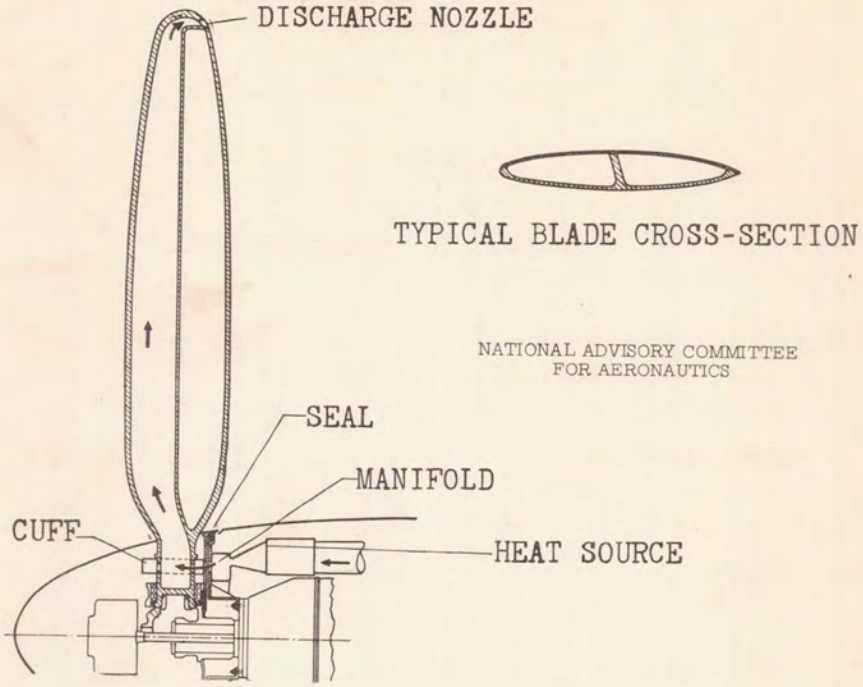

FIGURE 1.

HEAT-TRANSFER EQUATION

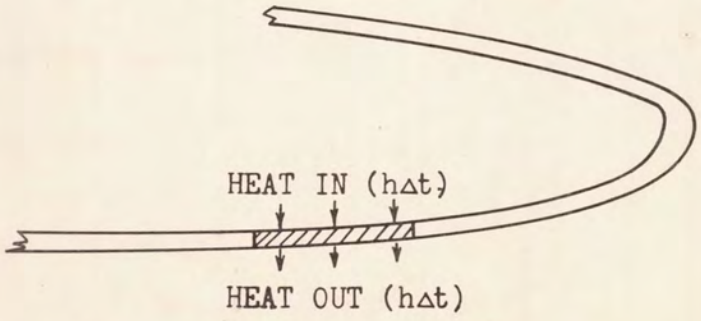

HEAT IN = HEAT OUT

CONVECTIVE HEAT = CONVECTIVE HEAT + EVAPORATIVE HEAT + SENSIBLE HEAT

$$h_g(t_{g,d} - t_s) = (h_a X + M)(t_s - t_{a,d})$$

FIGURE 2.

TYPICAL VARIATION OF EXTERNAL HEAT-TRANSFER COEFFICIENT

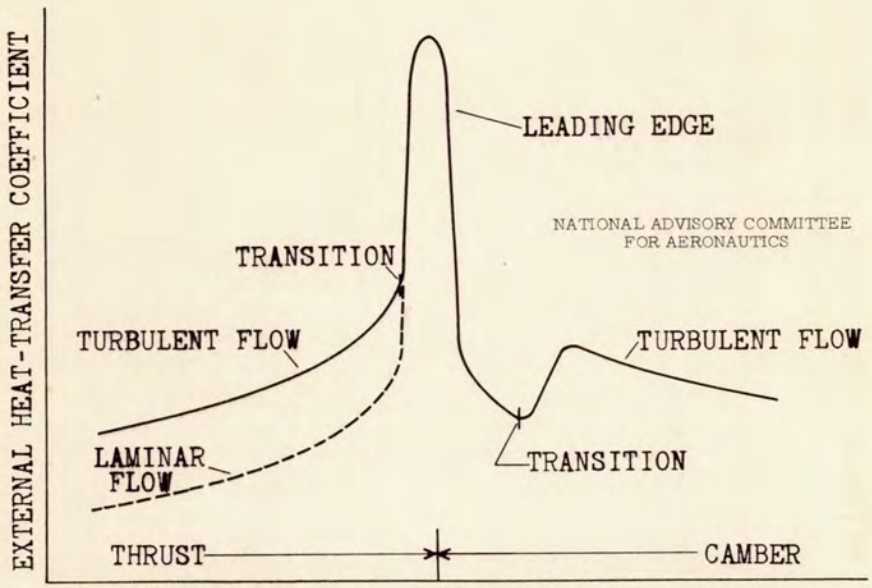

FIGURE 3.

CHORDWISE VARIATION OF BLADE SURFACE TEMPERATURE

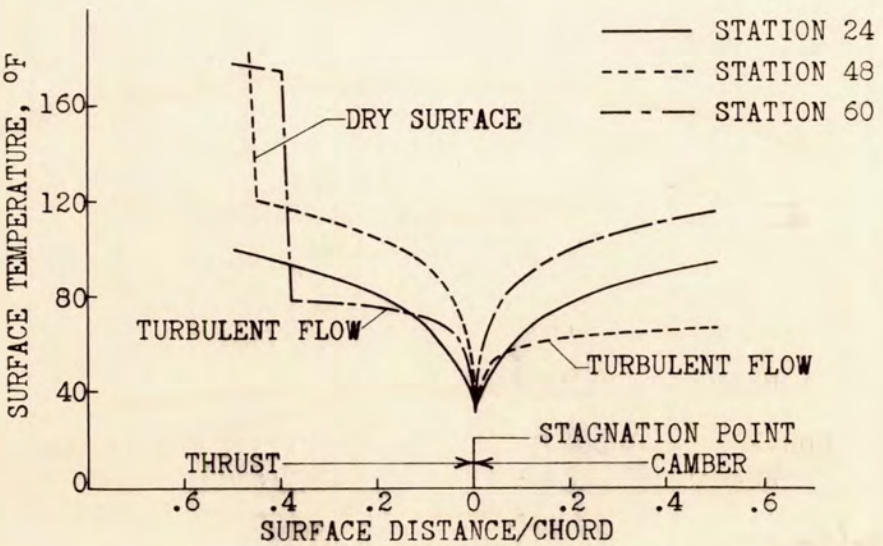

FIGURE 4.

HEAT-TRANSFER VARIABLES ALONG PROPELLER RADIUS

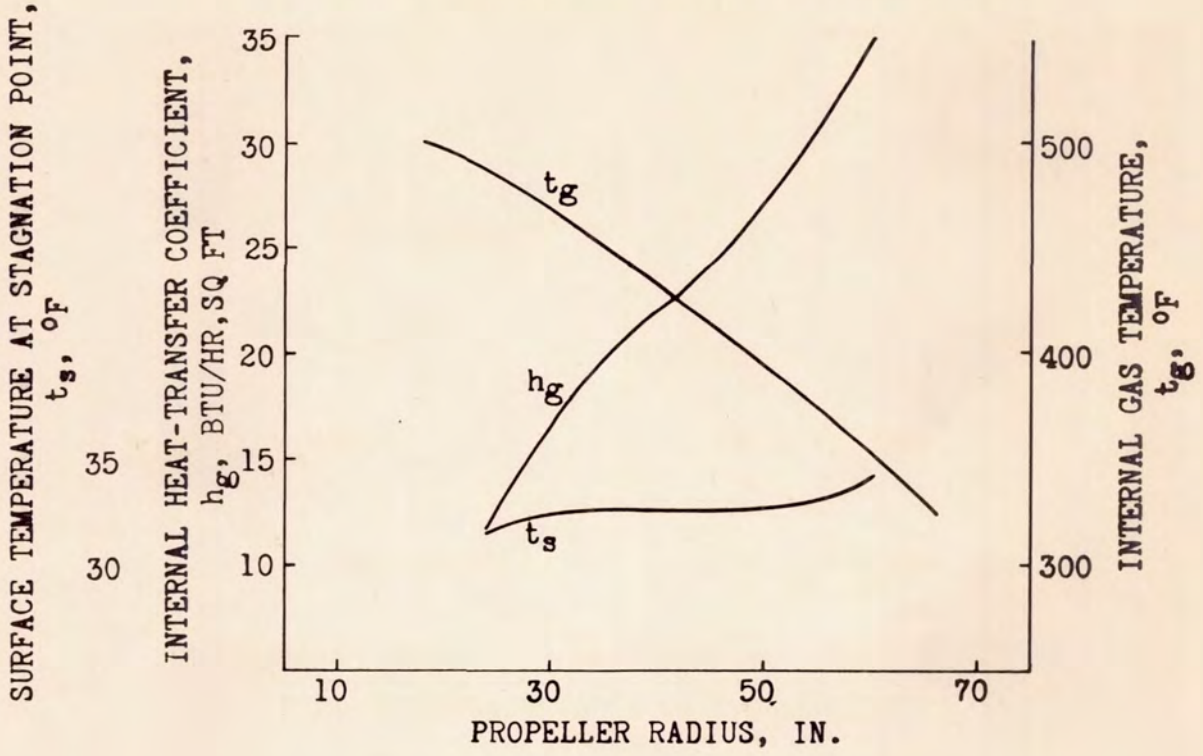

FIGURE 5.

MODIFICATION OF BLADE SECTION FOR IMPROVED HEAT TRANSFER

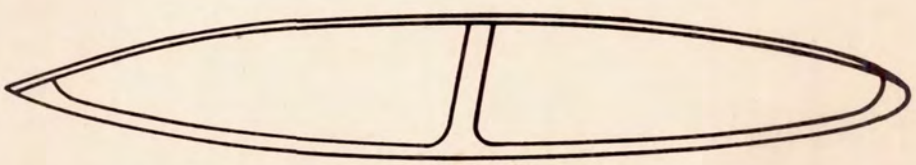

ORIGINAL

NATIONAL ADVISORY
COMMITTEE FOR AERONAUTICS

MODIFIED

FIGURE 6.

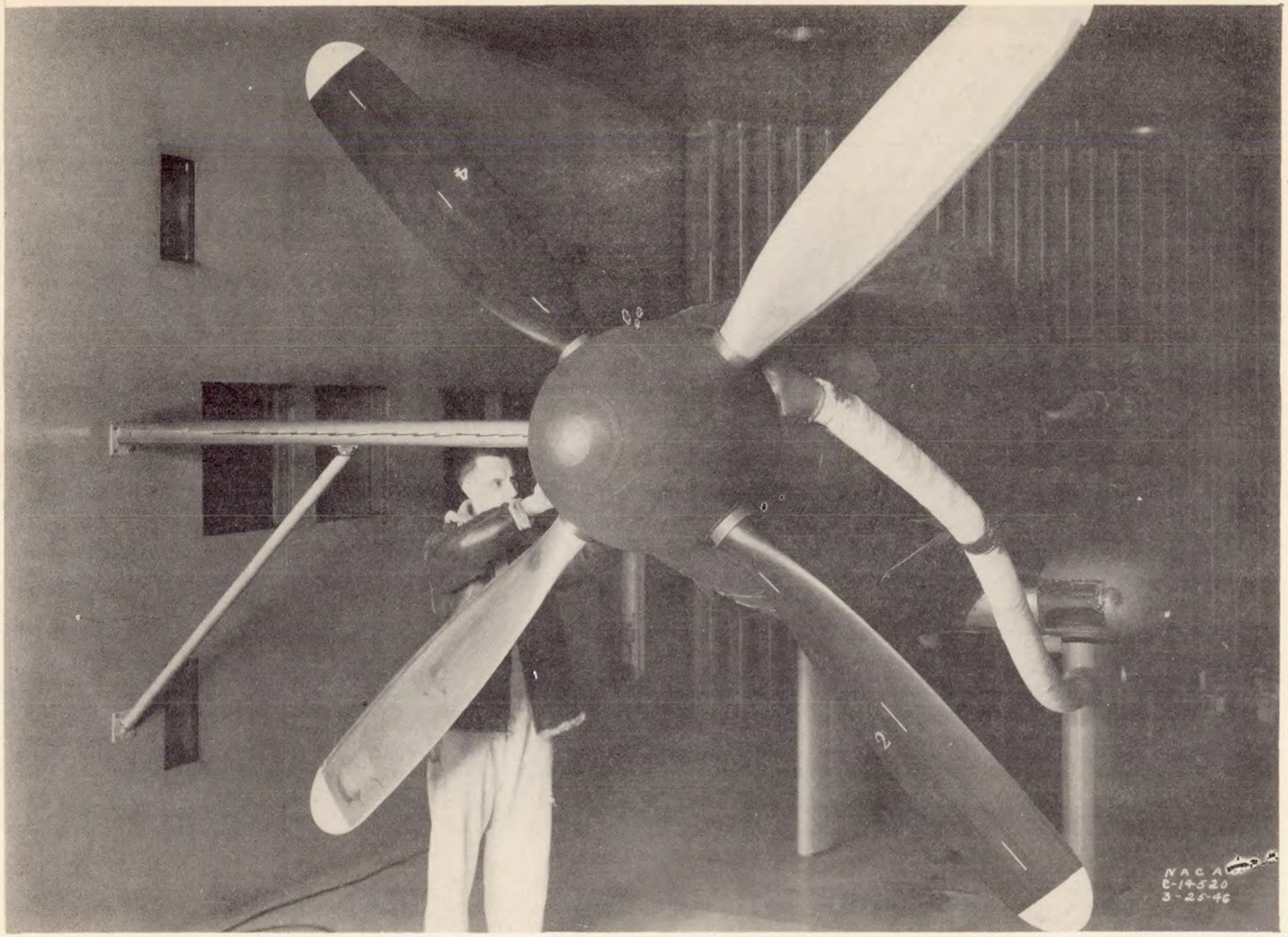

GAS-HEATED PROPELLER INSTALLATION
FIGURE 7.

MAXIMUM TEMPERATURE RISES IN ICING CONDITIONS

70% RADIUS

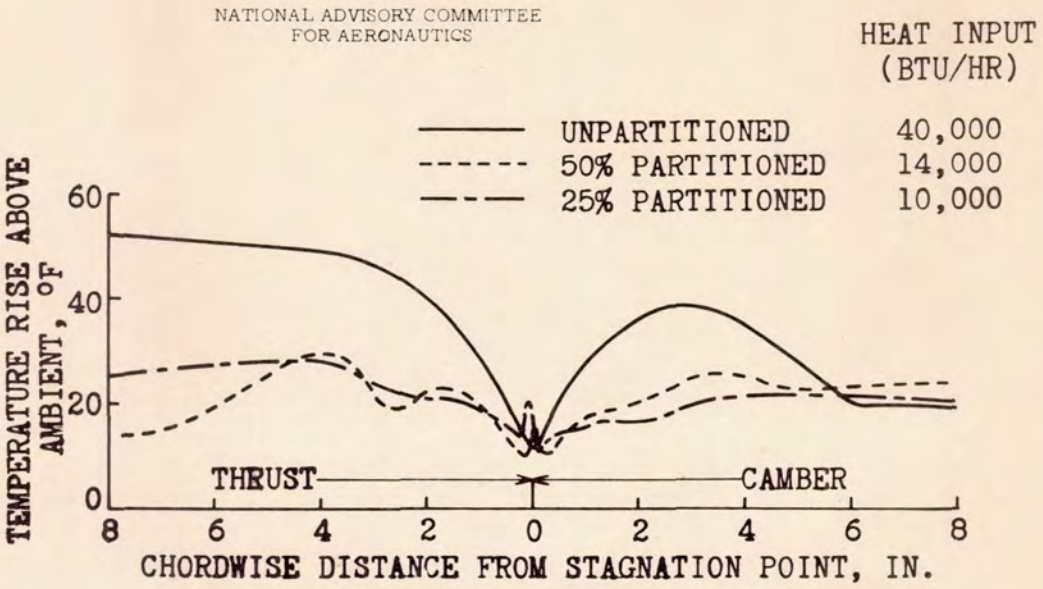

FIGURE 8.

ICING AND NON-ICING TEMPERATURE RISES

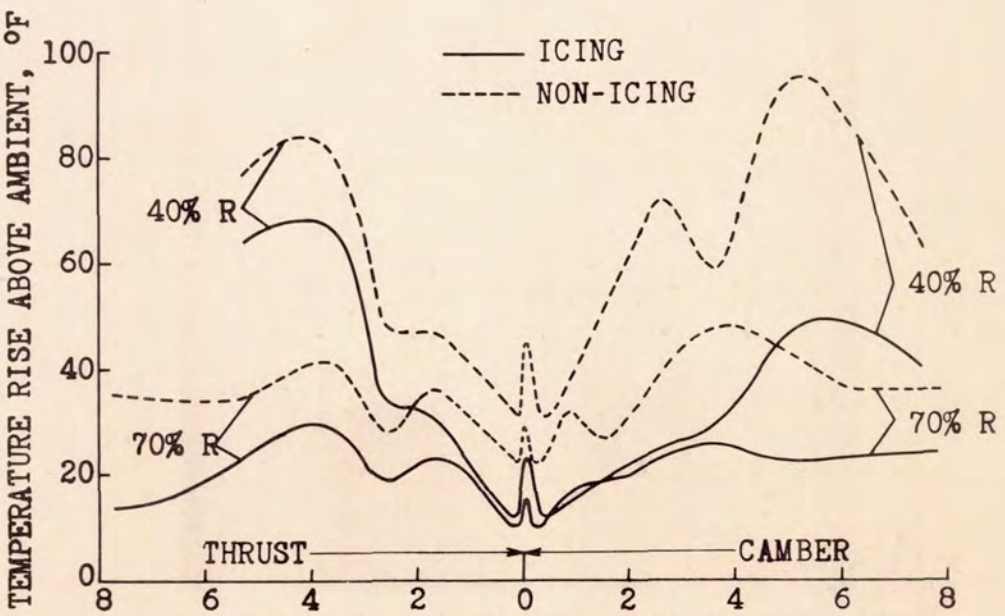

FIGURE 9.

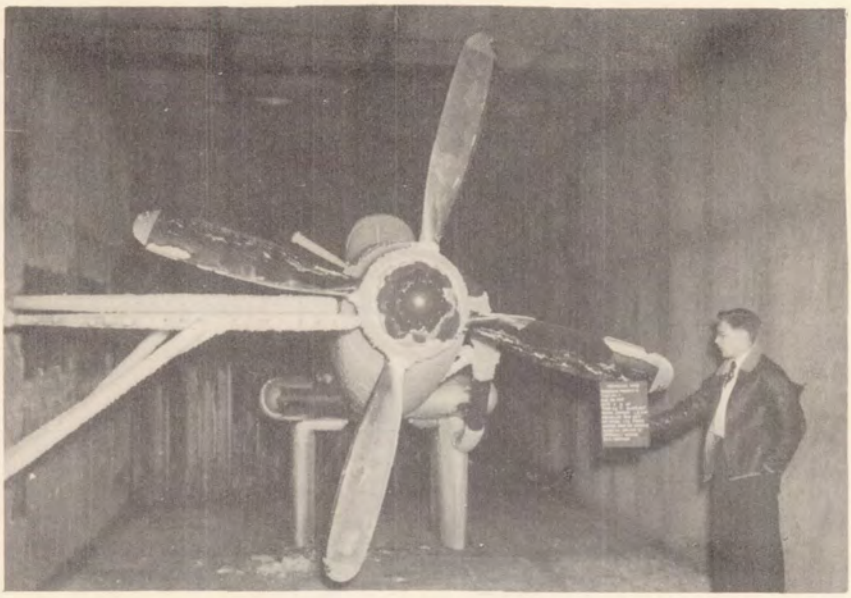

UNHEATED PROPELLER ICING
FIGURE 10.

CLOSE-UP OF ICING
FIGURE 11.

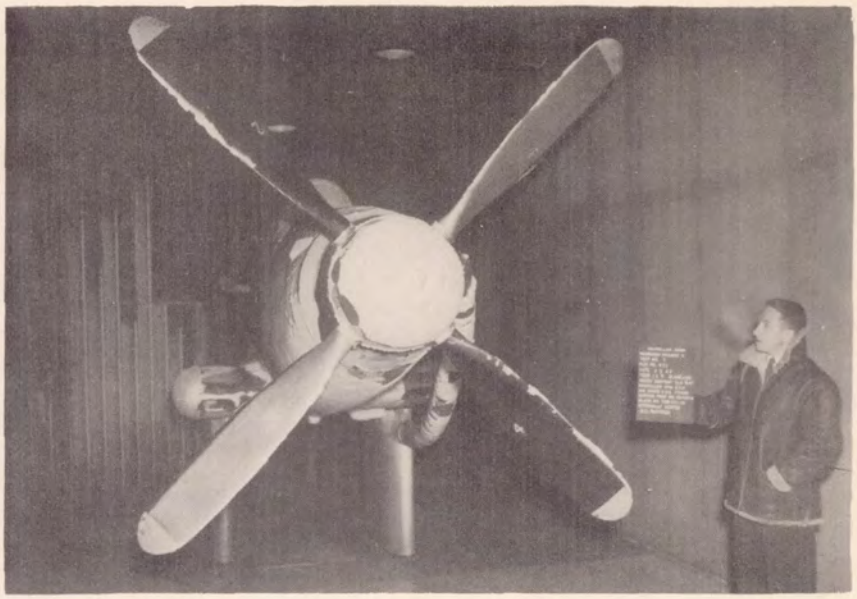

UNPARTITIONED BLADE RESIDUAL ICING
FIGURE 12.

CLOSE-UP OF ICING
FIGURE 13.

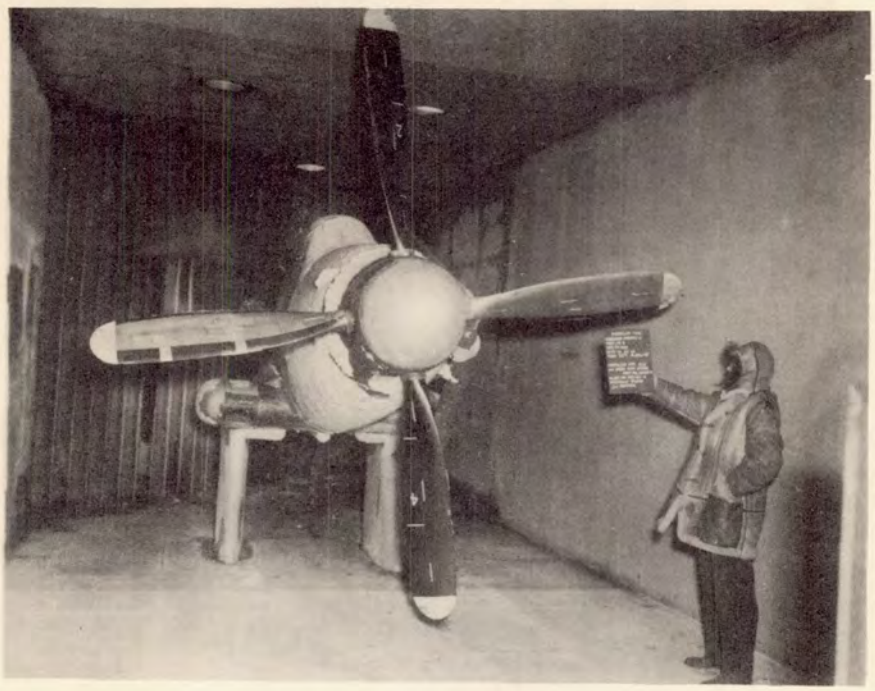

50% PARTITIONED BLADE RESIDUAL ICING
FIGURE 14.

25% PARTITIONED BLADE RESIDUAL ICING
FIGURE 15.

ELECTRO-THERMAL METHODS OF PROPELLER ICE PROTECTION

I - CYCLICAL DE-ICING BY EXTERNAL AND INTERNAL BLADE HEATERS

By J. P. Lewis

Flight Propulsion Research Laboratory

INTRODUCTION

A number of investigations has been made to obtain a solution to the problem of the protection of propellers in icing conditions. In the past, partial protection has been obtained by the use of pastes, lacquers, and alcohol in conjunction with blade feed shoes. None of these methods provided adequate and positive protection and, with the development of thermal de-icing systems for the rest of the airplane, attention has centered on the development of a thermal system for propellers. Two general methods for the thermal protection of propellers have been proposed; the first system employs electrical heating of the blades, and in the second system a hot gas is used as described by Gray. This paper discusses the electro-thermal system and reports the results obtained from an investigation of two types of electrically heated propellers in the NACA Cleveland icing research tunnel

The development of an electrical system for propellers began as early as 1938 (reference 1). Initial investigations and analyses showed the practicability and advantages of such a system of ice protection. Much of the early work was concerned with the details of the development of practical blade heaters and a power supply system with much of the experimental data being of a limited and inconclusive nature (reference 2). A considerable amount of experience and data were obtained by flights in natural and simulated icing conditions at the Ice Research Base, Minneapolis, Minnesota (reference 3). Investigations were conducted with two types of external-blade heater, one of which consisted of a rubber wire-insert blade shoe, whereas the second heater consisted of conductive rubber. From these investigations a minimum power input of 2.5 watts per square inch was recommended with the heated area extending to 20 percent of chord and 90 percent of the blade radius. These early investigations were primarily concerned with continuous heating of the blades to obtain ice prevention rather than de-icing. In addition the lack of suitable instrumentation prevented a definition and correlation of the icing conditions encountered.

Following these tests an analytical investigation of the power requirements for a thermal-electric system (reference 4) determined power input for ice prevention of 1700 watts per blade, which is equivalent to an average power density of 6 $\frac{3}{4}$ watts per square inch. For ice removal a power of 800 watts per blade was required, which is equivalent to an average power density of 3.2 watts per square inch. The indicated power requirement for continuous heating was in excess of that available on current aircraft. As a result, attention centered on the development of a cyclical or intermittent heating system. In this system the blades are allowed to ice and heat is then applied for a limited period to remove the ice deposit, the cycle is then repeated. In addition to the power economies obtained, cyclical heating was also presented as a solution to the problem of runback and refreezing.

Some of the important requirements for a cyclical de-icing system may be stated as follows: The ice removal must be prompt and complete with a minimum expenditure of power. The icing allowed during the heat-off period must not impair the aerodynamic performance of the propeller. The throw-off of ice during heating must be such that a low vibration level is maintained, no damage is suffered by the rest of the aircraft, and there is a minimum of discomfort to the passengers. The investigations of electro-thermal methods of propeller ice protection in the icing research tunnel (references 5 and 6) were primarily concerned with the determination of the power distribution and cycle time requirements for cyclical blade heating.

APPARATUS AND INSTRUMENTATION

The propeller research program was conducted in the diffuser section of the NACA Cleveland icing research tunnel which provided a test section large enough to permit investigation of full-scale propellers. The setup as shown in figure 1 was essentially the same for all the propeller icing investigations, differing only in the test propeller, the heat supply system, and details of instrumentation.

Two different types of propeller blade and blade heater were investigated. External rubber-clad blade heaters were installed upon a 10-foot, 5-inch-diameter 3-blade hollow-steel propeller. The second type of heater consisted of an internal heater installed in a 4-blade 11-foot-diameter propeller.

Figure 2 shows the construction of the external blade heater. The heater consisted of several small chromel heating ribbons, laid radially over two neoprene insulating plies and covered by an outer layer of abrasion resisting neoprene. The heating ribbons were

connected into 1/2-inch and 1-inch wide elements, thus permitting a variable chordwise heating distribution. The heating elements covered a constant chordwise surface distance on both the thrust and camber faces, extending to approximately 40 percent of chord on the camber face and approximately 50 percent on the thrust face at the 75 percent radius station. In a radial direction the heater extended 45 inches from the hub to the 88 percent station (55-inch station).

Figure 3 shows the internal heater, which consisted of a wire-woven blanket connected into a single circuit of a fixed distribution. The blade was constructed of a tubular main spar to which steel sheets, 0.037 inch thick, were fastened to form the blade profile. A sponge-type filler was inserted beneath the heater to prevent diaphragming of the blade skin. This filler also served as an excellent thermal insulation by effectively confining the heat to the forward section of the blade. The heating wires were arranged in groups to obtain the desired power distribution with the greatest heat power density at the leading edge. The heated area extended to 20 percent of chord on both faces and 48 inches radially from a point 2 inches from the shank end of the blade to the tip.

CONDITIONS AND PROCEDURES

A tunnel airspeed of 120 miles per hour was maintained throughout the investigation. The propellers were operated at two speeds with two corresponding blade angles. The higher propeller speeds investigated correspond to the cruise condition for the propellers while the lower speeds are representative of the speed range for large propellers on installations employing a large speed reduction ratio.

The investigation was made at three different icing conditions that were defined by the ambient-air temperature, liquid-water concentration, and droplet diameter. The conditions studied cover a range of nominal air temperature of 0° to 25° F with corresponding liquid-water concentrations of 0.2 to 1.0 gram per cubic meter. An average droplet size of 55 microns was obtained for the complete temperature and liquid-water range. These conditions are considered to be representative of moderate-to-heavy icing conditions.

Figure 4 shows several typical chordwise heating power distributions for the external heater. The first pattern (675 watts) is an approximation of the distribution stipulated in the current AAF specification (reference 7). The other configurations were obtained from this basic pattern by increasing both the power density and chordwise coverage. The patterns were chosen in order to obtain the maximum ice removal for the minimum expenditure of energy and also to

minimize runback and refreezing on the unheated areas. Figure 5 shows the radial and chordwise distribution for the internally heated blade. The values are the design distribution on the inner surface of the blade skin. The distribution at three radial stations are shown with the power density increasing with an increasing blade radius. The distribution on the outer surface of the blade differs because the fillet at the leading edge presents a relatively large mass of metal and hence distorts the heating pattern.

For cyclical de-icing several combinations of heating and cycle time were investigated. The heating and cycle times were selected on the basis of the AAF specification, the estimated rate of temperature rise, and the estimated icing rate. With the external blade heater, heating times of 12 and 24 seconds were used with cycle times in the ratio of 4:1 and 8:1. The internal heater was investigated at heating times of 5, 10, 20, 30, 40, and 50 seconds with cycle ratios of 2:1, 4:1, and 8:1.

RESULTS AND DISCUSSION

The results of the investigations in the icing research tunnel of electro-thermal methods of ice protection have been reported in terms of the ice formations obtained on unheated blades, the thermal characteristics of the blade heaters, the power requirements for ice removal, the heating and cycle times required for effective de-icing, and a comparison of the results of the icing tunnel investigation with those obtained in flight.

The ice formations obtained on the unheated three-bladed propeller with the external heaters were similar for all the operating and icing conditions investigated. At ambient-air temperature of 20° to 25° F, a rough, semiglaze ice formation was obtained. Lowering the air temperature gave a rime type of ice. The iced area was much the same for all conditions varying only slightly with propeller speed. The ice extended chordwise a distance of approximately 4 inches on both faces at the shank of the blades and tapered to about 1 inch at the tip end of the elements. Small ice formations around the blade tip were obtained at a propeller speed of 675 rpm. The smallest ice formations, extending only 50 to 70 percent of the blade radius, were obtained at the lowest temperature (5° F). An extremely low water content was obtained at 5° F and in addition a large percentage of the liquid water had frozen out as ice particles. This effect and other difficulties precluded the simulation of icing at temperatures below 0° F. As larger water contents are often encountered at this temperature in natural icing conditions, this limited coverage should not be used for design purposes. The maximum iced area was attained within 1 minute of icing and varied only slightly

thereafter. The ice built up on the leading edge at a rate of approximately 1/8 to 1/10 inch per minute. At the higher temperatures (20° to 25° F) natural throw-off occurred within 2 minutes, whereas at the lower temperatures (0° to 5° F) a single throw-off rarely occurred within a 10-minute period.

External Blade Heater. - Typical results of a study of the power and heating time required for an initial ice removal are shown in figure 6. Heat was applied after the blades had been allowed to ice for a period of 3 minutes and the time to remove the ice from the various area was noted. For the conditions shown a maximum heating time of 40 seconds was required at a power density of 3.5 watts per square inch. An upper limit for power density of approximately 8 to 9 watts per square inch is indicated with a corresponding heating time of 2 to 8 seconds. Raising the ambient-air temperature from 11° to 20° F reduced the heating time approximately 5 seconds. The data also indicate a greater power or time requirement at 925 rpm than at 675 rpm. Greater powers or times would also be required at lower ambient-air temperatures.

The typical variation of the blade surface temperature with time during cyclical de-icing with the external heater is shown in figure 7. The dash-dot lines represent the freezing isotherm 32° F. Results are given for two heating cycles and two ambient-air temperatures. At an ambient-air temperature of 10° F, heating time of 24 seconds, and total cycle time of 180 seconds, the blade temperatures rose quickly with the application of heat and reached a peak value of approximately 54° F. At a shorter cycle time and a lower air temperature, approximately the same peak temperatures were obtained. The short cycle (96 seconds) did not, however, allow the blade to cool completely as was the case with the 180 second cycle. In both cases the initial rate of cooling was similar and at the end of the heating period the surface temperatures quickly dropped below 32° F and a new ice formation was allowed to form. The surface temperature should eventually return to a value equal to the ambient temperature plus the local kinetic temperature rise. The average rate of blade temperature rise did not vary greatly with the icing or operating conditions nor with the radial or chordal position. An average rate of temperature rise of approximately 1.10° F per second was obtained for the conditions investigated. This rate of rise determines the heating time required for any particular condition. The average rate of cooling was such that blade temperatures dropped from 70 to 90 percent of the difference between the peak and minimum values in a period approximately equal to the heating period. Thereafter the rate of cooling decreased quickly, the minimum temperature being reached in a period two to four times the heating period. The heat-off period required is determined by this rate of cooling and by the amount of ice that can be allowed to form on the blades.

Figure 8 shows photographs of typical residual ice remaining on the blades after cyclical de-icing with the external heater. With the exception of investigations made at air temperatures greater than 20° F, a heating time of 12 seconds was insufficient for effective de-icing. At the lower temperatures both a longer heating time (24 seconds) and greater power input were required. In general, a ratio of the heating time to total cycle time of 1:4 gave the best results through the range of conditions investigated. As a result of investigations made with various chordwise heat distributions, the most effective heat distribution was found to be one approaching uniformity. At 20° to 25° F, a power density of approximately 5 to 6 watts per square inch was satisfactory. At 10° to 15° F, power densities of 7 to 8 watts per square inch were required and it is estimated that approximately 10 watts per square inch would be required at 0° F. The residual ice formations shown in figure 8 are in most cases caused by ice forming on unheated areas and bridging over to the heated region. For effective de-icing it is considered necessary to heat all the area where ice forms especially in the outer 60 percent of the blade where most of the thrust of the propeller is developed.

Internal Blade Heater. - With continuous heating of the blades the power requirements were found, as in the case of the external heater, to be a function of the icing and operating conditions. At a speed of 1000 rpm and an ambient-air temperature of 20° to 25° F, marginal ice protection in the heated area was obtained with a power input as low as 500 watts per blade. Full protection in the heated area at these conditions was obtained with an input of 750 watts per blade. At the same propeller speed (1000 rpm) and ambient-air temperatures of 5° to 10° F, 1000 watts per blade were required for full ice protection. At the same temperatures (5° to 10° F) but with a lower propeller speed of 800 rpm, a power input of 1000 watts per blade gave only marginal protection, with 1250 watts required for complete protection.

Figure 9 shows typical curves of the blade temperature rise above ambient temperature with the internal heater. These curves present some of the thermal characteristics of the blade heater and are of value in determining the heating time and power requirements. For both propeller speeds the temperatures showed an initial rate of rise of approximately 0.5°per second, with a rise to 32° requiring approximately 30 seconds for the heating power (fig. 9). At a propeller speed of 1000 rpm the temperatures reached a stable value of 51° F above ambient temperature in approximately 3 minutes. At a lower speed (800 rpm) a stable value of 62° F above ambient temperature was attained in approximately 4 minutes. The rise of the temper-

ature increment for the unheated blade can be attributed in part to release of the heat of fusion as well as changes in the ambient-air temperature.

Figure 10 shows typical variation of the blade surface temperature with time during cyclical de-icing with the internal heater. These curves are in general similar to the curves obtained with the external heater. The dash-dot lines represent the freezing isotherm 32° F. The initial temperature rise at -60 seconds was caused by the start of the icing sprays. The heating and cooling rates were much lower than the values obtained for the external heater. For the conditions shown the average rate of temperature rise was approximately 0.6° F per second. Because of the thermal capacity of the blades, a rather long cooling period following heating was required. This delayed cooling aggravated runback and refreezing at several conditions, causing ridges of ice to form at the rear edges of the heated area. A minimum cooling period of at least three times the heating period was required for the blade temperatures to return to the initial value. Because of the low rate of heating, a minimum heating time of 25 to 30 seconds was required. Temperature rise rates of from 0.25° to 0.75° F per second were obtained depending upon the ambient-air temperature.

Figure 11 shows photographs of typical results of cyclical de-icing with the internal heater. At 20° F for both power inputs shown, marginal de-icing was obtained with the results at 1250 watts per blade being only slightly better than those at 1000 watts per blade. At 5° F poor de-icing was obtained particularly at the lower input. The rather large formations at the shank of the blades should be noted. These formations were anchored to the unheated area at the shank and were extremely difficult, and, in some cases impossible to remove. The results shown in these photographs indicate the need for longer heating periods and increased power inputs as well as the necessity of proper heat distribution to prevent ice bridging over from an unheated area.

CONCLUSIONS

The results of the investigation of electrical blade heaters indicate that several important conclusions can be made as to the requirements for the design and operation of such systems of propeller ice protection.

The maximum heated areas should be at least equal to the maximum ice-covered area. For the propeller with the external heaters this maximum are extended a distance of 4 inches on both faces at the

shank, tapering to approximately 1 inch at the tip. Similar although slightly greater areas were indicated for the internally heated blade. The minimum heated area depends upon the effect of residual ice formations on propeller performance and the allowable tolerance of such performance losses.

For cyclical de-icing a power distribution approaching chordwise uniformity is indicated. For ice prevention, however, a concentration of heat at the leading edge is required. The radial extent and distribution of heat will depend chiefly upon the propeller operating conditions. The power density is a function of the ambient-air temperature and heating time. For heating times of less than 40 seconds, power densities of 5 to 10 watts per square inch are required for corresponding ambient temperatures of 25° to 0° F.

For the external heater, heating times of 12 to 30 seconds, depending upon power input and temperature are required. A cycle time four times the length of the heating period gave the best results for both heaters. With the internal heater a minimum heating time of 25 to 30 seconds is required.

By comparing the two types of heater, it can be seen that each has certain advantages and disadvantages. The external heater can be applied to all types of blades, both hollow and solid. Compared with the internal heater, the external heater has less thermal lag which results in a quicker ice removal with less danger of runback. The main disadvantage of the external heater is its susceptibility to wear and damage from abrasion. Experience has indicated that this abrasion damage may limit the radial coverage to approximately 65 percent of the blade radius. An installation with an internal heater suffers no aerodynamic penalties resulting from an external shoe and in addition is free from abrasion trouble. With the internal heater care must be taken in the disposition of the heater elements to obtain the correct heat distribution on the external surface, and in this respect it resembles the gas-heated blade. Compared with the hot-gas system, electrical de-icing has less thermal lag requiring little warm up and in general requires a less complicated heat supply system.

REFERENCES

1. Babbitt, J. D., Rose, D. C., and Orr, J. L.: Thermo-Electric Airscrew De-Icing. Nat. Res. Council, Canada, Rep. MM-38, Sept. 1940.

2. Loughlin, W. J.: Propeller Electrical Anti-Icing Systems. Memo. Rep. Ser. No. TSELA-3C-581-144-6, ATSC, Eng. Div., Army Air Forces, Sept. 25, 1944.

3. Scherrer, Richard, and Rodert, Lewis A.: Tests of Thermal-Electric De-Icing Equipment for Propellers. NACA ARR No. 4A20, 1944.

4. Scherrer, Richard: An Analytical Investigation of Thermal-Electric Means of Preventing Ice Formation on a Propeller Blade. NACA ACR No. 4H31, 1944.

5. Lewis, J. P.: An Investigation of the De-Icing Effectiveness of External Electrically Heated Propeller Blade Heaters. NACA TN (to be pub.).

6. Stevens, Howard C., and Lewis, J. P.: Icing and De-Icing of a Propeller with Internal Electrical Blade Heaters. NACA TN (to be pub.).

7. Anon: Army Air Forces Specification. De-Icing System; Aircraft Propeller Electrical. No. 29542, Nov. 15, 1945.

PROPELLER ICING RESEARCH SET-UP

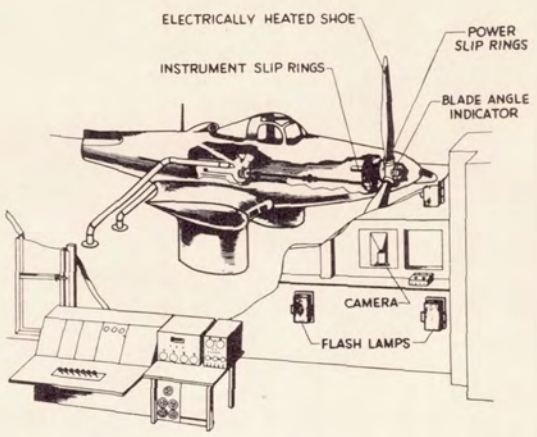

FIGURE 1.

NATIONAL ADVISORY
COMMITTEE FOR AERONAUTICS

EXTERNAL ELECTRICAL PROPELLER BLADE HEATER

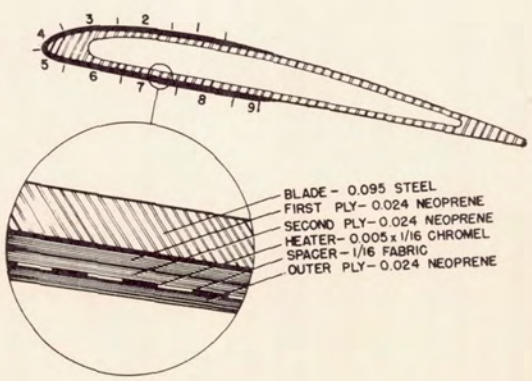

FIGURE 2.

INTERNAL ELECTRICAL PROPELLER BLADE HEATER

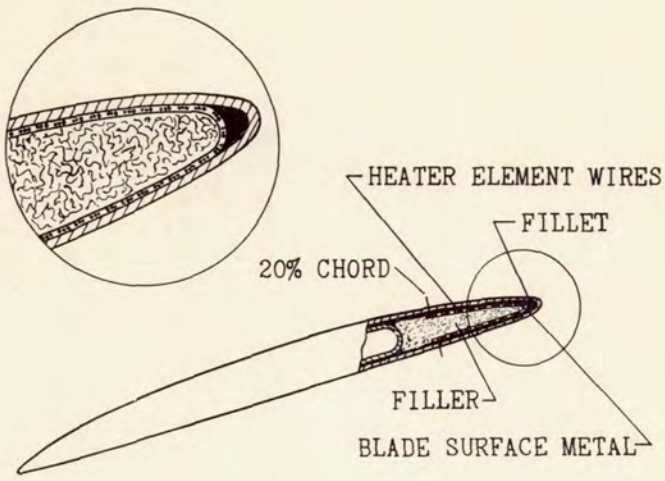

FIGURE 3.

CHORDAL-HEATING POWER DISTRIBUTION

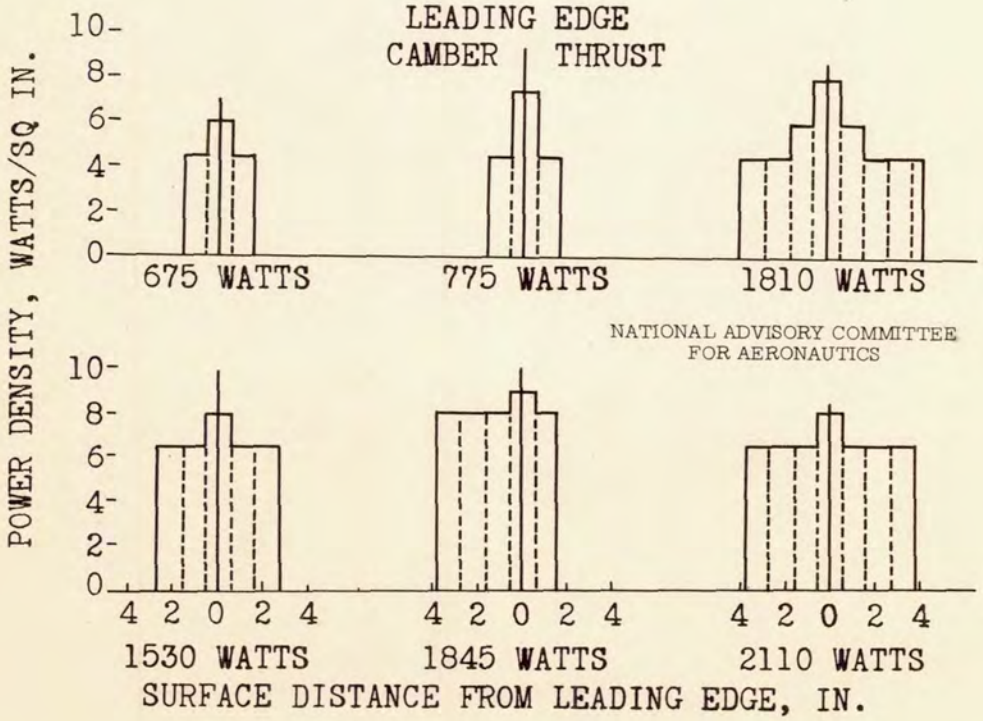

FIGURE 4.

HEAT DISTRIBUTION OF INTERNAL HEATER

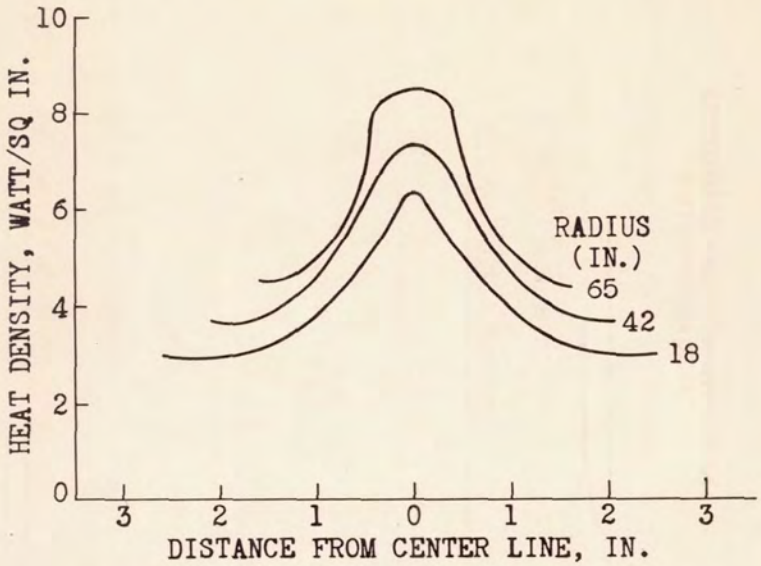

FIGURE 5.

EFFECTS OF POWER DENSITY ON DE-ICING TIME

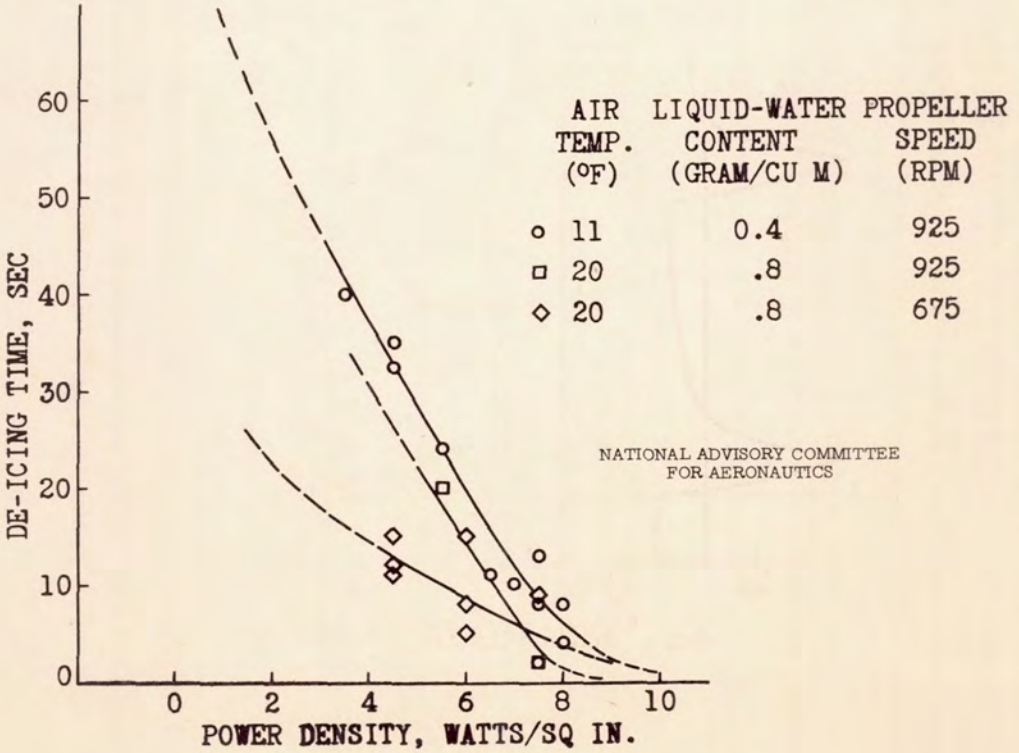

FIGURE 6.

CYCLICAL DE-ICING WITH EXTERNAL HEATER

LEADING EDGE AT 80% R; AIR SPEED, 120 MPH;
PROP SPEED, 925 RPM; HEAT INPUT, 9 W/SQ IN.

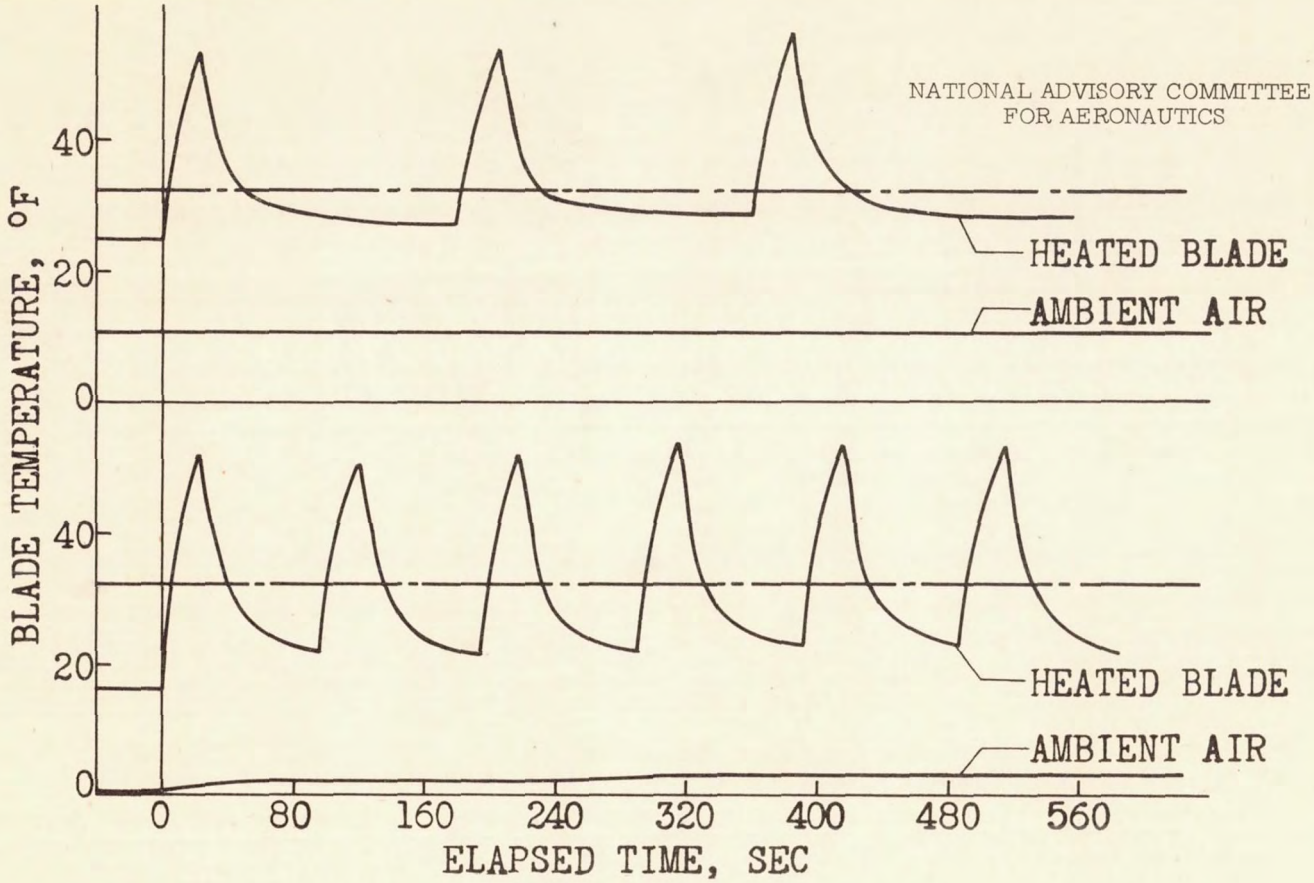

FIGURE 7.

CONFIDENTIAL

RESULTS OF CYCLICAL DE-ICING

NATIONAL ADVISORY COMMITTEE
FOR AERONAUTICS

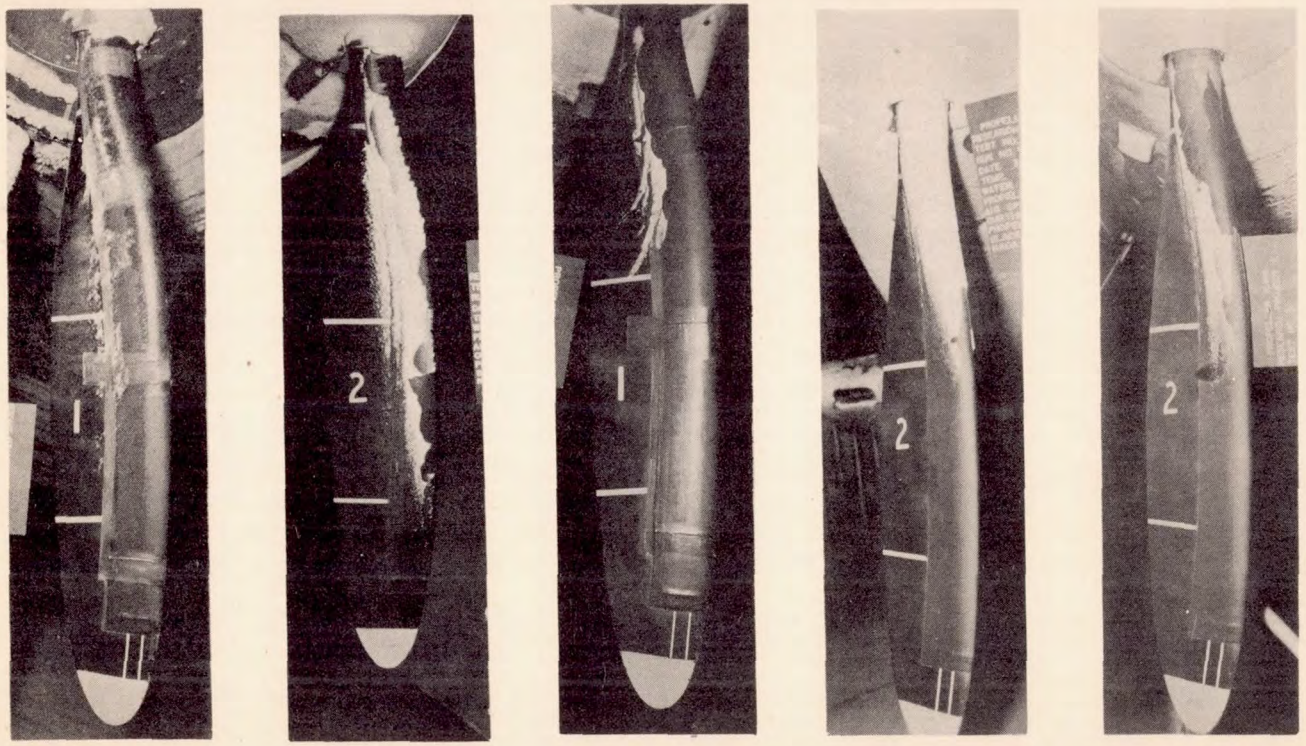

CONFIDENTIAL

°F	23	15	14	5	5
W/B	675	1810	1845	1845	2110
HEAT ON	12	12	23	12	24
CYCLE	8:1	4:1	8:1	4:1	4:1

FIGURE 8.

CONTINUOUS HEATING WITH INTERNAL HEATER

LEADING EDGE AT 33% R
AIR SPEED, 120 MPH
HEAT INPUT, 6.5 W/SQ IN.

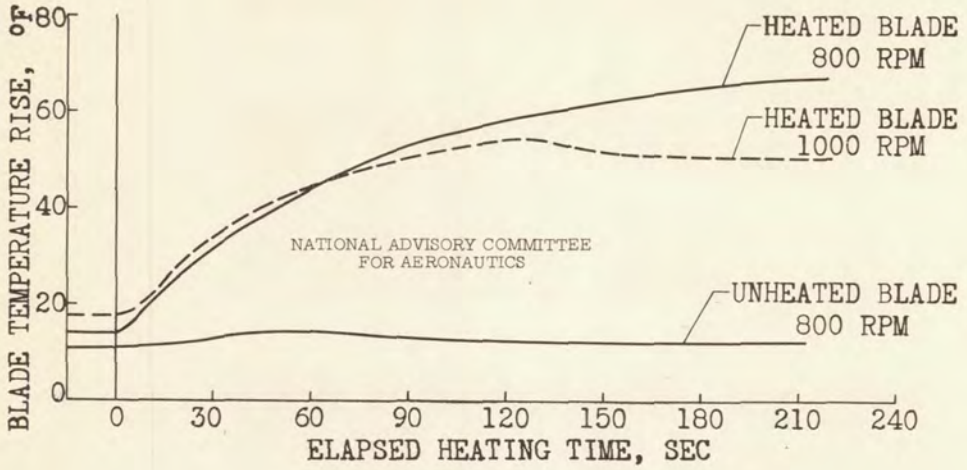

FIGURE 9.

CYCLICAL DE-ICING WITH INTERNAL HEATER

LEADING EDGE AT 33% R; AIR SPEED, 120 MPH;
PROP SPEED, 800 RPM; HEAT INPUT, 6.5 W/SQ IN.

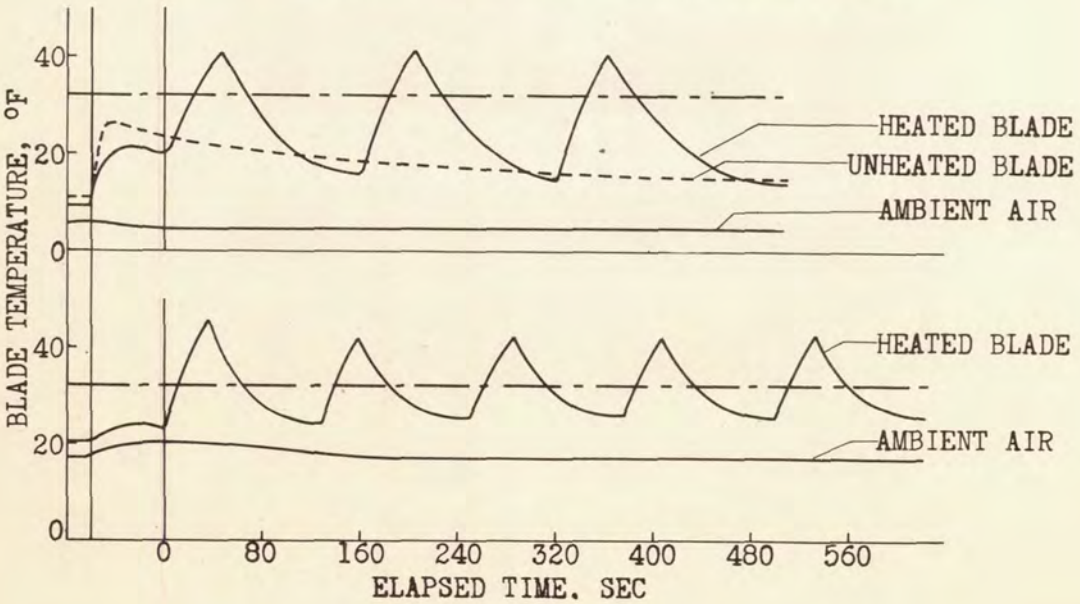

FIGURE 10.

CYCLICAL DE-ICING WITH INTERNAL HEATER
AIR SPEED, 120 MPH; PROP SPEED, 800 RPM

NATIONAL ADVISORY COMMITTEE
FOR AERONAUTICS

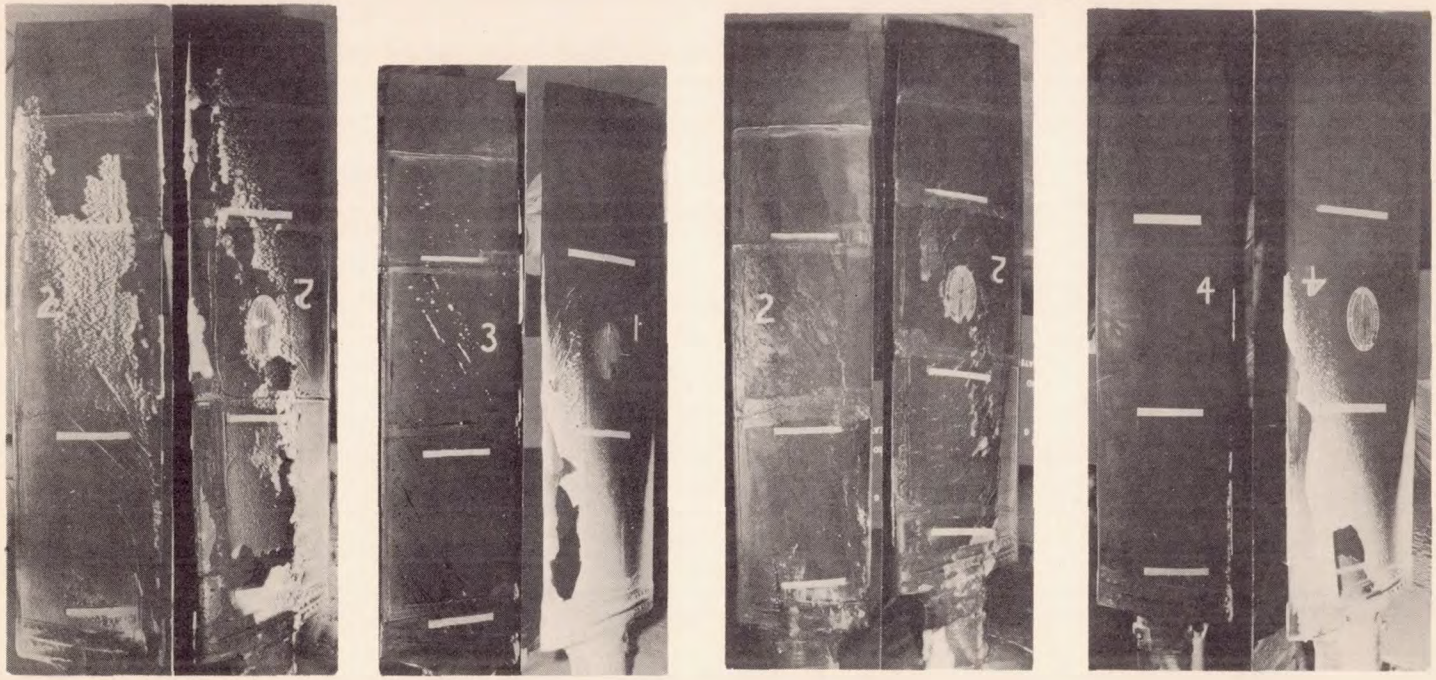

°F	20	5	20	5
W/B	1000	1000	1250	1250
HEAT ON	20	40	20	40
CYCLE	4:1	4:1	4:1	4:1

FIGURE 11.

ELECTRO-THERMAL METHODS OF PROPELLER ICE PROTECTION

II - SERVICE EXPERIENCE WITH ELECTRICAL BLADE HEATERS IN NACA FLIGHT OPERATIONS

By Gerard J. Pesman

Flight Propulsion Research Laboratory

INTRODUCTION

Information concerning the service performance of electrical propeller anti-icing systems is not plentiful; accordingly, a review of the service experience of NACA flight groups with such equipment during the winter of 1946-1947 is presented. The information was taken from service records of airplanes used for icing research and from interviews with service personnel and personnel who actually participated in the research flights. During these flights the airplanes were deliberately flown into the worst icing conditions that could be found.

The data presented are not the results of research programs and should therefore be considered as only qualitative indications of the service to be expected from such equipment in commercial service.

EQUIPMENT

Two different types of power system were used. One system consisted of propeller-hub generators excited by the standard airplane power supply. The other system utilized an auxiliary-aircraft power plant as a power source. Both wire-insert-rubber and conductive-rubber blade shoes were used.

The general configuration of the propeller-hub generator anti-icing system is shown in figure 1. The armature is fastened to the rear of the propeller hub. Separate leads run from the armature to each blade shoe. The field is attached to the front section of the crankcase and is excited by the 28-volt, direct-current, electrical system of the airplane. Inasmuch as the field is stationary and the armature rotates with the propeller, no slip rings are required.

The general details of the slip-ring system are illustrated in figure 2. Power is supplied by a standard commercial 110-volt, 400-cycle-per-second, auxiliary-aircraft power plant. The brush-holder slip-ring assembly of a reversible-pitch propeller was

substituted for the standard unit and the extra brushes were utilized for transferring the power to the propeller blade shoes.

Cross sections of the two types of blade shoe are shown in figure 3. The wire-insert blade shoes consist of rubber with wire-heating elements molded in place. The heating elements run parallel to the length of the blade. The high-heat section on the leading edge of the blade was designed to provide either 1.5 or 2 times the heating intensity of that on the cambered faces and extends farther toward the trailing edge of the blade on the forward face than on the rear face.

The conductive-rubber blade shoe is composed of an insulating layer, a conductive-rubber layer, and an abrasion-resistant layer on the outside. Copper braid is laid along each side of the shoe and the current flows across the blade through the conductive rubber. The center 32 percent of the shoe carries 1.5 times the heat intensity of the remaining section. The high-heat section is centered on the leading edge.

INDICATION OF HEAT INTENSITY REQUIRED

The various blade-shoe configurations provided four different heat intensities that could be compared for effectiveness. These heat intensities ranged from 4.8 to 7.5 watts per square inch on the leading edge and 2.4 to 3.8 watts per square inch on the cambered surfaces. A heat concentration of 4.8 watts per square inch on the leading edge and 2.4 watts on the remainder of the blade shoe did not provide adequate protection, although the maximum liquid-water content encountered during the icing season was only 0.42 gram per cubic meter. The pilots reported continual ice throw-off and figure 4 also indicates that the anti-icing was not complete.

A heat concentration of 5.25 watts per square inch on the leading edge and 3.50 watts per square inch on the cambered faces provided satisfactory protection up to 0.415 gram of liquid water per cubic meter, the maximum encountered with this configuration during the icing season. Figure 5 is a synchronized-flash photograph of one blade taken during flight and shows that the propeller remained free of ice.

Apparently the heat requirement to adequately protect the propeller for the general meteorological and operational conditions encountered is fairly critical. Changing the power input from 4.8 to 5.25 watts per square inch resulted in a change from unsatisfactory to satisfactory operation. It should be noted however, that the two

types of blade shoe are not directly comparable inasmuch as the ratio of leading-edge to camber-face heat intensity is not the same and more rapid heat conduction away from the leading edge takes place on the low-input blade shoe.

SERVICE DIFFICULTIES

Blade Shoes

Difficulties and failures encountered in the use of the wire-insert and conductive-rubber blade shoes were poor adhesion, short circuits, protruding heat elements, and erosion. Figure 6 shows the case histories of 10 sets of wire-insert blade shoes and one set of conductive-rubber blade shoes plotted against flight time and grouped according to difficulties. No definite cause was ascertainable for the broken leads of sets 1 and 2. Figure 7 shows a hole burned in one shoe of set 3 when an overheated or broken section of wire set fire to the rubber.

Difficulties with obtaining or maintaining proper adhesion of the blade shoes to the propeller were frequent. Part of the difficulty could be traced to poor room conditions during initial installation. It is recommended that blade shoes be installed by experienced men in rooms free from drafts and at the proper temperature.

The trouble experienced in obtaining proper adherence of the conductive-rubber blade shoes at installation (set 5, fig. 6) may have been associated with the curing process. This process requires that the blade shoe be brought to a prescribed temperature by passing electricity through it and then held at this temperature for a specified length of time. Unless the temperature is slowly raised and the entire surface temperature checked periodically at intervals of 1 or 2 minutes during the process, local overheating can occur and cause deterioration of the adhesive cement.

Some trouble was also experienced in maintaining the prescribed curing temperature because of varying room conditions. It is recommended that the curing be done in a room free from drafts and wide fluctuations in temperature.

The set of conductive-rubber shoes in current use has 60 hours of flight time and is apparently in good condition.

Figure 8 shows the photographs of the leading-edge erosion that occurred on one shoe of a set that had been in service for 123 hours and indicate that erosion may be a problem. The left photograph

shows the general extent of the erosion and the right photograph is a close up of the lower end of the shoe where the erosion was most severe. Another shoe in this set also had the broken end of a heating-element wire extending through a slit in the leading edge, as shown in figure 9.

Another indication of possible future trouble with the wire-insert blade shoes is indicated in figure 10. The blade shoes are not molded to the shape of the propeller blade and consequently must be stretched in some places and compressed in others to make them fit. The protrusions usually appear in the compressed sections and inspection shows that a buckled wire causes the protrusion. Gradually the top of these protrusions will erode and expose the wire.

Figure 11 shows the damage to a blade shoe caused by flying into a hail storm.

Gradual breakage of the heating-element wires during the life of the blade shoes may also be expected, as indicated by figure 12. The resistance of two of the shoes remained practically constant while the resistance of the other shoe increased during a two week period and then stabilized at a higher value. This indicates that one of the heating-element wires had broken and results in a decreased effectiveness of the blade shoe.

Power Supply

Propeller-hub generator. - The main difficulties encountered with the propeller-hub generators were insufficient capacity, problems associated with general mechanical design and fabrication, and one open circuit. The present generators have insufficient power output to anti-ice the propellers to which they are attached. This fault must be corrected before the generators can be considered satisfactory.

Improper seating of the armatures on the propeller-hub barrel necessitated modification of some of the generators by grinding or shimming to obtain proper seating. The Army also indicates that cracking of the stiffening ribs on the armature case has occurred after approximately 400 hours of operation. Such difficulties can be expected with developmental units and can be eliminated by redesigning.

SLIP RINGS

No difficulties were experienced with the slip-ring setup and brush wear was normal as compared to the other brushes in the propeller control assembly.

SUMMARY OF RESULTS

A study of the service records and service performance of electro-thermal anti-icing systems for propellers installed on NACA icing research airplanes during the winter of 1946-1947 gave the following qualitative results:

1. A heat concentration of 4.8 watts per square inch on the leading edge and 2.4 on the camber faces of the propeller blades was insufficient for satisfactory anti-icing at an atmospheric liquid-water content of 0.42 gram per cubic meter.

2. A heat concentration of 5.25 watts per square inch on the leading edge and 3.50 watts on the camber faces of the propeller blades was satisfactory in atmospheric liquid-water content to 0.415 gram per cubic meter.

3. Service troubles with the blade shoes included open or short circuits in the leads, breakage of heating-element wires, and poor adhesion of the shoes to the propeller blades.

4. Possible future trouble with blade shoes may be leading-edge erosion and eroding of protrusions caused by buckling of resistance wires leading to exposure of these wires.

5. The propeller-hub generators have insufficient capacity to take care of their present load and have design faults that must be corrected.

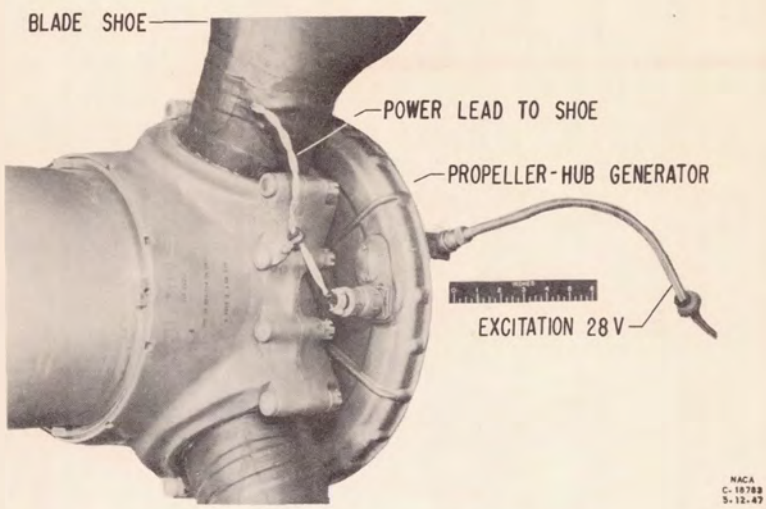

PROPELLER-HUB GENERATOR ANTI-ICING SYSTEM
FIGURE 1.

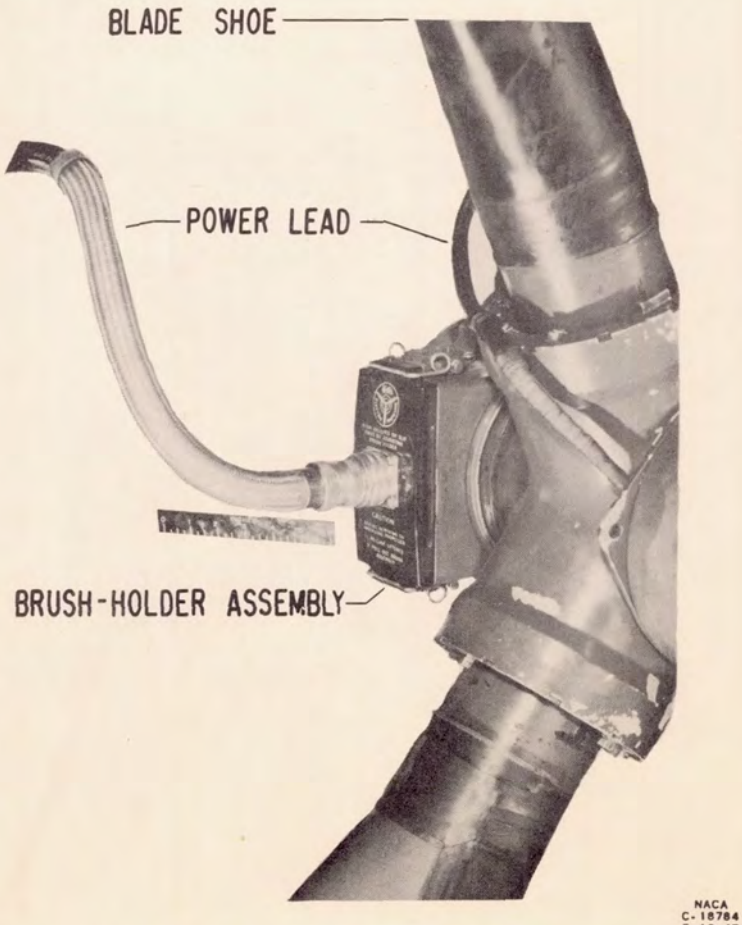

SLIP-RING PROPELLER DE-ICING SYSTEM
FIGURE 2.

BLADE-SHOE CROSS SECTIONS

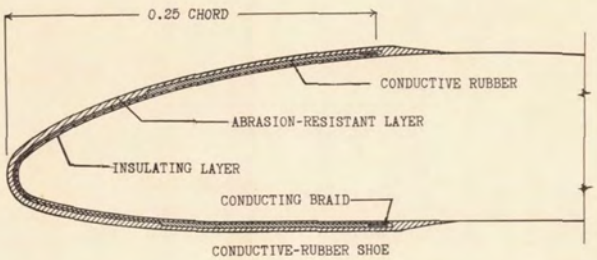

CONDUCTIVE-RUBBER SHOE

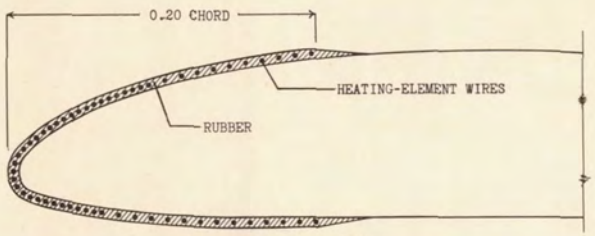

WIRE-INSERT SHOE

FIGURE 3.

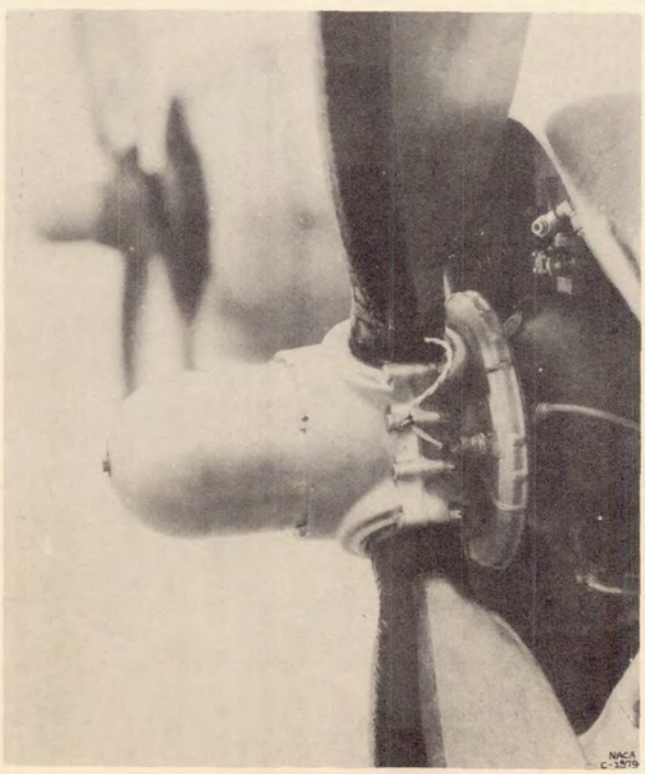

INCOMPLETE ANTI-ICING
FIGURE 4.

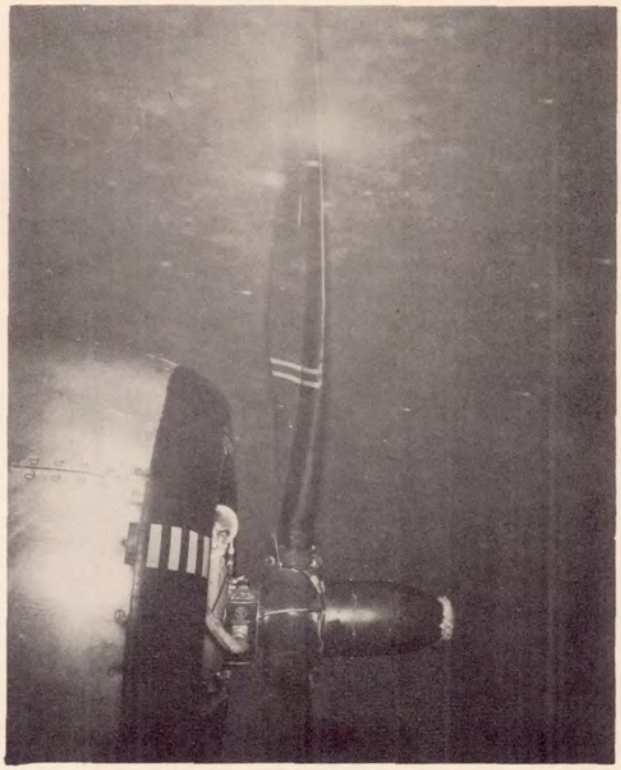

COMPLETE ANTI-ICING
FIGURE 5.

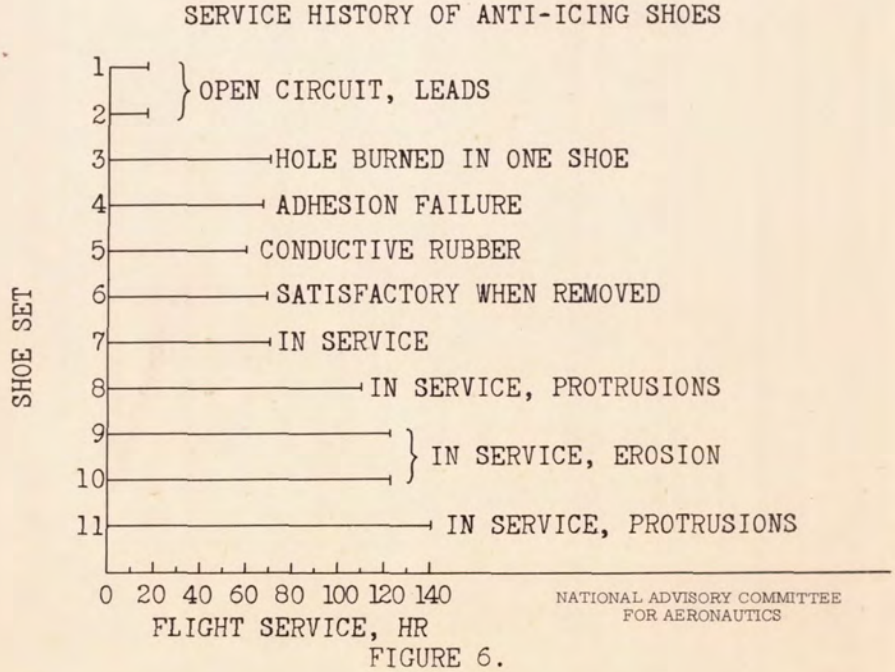

FIGURE 6.

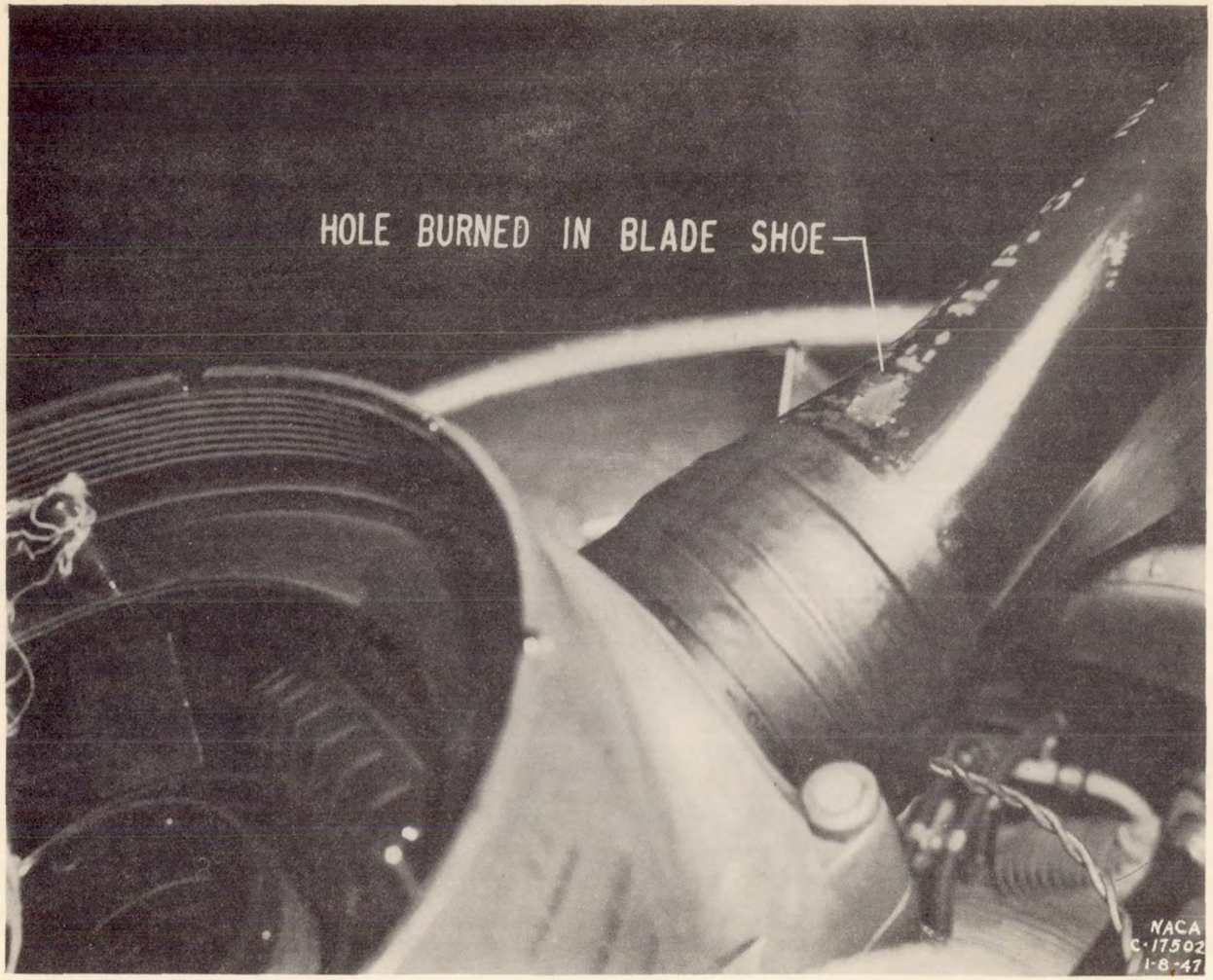

HOLE BURNED BY OVERHEATING OF RESISTANCE WIRE
FIGURE 7.

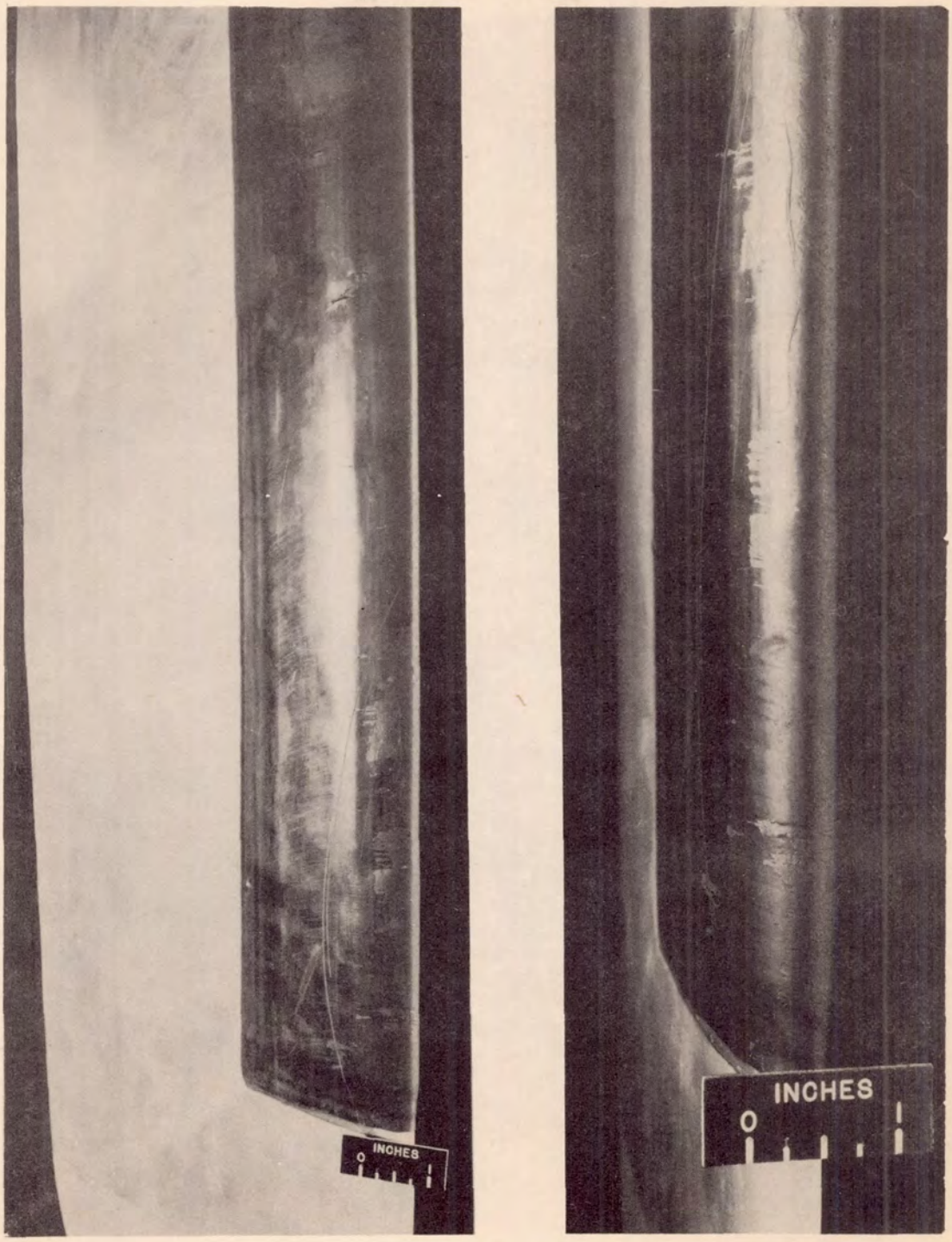

NATIONAL ADVISORY COMMITTEE
FOR AERONAUTICS

HEATING-SHOE EROSION
FIGURE 8.

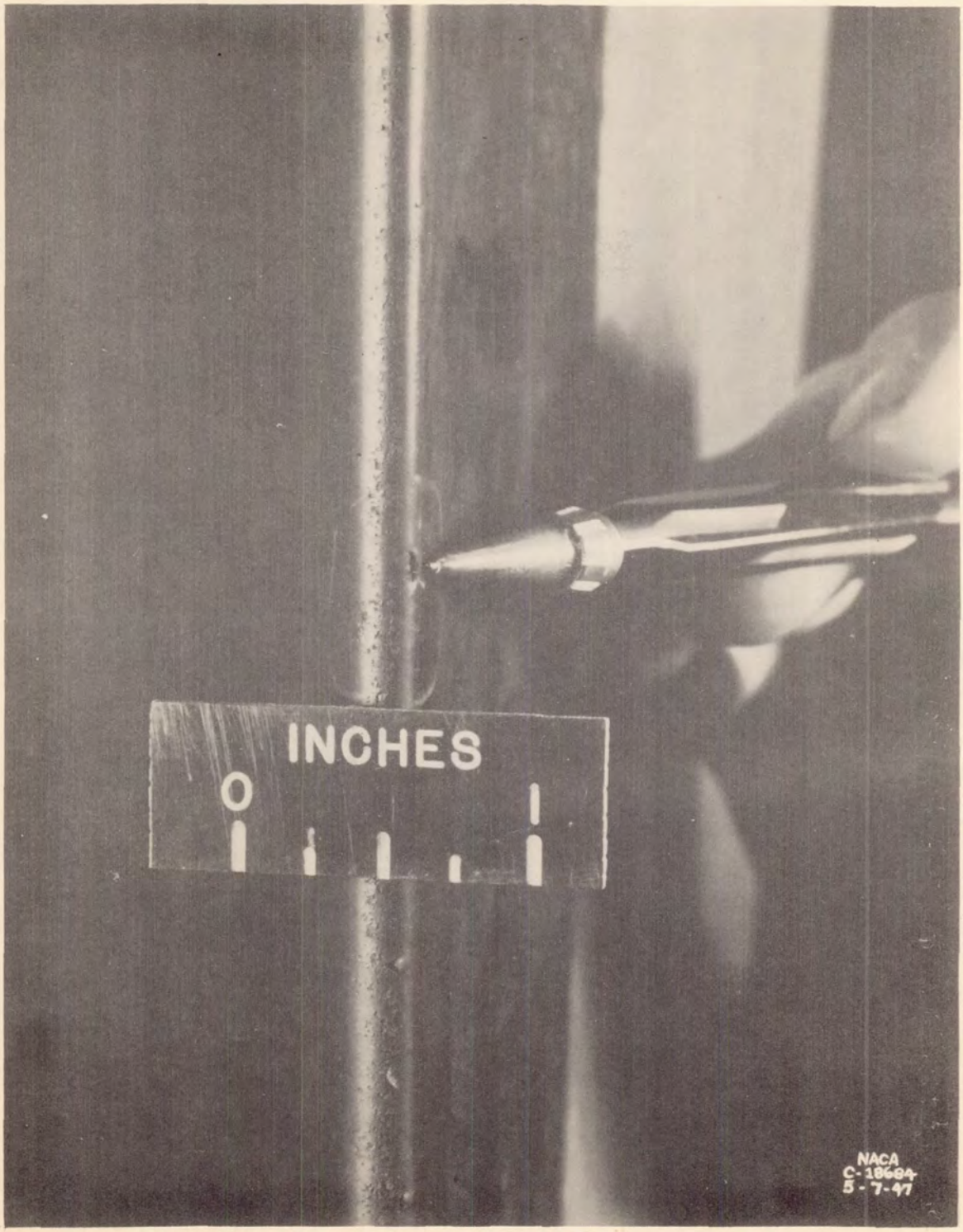

HEATING-ELEMENT WIRE BREAKAGE
FIGURE 9.

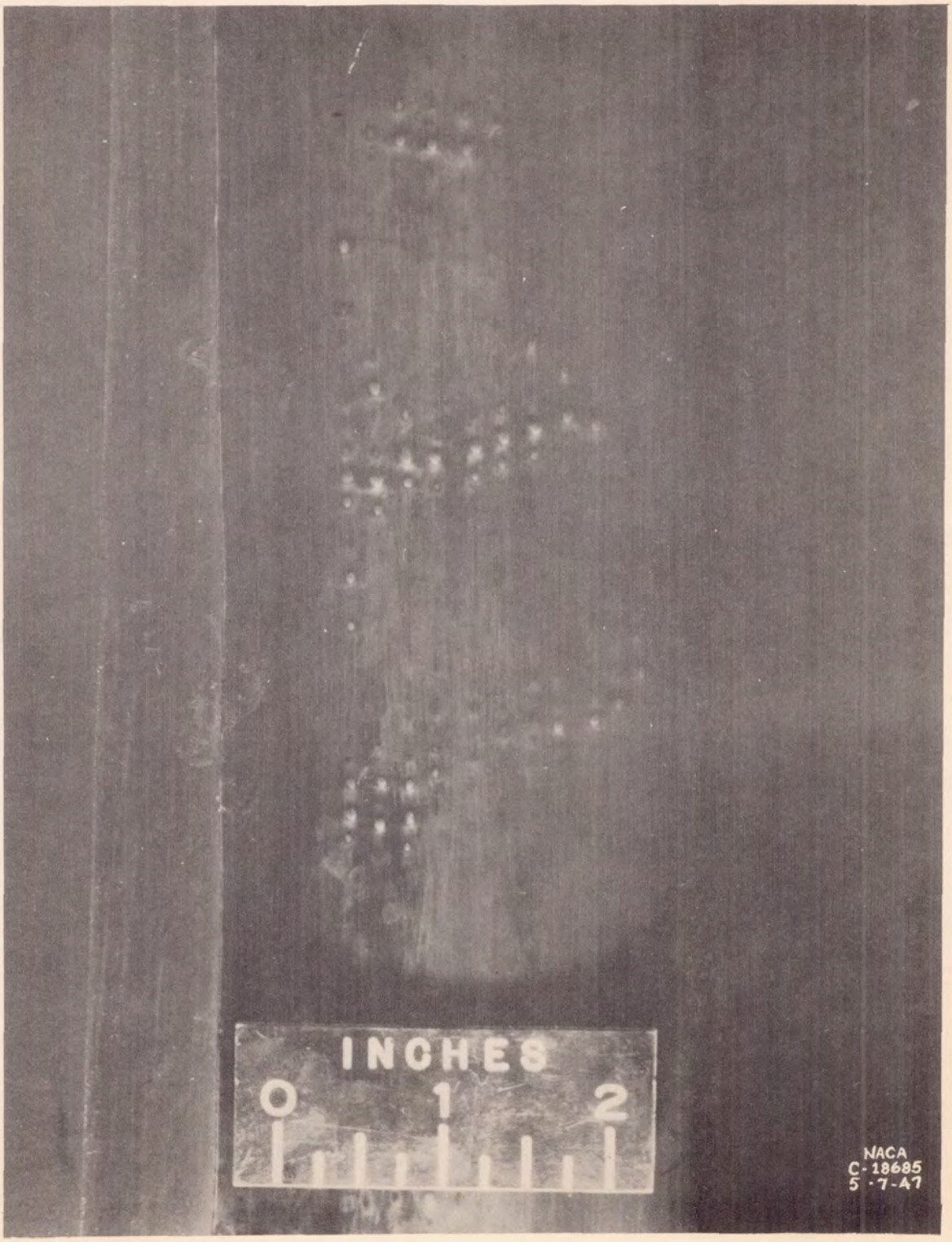

EROSION OF PROTRUSIONS
FIGURE 10.

HAIL DAMAGE TO DE-ICING SHOE
FIGURE 11.

BREAKAGE OF HEATING ELEMENTS

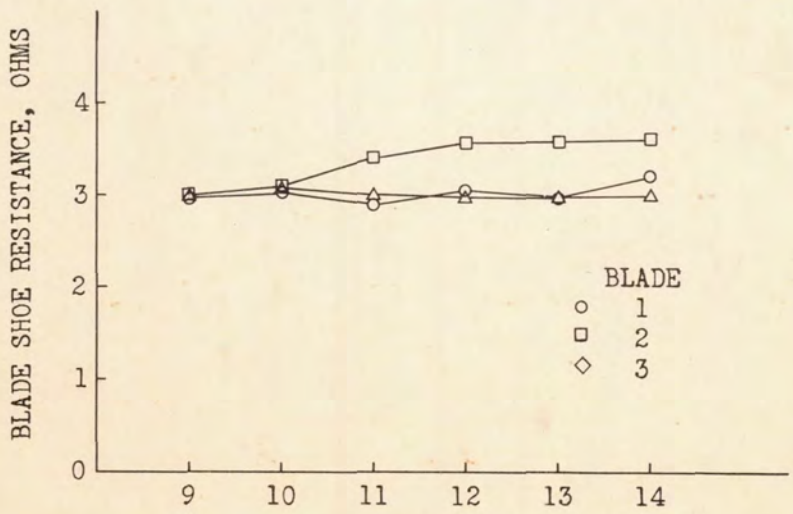

FIGURE 12.

CONFIDENTIAL

TITLE: NACA Conference on Aircraft Ice Prevention - A Compilation of the Papers Presented by NACA Staff Members.

AUTHOR(S) : (Not known)

ORIG. AGENCY : National Advisory Committee for Aeronautics, Washington, D. C.

PUBLISHED BY : (Same)

ATI- 8695

REVISION (None)

ORIG. AGENCY NO. (None)

PUBLISHING AGENCY NO. (None)

DATE	DOC. CLASS.	COUNTRY	LANGUAGE	PAGES	ILLUSTRATIONS
June '47	Confd'l	U. S.	English	248	photos, tables, diagr, graphs, drwgs

ABSTRACT:

Discussion of research on design, development, and flight application of aircraft ice-prevention equipment. Subjects discussed are NACA research on the thermal ice-prevention system, flight investigation of meteorological factors conducive to aircraft icing, calculation of heat required for wing thermal ice-prevention in specified ice conditions, tension in radio antenna wires resulting from ice formation, analytical study of thermal ice-prevention systems applied to light aircraft, effect of ice formations on aircraft performance, etc.

DISTRIBUTION: SPECIAL. All requests for copies must be addressed to: Originating Agency

DIVISION: 3

SECTION: Icing (1)

SUBJECT HEADINGS:

~~De-icing equipment~~ (28891.3)

ATI SHEET NO.:

Central Air Documents Office
Wright-Patterson Air Force Base, Dayton, Ohio

AIR TEC[illegible] INDEX

CON[illegible]TIAL

4 8